AD NUMBER
ADB015198
LIMITATION CHANGES

TO:

Approved for public release; distribution is unlimited.

FROM:

Distribution authorized to U.S. Gov't. agencies only; Test and Evaluation; NOV 1975. Other requests shall be referred to Air Force Flight Dynamics Lab., Wright-Patterson AFB, OH 45433.

AUTHORITY

AFFDL ltr 2 May 1979

AFFDL-TR-75-146 V.I

ACTIVE CONTROL SYNTHESIS FOR FLEXIBLE VEHICLES
Volume I KONPACT Theoretical Description

HONEYWELL
SYSTEMS & RESEARCH CENTER
2600 RIDGWAY PARKWAY
MINNEAPOLIS, MINNESOTA 55413

JULY 1976

TECHNICAL REPORT AFFDL-TR-75-146 FOR PERIOD APRIL 1975 - APRIL 1976

Prepared for
U.S. AIR FORCE FLIGHT DYNAMICS LABORATORY
WRIGHT-PATTERSON AIR FORCE BASE, OHIO 45433

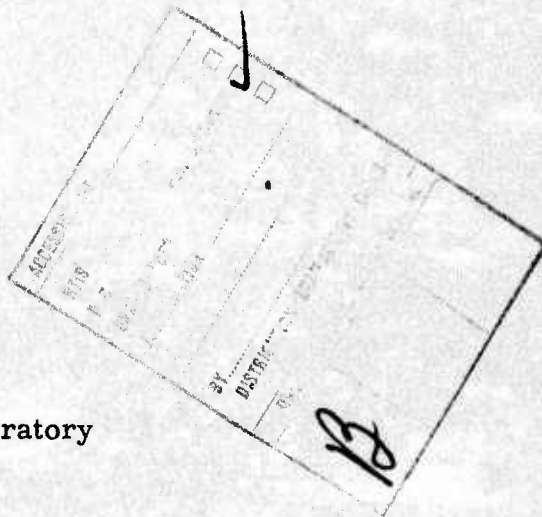| REPORT DOCUMENTATION PAGE		READ INSTRUCTIONS BEFORE COMPLETING FORM
1. REPORT NUMBER AFFDL-TR-75-146 Vol 1	2. GOV'T ACCESSION NUMBER	3. RECIPIENT'S CATALOG NUMBER
4. TITLE (AND SUBTITLE) ACTIVE CONTROL SYNTHESIS FOR FLEXIBLE VEHICLES. Volume I. KONPACT Theoretical Description		5. TYPE OF REPORT/PERIOD COVERED Final Report. Apr 1975 to Apr 1976.
		6. PERFORMING ORG. REPORT NUMBER 76SRC20 - Vol - 1
7. AUTHOR(S) A. F. Konar J. K. Mahesh C. R. Stone M. Hank		8. CONTRACT OR GRANT NUMBER(S) F33615-75-C-3046
9. PERFORMING ORGANIZATIONS NAME/ADDRESS Honeywell Inc., Systems and Research Center 2600 Ridgway Parkway Minneapolis, Minnesota 55413		10. PROGRAM ELEMENT, PROJECT, TASK AREA & WORK UNIT NUMBERS Project 8219, Task 82190221
11. CONTROLLING OFFICE NAME/ADDRESS U. S. Air Force Flight Dynamics Laboratory Wright-Patterson Air Force Base, Ohio 45433		12. REPORT DATE June 1976
		13. NUMBER OF PAGES 278
14. MONITORING AGENCY NAME/ADDRESS (IF DIFFERENT FROM CONT. OFF.)		15. SECURITY CLASSIFICATION (OF THIS REPORT) Unclassified
		15a. DECLASSIFICATION DOWNGRADING SCHEDULE

16. DISTRIBUTION STATEMENT (OF THIS REPORT)

Distribution limited to U. S. Government agencies only; test and evaluation statement applied November 1975. Other requests for this document must be referred to AF Flight Dynamics Laboratory (FGC), Wright-Patterson Air Force Base, Ohio 45433.

17. DISTRIBUTION STATEMENT (OF THE ABSTRACT ENTERED IN BLOCK 20, IF DIFFERENT FROM REPORT)

18. SUPPLEMENTARY NOTES

19. KEY WORDS (CONTINUE ON REVERSE SIDE IF NECESSARY AND IDENTIFY BY BLOCK NUMBER)

Active Control	C-5A
CCV (Control Configured Vehicles)	Optimal Control
Flight	FLEXSTAB
Flexible Vehicle	Modeling

20. ABSTRACT (CONTINUE ON REVERSE SIDE IF NECESSARY AND IDENTIFY BY BLOCK NUMBER)

KONPACT is a system of digital computer programs that will rapidly design optimal or suboptimal control systems especially for aircraft with lightly damped modes. This program represents advanced computational techniques to perform modern control synthesis, analysis, and design of automatic control systems. KONPACT augments aircraft mathematical models produced from such advanced programs as the FLEXSTAB Level 2.01.00 with control system dynamics and then designs and

→ next page

DD FORM 1473   EDITION OF 1 NOV 55 IS OBSOLETE
1 JAN 73

conti

analyzes quadratic optimal or suboptimal control systems.

The KONPACT Theoretical Description is the first volume of report prepared under Contract F33615-75-C3046.

It contains the mathematical description of algorithms used in KONPACT as well as active control synthesis procedures and their application to Active Life Description Control System (ALDCS) design. It also contains the results of a short study for the effects of model residualization and truncation procedures on control system performance.

FOREWORD

The research described in this report was prepared by Honeywell Inc.,
Minneapolis, Minnesota 55413, under Air Force Contract F33615-75-C-3046.
It was initiated under the AFFDL Task Number 82190221, "Optimal Control
of Flexible Aircraft," Project Number 8219, "Stability and Control of Aero-
space Vehicles." This work was directed by the Control Criteria Branch
(FGC), Flight Control Division of the Air Force Flight Dynamics Laboratory
and was administered by Mr. Charles R. Stockdale of the Control Criteria
Branch. Special thanks to Mr. Robert C. Schwanz of FGC and Mr. Gary
Grimes of ASD/ADDP for their continued support toward this contract.

The technical work reported in this volume was conducted by the Research
Department at the Systems and Research Center of Honeywell Inc. Dr. A.
F. Konar was the Honeywell Program Manager and the principal investigator
on this contract. He was assisted by Mr. C. R. Stone, Dr. J. K. Mahesh,
and Miss M. Hank. This report covers work done from April 1975 to April
1976.

The work under this contract was reported in three volumes entitled "Active
Control Synthesis for Flexible Vehicles."

Volume I	KONPACT Theoretical Description	
Volume II	KONPACT Program Listing	AD-B015 216L
Volume III	KONPACT Users Manual	AD-B015 025L

TABLE OF CONTENTS

TABLE OF CONTENTS (Continued)

TABLE OF CONTENTS (Concluded)

LIST OF FIGURES

LIST OF FIGURES (Continued)

LIST OF FIGURES (Continued)

LIST OF FIGURES (Continued)

LIST OF FIGURES (Continued)

LIST OF FIGURES (Continued)

LIST OF FIGURES (Continued)

LIST OF FIGURES (Continued)

LIST OF FIGURES (Concluded)

LIST OF TABLES

LIST OF TABLES (Continued)

LIST OF TABLES (Concluded)

SECTION I

INTRODUCTION

The general objective of this study is to develop techniques and tools necessary for rapid design of an active control system for aircraft with lightly damped structural modes. The synthesis techniques provided here are aimed at reducing the engineering man-hours presently required for a flight control system design, thus effecting a cost reduction. Improvements in the fatigue life, ride qualities, and/or handling qualities of military aircraft are sought by controlling the lightly damped modes and thus improving their mission performance.

The present scope of this study is to develop programs to interface the level 2.01.00 FLEXSTAB computer program system with existing Air Force-owned optimal control computer programs. These programs represent advanced computational techniques required to perform quantitative analysis of multisurface control systems. The resulting interface program system is called "KONPACT - Computer Programs for Active Control Technology." KONPACT provides the capability to model, synthesize, analyze, and design automatic control systems efficiently working together with FLEXSTAB. It can also be used as a stand alone program.

The work performed under this contract is reported in three volumes:

Volume I.   KONPACT Theoretical Description and Demonstration
Volume II. KONPACT Program Listing
Volume III. KONPACT Users Manual

1

This document reports the analytical techniques and algorithms used in KONPACT. It also demonstrates how these techniques are applied to flexible aircraft control system design.

An overview of the Honeywell theoretical approach to control system design using KONPACT is provided in Section II. The process of the Active Lift Distribution Control System (ALDCS) design, brief description of KONPACT, and the application results for the C-5A vehicle are described in this section.

In Section III the technique for mathematical modeling of the dynamics for the optimal controller design is presented. This is an automated process which has been applied to multivariable systems.

System performance analysis in state space is briefly reviewed in Section IV for completeness. The steady-state response modeling is considered in detail since it is required for the ALDCS design. Some of the analytical developments reported have not been incorporated into the existing software due to lack of resources.

In Section V active control synthesis procedures are reviewed. A description of performance criteria is given first. This is followed by the control configuration for the required steady-state performance. Subsequently, the full state and simplified optimal controller design steps are described. Finally, a demonstration example is given for the ALDCS design using the C-5A vehicle.

In Section VI the effects of modeling and model reduction procedures on control system performance is presented. Two vehicle modeling procedures,

i.e., Air Force FLEXSTAB and Honeywell/GELAC, are reviewed first for the C-5A vehicle. Subsequently, the theory of model reduction procedures is briefly described. The residualization and truncation methods are investigated using C-5A open-loop and closed-loop models.

Conclusions and recommendations are given in Section VII. Both future analytical work and software development work are described.

Computer programs which implement the mathematical analysis and models presented in this volume are listed in Volume II. Complete documentation of KONPACT is beyond the scope of this contract.

In Volume III users' information on KONPACT is given. The input cards are fully described for each program. A brief description of programs and the information flow in KONPACT are also presented for completeness. Demonstration examples are included to guide the user in data mechanics.

SECTION II

ACTIVE CONTROL SYNTHESIS APPROACH

This section presents the overview of Honeywell's work on the optimal and suboptimal active control design for the C-5A aircraft and design software.

First, the previous work of Honeywell on the subject (Reference 4) is briefly presented to provide background information. Subsequently an overview of the KONPACT package--Computer Programs for Active Control Technology, developed in this program is given.

Finally, the results of the Active Lift Distribution Control System (ALDCS) using the FLEXSTAB/LSA generated vehicle model are described.

REVIEW OF DESIGN PROCEDURE FOR THE C-5A ACTIVE LIFT DISTRIBUTION CONTROL SYSTEM (ALDCS)

Honeywell has conducted a study (Reference 4) which was part of Lockheed Georgia's (GELAC) program to increase the life of the C-5A airplane with the use of active control. The design goals for the ALDCS are listed in Table 1. The design rules were to meet these specifications with a single accelerometer in each wing (see Figure 1) and without the use of notch filters to remove unwanted flexure modes from the measurements. Four flight conditions were chosen as shown in Table 2.

4
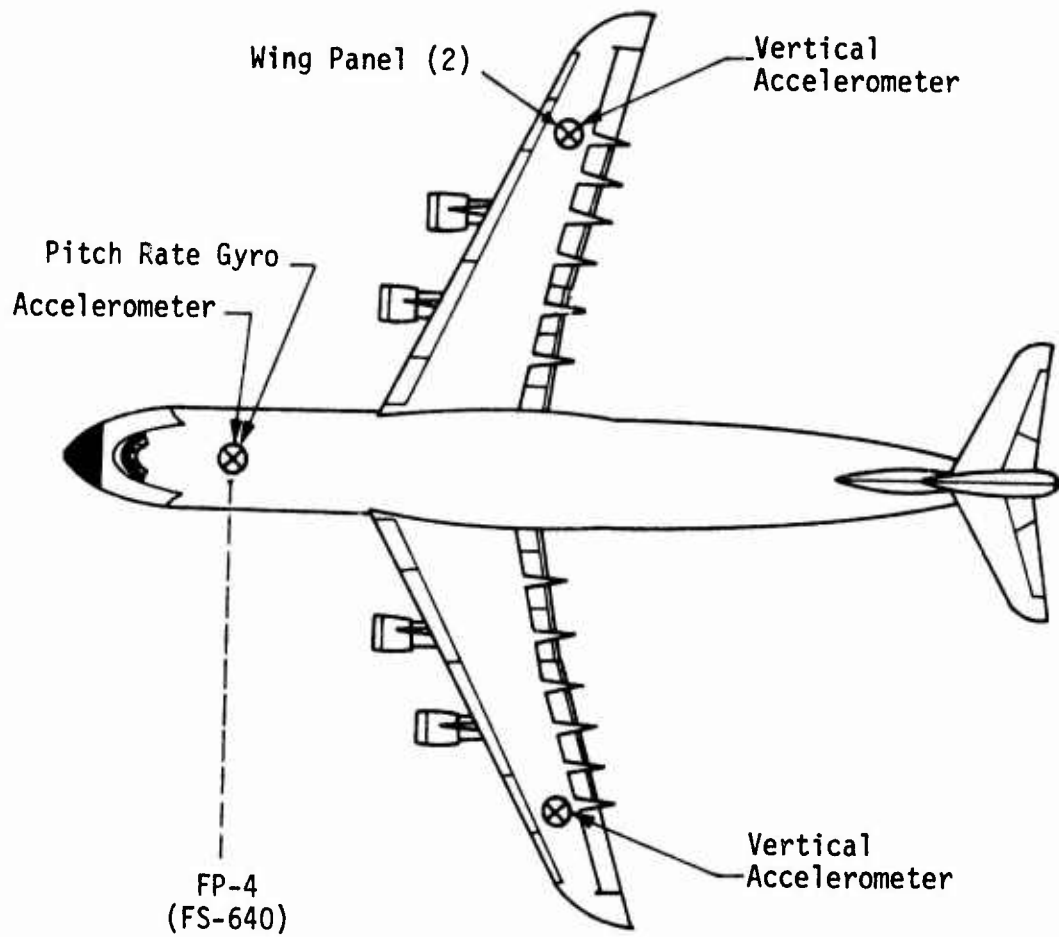
Figure 1. C-5A ALDCS Sensor Locations

Table 1. ALDCS Design Goals

No.	Performance Criterion	Specification
1	Wing root bending moment due to maneuvers and wind gusts	70% of free A/C values
2	Wing root torsion due to wind gusts	Less than 105% free A/C
3	Handling qualities	Same as A/C with existing SAS
4	Stick force per g	Same as A/C with existing SAS
5	Stability margins	10 db gain, 60° phase

Table 2. Flight Condition Definition

Flight Condition	KONPACT CHECKCASE CRUISE 412301	CLIMB 412502	TRAFFIC 412530	CONTOUR 412020	F.C. 37
Total Weight (lb)	578,430	698,400	698,400	529,500	593,154
Mach No.	.74	.448	.228	.533	.533
Altitude (ft)	30,000	7,500	1,500	0	10,000
Dynamic Pressure (psf)	240	191	73	418	292
Airspeed (fps) U_o	735	468	254	594	577
Fuel (lb)	94,250	214,500	214,500	94,250	159,750
Cargo (lb)	158,104	160,000	160,000	30,000	110,000
Center of Gravity (% M.A.C.) (c.g.)	30	31	30	29.9	31

6

The resulting system was called Active Lift Distribution Control System (ALDCS). It was developed as a means to reduce fatigue damage on the wing root due to aircraft flight maneuvers and wind gust forces. The control system developed by Honeywell (Reference 4) was designed to reduce the fatigue damage enough to double the actual flight life of the aircraft. The proposed system consisted of five sensors controlling the ailerons and the inboard elevators. An accelerometer was placed in each wing; an accelerometer and a pitch rate gyro were placed in the fuselage, and a sensor was placed on the pilots pitch control column (see Figure 2).

The control system reduces wing bending during maneuvers by putting an upward bias on the ailerons proportional to the g load. This causes the life to be distributed inboard on the wing and requires the elevator to deflect more. The wing bending due to wind gusts and maneuver are reduced by sensing these forces with the accelerometer and cancelling them with the aerodynamic surfaces. The aileron most effectively damps the higher frequency bending modes. The elevator most effectively damps the low frequency bending modes.

Structural mode control technology has been developed for aircraft in programs with the XB-70, B-52, C-5A and YF-12A (References 11 and 18 through 21). The XB-70 program demonstrated the effectiveness of the ILAF (identical location of accelerometer and force) configuration where the sensor and control force producers are placed near one another. The control surfaces effectively cancelled out sensed aeroelastic forces due to lower local acceleration.
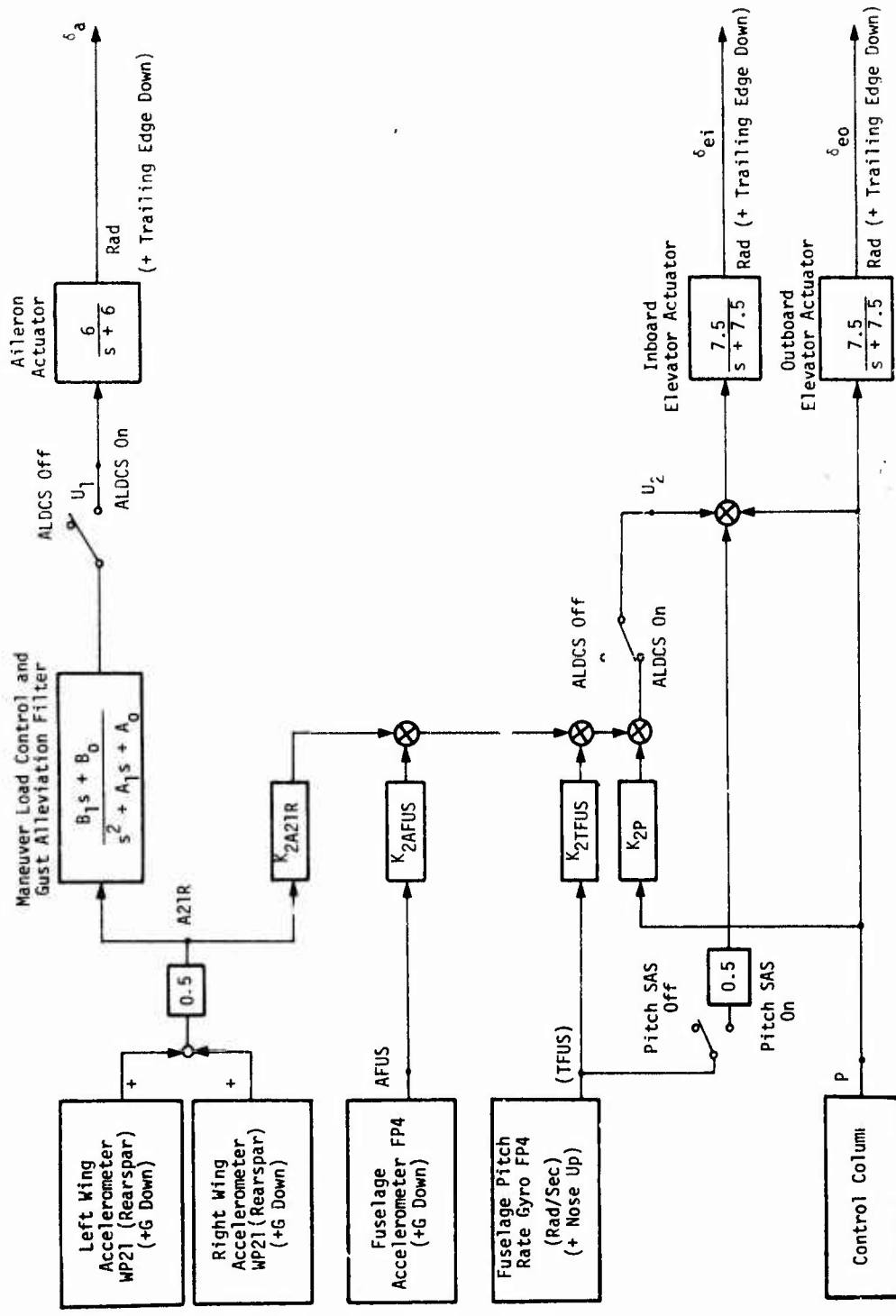
Figure 2. ALDCS Simplified Controller Configuration for Cruise - F. C. 412301

8

The B-52 and C-5A LAMS programs established the feasibility of using control forces to reduce fatigue damage ratio in air turbulence. The C-5A LICS program showed the special effectiveness of the inboard spoilers in reducing wing root fatigue. The YF-12A study extended the LAMS technology by examining additional control force producers. A canard vane proved to be the most effective force producer for reducing structural mode contributions to local accelerations.

In the C-5A ALDCS program all aspects of the control problem were considered. These included handling qualities, flutter margins, and cost effective sensor configurations. The elevators proved to be effective force producers in combination with the ailerons for reducing wing root bending moments. In addition to low frequency bending mode suppression, the ailerons were up-rigged for steady-state g loads to distribute the maneuver's lift forces inboard to reduce root stress.

Honeywell-GELAC C-5A Vehicle Modeling

Modeling Procedure--One of the most difficult and crucial tasks in the design of the flexure control system is constructing an accurate model of the aircraft (Reference 5). The Lockheed Georgia Company provided the complex model of the C-5A structural dynamics with 15 flexure modes (Reference 4). The model allowed accurate determination of flexure mode states over the aircraft wing as a function of aerodynamic and control surface forces. The provided data also allowed the calculation of accelerometer outputs for any sensor location. In addition, shear, torsion, and bending moment equations were provided to calculate the control performance. The above data were supplied for the four critical flight conditions presented in Table 2.

9

The model was transformed from second order airframe standard form to first order differential equations for state space analysis. Other minor changes were made to the model to simplify the state space analysis. First order actuator models were added. The Von Karman wind gust model was replaced by the second order Dryden model. The Wagner dynamics for the flexure modes were reduced from the second to first order to represent unsteady model. The phugoid dynamics were removed so that the unstable roots would not affect the design calculations. After the above transformations, the steady and unsteady aircraft models contained 42 and 79 states, respectively.

In order to make the design optimization cost effective, the design model was obtained by reducing the 7th through 15 flexure modes in the steady model through residualization. By this process the highest frequency flexure modes were removed. This procedure is more accurate for SS maneuver load calculations than modal truncation.

Specific modeling software was developed to perform the above data manipulations, transformations, and reductions (Reference 26). We note, however, that, because of the way the unsteady effects (Wagner dynamics) were modeled, the steady low order models could not be obtained directly from the high order unsteady model either by truncation or by the residualization processes.

This fact was overlooked in some current programs at Honeywell using the C-5A high order model. It was also a source of some confusion in this program when the comparison of Honeywell/GELAC and FLEXSTAB/LSA models were made. The late discovery of this fact prevented reactivating specific modeling software reported in Reference 26 to obtain accurate reduced order models using the GELAC data for this study.

10

Coordinate Systems--The rigid body dynamics of the Honeywell study are
described in the body fixed axis systems. The origin of this system is at
the aircraft's center of gravity (c. g.) and moves with the c. g. along the
flight path. (See Reference 4 for additional details.)

Bending moments and torsional moments provided by Lockheed are
described at the five wing station local coordinate systems shown in
Figure 3. Polarity is established by the "right-hand" sign convention.
Bending moments are about an axis perpendicular to the elastic axis
(+ bending moment produces right wing-tip up). Torsional moments are
about an axis parallel to the elastic axis (+ torsion produces leading-
edge up).

Active Control Using Quadratic Optimization

The quadratic optimization design methods were carried out on a six mode
model without Wagner dynamics. The design model required 28 states with
various compensator states included.

Quadratic optimization is a numerical technique. The technique is especially
suited to complex problems with many interactive loops and many conflicting
performance criteria. In such problems, intuition is confused. The
numerical technique provides a systematic procedure for making complex
tradeoffs. By simply adding all the performance parameters to a response
vector and weighing their relative importance, the method gets near the
desired result very quickly.

For quadratic optimization the model and its responses are reduced to
algebraic quantities. The rms responses are described by the coefficients

11
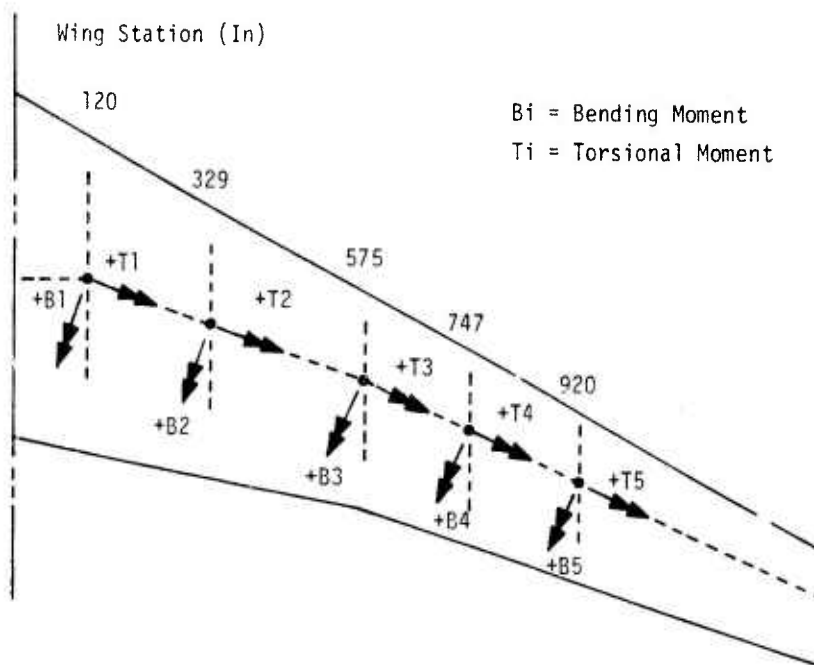
Figure 3. Equivalent Honeywell/GELAC C-5A Load Axis Systems
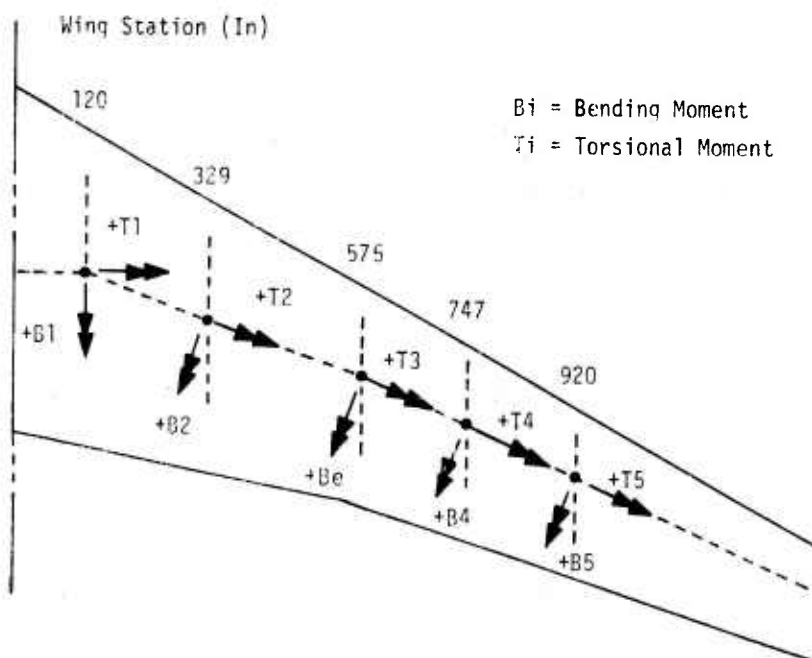
Figure 4. Equivalent FLEXSTAB C-5A Load Axis Systems

12

of the differential equations of the system. These responses can be summed in a cost function with variable weights. The feedback gains are chosen to minimize the sum of the responses. The design problem is to pick the proper responses for the cost function with the proper weight ratio for the performance tradeoff. Initially, feedback gains are chosen for all the states (dynamic elements) of the system. Since only a limited number of states can be fed back through the sensors, the gains have to be adjusted later for that condition in order to make the system practical.

Cost Function

The cost function for the quadratic design was made up of flexure mode rates, bending and torsion moments at several wing stations, control surface position and velocity, and pitch response model error. All of the above responses were minimized in accordance with selected weighting ratios. The pitch response of the C-5A with the stability augmentation system (SAS) was used as a model for handling qualities.

Design Procedure

The quadratic optimization of the above cost function produced a full state feedback design. The design was then "practicalized" by adjusting the feedback gains to be compatible with the actual sensors. This process is accomplished with a numerical search algorithm which seeks to adjust the feedback gains with the least amount of increase in the cost function.

In this design procedure, for each response weights, the DIAK program generates full state feedback. Successive response weights are chosen until performance specifications are exceeded. Then the design is practicalized using the FFOC program. If the practicalized design meets performance specifications, performance plots are calculated using the analysis model. If not, a new full state design is calculated. If the frequency response plot shows insufficient stability margin, slight gain or filter changes are made. Then the rms responses and transient responses are rechecked.

Performance Evaluation

During the design process, the performance of the system was evaluated by examining the rms values of the wing root bending and torsion moments. The handling qualities were evaluated by comparing the ALDCS design transient response to a step pilot command with similar SAS aircraft responses. In addition, the damping ratios and the natural frequency of the short period roots are compared with that of the SAS aircraft. The stability of the ALDCS system is qualitatively evaluated by looking at the damping ratios of all of the roots of the characteristic equation. A quantitative measure of stability margin is obtained from loop breaking frequency response plots. One sensor or actuator loop is opened at a time to determine the gain margin for each loop.

ACTIVE CONTROL TECHNOLOGY COMPUTER PROGRAM

A computer program (KONPACT) was generated to facilitate dynamic modeling, optimal and suboptimal controller synthesis, and performance analysis of vehicles with lightly damped modes.

14

This program utilizes advanced computational techniques to perform system modeling, modern control synthesis, analysis, and design of automatic control systems. Figure 5 shows its functional block diagram. It interfaces with the FLEXSTAB/LSA program for vehicle description as well as performance evaluation of the optimal closed loop system. Figure 6 shows the LSA/KONPACT interface and also shows a proposed version of an advanced FLEXSTAB program. KONPACT is also used as a stand alone program with externally input vehicle descriptions. Specifically, KONPACT integrates the relevant computer programs in aerodynamics, and structures (FLEXSTAB/ LSA level 2.01.00) with programs in modern control theory (DIAK, FFOC) into a single interdisciplinary design tool. This integration is shown in detail in Figure 7. Its variable dimensioning feature reduces the workload on the interface data mechanics for design and analysis of large scale systems.

In the following a brief description of KONPACT is given.

Overlay Organization

KONPACT consists of two programs, namely, a modeling program (KONPACT-1) and a design program (KONPACT-2). KONPACT-1 interfaces with FLEXSTAB through the LSA program to obtain the vehicle model and augments the specified dynamics to obtain the state space description (quadruple data) of the flight control system. These data are utilized by KONPACT-2 which contains the subprograms DIAK and FFOC (documented in Reference 1) in the design of the optimal feedback gains. Also KONPACT-2 interfaces with FLEXSTAB through the LSA program to evaluate performances of the above designed optimal flight control system.

15
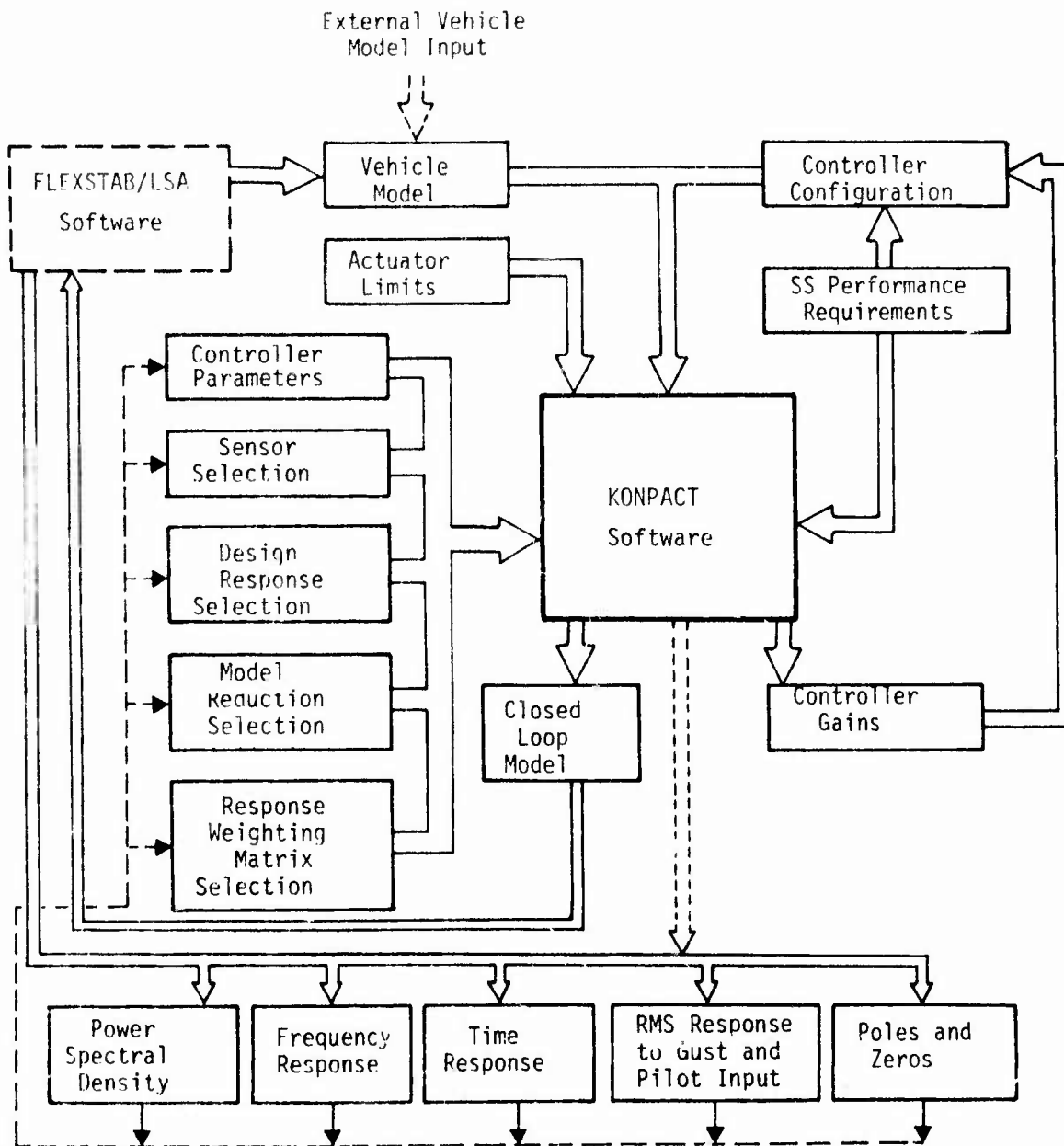
Figure 5. Functional Block Diagram of KONPACT Software
(Dotted lines show future work)

16
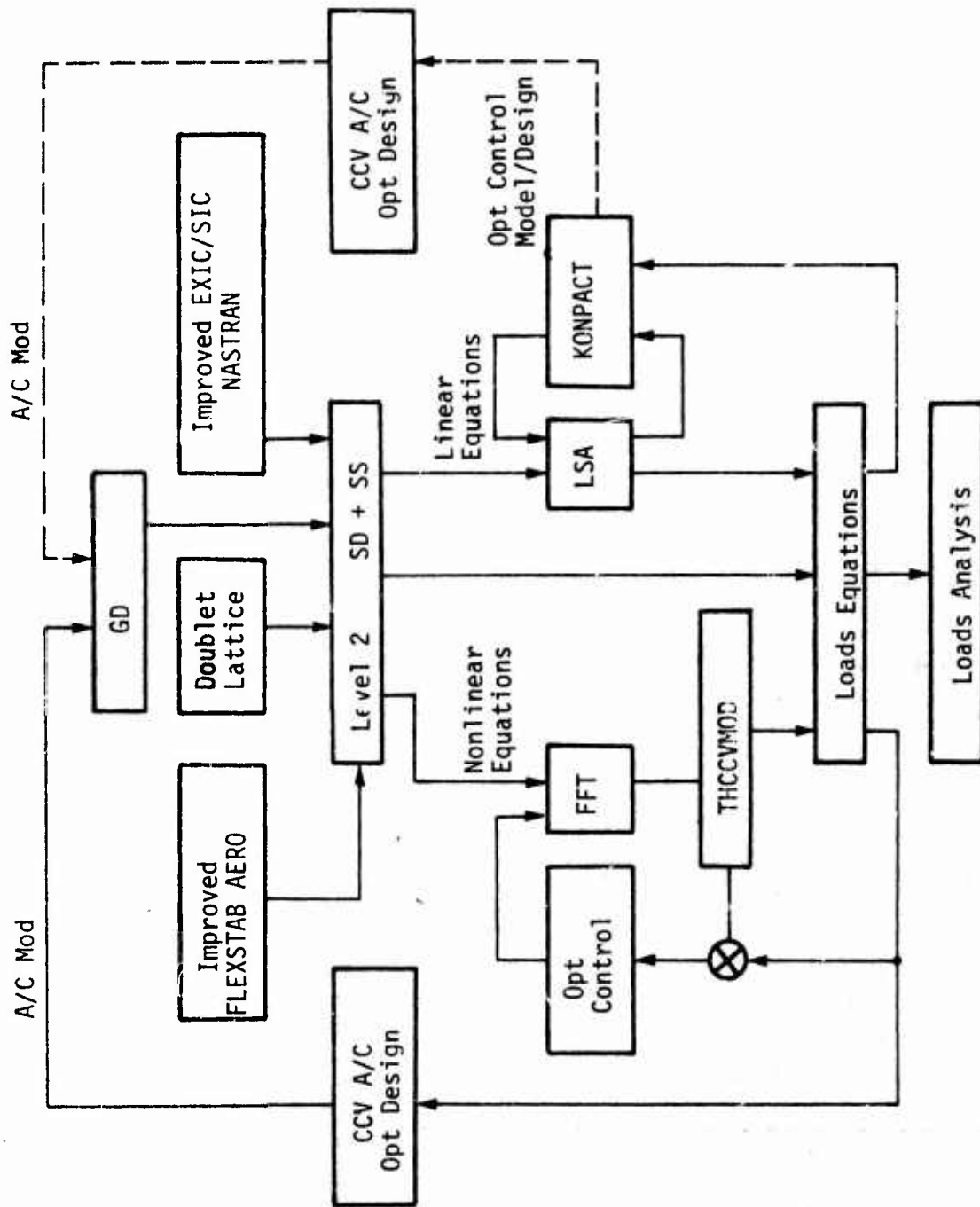
Figure 6. Advanced FLEXSTAB Program
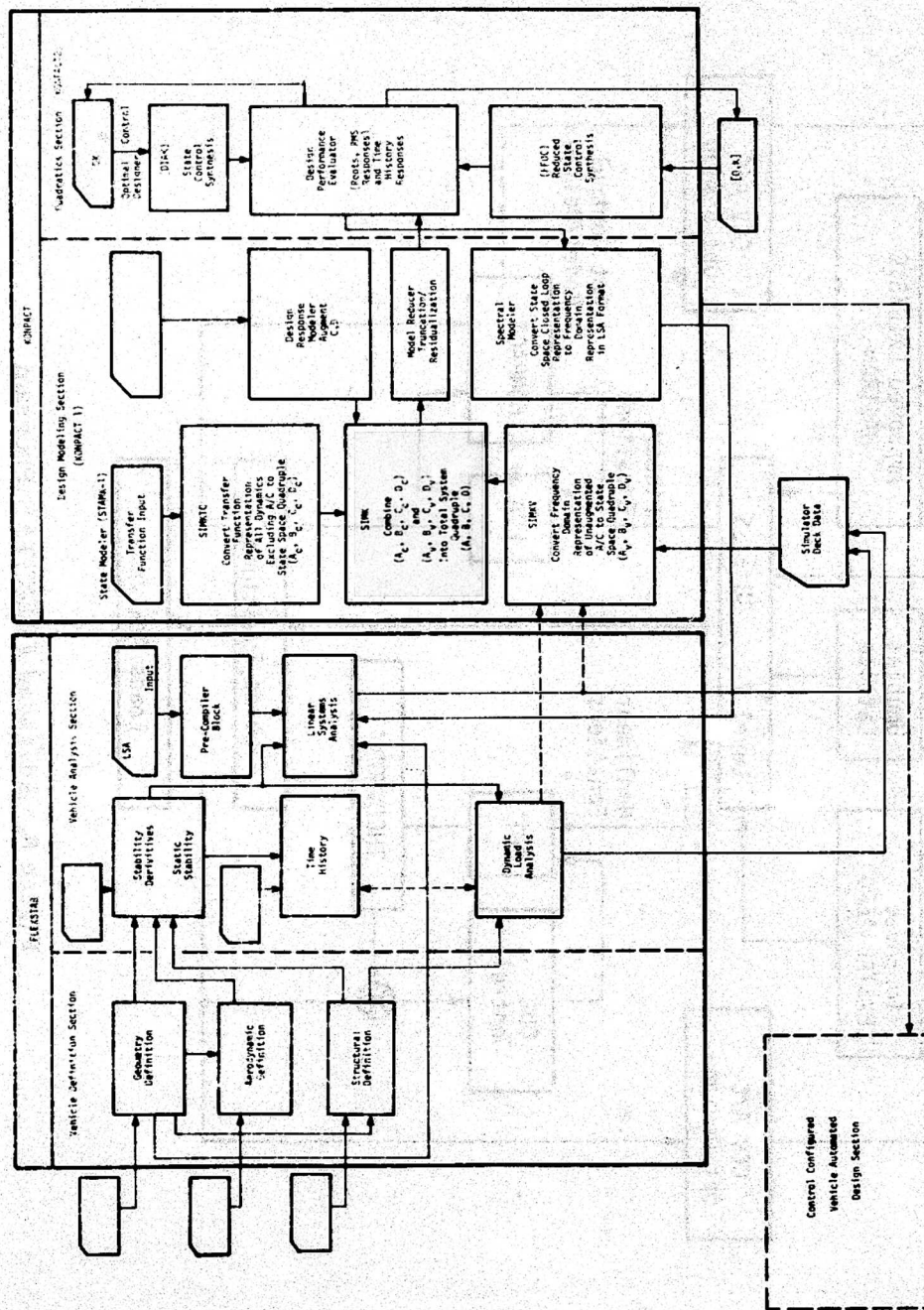
Figure 7. KONPACT Program Organization
(Dotted lines show future work)

Table 3 provides a brief description of programs KONPACT-1 and KONPACT-2 and their subprograms. The detailed interface between KONPACT and the LSA program is illustrated in Figure 8. The overlay structure of KONPACT is discussed in References 51.

Information Flow

The normal sequence for obtaining an overall state space model of a flight control system using the modeling program (KONPACT-1) is as follows:

- The vehicle model is obtained by using either subprogram STAMK1 for LSA data or subprogram STAMK4 for other types of vehicle data.

- The actuator, sensor, controller, implicit and explicit models are obtained by using either subprogram STAMK2 with transfer function input data or subprogram STAMK3 with quadruple input data.

- The subsystems defined above are combined to get an overall system by using subprogram STAMK3 with interconnection input data.

- The overall system model is conditioned (modified) by scaling and/or shuffling and/or truncating and/or residualizing the variables using the CONDK program. This program also develops the rate of change of response variables when required.

The normal sequence for designing optimal feedback controllers and evaluating the performance of the resulting system using the design program KONPACT-2 is as follows:

19

Table 3. KONPACT Program Descriptions

PROGRAM	SUBPROGRAM	DESCRIPTION
KONPACT-1		State space modeling program
	STAMK1	Obtains state space model from LSA simulator deck data
	STAMK2	Obtains state space model from transfer function data
	STAMK3	Obtains state space model from quadruple data and interconnection data
	STAMK4	Obtains state space model from simulation equations (User Written)
	CONDK	Modifies the state space model by scaling, shuffling, truncating and residualizing the system variables
KONPACT-2		Optimal design program
	DATAK	Prepares data for DIAK, FFOC and LSA programs
	DIAK	Designs full state feedback optimal controllers
	FFOC	Designs reduced state (practical) feedback optimal controllers
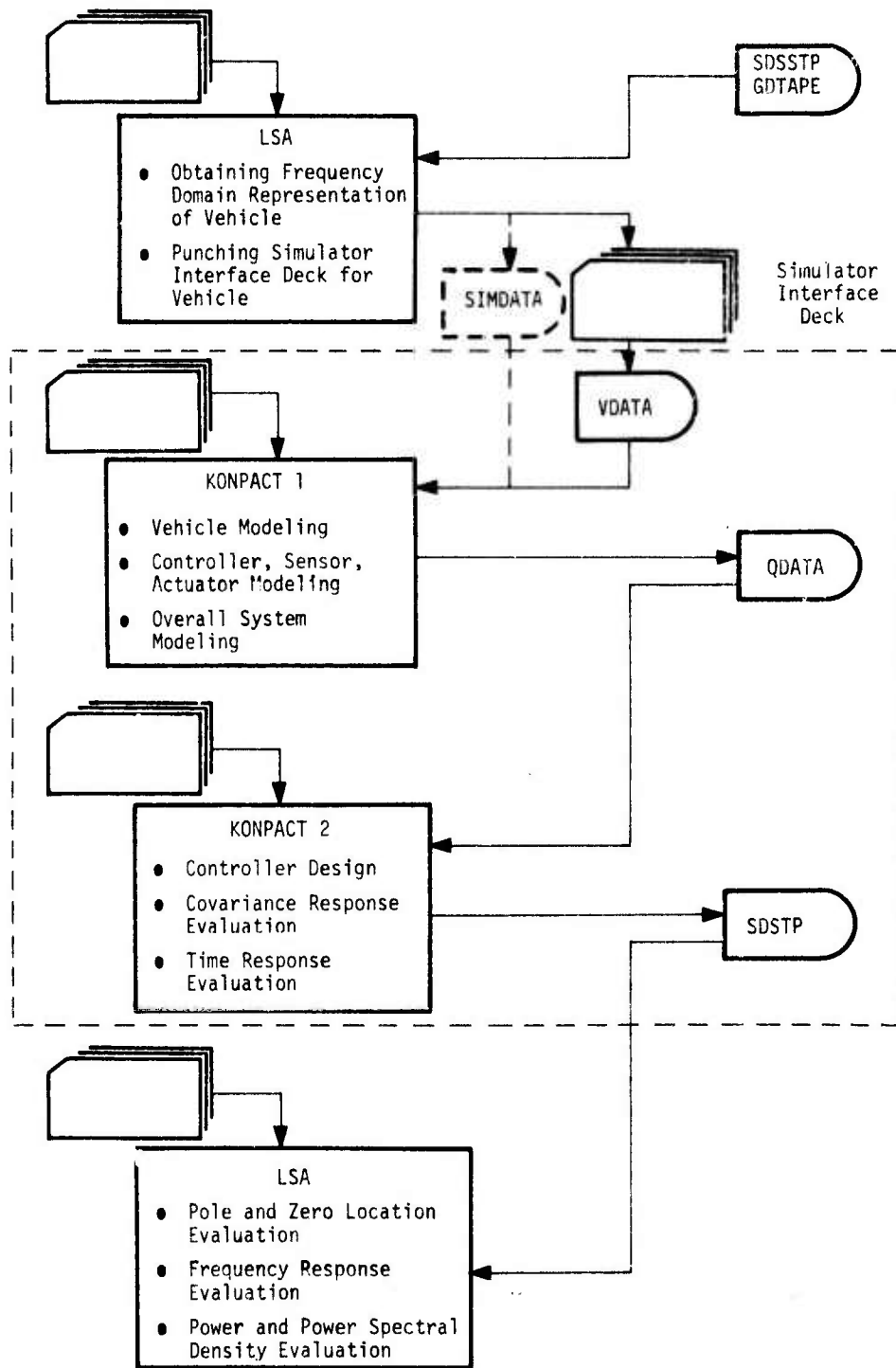
Figure 8. Interface Between LSA and KONPACT Programs

- Full state feedback control gains are obtained by using the DIAK program and by varying the quadratic weights until performance design requirements are satisfied.

- The resulting full state feedback control gains are reduced to gains only on specified measurements by using the FFOC subprograms.

- The performance of the resulting closed loop system is evaluated using the LSA program.

- The above steps are repeated until a satisfactory design is obtained.

Table 4 describes all the data tapes used in the KONPACT-1 and KONPACT-2 programs. The state space model data (quadruple data) and the name list

Table 4. KONPACT Data Tapes

TAPE NAME		GENERATING PROGRAM	BENEFITING PROGRAM(S)
VDATA	Simulator Interface data in the form of card images	LSA	KONPACT-1
QDATA	Quadruple (A, B, C, D) or state variable representation data	KONPACT-1	KONPACT-1 KONPACT-2
NDATA	Name list data of the state variable representation	KONPACT-1	KONPACT-1
DDATA	Full state feedback gain data in the form of card images	KONPACT-2	KONPACT-2
FDATA	Reduced feedback gain data in the form of card images	KONPACT-2	KONPACT-2
SDSTP	Frequency domain representation of quadruple data	KONPACT-2	LSA

data are written on tapes QDATA and NDATA, respectively. The vehicle data (simulator deck data) are written on tape VDATA. The feedback gain data from DIAK and FFOC are written on tapes DDATA and FDATA, respectively. The overall system data in frequency representation form are written on tape SDSTP for use by the LSA program.

The DATAK subprogram is used in preparing data tapes for DIAK, FFOC, and LSA.

Variable Dimensioning

Dynamic data storage variable dimensioning techniques (Reference 7) are used for efficient data storage. This technique also facilitates changing the amount of allocated (required) storage space by a data card input. In KONPACT the subprogram arrays, whose size depends on the maximum system dimension inputs, are stored in scratch storage blocks using variable entry points. In the subprograms the arrays are dimensioned with integer variables. These "variable DIMENSION statements" remain unchanged although the amount of required data storage is altered. The maximum size of the scratch storage blocks is specified, in a "fixed DIMENSION statement," in the main program.

The size of storage actually needed by the arrays varies depending on the maximum system dimension inputs. Thus, if the maximum size a user allows for his program changes, there is only the "fixed DIMENSION statements" in the main program to be changed. Changing the main program of KONPACT-1 is done by a precompiler. The user provides the new maximum system dimensions by data cards. Updating and running with the

updated main program are done with control cards in a single run. For more details on variable dimensioning the reader is referred to Volume II (Reference 3).

ALDCS DESIGN WITH FLEXSTAB C-5A VEHICLE DATA

Two of the contract objectives were 1) to check out KONPACT by repeating the past Honeywell design work (Reference 4) using the FLEXSTAB generated C-5A vehicle data and 2) to compare and correlate the resulting FLEXSTAB controller to a Reference 4 ALDCS.

Modeling Procedures

The Air Force supplied C-5A data for the cruise flight condition in the form of cards (simulator data deck). The FLEXSTAB simulator data were converted to state format and augmented by the wind and wind distribution states, actuators, and controller dynamics as shown in Figure 9. Subsequently, the augmented data were scaled and shuffled to correspond with Honeywell/ GELAC data.

Controller Design

After having obtained agreement between the two sets of data, a full state design was obtained using the weights of Reference 4 and the DIAK program in KONPACT software.

Subsequently, the gains on the measured variables were retained and other gains were reduced to zero using the FFOC program in KONPACT software.
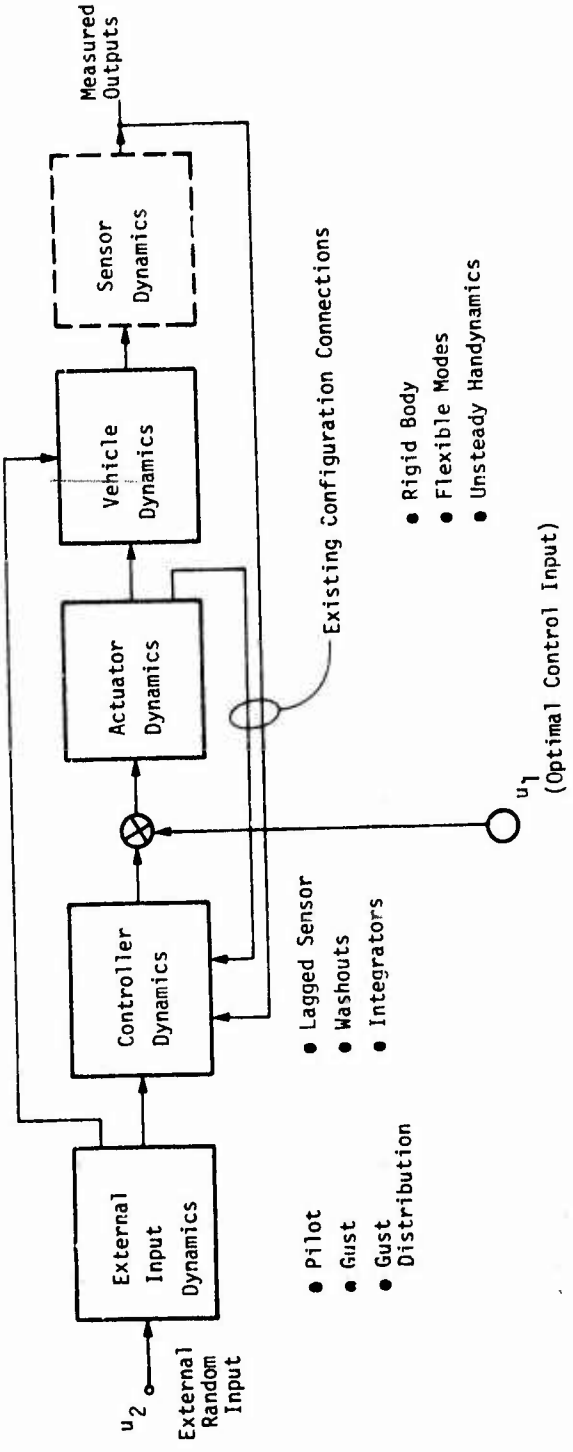
Figure 9. General Overall System Block Diagram

25

Finally the pilot gain the reduced control law was adjusted to maintain the same stick gradient per g as that of SAS. The closed-loop model was produced using KONPACT software with the final ALDCS controller to evaluate several performances.

Time history plots were made using DIAK. Power spectral density plots were made using the FLEXSTAB/LSA program. These results are presented in detail in Section V.

This repeat design process thoroughly checked out the total KONPACT system with respect to communication with its internal programs as well as with the FLEXSTAB/LSA program system.

Coordinate Systems

The FLEXSTAB rigid body dynamics are described in the body fixed axis system. The origin of this system is at the aircraft's c.g. and moves with the c.g. along the flight path. (See Reference 2 for additional details.)

Bending moments and torsional moments are described at the five wing station local coordinate systems shown in Figure 4. The polarity, orientation, and location of these load axis systems are equivalent to the Honeywell/GELAC data with one exception: the FLEXSTAB inboard (w.s. = 120 in) system is rotated 18.6° right wing tip forward. Due to the late discovery of this fact, all design performed with the FLEXSTAB model includes this discrepancy.

SECTION III

DYNAMIC MODELING FOR OPTIMAL
CONTROLLER DESIGN

In this section we briefly present procedures on the automatic modeling
of interconnected dynamic systems for optimal control synthesis and
analysis. State variable form is selected to characterize the dynamic
elements of a system. This is necessary for optimal control synthesis.
Also a uniformity in the model form (irrespective of the size or the internal
structure of subsystems) facilitates the analysis during the evaluation of
various performance measures.

In the state space representation a dynamic model is characterized by
four matrices (A, B, C, D) for the continuous model and (F, G, H, E) for the
discrete model. These four matrices are referred to as a system quadruple.
First we present an approach to develop a system quadruple from the
physical equations describing the dynamics of a system. Converting the
FLEXSTAB/LSA simulator data matrices to quadruple format is treated
here. This is followed by an approach for modeling with transfer function
inputs. This facilitates the augmentation of vehicle dynamics with the
actuator, filtered measurements, and controller dynamics. Subsequently
modeling of transport delays in the vehicle aerodynamics is treated using
the Pade' approximation and developing the corresponding quadruple.
This is followed by the overall system modeling using the dynamic blocks
and the interconnections between them. The response rate modeling is
treated next. Successful optimal control synthesis requires careful

construction of design responses to force the desired performance. The desired performance in general contain responses and response rates.

Finally we present briefly the conditioning of a model for optimal control design. Model conditioning includes reduction, shuffling, and scaling operations. Model reduction can be achieved in several ways. Here we present only the residualization and truncation procedures.

Reordering of states is called shuffling. This operation is needed to bring two different model variables into a common base for comparison as well as to reduce the system order. The scaling operation also facilitates the data comparison and overall system modeling by bringing subsystem units into a common base.

DEVELOPMENT OF THE LINEAR SYSTEM MATRICES
FROM THE SIMULATION EQUATIONS

In general, the simulation equations of the system take the following form:

$$\dot{x} = f(\dot{x}, y, x, u) \tag{1}$$

$$y = g(\dot{x}, y, x, u) \tag{2}$$

$$r = h(\dot{x}, y, x, u) \tag{3}$$

where

$x = n_x \times 1$ vector of the output of integrators

$y = n_y \times 1$ vector of the output of summing points

$r = n_r \times 1$ vector of the system variables of interest (response outputs)

$u = n_u \times 1$ vector of the external inputs

The functions f, g and h are usually nonlinear. For the linear analysis they can be linearized about a given operating point. In the following, we shall assume that the simulation equations represent the linearized model. In this case, Equations (1), (2) and (3) can be put in the following form:

$$\dot{x} = F_{\dot{x}} \dot{x} + F_y y + F_x x + F_u u \tag{4}$$

$$y = G_{\dot{x}} \dot{x} + G_y y + G_x x + G_u u \tag{5}$$

$$r = H_{\dot{x}} \dot{x} + H_y y + H_x x + H_u u \tag{6}$$

and this set of equations can be reduced to the following standard form by algebraic operations

$$\dot{x} = Ax + Bu \tag{7}$$

$$r = Cx + Du \tag{8}$$

On the surface, this task appears to be very simple to carry out with paper and pencil. However, for large systems the writing of simulation equations in the format given in Equations (4), (5), and (6) is prone to human error and should be avoided.

In the following, we present an algorithm which automates the transition from the physical equations (analog simulation equations) to the state variable representation given by Equations (7) and (8).

Let us define two vectors as follows.

$$v = \text{col}\,(\dot{x},\ y,\ r) \tag{9}$$

$$w = \text{col}\,(\dot{x},\ y,\ x,\ u) \tag{10}$$

Obviously, Equations (4), (5) and (6) can be written as

$$v = F(w) \tag{11}$$

The matrix coefficients given in Equations (4), (5) and (6) are then obtained by first finding

$$\left(\frac{\partial F}{\partial w} \right)$$

and then properly partitioning it. This term $\dfrac{\partial F}{\partial w}$ is called the simulation matrix. The sizes of its rows and columns are given respectively by

$$n = n_x + n_y + n_r \tag{12}$$

$$m = 2n_x + n_y + n_u \tag{13}$$

The coefficient matrices obtained by partitioning the simulation matrix is indicated in Figure 10.
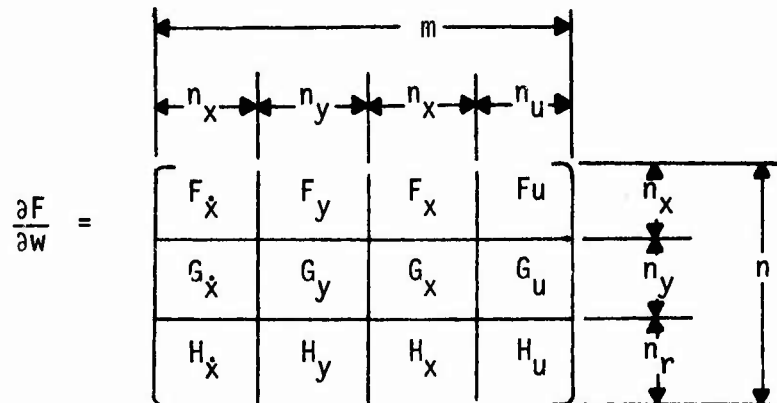
Figure 10. The Simulation Matrix

30

The column vectors $\dfrac{\partial F}{\partial w_i}$ $i = 1, 2, \ldots , m$ are obtained simply by setting

$$w_i = 1$$
$$w_j = 0, \ j = 1, 2, \ldots , m, \ j \neq i \tag{14}$$

and evaluating (11). This yields the coefficient matrices.

In the sequel, the algebraic reduction process will be described. First, Equations (4) and (5) are written in the following form:

$$\left[\begin{array}{c|c} (I - F_{\dot{x}}) & -F_y \\ \hline -G_{\dot{x}} & (I - G_y) \end{array} \right] \begin{pmatrix} \dot{x} \\ y \end{pmatrix} = \left[\begin{array}{c|c} F_x & F_u \\ \hline G_x & G_u \end{array} \right] \begin{pmatrix} x \\ u \end{pmatrix} \tag{15}$$

Then $\begin{pmatrix} \dot{x} \\ y \end{pmatrix}$ is obtained in terms of x and u by solving Equation (15).

Then r is obtained in terms of x and u by substituting (15) into (16):

$$r = (H_x \mid H_y) \begin{bmatrix} \dot{x} \\ y \end{bmatrix} + (H_x \mid H_u) \begin{bmatrix} x \\ u \end{bmatrix} \tag{16}$$

The subroutine which implements this algorithm is called STAMK.

Implementation of the Simulation Equations

The physical (simulation) equations describing the system dynamics (Equations (4), (5) and (6)) are implemented in subroutines SIMK1 and SIMK2.

The physical equations describing the vehicle dynamics in the FLEXSTAB system (Reference 2) are shown in Volume III, Figure 9 (Reference 51). These equations are implemented in subroutine SIMK1. The coefficient matrices are read from the simulator interface deck in the beginning of the above subroutine.

MODELING WITH TRANSFER FUNCTION INPUT

In the following we present an approach to carry out system modeling by software with transfer function input. The approach consists of two parts: 1) obtaining the corresponding quadruple for each transfer function block, and 2) combining the blocks using the connection equations and obtaining the system quadruple. In the following we discuss each in that order.

Consider a system characterized by its output/input relation:

$$\frac{R(s)}{U(s)} = H(s) = \frac{b_n s^n + b_{n-1} s^{n-1} + \ldots + b_1 s + b_o}{a_n s^n + a_{n-1} s^{n-1} + \ldots + a_1 s + a_o} \quad , \quad a_n \neq 0 \qquad (17)$$

There are many ways of realizing this transfer function. (See Reference 31 for major realization forms.) In the following we shall develop input Frobenius form realization and obtain corresponding quadruple in parametric form for software implementation.

The long division of Equation (17) yields

$$H(s) = \frac{b_n}{a_n} + \frac{\left[b_{n-1} - \left(\frac{b_n}{a_n}\right) a_{n-1}\right] s^{n-1} + \ldots + \left[b_o - \left(\frac{b_n}{a_n}\right) a_o\right]}{a_n s^n + a_{n-1} s^{n-1} + \ldots + a_1 s + a_o} \quad (18)$$

This can be written as

$$H(s) = \left(\frac{b_n}{a_n}\right) + \left(\frac{1}{a_n}\right) \frac{\left[b_{n-1} - \left(\frac{b_n}{a_n}\right) a_{n-1}\right] s^{n-1} + \ldots + \left[b_o - \left(\frac{b_n}{a_n}\right) a_o\right]}{\left[s_n + \left(\frac{a_{n-1}}{a_n}\right) s^{n-1} + \ldots + \left(\frac{a_o}{a_n}\right)\right]} \quad (19)$$

Figure 11 shows the state diagram corresponding to Equation (19)   The
corresponding quadruple (A, B, C, D) is directly obtained from the state
diagram and is presented on the following page.

$$A = \begin{bmatrix} 0 & 1 & & & \\ & & & 1 & \\ & & & 0 & 1 \\ -\frac{a_o}{a_n} & -\frac{a_1}{a_n} & \ldots\ldots & -\frac{a_{n-2}}{a_n} & -\frac{a_{n-1}}{a_n} \end{bmatrix} \quad (20)$$

$$B = \text{col} \begin{bmatrix} 0 & 0 & \ldots\ldots\ldots\ldots & \frac{1}{a_n} \end{bmatrix}$$
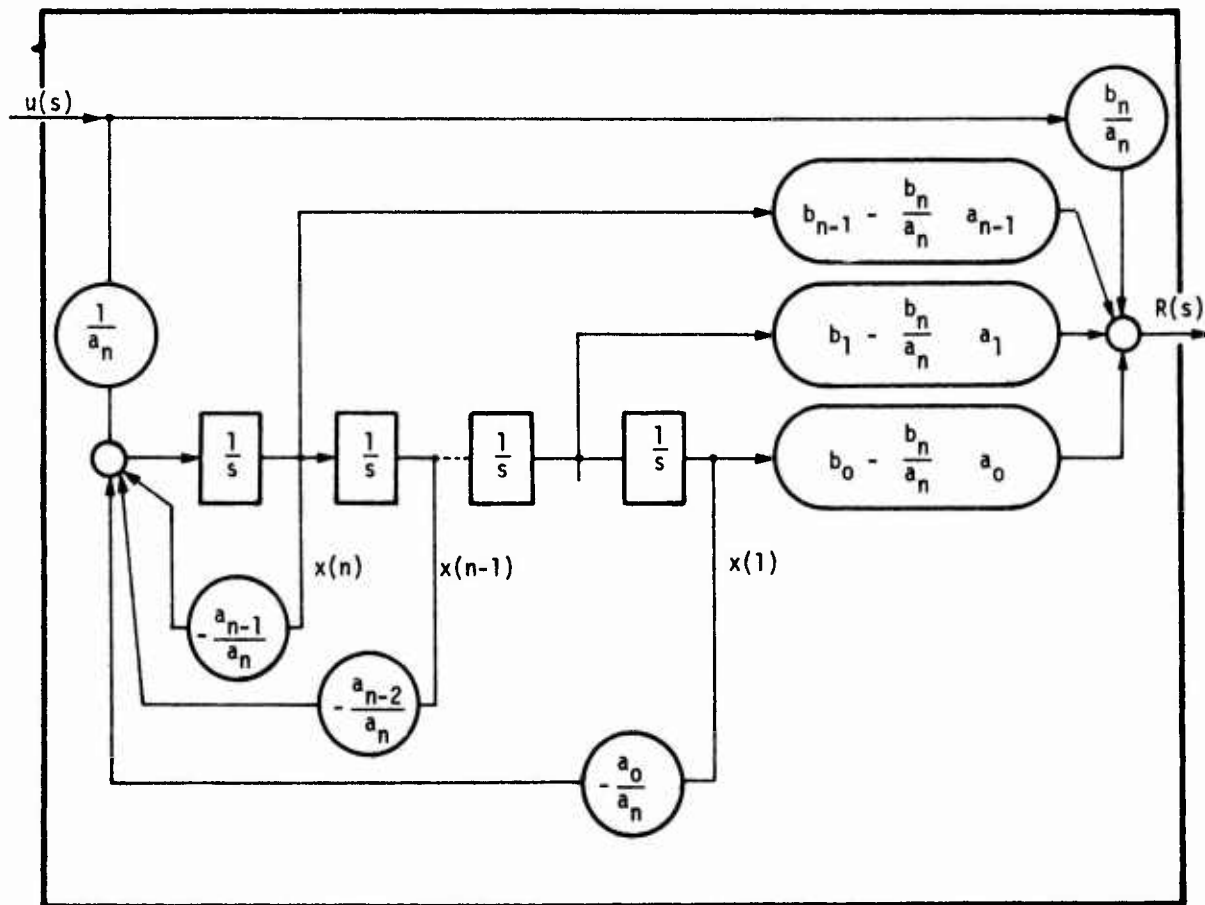
Figure 11. Input Frobenius Form State Diagram of a Single Input, Single Output Transfer Function

$$C = \left[b_0 - \left(\frac{b_n}{a_n}\right) a_0 \;\middle|\; b_1 - \left(\frac{b_n}{a_n}\right) a_1 \;\middle|\; -- \;\middle|\; b_{n-1} - \left(\frac{b_n}{a_n}\right) a_{n-1} \right]$$

$$D = \frac{b_n}{a_n}$$

The transfer function coefficients in Equation (17) form a 2 x n array as indicated below.

$$H(s) = \begin{bmatrix} b_n & | & b_{n-1} \\ \hline a_n & | & a_{n-1} \end{bmatrix} \quad \cdots \cdots \quad \begin{bmatrix} b_1 & | & b_o \\ \hline a_1 & | & a_o \end{bmatrix} \tag{21}$$

Equations (20) and (21) form an algorithm for obtaining the quadruple of an nth order transfer function. Subroutine TRANSK implements this algorithm.

To develop the system quadruple, one must combine the block quadruples obtained as described above using the connection relations. To demonstrate the approach taken, consider a block diagram of a system containing three transfer function blocks as shown in Figure 12.
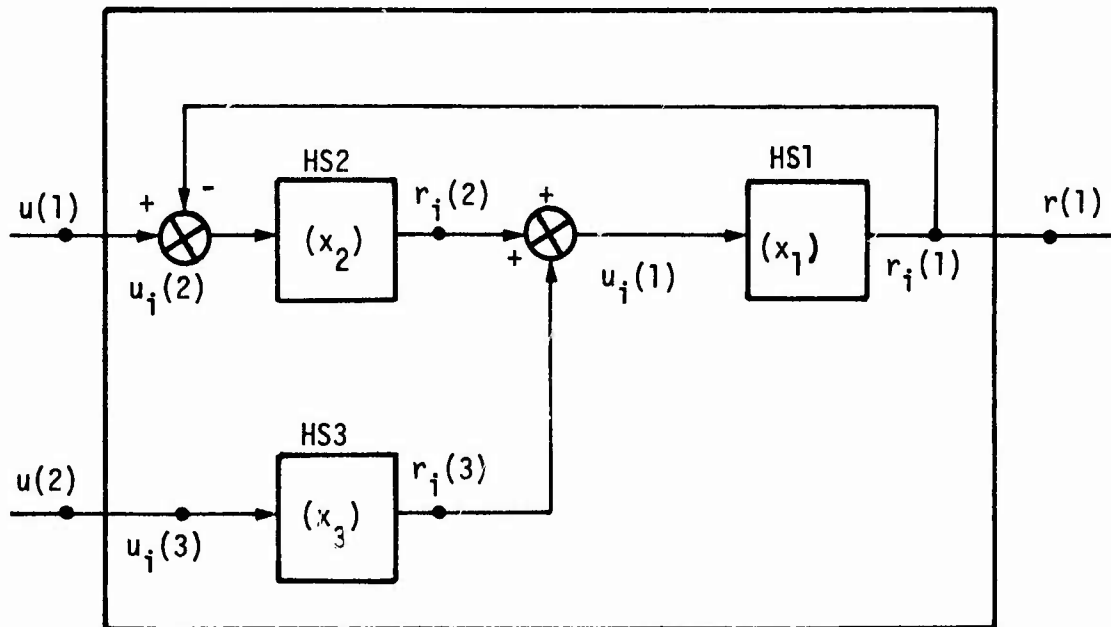
Figure 12. Block Diagram of a System Containing Three
Transfer Function Blocks

Each block is identified by four quantities: 1) a block number, 2) HS array representing the transfer function data, 3) state number, and 4) output-input pair. We note that the inputs and outputs (i.e., $u(1)$, $u(2)$ and $r(1)$) external to the box are unsubscripted variables, whereas inside the box they are subscripted with i denoting that they are internal variables.

With these definitions the simulation equations corresponding to the system shown in Figure 12 can be written as follows.

$$\left.\begin{aligned}
\dot{x}_1 &= A_1 x_1 + B_1 u_i(1) \\[2mm]
\dot{x}_2 &= A_2 x_2 + B_2 u_i(2) \\[2mm]
\dot{x}_3 &= A_3 x_3 + B_3 u_i(3)
\end{aligned}\right\} \text{Dynamics} \tag{22}$$

where HSi is defined by $(A_i\ B_i\ C_i\ D_i)$.

$$\left.\begin{aligned}
r_i(1) &= C_1 x_1 + D_1 u_i(1) \\[2mm]
r_i(2) &= C_2 x_2 + D_2 u_i(2) \\[2mm]
r_i(3) &= C_3 x_3 + D_3 u_i(3)
\end{aligned}\right\} \text{Internal outputs} \tag{23}$$

$$\left.\begin{aligned}
u_i &= P\, r_i + Qu \qquad\qquad &&\text{Internal inputs} \tag{24} \\[4mm]
r &= R\, r_i + Su &&\text{External output} \tag{25}
\end{aligned}\right.$$

The set of equations given above are implemented in subroutine SIMKT. The quadruple (P, Q, R, S) appearing in Equations (24) and (25) are called the connection quadruple. For the system shown in Figure 12 their values are given below.

$$P = \begin{bmatrix} 0 & 1 & 1 \\ -1 & 0 & 0 \\ 0 & 0 & 0 \end{bmatrix}, \qquad Q = \begin{bmatrix} 0 & 0 \\ 1 & 0 \\ 0 & 1 \end{bmatrix} \tag{26}$$

$$R = (1 \quad 0 \quad 0), \qquad S = (0 \quad 0)$$

The system quadruple is obtained via STAMK as described previously.

MODELING FOR TRANSPORT DELAYS

The transport delays resulting from the gust penetration effect in the development of aerodynamic forces and moments are represented by

$$H(s) = e^{-sT_i} \qquad i = 1, 2, 3 \tag{27}$$

where T_i is the time delay at the ith gust input station. This irrational transfer function in s-plane may be converted to a rational transfer function

$$\tilde{H}_i(s) = \frac{N(s)}{D(s)} \tag{28}$$

in different ways. Here we adopt the Pade' approximation (Reference 30) for this conversion, and Table 5 provides the numerator and denominator polynonial coefficients for a specified degree of these polynomials. The Pade' table is inplemented in subroutine DFN.

Table 5. Padé Table for e^{-x} $(x = Ts)$

T = time in seconds

S = Laplace transform variable

Degree of Numerator Polynomial

Degree of Denominator Polynomial	0	1	2	3
0	$\dfrac{1}{1}$	-	-	-
1	$\dfrac{1}{1+x}$	$\dfrac{1 - x/2}{1 + x/2}$	-	-
2	$\dfrac{1}{1 + x + x^2/2!}$	$\dfrac{1 - 1/3\,x}{1 + 2/3\,x + 1/3\,x^2/2!}$	$\dfrac{1 - 1/2\,x + 1/6\,x^2/2!}{1 + 1/2\,x + 1/6\,x^2/2!}$	
3	$\dfrac{1}{1 + x + x^2/2! + x^3/3!}$	$\dfrac{1 - 1/4\,x}{1 + 3/4\,x + 2/4\,x^2/2! + 1/4\,x^3/3!}$	$\dfrac{1 - 2/5\,x + 1/10\,x^2/2!}{1 + 3/5\,x + 3/10\,x^2/2! + 1/10\,x^3/3!}$	$\dfrac{1 - 1/2\,x + 1/5\,x^2/2! - 1/20\,x^3/3!}{1 + 1/2\,x + 1/5\,x^2/2! + 1/20\,x^3/3!}$
4	$\dfrac{1}{1 + x + x^2/2! + x^3/3! + x^4/4!}$	$\dfrac{1 - 1/5x}{1 + 4/5x + 3/5\,x^2/2! + 2/5\,x^3/3! + 1/5\,x^4/4!}$	$\dfrac{1 - 1/3\,x + 1/15\,x^2/2!}{1 + 2/3\,x + 2/5\,x^2/2! + 1/5\,x^3/3! + 1/15\,x^4/4!}$	$\dfrac{1 - 3/7\,x + 1/7\,x^2/2! - 1/35\,x^3/3!}{1 + 4/7\,x + 2/7\,x^2/2! + 4/35\,x^3/3! + 1/35\,x^4/4!}$

38

OVERALL SYSTEM QUADRUPLE

To develop the overall system quadruple, one must combine the subsystem
quadruple using the interconnection relations. The approach is similar
to the previous case. The main difference in this case is that quadruples
for the subsystem are part of the input data, and each subsystem may
have multiple inputs and outputs. Consider the block diagram of the system
consisting of two subsystems as shown in Figure 13. Each subsystem is
identified by four quantities: 1) system number, 2) quadruple data for the
system, 3) system states, 4) system outputs and inputs. Again the inputs
and outputs of the overall system are unsubscripted variables, whereas
inside the box they are subscripted with i denoting that they are internal
variables.
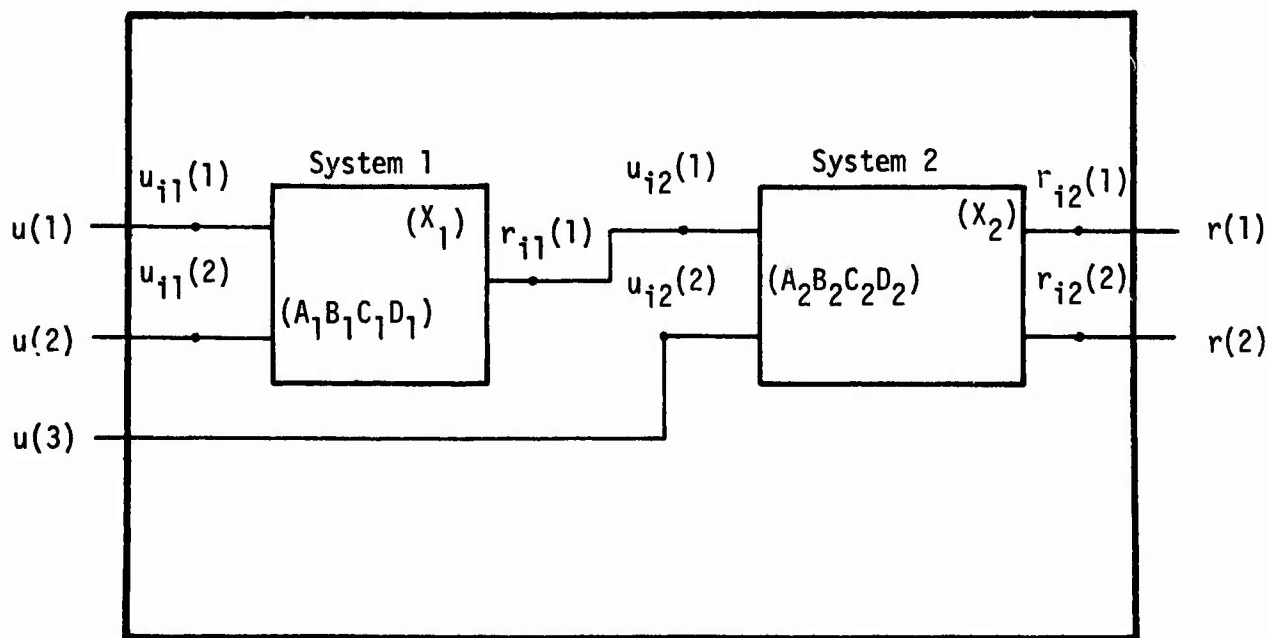
Figure 13. Overall System Block Diagram

The simulation equations corresponding to the system can be written as follows:

$$\left.\begin{array}{l} \dot{x}_1 = A_1 x_1 + B_1 u_{i1} \\[2em] \dot{x}_2 = A_2 x_2 + B_2 u_{i2} \end{array}\right\} \quad \text{Dynamics} \tag{29}$$

$$\left.\begin{array}{l} r_{i1} = C_1 x_1 + D_1 u_{i1} \\[2em] r_{i2} = C_2 x_2 + D_2 u_{i2} \end{array}\right\} \quad \text{Internal Outputs} \tag{30}$$

where System i is defined by quadruple $(A_i B_i C_i D_i)$.

$$\left.\begin{array}{l} u_{i1} = P_{11}\, r_{i1} + P_{12}\, r_{i2} + Q_1 u \\[2em] u_{i2} = P_{12}\, r_{i1} + P_{22}\, r_{i2} + Q_2 u \end{array}\right\} \quad \text{Internal Inputs} \tag{31}$$

$$r = R_1\, r_{i1} + R_2\, r_{i2} + Su \quad \left.\right\} \quad \text{External Output} \tag{32}$$

The above set of equations are implemented in subroutine SIMK. The set of matrices $\{P_{ij},\ Q_i,\ R_j,\ S\}$ are called the interconnection quadruples. The combined system quadruple is obtained via STAMK as before.

40

MODELING FOR RATE RESPONSES

The original system is described by

$$\dot{x} = Ax + Bu \tag{33}$$

$$r = Cx + Du \tag{34}$$

From the response set specification the program computes

$$r_s = C_s x + D_s u \tag{35}$$

Then, Equations (33) and (35) form the description of the new system with specified responses. The elements of C_s and D_s matrices are constructed as shown in Table 6.

As can be seen from this table, unless D_j is a null matrix, the input space should be extended to include $\dot{u}$. When the implicit model error rate response is specified in the response set, the program computes it using the following algorithm.

Implicit Model Following Error Response

In general the description of the original system (33) and (34) contains the implicit model as follows:

$$\begin{bmatrix} \dot{x}_p \\ \dot{x}_m \end{bmatrix} = \begin{bmatrix} A_p & 0 \\ 0 & A_m \end{bmatrix} \begin{bmatrix} x_p \\ x_m \end{bmatrix} + \begin{bmatrix} B_p \\ B_m \end{bmatrix} u \tag{36}$$

Table 6.   Construction of the Response Matrix

Specified Response	Construction of Equation $r_s(i) = C_{si} x + [D_{si} u + \dot{D}_{si} \dot{u}_j]$		
	C_{si}	D_{si}	$\dot{D}_{si}$
$r_s(i) = x(j)$	j^{th} Column $(0 - - - 1 - - 0)$	$(0 - - - 0)$	0
$r_s(i) = \dot{x}(j)$	A_j (j^{th} row of A)	B_j (j^{th} row of B)	0
$r_s(i) = r(j)$	C_j (j^{th} row of C)	D_j (j^{th} row of D)	0
$r_s(i) = \dot{r}(j)$	$C_j A$	$C_j B$	D_j

42

$$
\begin{bmatrix} r_p \\ r_\epsilon \end{bmatrix} = \begin{bmatrix} C_p & 0 \\ C_1 & C_2 \end{bmatrix} \begin{bmatrix} x_p \\ x_m \end{bmatrix} + \begin{bmatrix} D_p \\ 0 \end{bmatrix} u \tag{37}
$$

where x_p is the plant state vector and x_m the implicit model state vector and r_ϵ is the error vector in the responses between plant and implicit model. If the specified response set includes implicit model error rates, we obtain from (36) and (37)

$$
\dot{r}_\epsilon = C_1 A_p x_p + C_2 A_m x_m + (C_1 B_p + C_2 B_m) u \tag{38}
$$

It is assumed that the implicit model following error is small. This yields approximately

$$
r_\epsilon = C_1 x_p + C_2 x_m = 0 \tag{39}
$$

or

$$
x_m = -C_2^{-1} C_1 x_p \tag{40}
$$

Substituting this in (38) we get

$$
\dot{r}_\epsilon = (C_1 A_p - C_2 A_m C_2^{-1} C_1) x_p + (C_1 B_p + C_2 B_m) u \tag{41}
$$

Finally the overall system description with implicit model following error rates is given by

$$
\dot{x}_p = A_p x_p + B_p u \tag{42}
$$

43

$$\begin{bmatrix} r_p \\ \dot{r}_\epsilon \end{bmatrix} = \begin{bmatrix} C_1 \\ C_\epsilon \end{bmatrix} x_p + \begin{bmatrix} D_p \\ D_\epsilon \end{bmatrix} u \qquad (43)$$

where

$$C_\epsilon = (C_1 A_p - C_2 A_m C_2^{-1} C_1) \qquad (44)$$

$$D_\epsilon = (C_1 B_p + C_2 B_m) \qquad (45)$$

If the specified response set does not include implicit model following error rates, then the implicit model states are directly truncated to obtain

$$\dot{x}_p = A_p x_p + B_p u \qquad (46)$$

$$r_p = C_p x_p + D_p u \qquad (47)$$

MODEL CONDITIONING (REDUCTION, SHUFFLING AND SCALING)

Reduction of Order

Reduction of the size of a dynamic equation of a system can be achieved in several ways depending upon the reduction criteria.

In the following we present two approaches for reduction. Table 7 shows these and criteria for reduction.

Table 7. Reduction Criteria (x_2 = collection of states to be reduced)

Reduction Procedure	Criteria for Reduction
Truncation	$x_2 = 0, \; \dot{x}_2 = 0$
Residualization	$x_2 = x_{2ss}, \; \dot{x}_2 = 0$

Now consider the system described by

$$\dot{x} = Ax + Bu \tag{48}$$

$$r = Cx + Du$$

where x and r are the state and response vectors of appropriate sizes. Partition the state vector $x = \text{col}\,(x_1, x_2)$ where x_2 represents the collection of state components to be reduced. Equation (53) can be written as

$$
\begin{bmatrix} \dot{x}_1 \\ \dot{x}_2 \end{bmatrix} =
\begin{bmatrix} A_{11} & A_{12} \\ A_{21} & A_{22} \end{bmatrix}
\begin{bmatrix} x_1 \\ x_2 \end{bmatrix} +
\begin{bmatrix} B_1 \\ B_2 \end{bmatrix} u
$$

$$
r = (C_1 \; C_2) \begin{bmatrix} x_1 \\ x_2 \end{bmatrix} + Du
\tag{49}
$$

The truncated model is obtained by setting $\dot{x}_2 = 0$ and $x_2 = 0$. The reduced system is described by ($\sim$ denotes reduced system variables)

$$\dot{\tilde{x}}_1 = A_{11} \tilde{x}_1 + B_1 u$$

$$\tilde{r} = C_1 \tilde{x}_1 + D u \tag{50}$$

Residualized model is obtained by setting $\dot{x}_2 = 0$ and $x_2 = x_{2ss}$.
This implies

$$0 = A_{21} \tilde{x}_1 + A_{22} \tilde{x}_2 + B_2 u \tag{51}$$

Assuming that A_{22} is a stable matrix we get

$$\tilde{x}_2 = -A_{22}^{-1} (A_{21} \tilde{x}_1 + B_2 u) \tag{52}$$

The substitution of (52) into (49) yields the residualized system model as follows:

$$\dot{\tilde{x}}_1 = (A_{11} - A_{12}A_{22}^{-1} A_{21}) \tilde{x}_1 + (B_1 - A_{12} A_{22}^{-1} B_2)u \tag{53}$$

$$\tilde{r} = (C_1 - C_2 A_{22}^{-1} A_{21}) \tilde{x}_1 + (D - C_2 A_{22}^{-1} B_2) u$$

$$\dot{\tilde{x}}_2 = A_{21} \tilde{x}_1 + A_{22} \tilde{x}_2 + B_2 u$$

The smaller the time constants associated with states x_2 (compared with the time constants associated with states x_1) the closer the agreement is

between the time responses of the residualized system (53) and the original system (49) to step inputs.

Define

$$x = \tilde{x} + \epsilon \tag{54}$$

where x, $\tilde{x}$ and ϵ denote actual state response, approximate state response and error response, respectively.

Using Equations (49) and (53) in (54) one obtains the differential equation of the residualization error as follows

$$\dot{\epsilon}_1 = \tilde{A}_{11}\epsilon_1 + (A_{11} - \tilde{A}_{11}) x_1 + A_{12}x_2 + (B_1 - \tilde{B}_1) u \tag{55}$$

$$\dot{\epsilon}_2 = A_{21}\epsilon_1 + A_{22}\epsilon_2 \tag{56}$$

with the initial conditions $\epsilon_1(0) = 0$, $\epsilon_2(0) \neq 0$.

Equation (55) shows that the residualization error is driven by the input u as well as actual system states x_1 and x_2.

The integral of the square error can be computed by augmenting (55) to (40) and using the Lyapunov equation (Reference 31). The resulting performance number can be used to measure the goodness of the residualization and for selecting variables to be residualized.

The two options of the reduction algorithm presented above are implemented in a subroutine called REDUCE.

Shuffling (Reordering of States)

Denoting the reordered (shuffled) system variables by x_p, u_p and r_p the relation between reordered variables and the original variables is expressed by

$$x_p = P_x x$$

$$u_p = P_u u \tag{57}$$

$$r_p = P_r r$$

where P_x, P_u, and P_r are the shuffling matrices (obtained internally by software from the shuffling data provided by the user).

Substituting (57) into (48) we get

$$\dot{x}_p = A_p x_p + B_p u_p$$

$$r_p = C_p x_s + D_p u_p \tag{58}$$

where

$$A_p = P_x A P_x^{-1}$$

$$B_p = P_x B P_u^{-1}$$

$$C_p = P_r C P_x^{-1} \tag{59}$$

$$D_p = P_r D P_u^{-1}$$

48

Note that the operations described by (59) to obtain A_p, B_p, C_p and D_p are merely row and column operations (i.e., permutations) on A, B, C and D.

The shuffling algorithm is implemented in the subroutines SHUFF, SHUF 1 and SHUF 2 (SHUF 2 shuffles the name list table).

Scaling of States

Denoting the rescaled variables by x_s, u_s and r_s, we have

$$x_s = S_x x$$

$$u_s = S_u u \qquad (60)$$

$$r_s = S_r r$$

where S_x, S_u, and S_r are the scaling matrices (obtained internally by software from the scaling data provided by the user).

As before, the scaled system is described by

$$\dot{x}_s = A_s x_s + B_s u_s$$

$$r_s = C_s x_s + D_s u_s \qquad (61)$$

49

where

$$A_s = S_x A S_x^{-1}$$

$$B_s = S_x B S_u^{-1}$$

$$C_s = S_r C S_x^{-1}$$ (62)

$$D_s = S_r D S_u^{-1}$$

The subroutine which computes the scaled matrices is called SCAL.

SECTION IV

SYSTEM PERFORMANCE MODELING

In this section we briefly review specific performance modeling procedures for the ALDCS design process. First, general performance measures are stated for completeness. Subsequently, the steady-state modeling procedure is described in detail. This is followed by the frequency domain modeling in the form of a system matrix. Finally, the closed loop response modeling is given with output feedback.

GENERAL PERFORMANCE MEASURES

As illustrated in Section II, general performance measures for design and analysis can be listed as:

- Poles and zeros

- Frequency response and phase and gain margins

- rms response to turbulence and random pilot inputs

- Power spectral density and power in a given band

- Time response

Detailed models for the development of these performance measures are given in References 1, 31, and 50. In addition to these, ALDCS design requires the steady-state values of time response with step inputs for prescribed steady-state specification. In the following subsection, we give an approach for this requirement.

STEADY-STATE RESPONSE MODELING

Consider a system described by

$$\dot{x} = Ax + Bu_i \tag{63}$$

$$r_i = Cx + Du_i \tag{64}$$

where x, r_i, and u_i are the state, response, and input vectors of sizes nx, nr, and nu, respectively.

As previously discussed, the maneuver load control calculations involve computation of steady-state control surface deflections for prescribed steady-state responses. For the steady-state response modeling, the input vector u_i in general consists of three parts

$$u_i = \text{col} \{u_o, u_d, u\}$$

where

u_o = set of inputs with prescribed steady-state values,

u_d = set of inputs defined by prescribed interconnections, and

u = set of inputs with unknown steady-state values.

The response vector is also divided into two parts, namely

r_s = a set of specified outputs with prescribed steady-state values r_o

r = total outputs

The input vector u_i and the specified response vector r_s can be represented by the steady-state interconnection quadruple (P_s, Q_s, R_s, S_s) as follows:

$$u_i = P_s r_i + Q_s u \tag{65}$$

$$r_s = R_s r_i + S_s u \tag{66}$$

Figure 14 shows the input/output definition for the steady-state response calculations.
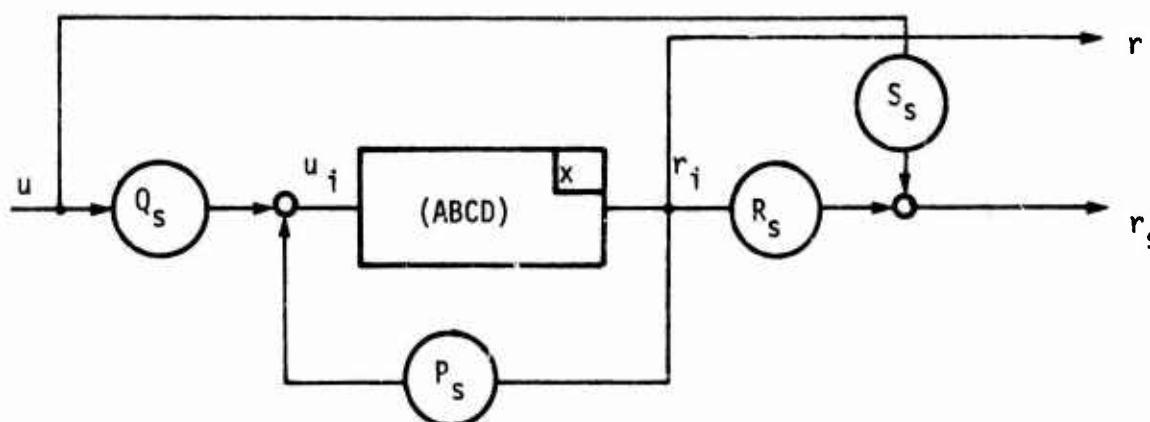
Figure 14. Interconnection Model for Specified Steady-State Inputs and Outputs

The set of equations defining the steady-state system is given by:

$$Ax + Bu_i = 0 \tag{67}$$

$$r_i = Cx + Du_i \tag{68}$$

$$u_i = P_s r_i + Q_s u \tag{69}$$

$$r_s = R_s r_i + S_s u = r_o \tag{70}$$

$$r = r_i \tag{71}$$

53

with the unknowns x, and u. When r_i and u_i are eliminated from the above set as described in Reference 31, we obtain the following set of equations in terms of x and u.

$$\tilde{A}x + \tilde{B}u = 0 \tag{72}$$

$$\tilde{C}x \quad \tilde{D}u = r_o \tag{73}$$

$$r = \hat{C}x + \hat{D}u \tag{74}$$

The solutions of (72) and (73) yield the required steady-state input for the prescribed steady-state output. Equation (74) provides the steady-state value of the total response vector.

In case no response steady-state value is specified and all steady-state inputs are given, Equation (67) is directly solved for x and the total response is computed from (66).

As an example, consider ALDCS design for the C-5A. For the stick per G specification, the outboard elevator deflection is to be computed for 1G maneuver with SAS system and no aileron. The steady-state interconnection diagram for this case is given in Figure 15.
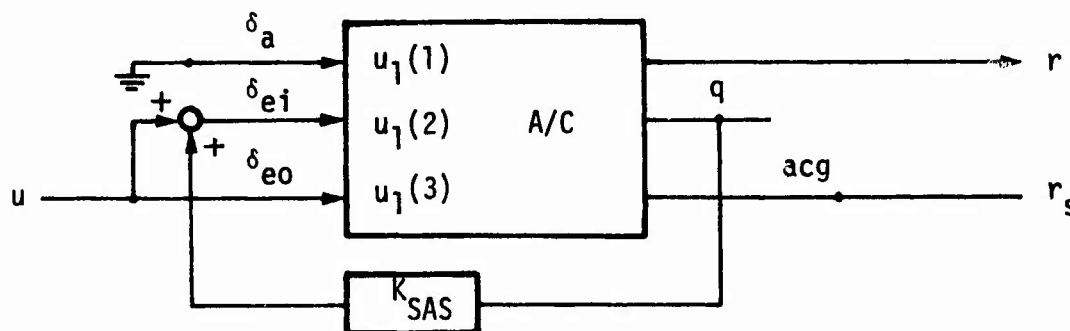
Figure 15. Steady-State Interconnection Diagram

The input and specified response equations are given by:

$$\delta_a = 0$$

$$\delta_{ei} = K_{SAS} \, q + \delta_{eo}$$

(75)

$$\delta_{eo} = u$$

$$a_{cg} = -\frac{q \, u_o}{g}$$

where

q = pitch rate

u_o = forward velocity

g = acceleration due to gravity

Using these equations, the interconnection quadruple is formed and combined system quadruple $(\tilde{A} \; \tilde{B} \; \tilde{C} \; \tilde{D})$ is obtained. Finally (77) and (78) are solved for the required $u = \delta_{eo}$ given the steady-state value $a_{cg} = -1G$. (See Reference 51, Figure 18, for definitions of variables.)

The Honeywell Software which implements this algorithm is called Program SSK. This program is not integrated into KONPACT System due to present scope of this contract.

FREQUENCY DOMAIN MODEL FOR OVERALL SYSTEM

Consider the system described by

$$\dot{x} = Ax + Bu$$

(76)

$$r = Cx + Du$$

(77)

where x, r, and u are the state, response, and input vectors of sizes NX, NR, and NU, respectively. The s-plane (or frequency domain) description of the system in the FLEXSTAB/LSA form is given by

$$\left[C(s) \right] \begin{bmatrix} x \\ r \\ u \end{bmatrix} = 0 \tag{78}$$

where $C(s)$ is called the system matrix (Reference 2). For systems described by quadruple (A, B, C, D), it takes the form of

$$C(s) = C_1 s + C_o \tag{79}$$

The steps to compute C_1 and C_o from the quadruple data (A, B, C, D) are given below:

Taking the s-transform of Equations (76) and (77) we get:

$$(sI - A) x - Bu = 0 \tag{80}$$

$$r - Cx - Du = 0$$

Equations (80) and (81) can be combined and written as follows:

$$\left[\begin{array}{c|c|c} sI - A & 0 & -B \\ \hline -C & I & -D \end{array} \right] \begin{bmatrix} x \\ r \\ u \end{bmatrix} = 0 \tag{82}$$

56

Hence C_1 and C_o are given by:

$$C_1 = \begin{bmatrix} I & 0 & 0 \\ \hline 0 & 0 & 0 \end{bmatrix} \tag{83}$$

$$C_o = \begin{bmatrix} -A & 0 & -B \\ \hline -C & I & -D \end{bmatrix} \tag{84}$$

CLOSED-LOOP MODEL WITH OUTPUT FEEDBACK

Consider the design model of the system described by

$$\dot{x} = Ax + Bu \tag{85}$$

$$r = Cx + Du \tag{86}$$

where x, r, and u are the state, response, and input vectors of sizes NX, NR, and NV, respectively.

The input and output vectors are in the form of

$$u = col \{u_c, \eta\} \tag{87}$$

$$r = col \{r_d, r_m\} \tag{88}$$

where

$$u_c = \text{control input vector}$$

57

η = disturbance input vector

r_d = design response vector

r_m = measurement response vector

Equations (85) and (86) can be written in terms of these subvectors as follows

$$\dot{x} = Ax + B_1 u_c + B_2 \eta \tag{89}$$

$$r_d = C_1 x + D_1 u_c \tag{90}$$

$$r_m = C_2 x \tag{91}$$

The closed-loop equations are obtained by defining the output feedback control as:

$$u_c = u + K r_m \tag{92}$$

Substitution of (92) into (89) and (90) yields

$$\dot{x} = (A + B_1 K C_2) x + B_1 u + B_2 \eta \tag{93}$$

$$r_d = (C_1 + D_1 K C_2) x + D_1 u \tag{94}$$

$$r_m = C_2 x \tag{95}$$

The corresponding closed-loop quadruple is given by

$$\tilde{A} = (A + B_1 K C_2) \tag{96}$$

$$\tilde{B} = B = (B_1 \ B_2) \tag{97}$$

58

$$\widetilde{C} = \begin{bmatrix} \widetilde{C}_1 \\ \hline \widetilde{C}_2 \end{bmatrix} = \begin{bmatrix} (C_1 + D_1 K C_2) \\ \hline C_2 \end{bmatrix} \qquad (98)$$

$$\widetilde{D} = D = \begin{bmatrix} D_1 & \vdots & 0 \\ \hline 0 & \vdots & 0 \end{bmatrix} \qquad (99)$$

SECTION V

ACTIVE CONTROL SYNTHESIS PROCEDURE

INTRODUCTION

This section presents a design procedure for the longitudinal Active Load
Distribution Control System (ALDCS). First, applicable performance
objectives are described in general. Then specific ALDCS design goals
are stated. Subsequently, a controller configuration for the Active Load
Distribution Control System is given. This is followed by a brief descrip-
tion of full state optimal controller design and simplified optimal controller
design. Finally, the ALDCS design results using the FLEXSTAB C-5A
residual elastic math model as documented in References 5 and 6 are presented.

PERFORMANCE OBJECTIVES FOR ACTIVE CONTROL SYNTHESIS

The goal of a Control Configured Vehicle (CCV) design is to improve the
performance of an aircraft using active control. The CCV concepts include
the following areas (Reference 13).

- Improved handling qualities

- Flight envelope limiting

- Reduced static stability

- Gust acceleration reduction

- Maneuver load control

- Active control of structural modes

60

In the following, each area is discussed briefly for the longitudinal active control design. For detailed lateral specifications, see Reference 13. The enforcement of each criteria is achieved by properly weighted response vectors as described later.

Improved Handling Qualities (Handling Quality Control)

The longitudinal axis-handling qualities are specified in various ways. The major ones are $C*$ model response, the short period pole locations, and the Time Response Parameter (TRP).

The lateral directional handling qualities include good roll rate response, improved Dutch roll damping, and good turn coordination over a wide variation in angle-of-attack.

Time Response Parameter (TRP) Criteria--The command performance is specified for a step stick input in terms of normal acceleration at the c.g. and pitch rate. A figure of merit called Time Response Parameter (TRP) (see Reference 15) is defined to measure the command response (Figure 16). The requirement is for a TRP below a specified number.

This criterion is generally applicable to any system order and degree of linearity. It appears to correlate reasonably well with existing specifications, e.g., MIL-F-8785B(ASG), without many of the interpretation problems of the latter. It is amenable to both computerized performance evaluation and pilot response assessment. Furthermore, it deals directly with input/output relationships which are significant to the aircraft function as a weapon system.

Note: (1) Bracket Terms Zero if Negative.
(2) $t_c = \infty$ for No Overshoot.
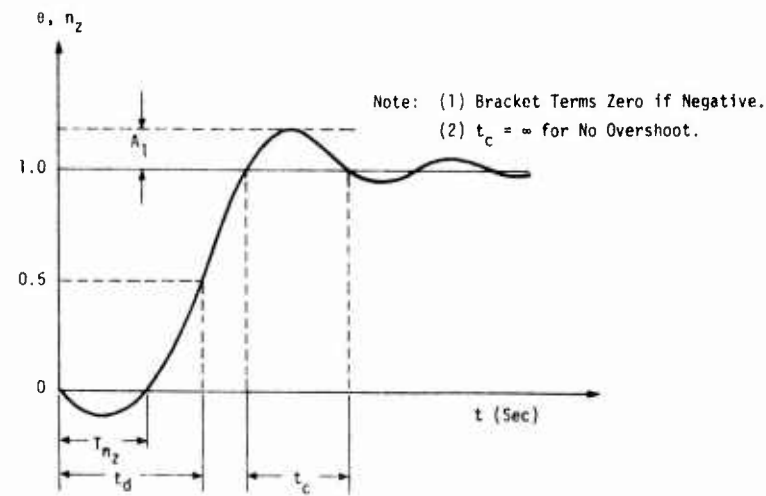
$$TRP = (TRP)_{\dot\theta} + (TRP)_{n_z}$$

$$(TRP)_{\dot\theta} = \left(\frac{t_d}{t_c}\right)_{\dot\theta} + 0.08\,(A_{1_{\dot\theta}} - 1.0)$$

$$(TRP)_{n_z} = 0.5\,(t_{d_{n_z}} - 0.7) + 0.3\,(A_{1_{n_z}} - 0.3) + 0.2\,(T_{n_z} - 0.2)$$

Figure 16. Definition of Time Response Parameter

There are certain difficulties with the TRP in its current form, however, which merit consideration. (See Reference 14.)

C* Criterion--The C* criterion is an example of specifying short period handling qualities in terms of aircraft parameters familiar to a pilot. The concept implicitly includes the traditional short period frequency and damping requirements but is more general in its application. The usual definition for C* is

$$C^* = K_a N_z + K_b \dot\theta + K_c \ddot\theta$$

where K_a, K_b, K_c are dimensional constants. The $\ddot\theta$ term represents the normal acceleration increment at the pilot's location caused by the

moment arm from vehicle center-of-gravity. Therefore, the expression can be written as

$$C^* = N_{z_{Pilot}} + K_{co} = \frac{U_o}{g}$$

where K_{co} = "crossover" velocity. The steady-state perturbation relation between q and N_z is

$$q_{ss} = \frac{N_z}{U_o} \, , \quad U_o = \text{forward velocity}$$

The velocity at which the contribution of pitch rate equals the contribution of N_z to the C^* response is the so-called crossover velocity.

The C^* criterion for flight control has evolved because it allows the designers to control one response with one forcing function (the elevator). At high dynamic pressures the elevator produces primarily normal acceleration, and at low dynamic pressures it produces a composite variable that is significant at all flight conditions. (References 52, 53)

The handling qualities can be summarized as:

- The dominant short period frequency as excited by a sharp-edged gust shall have a minimum damping ratio of 0.3

- For a step pilot input, the time response shall meet the C^* envelope of Figure 17 where the categories are defined as: (Reference 13)

63

I   Optimum response (aerial combat, etc.)

II   Not as critical (refueling, cruise, etc.)

III Categories for conditions not covered by 1, 2, 4

IV   Power approach

For details see References 52 and 53.
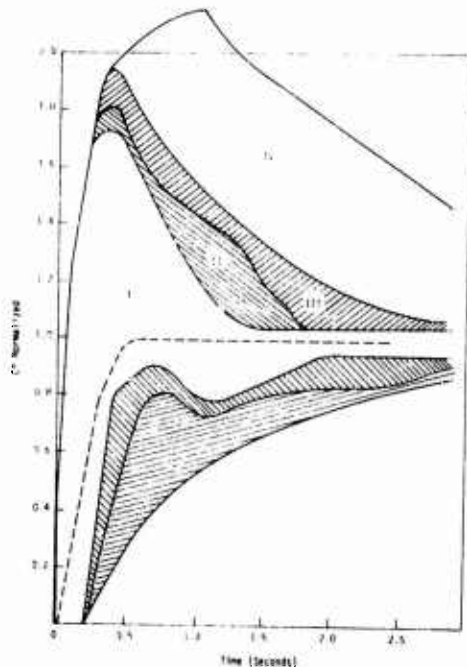
Figure 17. Typical C* Envelope

- The pitch Command Augmentation System (CAS) will produce
  a steady-state short period control stick gradient consistent with
  MIL-F-8785 requirements (Reference 16). A C* feedback
  permits the stick gradient requirements to be met without scheduling
  the stick gain (K_f). This is illustrated in Figure 18 for several
  points representing extremes in the F-8C data (note $\frac{n}{\alpha} \approx -z_\alpha$).
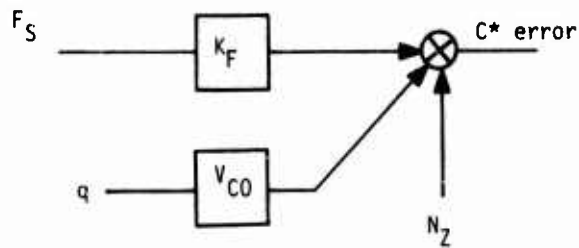
$$\frac{F_S}{N_Z} = - \frac{(1 + \frac{V_{CO}}{V})}{K_F}$$
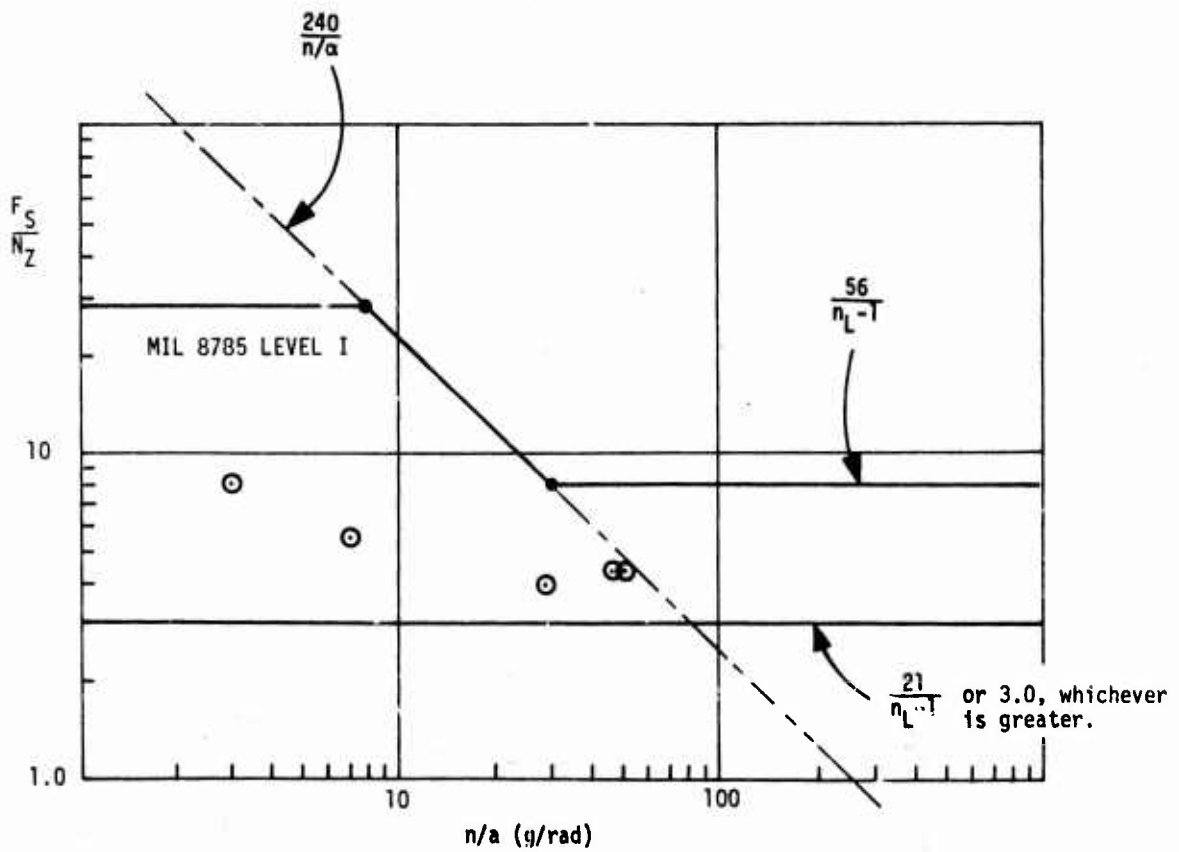
Figure 18. Typical Pitch Stick Gradient

Short Period Pole Locations--In this criteria the natural frequency (ω_n) and the damping factor (ζ) of the short period dynamics are specified. It is the simplest criteria for handling quality specification.

Flight Envelope Limiting (Boundary Control)

The flight envelope limiting controller design involves two steps. First, control laws are defined for limiting certain variables of the aircraft (i. e., α) during maneuvers. Second, a method of transition (i. e., mode switching) between boundary control laws and normal control augmentation system is developed (Reference 13).

Reduced Static Stability (RSS Control)

For a conventionally designed aircraft, static stability and acceptable handling characteristics are obtained through aerodynamic design which includes proper location of the c.g. This is shown in Figure 19.
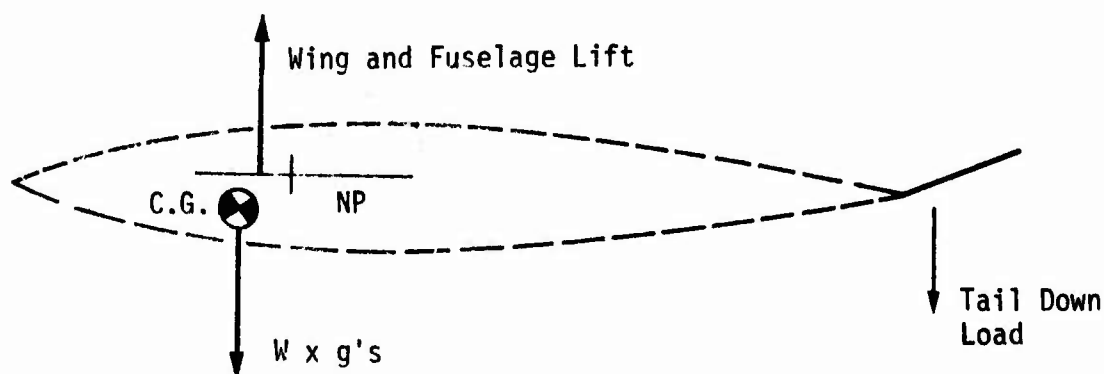
Figure 19. Conventional Static Stability

In maneuvering subsonic flight and in supersonic flight this usually results in significant tail down loads to provide the required moment balance for the aircraft.

If a high authority feedback control system is used to provide artificial stability, then the unaugmented aircraft's longitudinal static stability can be relaxed. This enhances the maneuvering capability of the aircraft by reducing the drag. Figure 20 shows this case.

Wing and Fuselage Lift

NP — C.G.

Tail Up Load

W x g's
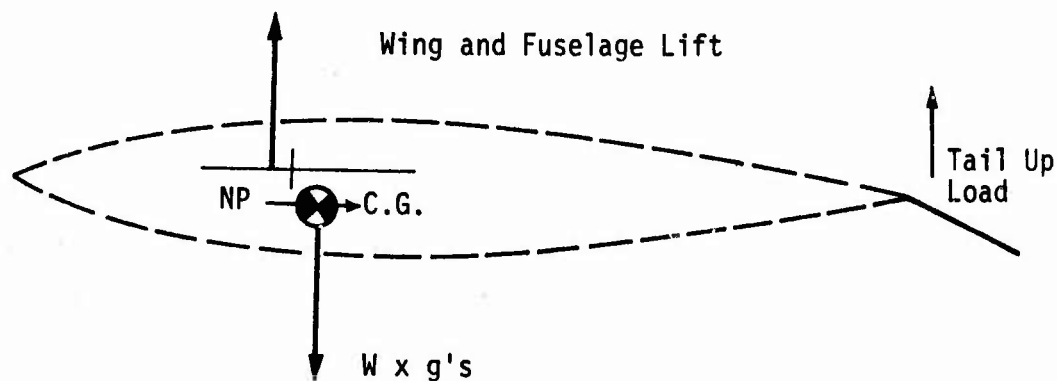
Figure 20. Relaxed Static Stability A/C with Active Control

The reduced static stability controller (M_α augmenter) restores the stability lost in the CCV aircraft due to shifting the c.g. aft. It basically consists of additional pitch rate feedback to the elevator.

67

Gust Acceleration Reduction

Reduction of the aircraft accelerations due to wind gusts without deteriorating the response to pilot commands normally enhances the stability of the aircraft and results in improved mission performance. It also improves the ride qualities for the pilot as well as enhancing his ability to perform precision tracking tasks. It is well-known that the conventional elevator together with direct lift force producers (canards, flaps and symmetric ailerons) can be effective in reducing gust induced accelerations. Combining these control surfaces with the elevator controller to produce direct lift for gust alleviation is an important mode in active control laws.

Maneuver Load Control (Steady-State Load Relief Control)

For transport A/C the reduction of the wing root bending moments during maneuvering flight (i.e., 1 incremental g pitch up) is described to alleviate structural load and fatigue of the wing. This reduction in wing bending is obtained by shifting the wing lift distribution center of pressure inboard as shown in Figure 21.
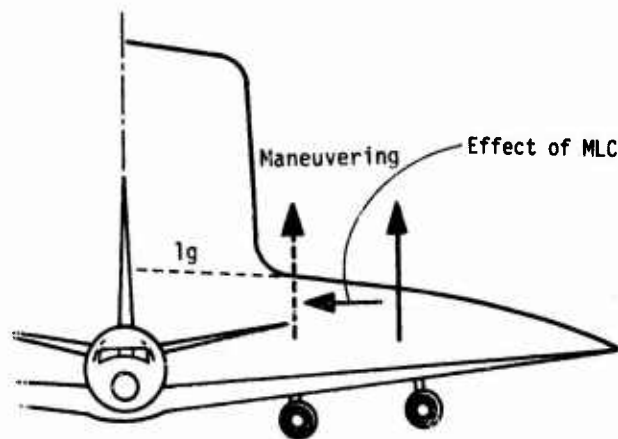
Figure 21. Transport Aircraft Ideal Lift Distribution

A Maneuver Load Control System (MLC) positions control surfaces with steady-state accelerations to redistribute the loading on a wing. For fighter type A/C, the objective is to redistribute the wing loading to reduce drag during high-g maneuvers (Reference 13).

Structural Mode Damping (Flexure Control)

Active control is used to regulate the response of flexure modes to turbulent air or pilot commands for reducing fatigue damage. These can be extended to damping of flexure modes for flutter suppression also.

By placing the sensor and control force producers near one another the sensed aeroelastic forces can effectively be cancelled out by the control surfaces to lower local acceleration (References 18 through 21).

ALDCS DESIGN GOALS - FORMULATIONS AND PROCEDURES

Active Lift Distribution Control System (ALDCS) Design Goals

One of the objectives of this contract was to repeat Honeywell's ALDCS design (Reference 4) using the FLEXSTAB generated C-5A A/C data and KONPACT software. The cruise flight condition was selected for this demonstration as shown in Table 2.

Full State Quadratic Design Formulation

The theory and numerical techniques used in quadratic design are well documented in other sources (References 12, 23, 24, and 25) and therefore

will not be repeated here. We shall be concerned here primarily with formulation of the problem. The system description has the form

$$\dot{x} = Ax + B_1 u + B_2 \eta \tag{100}$$

$$r_1 = C_1 x + D_1 u \tag{101}$$

$$r_2 = C_2 x \tag{102}$$

where

x = state vector (including rigid-body states, actuator and servo states, flexure-mode states, sensor states, model-following states, and wind states)

u = control input vector

η = unit-variance white noise vector

r_1 = design response vector

r_2 = measurement vector (consists of actual and complementary measurements)

We wish to find a time-invariant controller of the form

$$u = K*r_2 = K*C_2 x \tag{103}$$

which minimizes the performance index

$$J = E\{r_1' Q r_1\} = tr[Q R_1] \tag{104}$$

70

where Q is a symmetric weighting matrix, and R_1 is the response covariance matrix given by

$$R_1 = (C_1 + D_1 K*C_2) \ X \ (C_1 + D_1 K*C_2)' \tag{105}$$

and X is state covariance matrix given by the solution to Equation (108).

Figure 22 shows the block diagram of the overall system.
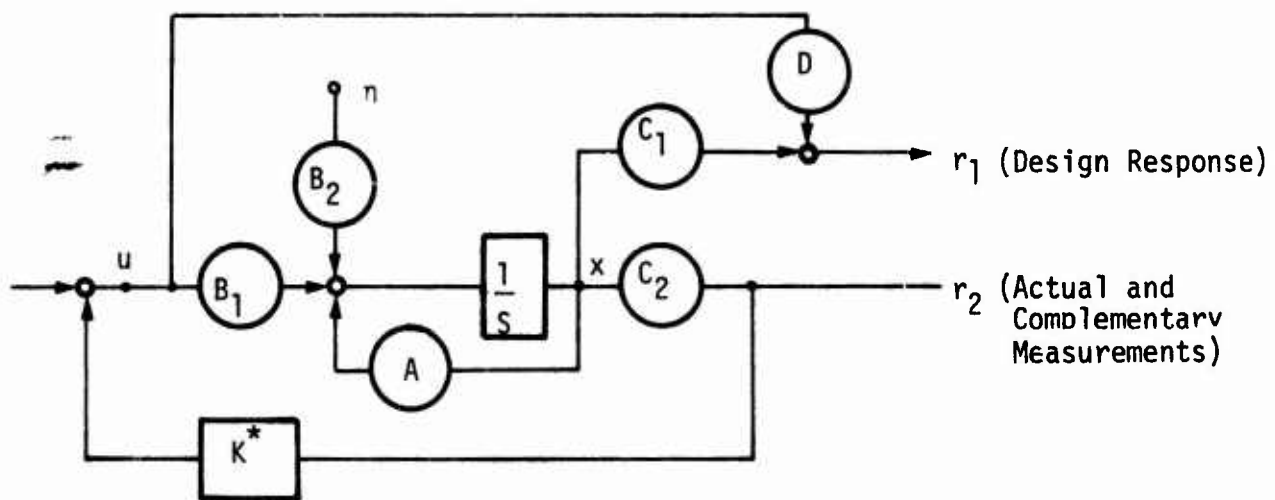
Figure 22. Optimal System Block Diagram

The optimal gain on the full measurements is given by

$$K* = -(D_1' \ QD_1)^{-1} \ (D_1' \ QC_1 + B_1' \ P) \ X \ C_2' \ (C_2 \ X \ C_2')^{-1} \tag{106}$$

71

where P (Riccati matrix) and X (covariance matrix) are determined from

$$(A + B_1 K*C_2)' \, P + P(A + B_1 K*C_2) + (C_1 + D_1 K*C_2)' \, Q(C_1 + D_1 K*C_2) = 0$$

(107)

$$(A + B_1 K*C_2) \, X + X(A + B_1 K*C_2)' + B_2 B_2' = 0$$

(108)

When C_2 is invertible (for full measurement feedback), the solution of
Equation (106)

$$K* = -(D_1' \, Q \, D_1)^{-1} \, (D_1' \, Q \, C_1 + B_1' \, P)C_2^{-1}$$

(109)

and does not depend on the covariance X. For limited-measurement feed-
back, C_2 is not invertible since the number of measurements is generally
fewer than the number of states, so that K* will be a function of both P and X.

Simplified Quadratic Design Formulation

The design procedure described in References 12, 23, and 25 is used
to simplify the full state controller. In this procedure, the measurement
gains are written as a function of a scalar parameter, λ, such that

$$u = K*(\lambda) \, r_2$$

(110)

where

$$K*(\lambda) = K_1(\lambda) + \lambda \, K_2 \qquad 0 \le \lambda \le 1$$

The starting point ($\lambda = 1$) is four d by using the optimal state feedback gains
and the measurement matrix (corresponding to actual measurements

augmented with complementary measurements so that C_2^{-1} exists)

$$K*(1) = KC_2^{-1} \qquad (111)$$

The measurement constraints are applied gradually by stepping λ to zero, thereby reducing gains on the complementary measurements. The matrix $K_1(0)$ is the fixed-form solution and has the gain structure desired.

This procedure of "backing off" from the state feedback controller is illustrated in Figure 23.
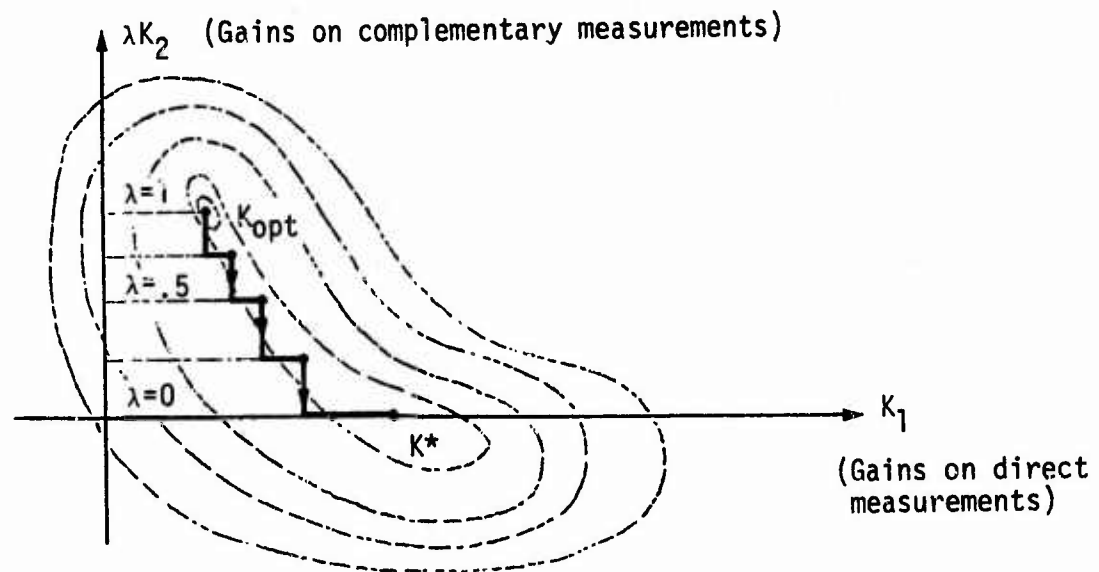
Figure 23. Optimal Control with Measurement Constraint

The same quadratic performance index as of the full state feedback is minimized using the K_1 gains after each stepping down of λ parameter.

Constrained Quadratic Design Formulation

As will be shown later, the maneuver load control requirements generate an equation in the form of

$$x'_{ss} K - \delta_{a_{ss}} = 0 \tag{112}$$

where

x_{ss} = state of the overall system at one incremental g

$\delta_{a_{ss}}$ = required steady-state aileron deflection to reduce bending moment by specified amount

K = aileron feedback gains

This equation generates additional constraints on optimal gains. Dynamically enforcing the related equation will be given later. Figure 24 shows algebraic forcing with two gains.
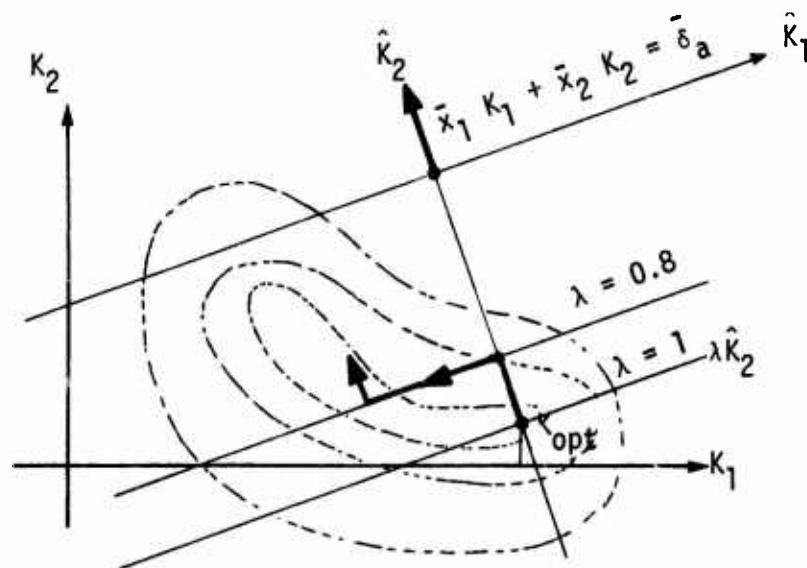
Figure 24. Optimal Control with Gain Constraints

This problem can be handled the same way by performing a transformation in the gain space and stepping down of λ parameter on $\hat{K}_2$ and optimizing with $\hat{K}_1$.

Response Selection Procedure

Quadratic design formulation shows that design problem is essentially reduced to defining proper responses (response selection) for the cost function and finding proper weights (weights selection) for the performance achievement.

These two steps require design experience and insight to the physics of the problem as well as familiarity with the synthesis software.

Response selection for design depends on the design criteria to be enforced. Converting a set of design criteria into a minimization of a set of responses is one of the fundamental steps in optimal control synthesis.

In the following, we will discuss typical cases briefly to demonstrate the mechanics of the response selection.

Response Selection for Enforcing Handling Quality Criteria--The C-5A aircraft is augmented with a simple Stability Augmentation System (SAS) to enhance the handling qualities of the aircraft. It consists of pitch rate feedback to the inboard elevator input in the form of

$$\delta_{eic} = K_{SAS}q \tag{113}$$

One way of incorporating the effect of this SAS into optimal handling quality controller design with an aileron input is to define the inboard elevator residual response (deviation from ideal) using (113).

$$r = (K_{SAS}q - \delta_{eic})$$ (114)

Thus by varying the weights on r, the short period roots can be indirectly controlled.

Implicit Model Following

When handling quality criteria specifies the desired short period locations, as in C-5A case, the model following error rate response may be generated to enforce the specified pole locations in the following way.

The rigid body (RB) and model M equations are given by

$$\dot{x}_{RB} = A_{RB} x_{RB} + B\delta_e$$ (115)

$$\dot{x}_M = A_M x_M + B\delta_e$$ (116)

The rate of residual is defined as

$$\dot{r} = \frac{d}{dt} [x_{RB} - x_M]$$ (117)

and given by

$$\dot{r} = A_{RB} x_{RB} - A_M x_M$$ (118)

Assuming that rigid body and model states are close together

$$x_M \approx x_{RB}$$ (119)

76

yields

$$\dot{r} = (A_{RB} - A_M)\, x_{RB} \tag{120}$$

Let ω_M and ζ_M be the natural frequency and damping factor of the model short period modes. The corresponding characteristic equations are given as

$$s^2 + (2\zeta_M\,\omega_M)\, s + \omega_M^2 = 0 \tag{121}$$

In terms of the model transition matrix

$$s^2 + (\text{tr } A_M)\, s + \det A_M = 0 \tag{122}$$

Equations (121) and (122) provide two equations to determine the elements of model transition matrix A_M. If we assume that the $\dot{w}$ equations for model and vehicle are identical, then the remaining elements of A_M can be found from (121) and (122). Equation (120) is the response equation to force the desired pole locations, with the coefficient matrix as computed above.

If symmetric ailerons are used together with the inboard elevators for Manevuer Load Control (MLC) and Gust Load Alleviation (GLA), then handling quality can be enforced in the following way.

Figure 25 shows the block diagram of the rigid body part of the flexible vehicle dynamics and corresponding handling quality model which generates existing SAS pitch responses (w_M, q_M).

77
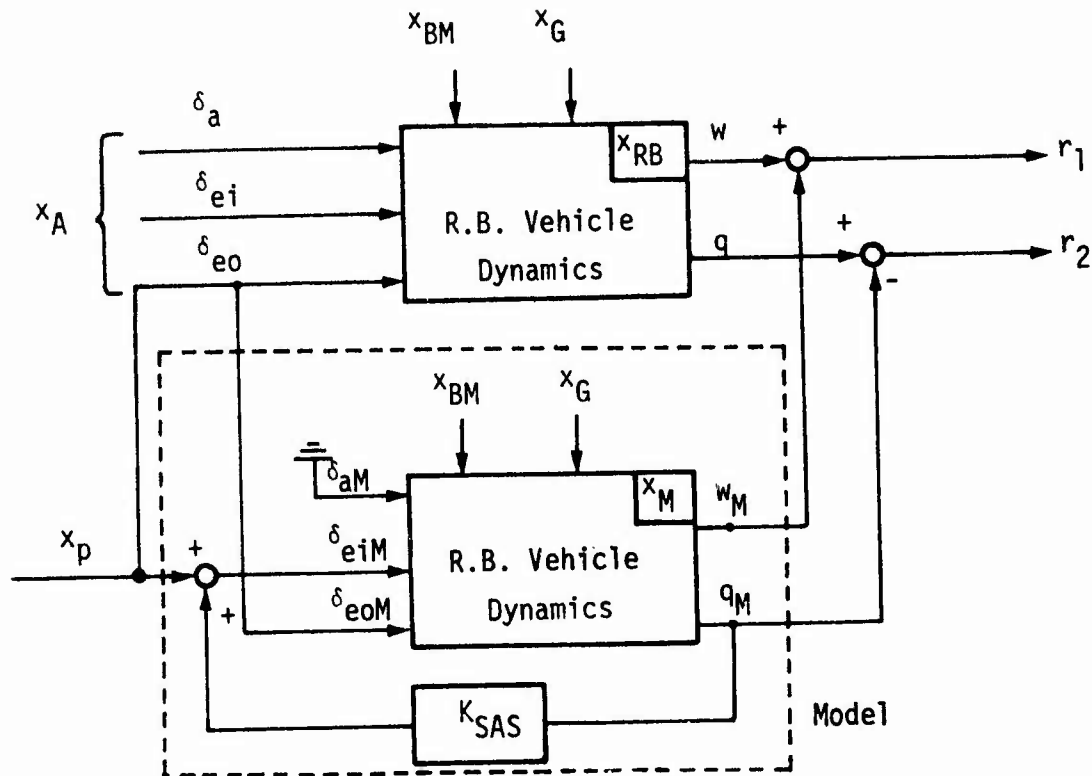
Figure 25. Response Generation to Enforce Handling Quality Criteria

The rigid body part of the flexible vehicle equations are in the form of:

$$\dot{x}_{RB} = A_{11} x_{RB} + A_{12} x_{BM} + A_{13} x_A + A_{14} x_G \tag{123}$$

where

x_{RB} = Rigid body states

x_{BM} = Bending mode states

x_A = Control surface states

x_G = Gust states

x_p = Pilot states

78

Handling quality open-loop model is in the same form of rigid body equations and given by

$$\dot{x}_M = A_{11} x_M + A_{12} x_{BM} + A_{13} x_{AM} + A_{14} x_G \tag{124}$$

where

x_M = model states

x_{AM} = model control surface states

Here the model control surface states are specified as

$$\begin{bmatrix} \delta_{aM} \\ \delta_{eiM} \\ \delta_{eoM} \end{bmatrix} = \begin{bmatrix} 0 \\ K_{SAS} q_M + x_p \\ \delta_{eo} \end{bmatrix} \tag{125}$$

This assumes that the SAS aircraft is the ideal model. The residual response rate on the rigid body state is defined as

$$\dot{r}_{RB} = \dot{x}_{RB} - \dot{x}_M \tag{126}$$

Substituting (123) and (124) into (126) yields

$$\dot{r}_{RB} = A_{11}(x_{RB} - x_M) + A_{13}(x_A - x_{AM}) \tag{127}$$

Assuming that

$$x_{RB} \approx x_M \tag{128}$$

79

Equation (127) yields the residual response rates in terms of the linear combination of states and the system coefficients

$$
\dot{r}_{RB} = \begin{bmatrix} \dot{\epsilon}_w \\ \\ \dot{\epsilon}_q \end{bmatrix} = \begin{bmatrix} Z_{\delta_a} & Z_{\delta_{ei}} & Z_{\delta_{eo}} \\ \\ M_{\delta_a} & M_{\delta_{ei}} & M_{\delta_{eo}} \end{bmatrix} \begin{bmatrix} \delta_a \\ \\ \delta_{ei} - K_{SAS}q - x_p \\ \\ 0 \end{bmatrix} \tag{129}
$$

Thus by varying the weights on $\dot{r}_{RB}$, the handling quality is enforced in optimal ALDCS design.

Explicit Model Following

In the preceding analysis, the response equations contain only the original system states. The model states are discarded using the rates of the residuals and the assumption that model and system states are approximately the same. This technique is known as the implicit model following. It has the benefit of not increasing the system order and not yielding high gains in the controller design.

In the following, we present for completeness another form of response development to enforce handling qualities which is known as explicit model following.

Figure 26 shows handling quality controller which produced improved short period response with an explicit model (Reference 13). The integrator in the controller enforces the following equation in the steady-state

$$
\epsilon = y_M - y = 0
$$

80

81
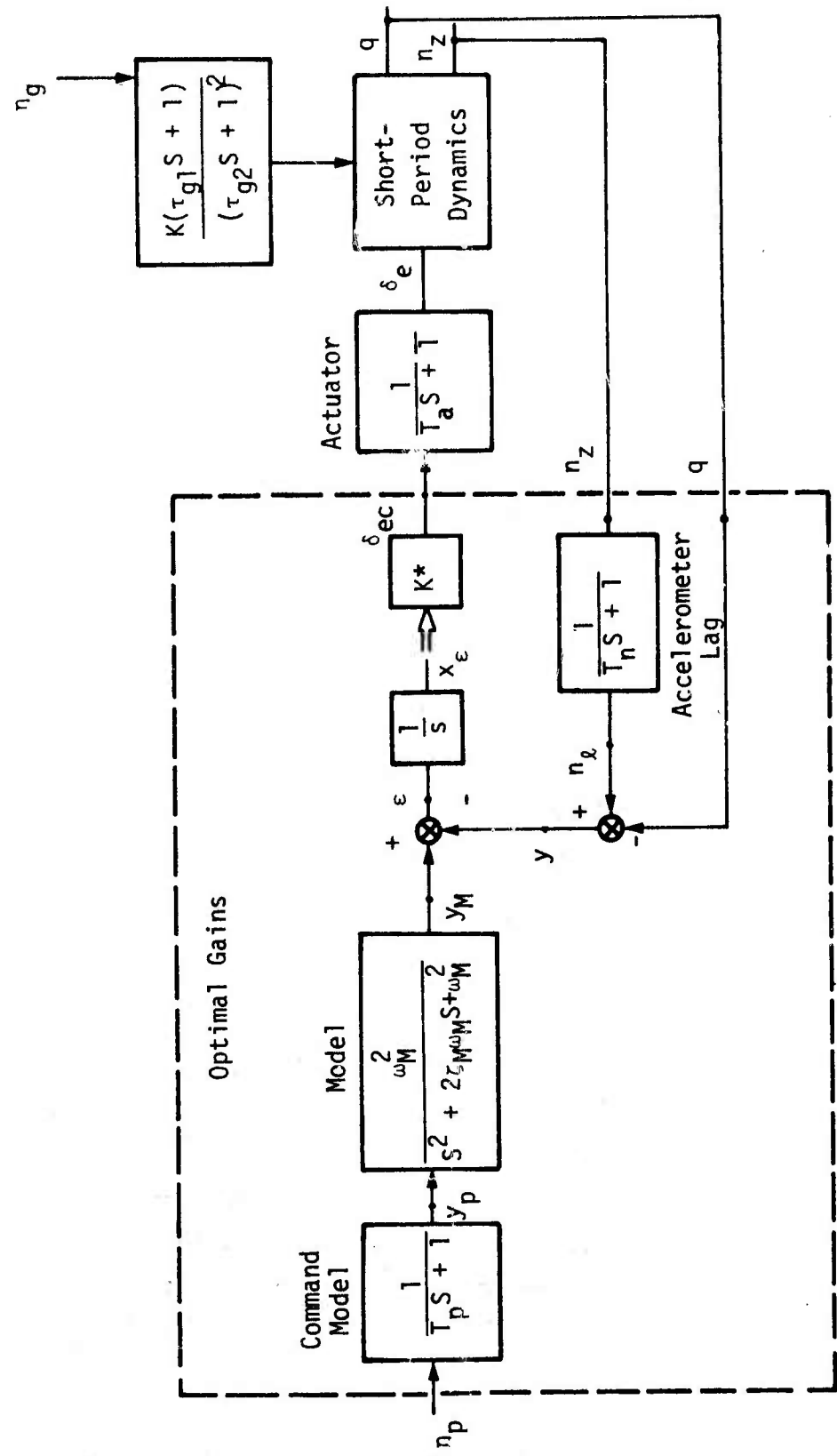
where

y_M = Model response to command

y = Blended pitch rate and lagged normal acceleration

The design response to enforce the desired handling quality is in the form of:

$$r = \text{col} \, (\epsilon, \, x_\epsilon, \, \dot{\delta}_e)$$

which contains the model following error and its integral. It also contains actuator rate response to limit the bandwidth of the actuator due to feedback.

Figure 27 shows the general structure of controller with explicit model (Reference 23). The actual model in the control law to generate model response x_M increases the dynamical order of the controller and generally yields higher gain values as compared to controller with implicit model.
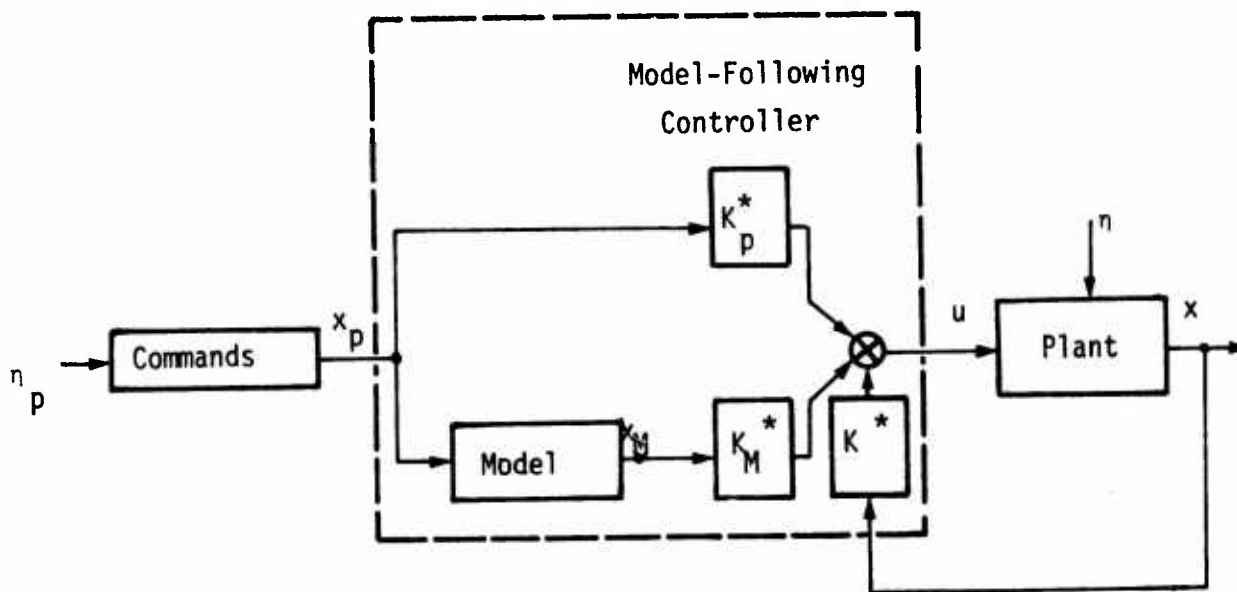
Figure 27. Explicit Model-Following Structure

82

The control law is in the form of

$$u = K^*_x x + K^*_M x_M + K^*_p x_p$$

where

x = plant state including vehicle, actuator, sensor and gust filters

x_M = model states

x_p = pilot input states

Response Selection to Enforce Maneuver Load Control--Maneuver load control involves computing bending moment response of free A/C for 1G normal acceleration pitching maneuver at the level flight and determining control surface positions to reduce the bending moment as specified by the specification (see Figure 28).

The normal acceleration is given by

$$a_{cg} = \dot{w} - U_o q \qquad (132)$$

where U_o is the cruise speed and $\dot{w}$ = o for level flight.
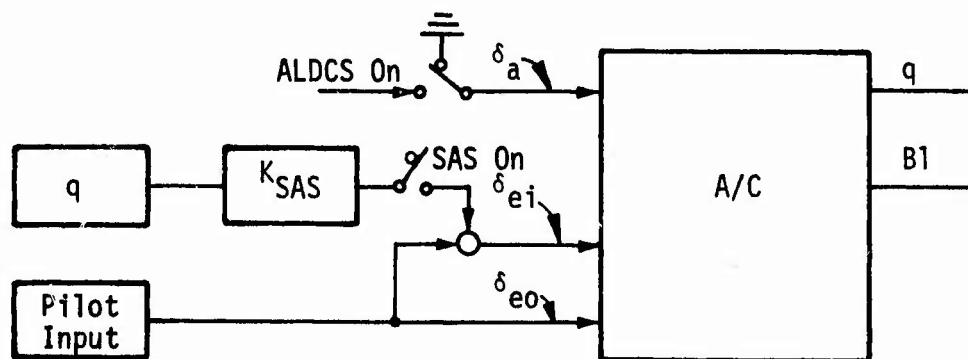
Figure 28. Maneuver Load Control Surface Position Calculation

First pilot stick input to free A/C as shown in Figure 28 is calculated to produce a steady-state pitch rate corresponding to 1G normal acceleration. The value of the specified-bending moment is obtained at this maneuver.

Subsequently, the pilot input for 1G maneuver with SAS'd A/C is calculated to enforce the stick/g requirement. This determines the steady-state deflection for the outboard elevator δ_{eo}. Now the aileron and inboard elevator deflections are computed to obtain 1G maneuver and reduced bending moment response, with the fixed value of δ_{eo}.

After having determined the steady-state surface positions, the next task is to enforce these positions by properly selected controller configuration.

Maneuver load control can be enforced either by integral control or by a high-passed aileron control. The integral control enforces the following aileron deflection equation at steady-state.

$$K_{SS} n_a - \delta_{a_{SS}} = 0 \tag{133}$$

Figure 29 shows the MLC configuration with integral control.

The integral control has one obvious drawback - it may require a sensor to measure aileron position (Reference 8). High passed aileron control, as shown in Figure 30, washes out all steady-state aileron commands except for MLC.

CONTROLLER CONFIGURATIONS

Handling quality controller with explicit model and state feedback corresponding to Figure 26 is shown in Figure 31. The desired reduced form is shown in
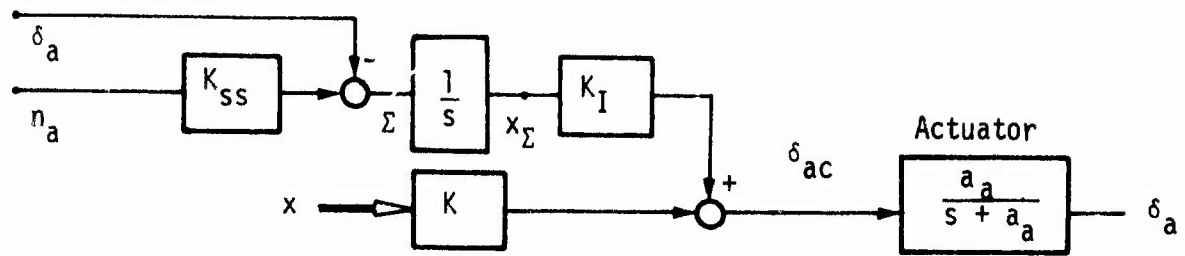
δ_{ac} = Aileron actuator input

K_I = Gain integral of error state

Σ = Error

x_Σ = Error state

x = Total system state

K = State feedback gain matrix

Figure 29. Integral Control Configuration to Enforce MLC
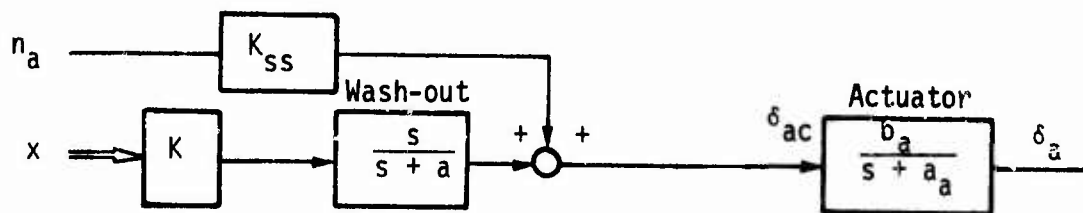
Figure 30. High-Passed Aileron Control Configuration to Enforce MLC

Figure 32. Boundary controller require isolation of a common proportional plus integral function, as given in Reference 13. Gain scheduling is also facilitated by this configuration. The factorization process is not unique. One such factorization is given in Reference 13.

Figure 33 shows the configuration used in Reference 4. Design problem is to determine the coefficients of the second order maneuver load control and gust alleviation filter and the four feedback gains shown in the diagram.
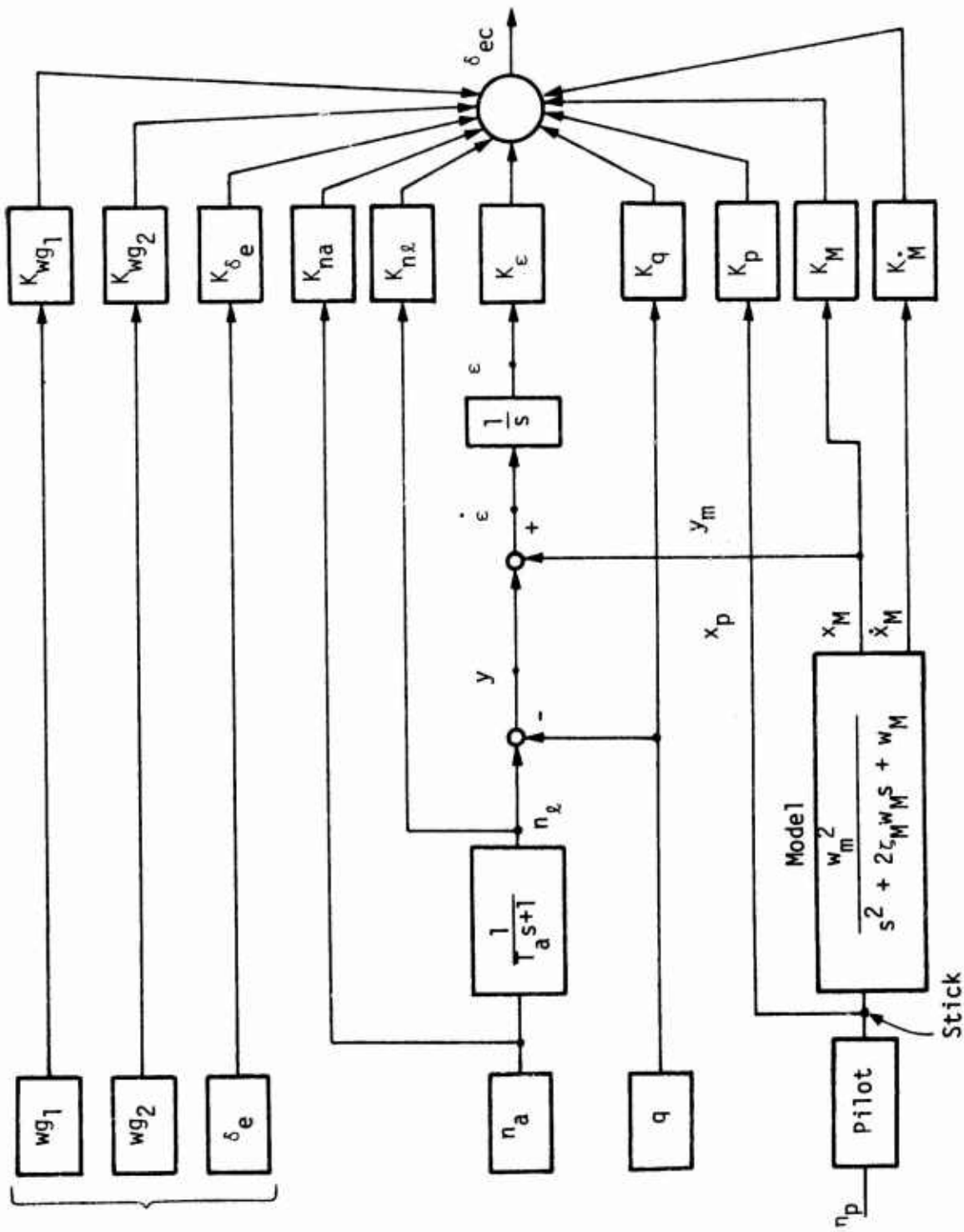
Figure 31. Handling Quality Controller Configuration with Explicit Model
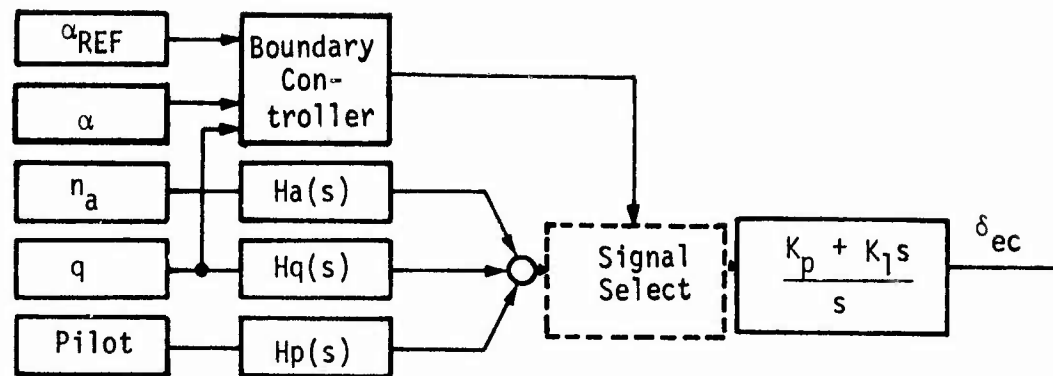
Figure 32. Desired Form of Handling Quality Controller Configuration
(Proportional and Integral Control Factorized)

This configuration provides steady-state aileron deflection proportional to
steady-state normal acceleration as given by

$$\delta_a = K_{SS} \; A_{21R} \tag{134}$$

The K_{SS} is obtained from the steady-state maneuver load control require-
ments as described previously. In addition, this filter shapes the frequency
response of the aileron loop to provide gust load alleviation.

The decomposition of this filter into a lagged acceleration and an integrator
is shown in the state diagram as given by Figure 34. Table 8 provides
a relationship between the filter coefficients and the optimal feedback gains.
Again this decomposition is not unique, and can be accomplished in different
ways. For instance, the filter decomposed as shown in Figure 34 enforces
the relation given by Equation 134 whereas the decomposition given in Figure 38
enforces an equivalent relation given by

$$6 \; \delta_a = K_{AF} \; \frac{A_{21R}}{6} \tag{134a}$$

87
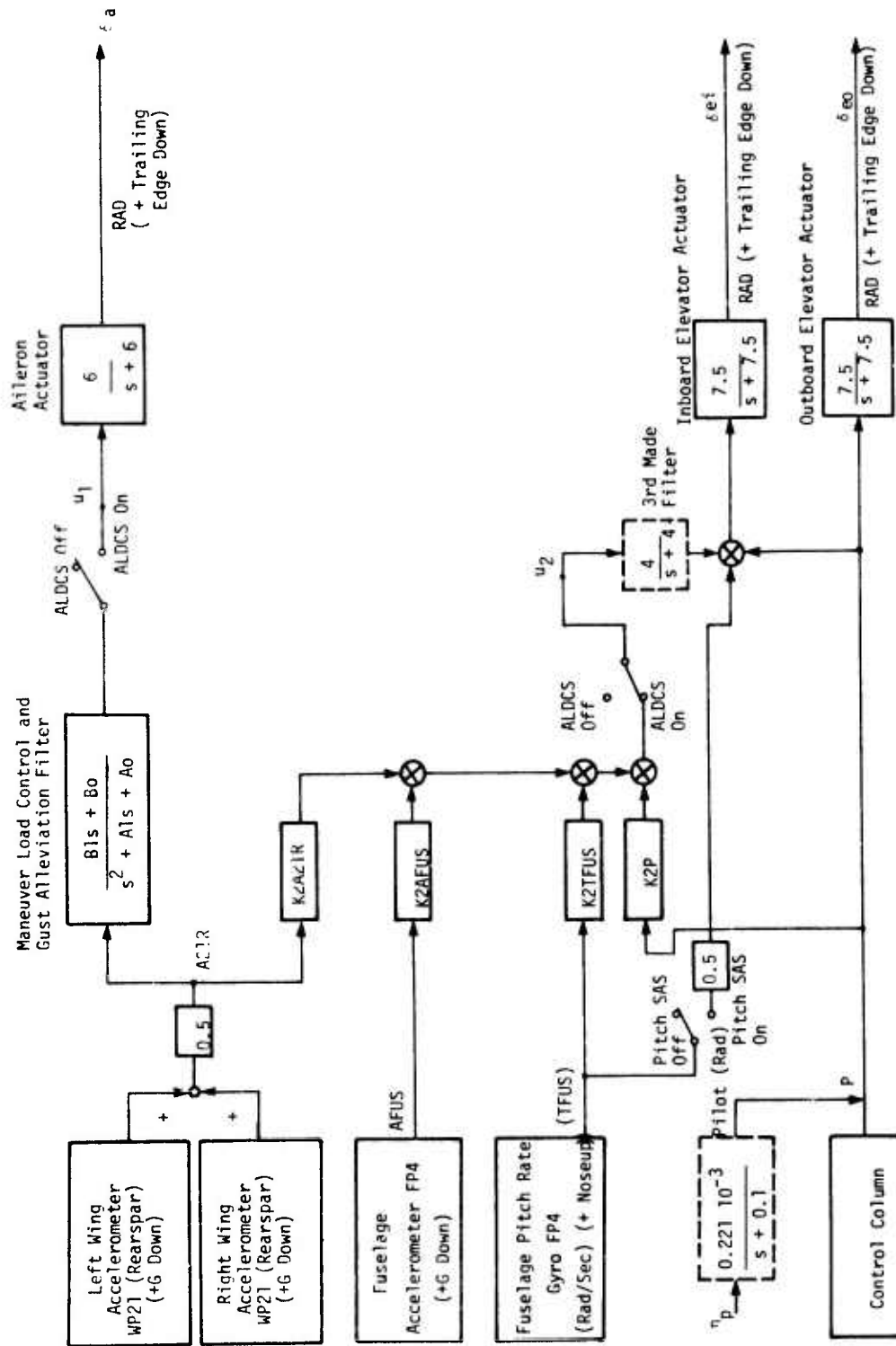
Figure 33. ALDCS Controller Configuration for CRUISE - F. C. 412301
(See Tables 13 and 14 for Gain Values)

88
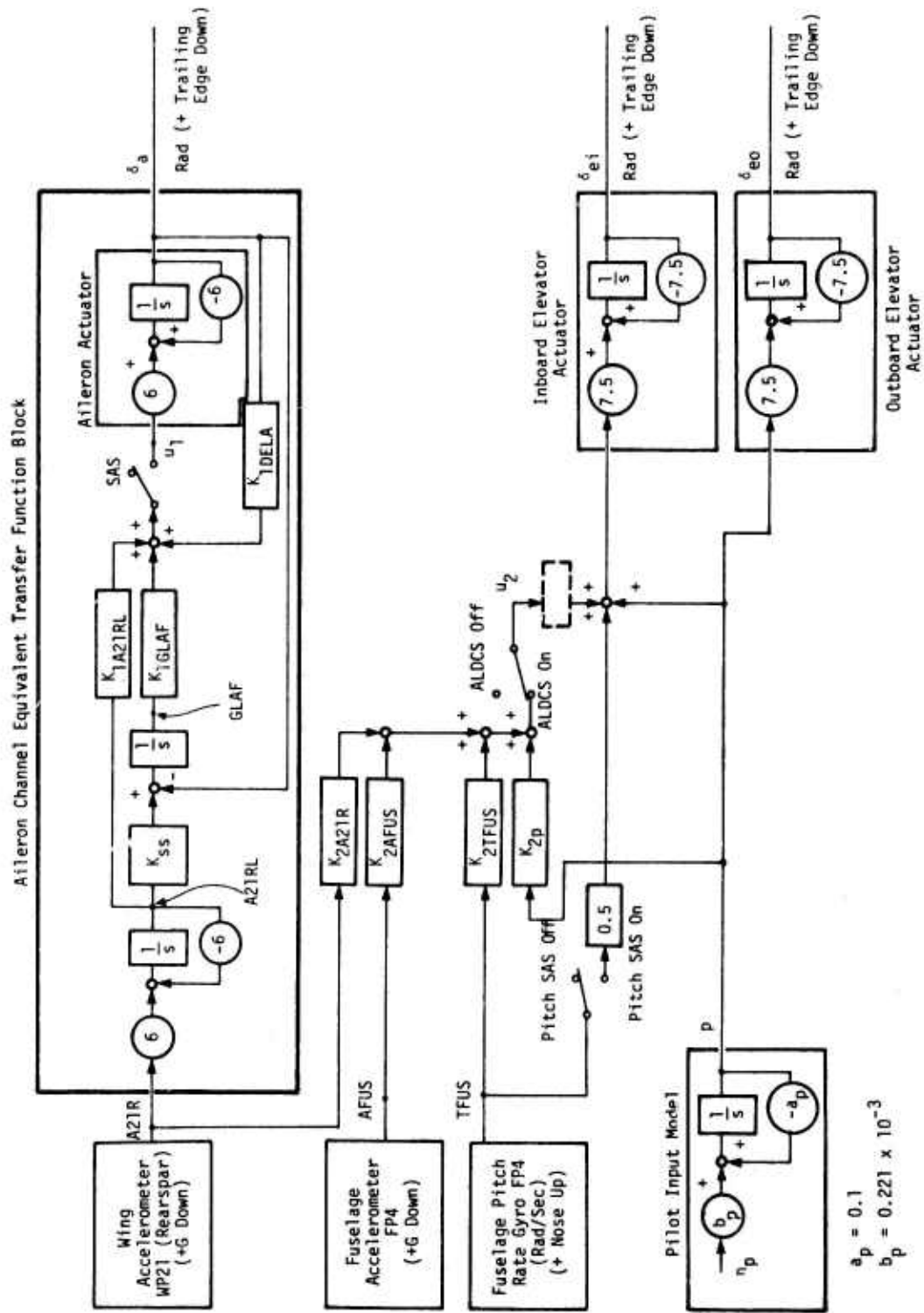
Figure 34. ALDCS Controller State Diagram

89

Table 8. Relation of Filter Coefficients to Controller Gains
(as implemented in Figure 34)

$$A_1 = 6(1 - K_{1DELA})$$

$$A_o = 6 K_{1GLAF}$$

$$B_1 = 6 K_{1A21RL}$$

$$B_o = K_{ss} A_o$$

In both configurations additional states are introduced into the control law. These states are included in the response set so that they can be weighted for proper overall response.

The lagged normal acceleration (A21RL) time constant is chosen to be the same as aileron actuator (δ_a) time constant. This selection eliminates the need for the aileron actuator sensor.

Past Honeywell work (Reference 4) indicates that the third bending mode damping is difficult to control during the ALDCS design. To facilitate design and reduce damping factor sensitivity to gains, one may include a roll-off filter in the elevator loop as shown in Figure 33.

C-5A ALDCS EXAMPLE

The ALDCS example presented here is based on Reference 4 and utilized to verify the KONPACT software results. The ALDCS design goals are shown in Table 9. The C-5A ALDCS controller design via the optimal control

Table 9. ALDCS Design Goals

Design Goal	Criterion Specification
Handling Qualities	• Same stick displacement/g (steady state) as A/C with SAS* • α, $\dot{\theta}$ command response close to that for A/C with SAS
Gust Load Alleviation	• rms value of B120.4 (wing root bending) due to wind less than 0.70 of that for the free A/C • rms value of T120.4 (wing root torsion) due to wind not more than 1.05 of that for the free A/C
Maneuver Load Control	• Steady-state B120.4/g due to commands should be less than 0.70 of that for the free A/C • The B120.4 response to step commands should not markedly reverse directions

* SAS may be taken as $U_{\delta ei} = 0.5 \, q_s$

91

synthesis technique is carried out in three steps: a) Design Model Generation, b) Controller Design, and c) Performance Evaluation.

Design Model Generation

The detailed steps to obtain the design model are described in Section VI of Volume III (Reference 51). Essentially it involves converting the FLEXSTAB/ LSA, 15 mode, residual elastic simulator deck data into state space form and augmenting it with the gust model and actuator to obtain the plant model. These are done by the software. This plant model is subsequently reduced by residualization procedure (see Section VI) and the reduced model is augmented with the controller. After this, design responses are selected to obtain the design model. Figure 35a and b show the input/output diagram of the design model. The actuator state diagram is shown in Figure 36. The form of the gust model transfer function block diagram is shown in Figure 37. Parameter values are given in Reference 4. The ALDCS controller state diagram used in Reference 4 is shown in Figure 38. In the controller, the constants K_{AF} and KM1 are determined to satisfy the steady-state maneuver load control requirements. The steady-state response computations on the plant model are illustrated in Table 10. In the first case we set $\delta_a = 0$ and $\delta_{ei} = \delta_{eo} = p$. The value of p is determined to obtain $q = \bar{q} = 0.04377$. (For consistency, the steady-state values are computed at +1 incremental g, i.e., 2g, in level flight. At the cruise speed of 735 fps this corresponds to a pitch rate of 0.04377 rad/sec.) The corresponding steady-state value of B_1 is also obtained. This is designated as $\overline{B_1}$. In the second case, we set $\delta_a = 0$, $\delta_{ei} = p + 0.5\,\bar{q}$ and $\delta_{eo} = p$ and again the value of p is determined to obtain $q = \bar{q}$. This is designated as $\bar{p}$. In the third case, we set $\delta_{eo} = \bar{p}$ and compute δ_a and δ_{ei} to obtain $q = \bar{q}$ and $B_1 = 0.7\,\overline{B_1}$.

92
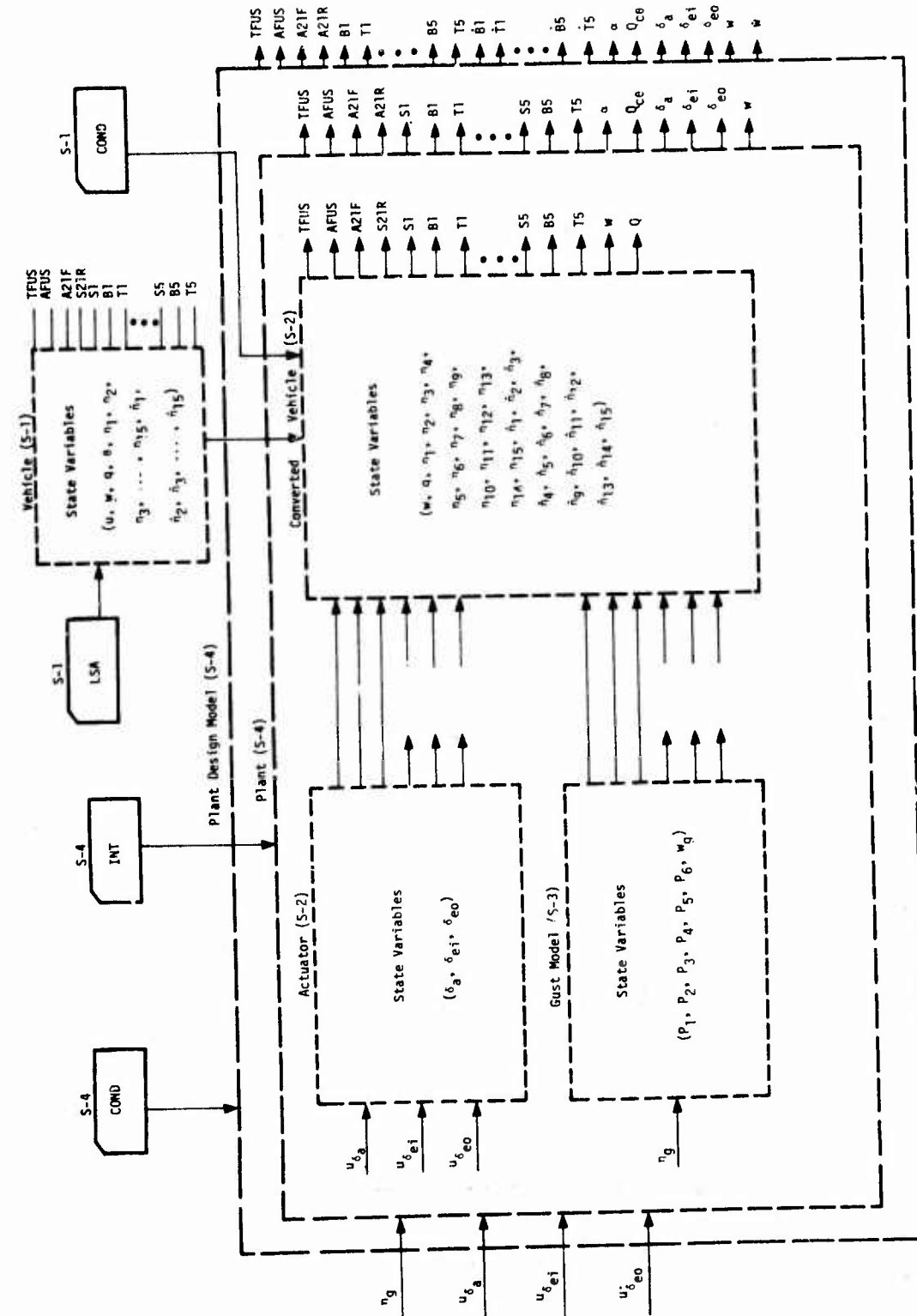
Figure 35a. Design Model Generation for ALDCS Controller Design (C-5A Cruise Flight Condition)
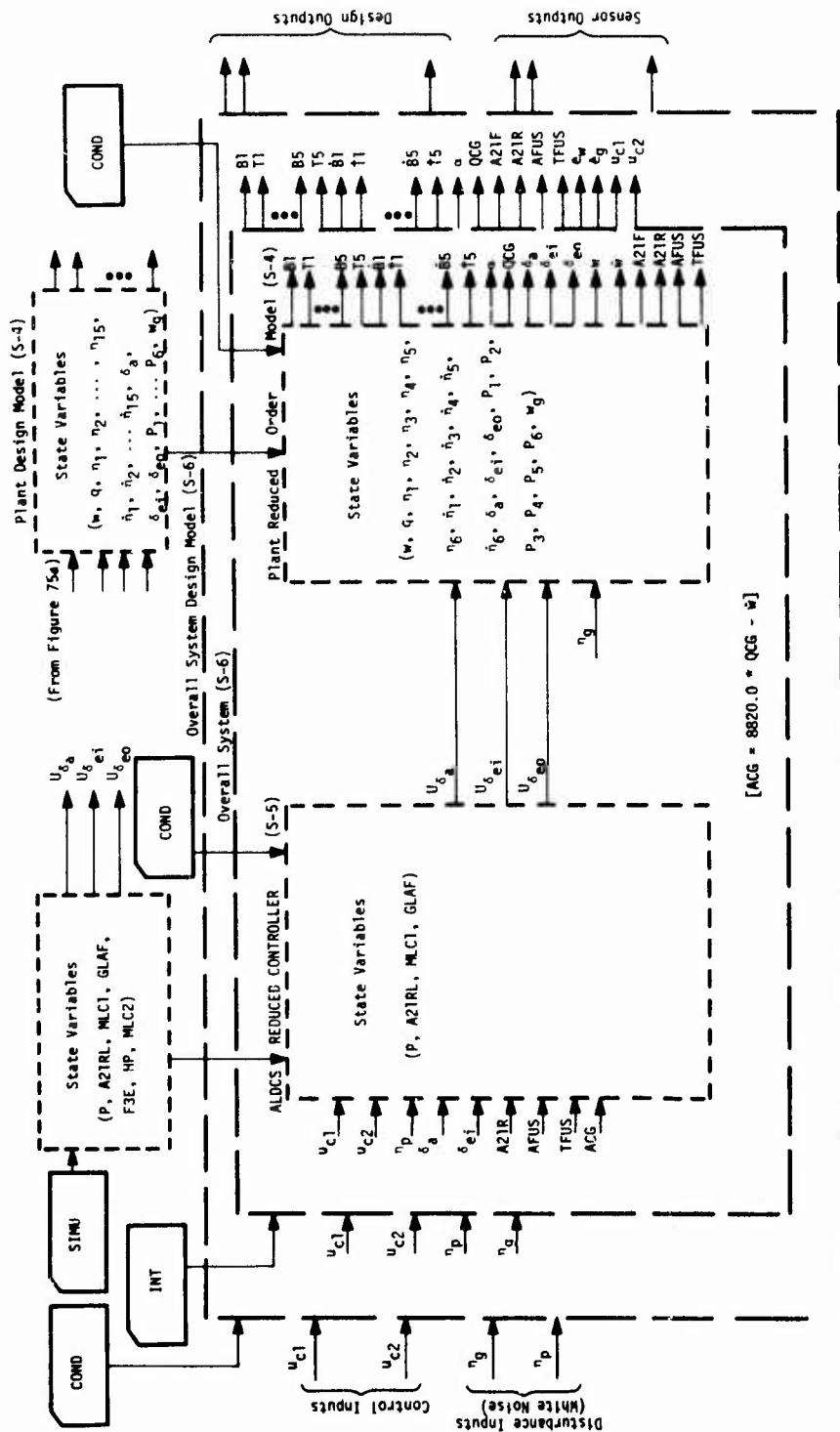
Figure 35b. Design Model Generation for ALDCS Controller Design (C-5A Cruise Flight Condition)

94
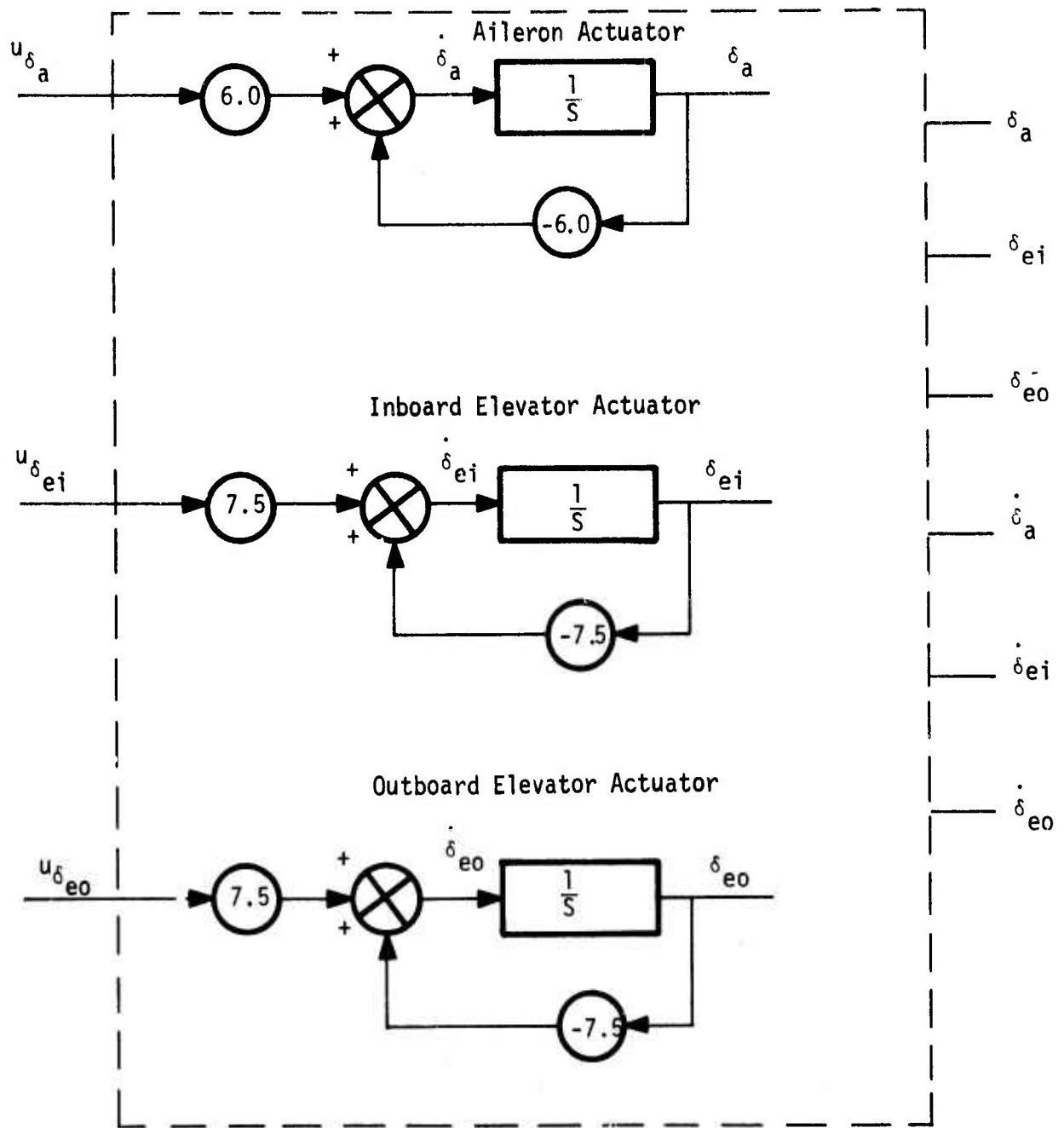
Figure 36. Actuator State Diagram

95

W-Gust Filter

$$\frac{K_g(T_q s+1)}{(T_8 s+1)^2}$$

n_g → W-Gust Filter → w_g

Nose Tail Kussner

$$\frac{1}{T_1 s+1}$$

→ Nose Section

Wing Kussner

$$\frac{1}{T_7 s+1}$$

Wing Time Delay

$$\frac{1}{T_2 s+1}$$

→ Wing Section

Tail Time Delay

$$\frac{(T_5)s + (T_6)}{T_3 s^2 + (T_4) s+1}$$

→ Tail Section
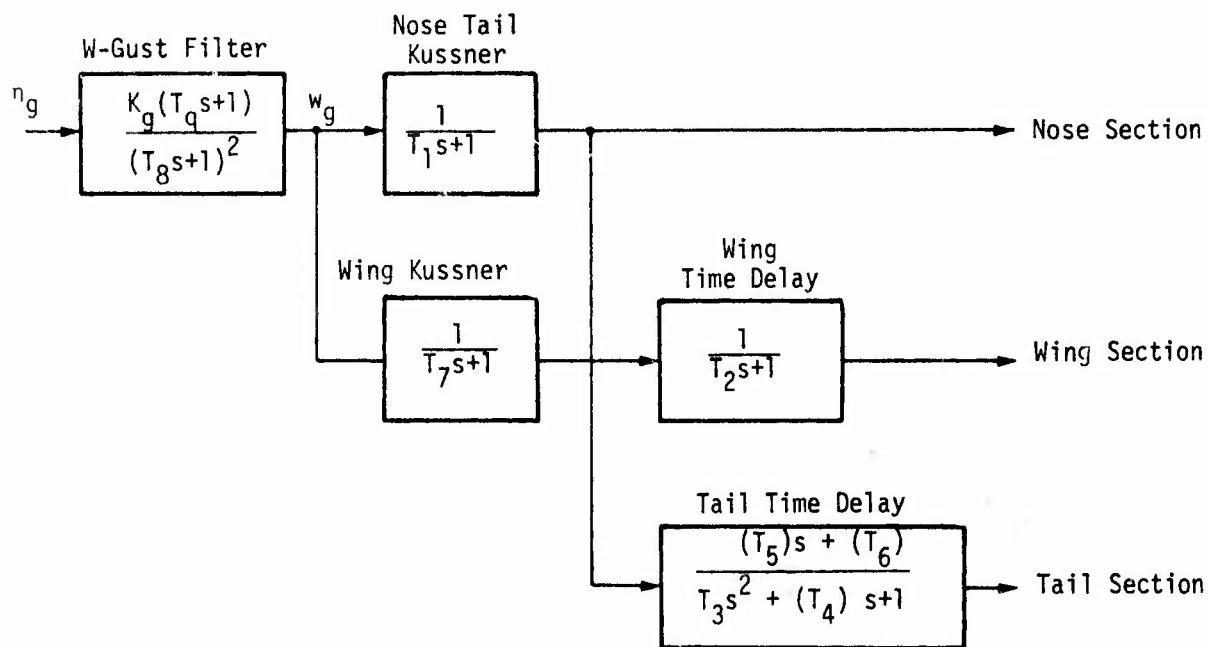
Figure 37. Gust Model Transfer Function Block Diagram

Referring to Figure 38 and Table 10, for the full state feedback design, the MLC1 integrator input gain for aileron is calculated as

$$KM1 = \frac{ACG/g}{\delta_a/g}\bigg|_{ss} = \frac{-1.0}{-0.2752} = 3.63$$

Similarly the maneuver load control gain is calculated as

$$K_{AF} = \frac{6.0\ \delta_a/g}{A21RL/g}\bigg|_{ss} = \frac{(6.0)\ (-0.2752)}{(1/6.0)\ (-1.0)} = 9.91$$

96
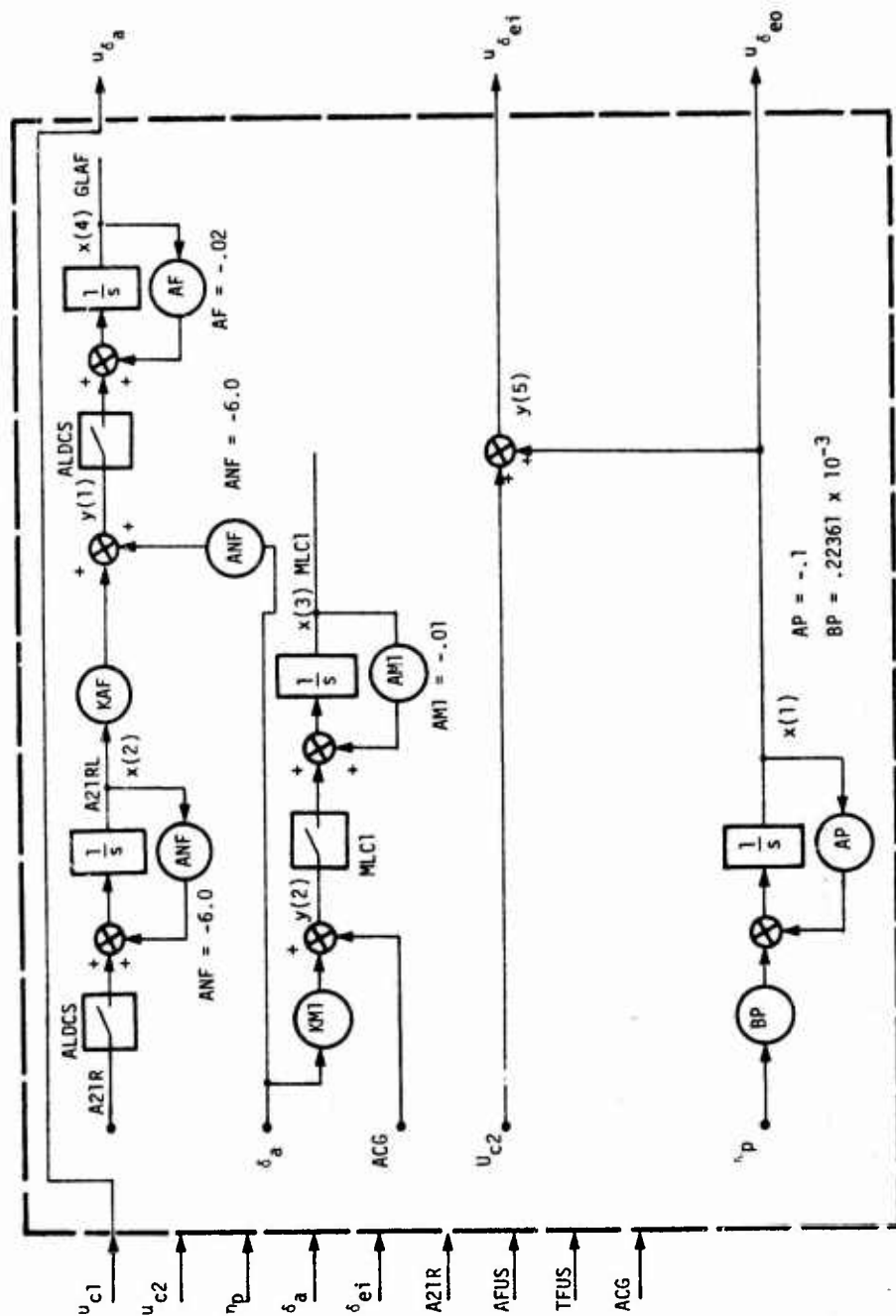
Figure 38. ALDCS Controller State Diagram

Table 10. Steady-State Responses

Case	SS Connection	Prescribed Output	Required Input	Additional Computed Outputs
Free A/C	FLEXSTAB Plant Model ($\delta_a = 0$, δ_{ei}, δ_{eo}, p; outputs $\bar{q}$, $\overline{B1}$)	$\bar{q} = 0.04377$ (rad/sec)	$\bar{p} = -0.0737$ $S_{ei} = S_{eo} = p$	$\overline{B1} = 0.6479 * 10^8$ (in-lbs)
A/C + SAS	FLEXSTAB Plant Model ($\delta_a = 0$, δ_{ei}, δ_{eo}, p; .5 gain; output $\bar{q}$)	$\bar{q} = 0.04377$ (rad/sec)	$\bar{p} = -0.0896$ $\overline{\delta_{eo}} = \bar{p}$ $\overline{\delta_{ei}} = \bar{p} + 0.5\bar{q}$	$\bar{\delta}_{ei} = -0.0677$
A/C + ALDCS	FLEXSTAB Plant Model (δ_a, δ_{ei}, δ_{eo}, $\bar{u}_2$, p; outputs $\bar{q}$, $.7\overline{B1}$, $\overline{\delta_{eo}} = -.1284$)	$\bar{q} = 0.94377$ $.7\overline{B1} = 0.4531 * 10^8$ $\overline{\delta_{eo}} = -0.0896$	$\bar{\delta}_a = -0.2752$ $\overline{\delta}_{ei} = -0.0226$	

98

The steady-state value $\bar{\delta}_{ei}$ is used to adjust the feedback gains of the ALDCS controller in the end to meet the steady-state requirements for maneuver load control.

Controller Design

The ALDCS controller design presented here is repeat design. Figure 39 represents a block diagram of the design process. The design response weights are shown in Table 11. The following steps describe the controller design.
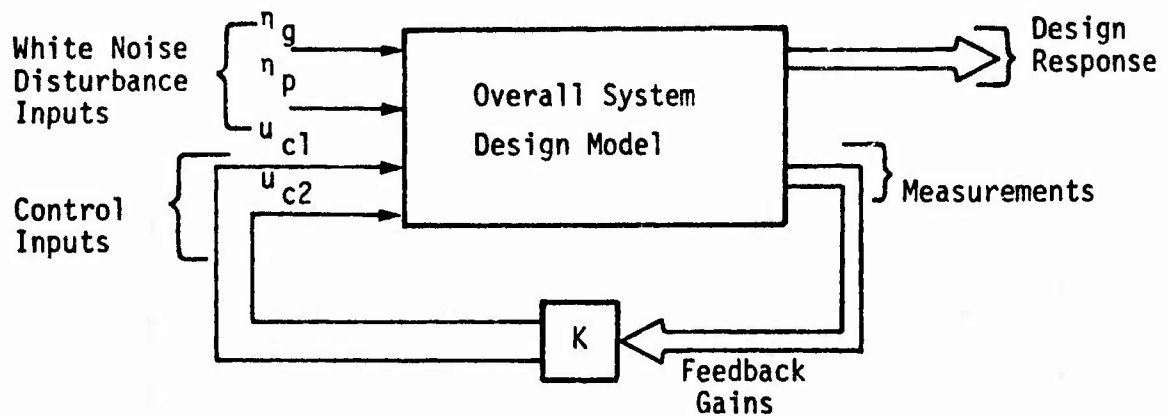
Figure 39. ALDCS Controller Design Process

Table 11. Design Response Weights for ALDCS Controller Design
(C-5A Cruise Flight Condition)

Responses	Weights	Value
MLC1	Q_1	0.800E+01
B_1	Q_2	0.100E-01
T_1	Q_3	0.100E-08
q_s	Q_4	0
B_2	Q_5	0
T_2	Q_6	0
$\dot{\delta}_a$	Q_7	0.500E+04
B_3	Q_8	0
T_3	Q_9	0
$\dot{\delta}_{ei}$	Q_{10}	0.600E+06
B_4	Q_{11}	0
T_4	Q_{12}	0
δ_a	Q_{13}	0
B_5	Q_{14}	0
T_5	Q_{15}	0
δ_{ei}	Q_{16}	0
$\dot{B}_1$	Q_{17}	0.750E-13
$\dot{T}_1$	Q_{18}	0.100E-10

Table 11. Design Response Weights for ALDCS Controller Design
(C-5A Cruise Flight Condition) (Concluded)

Responses	Weights	Value
$\dot{\eta}_1$	Q_{19}	0
$\dot{B}_2$	Q_{20}	0.100E-13
$\dot{T}_2$	Q_{21}	0.100E-11
$\dot{\eta}_2$	Q_{22}	0
$\dot{B}_3$	Q_{23}	0.200E-13
$\dot{T}_3$	Q_{24}	0.200E-11
$\dot{\eta}_3$	Q_{25}	0
$\dot{B}_4$	Q_{26}	0.800E-13
$\dot{T}_4$	Q_{27}	0.100E-10
$\dot{\eta}_4$	Q_{28}	0
$\dot{B}_5$	Q_{29}	0.200E-12
$\dot{T}_5$	Q_{30}	0.200E-10
η_5	Q_{31}	0
$\dot{\eta}_6$	Q_{32}	0
$\dot{e}_w$	Q_{33}	0.100E+01
$\dot{e}_q$	Q_{34}	0.100E+01
α	Q_{35}	0
u_{c_1}	Q_{36}	0
u_{c_2}	Q_{37}	0

Full State Optimal Controller Design--Full state optimal control is unique and is used for initial studies. It determines what performance can be achieved from the system under idealized conditions.

Using the overall system design model described earlier, the optimal full state feedback gains are computed for the specified quadratic weights.

Simplified Optimal Control Design--Starting from the optimal full state feedback gains, simplified feedback gains are obtained as described in References 25 and 4. The reduced control law is given by the following equations (see Figure 38).

$$u_{\delta_a} = (K1_{\delta_a})\,\delta_a + (K1_{A21RL})\,A21RL + (K1_{GLAF})\,GLAF \tag{135}$$

$$u_{\delta_{ei}} = (K2_{A21R})\,A21R + (K2_{AFUS})\,AFUS + (K2_{TFUS})\,TFUS + \tag{136}$$

$$(K2p)P$$

The reduced feedback gains are shown in Table 12.

Adjustment of Gain $K2_p$ and Calculation of the MLC Filter Coefficients-- The gain $K2_p$ obtained in the previous step is adjusted so that the steady-state maneuver load control requirements are met for the elevator channel. From the steady-state response calculations

$$\bar{\delta}_{ei} = -0.0226 \text{ rad} \qquad \bar{\delta}_{eo} = -0.0896 \text{ rad}$$

Since the actuator steady-state gain is unity (refer to Figure 38) we have:

102

Table 12. Reduced Feedback Gains for ALDCS Controller Design
(C-5A Cruise Flight Condition)

Gains	Values
$K1_{DELA}$	-7.81200
$K1_{A21RL}$	11.94000
$K1_{GLAF}$	1.96900
$K2_{A21R}$	0.00256
$K2_{AFUS}$	-0.06400
$K2_{TFUS}$	0.49040
$K2_p$	-0.40150

$$\bar{\delta}_{ei} = \bar{u}_{\delta_{ei}} = \bar{u}_{c_2} + \overline{P} = (K2_{A21R})\,\overline{A21R}\ + \tag{137}$$

$$(K2_{AFUS})\,\overline{AFUS} + (K2_{TFUS})\,\overline{TFUS} + (K2*_p + 1.0)\overline{P}$$

Substituting the steady-state values for 1G maneuver and solving for $K2*_p$, we obtain $K2*_p = 0.178$.

Table 13 shows the adjusted reduced gains. Figure 40 shows the final form of the ALDCS controller configuration for cruise flight condition. The final maneuver load control and gust alleviation filter coefficients are obtained from A21RL and GLAF filters (Figure 38) by setting the integrator feedback

gain AF = 0.0. These calculations are shown in Table 14. The final ALDCS controller is shown in Figure 41.

Table 13. Final Gains for ALDCS Controller Design
(C-5A Cruise Flight Condition)

Gains	Values
$K1_{DELA}$	-7.812000
$K1_{A21RL}$	11.940000
$K1_{GLAF}$	1.969000
$K2_{A21R}$	0.002565
$K2_{AFUS}$	-0.064010
$K2_{TFUS}$	0.490400
$K2_p$ *	0.178000

* $K2_p$ Gain obtained by FFOC is subsequently adjusted to satisfy the steady-state ALDCS requirements for δ_{ei}.

Table 14. MLC and GLAF Filter Coefficients
(As implemented in Figure 38)

Filter Coefficient	Equation	Value
A_1	$6(1-K1_{DELA})$	52.872
A_o	$36*K1_{GLAF}$	70.88
B_1	$K1_{A21RL}$	11.94
B_o	$KAF*K1_{GLAF}$	19.51

104
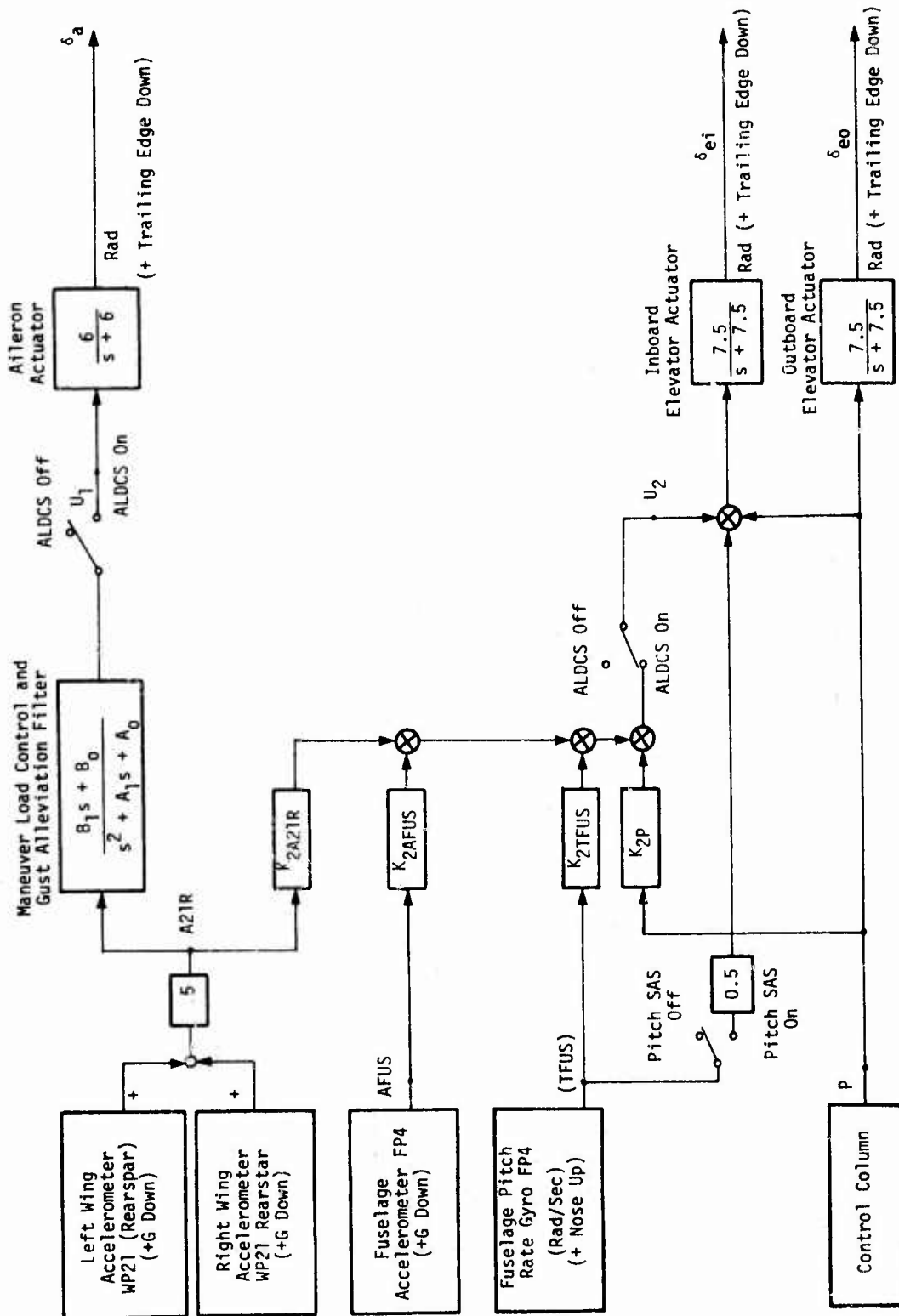
Figure 40. ALDCS Controller Configuration for Cruise F. C. 412301

105
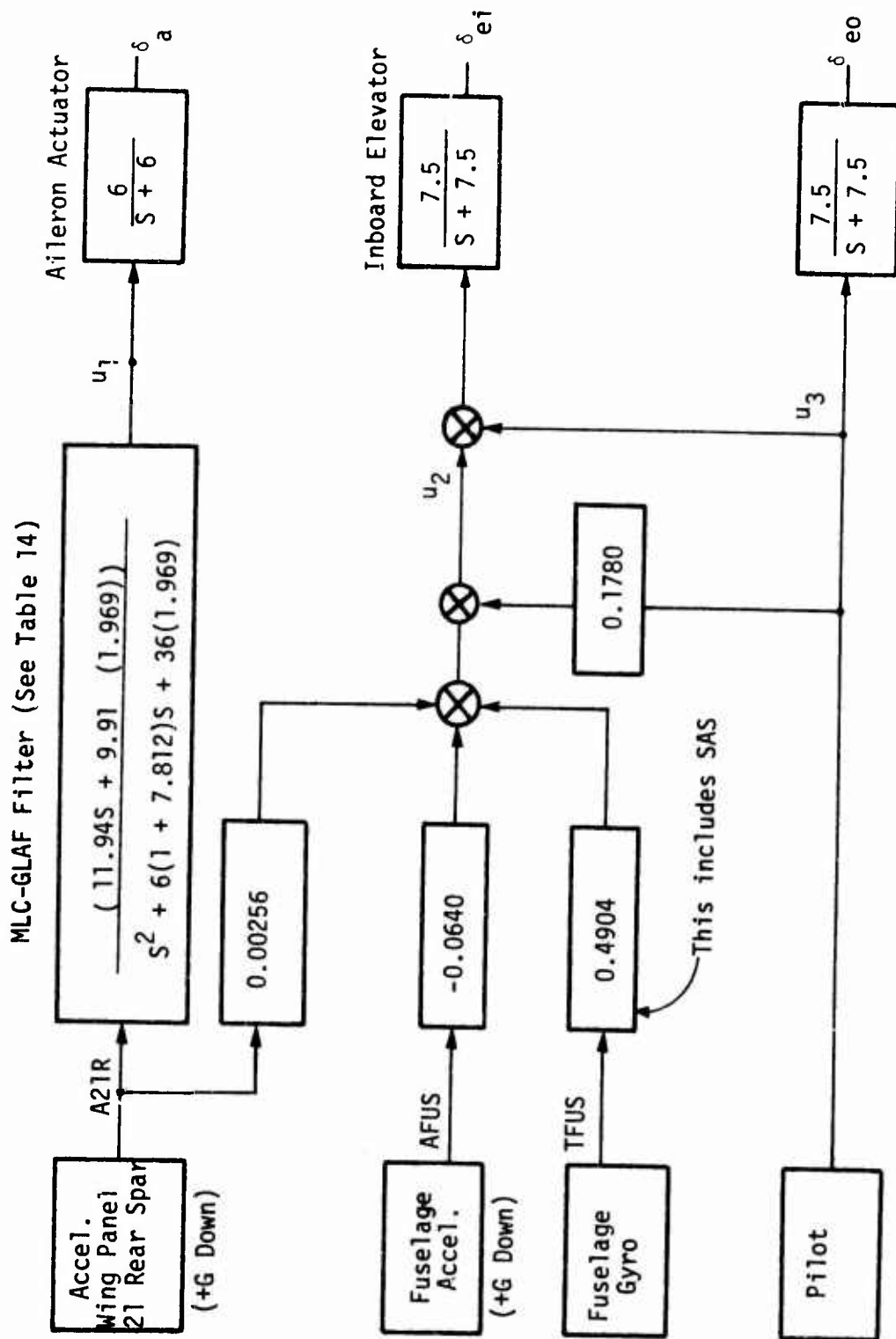
Figure 41. Final ALDCS Block Diagram for Cruise F. C. 412301

106

Performance Evaluation

The detailed performance results are presented in the next section. Here the variation of some key performance variables as we move from full state feedback to simplified feedback (i.e., as $(1-\lambda)$ goes to 1) is presented.

Figures 42, 43, and 44 present the variation of quadratic cost and the sensor feedback gains as $(1-\lambda)$ varies from 0 to 1. These variations are fairly smooth (an erratic variation would indicate that the step size in λ was too large). Note that the aileron feedback gains essentially remain zero until $(1-\lambda)$ approaches zero and then suddenly shoot up. This corresponds to taking out the temporary MLC1 integrator and putting in the GLAF integrator in Figure 38.

Figures 45, 47, 49, and 51 present the variation of rms responses ($\dot{e}_q$, $\dot{e}_w$, T1, B1) due to wind gust as $(1-\lambda)$ varies from 0 to 1. And Figure 46, 48, 50, and 52 present the variation of rms responses ($\dot{e}_q$, $\dot{e}_w$, T1, B1) due to pilot as $(1-\lambda)$ varies from 0 to 1. In all of these figures, we observe that full state feedback determines what performance can be obtained from the system under ideal conditions and the simplified feedback is obtained by a minimum loss of the performance obtained by full state feedback. Also note that the final ALDCS performance is slightly different from the simplified (reduced) feedback controller performance. (Final ALDCS controller satisfies the steady-state requirements completely whereas the simplified feedback controller does not. This is because of the small feedback around the GLAF filter (i.e., AF $\neq$ 0 in Figure 38) in the simplified controller as well as the adjustment of pilot gain K_{2p} to K^*_{2p} for meeting steady-state requirements.)

Figures 53, 54, and 55 present the variation of the closed-loop roots (rigid body, first flexure mode, and third flexure mode) as $(1-\lambda)$ varies from 0 to 1.
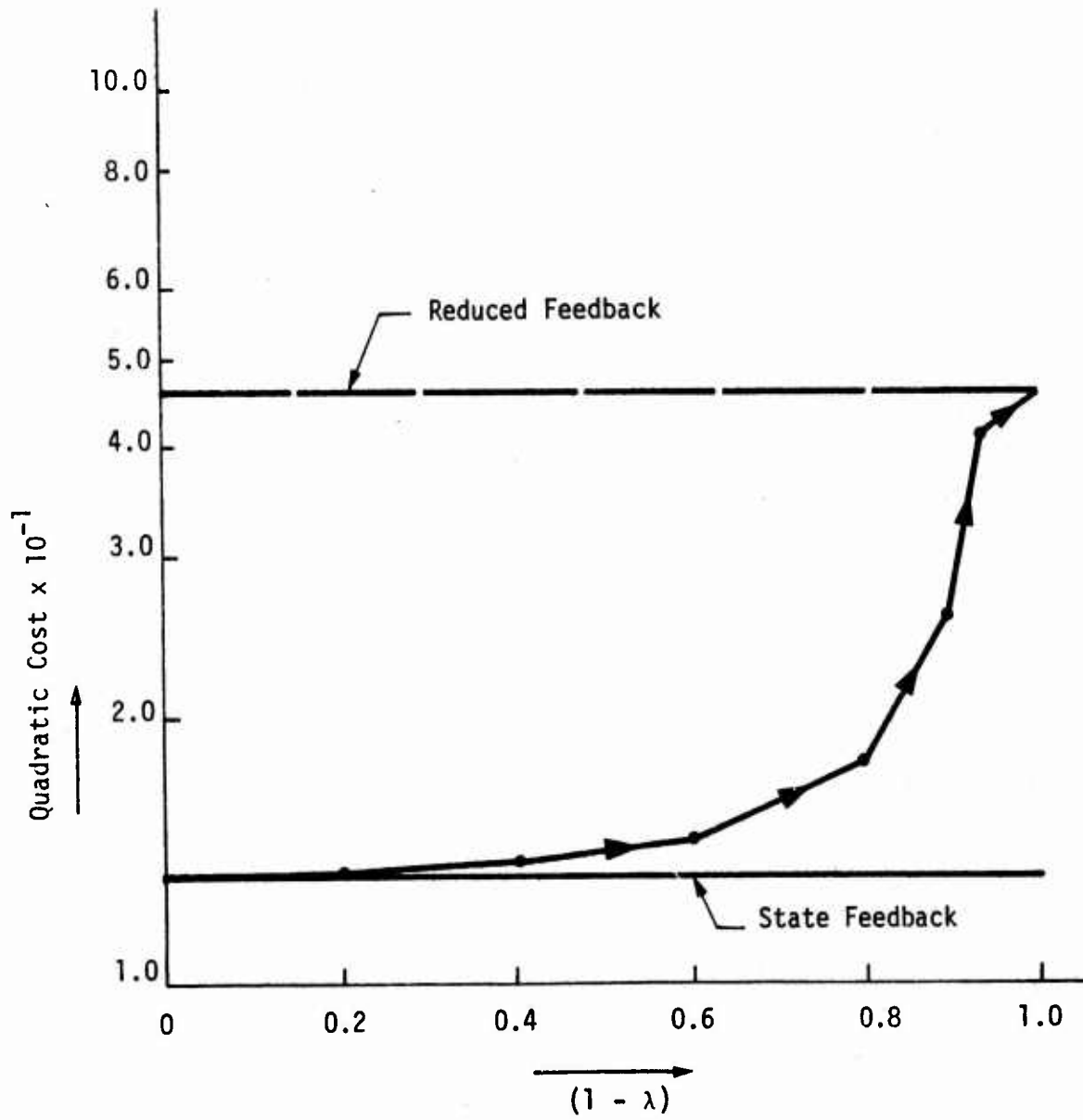
Figure 42. Variation of Quadratic Cost with (1-λ)
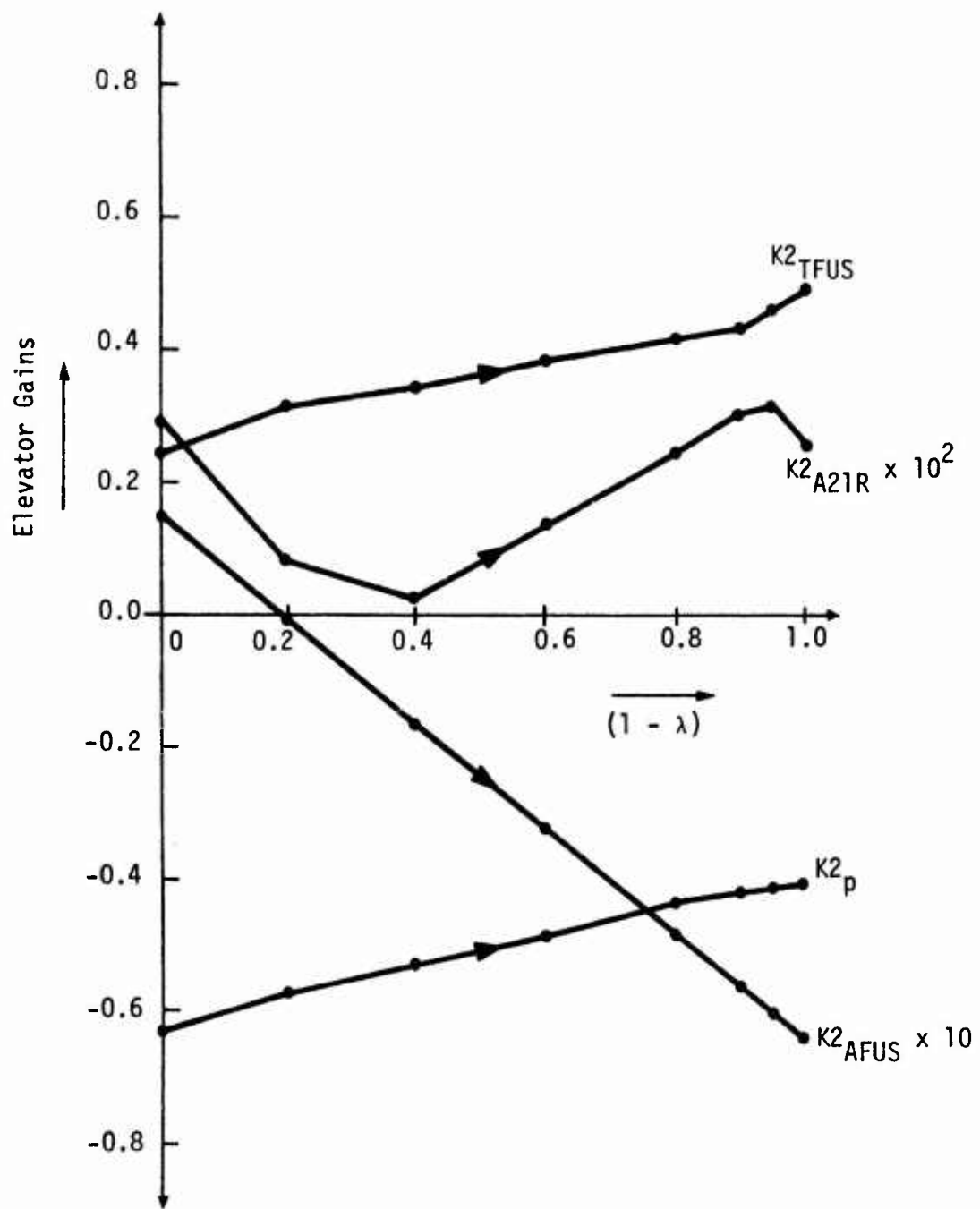
Figure 43. Variation of Elevator Feedback Gains with (1-λ)
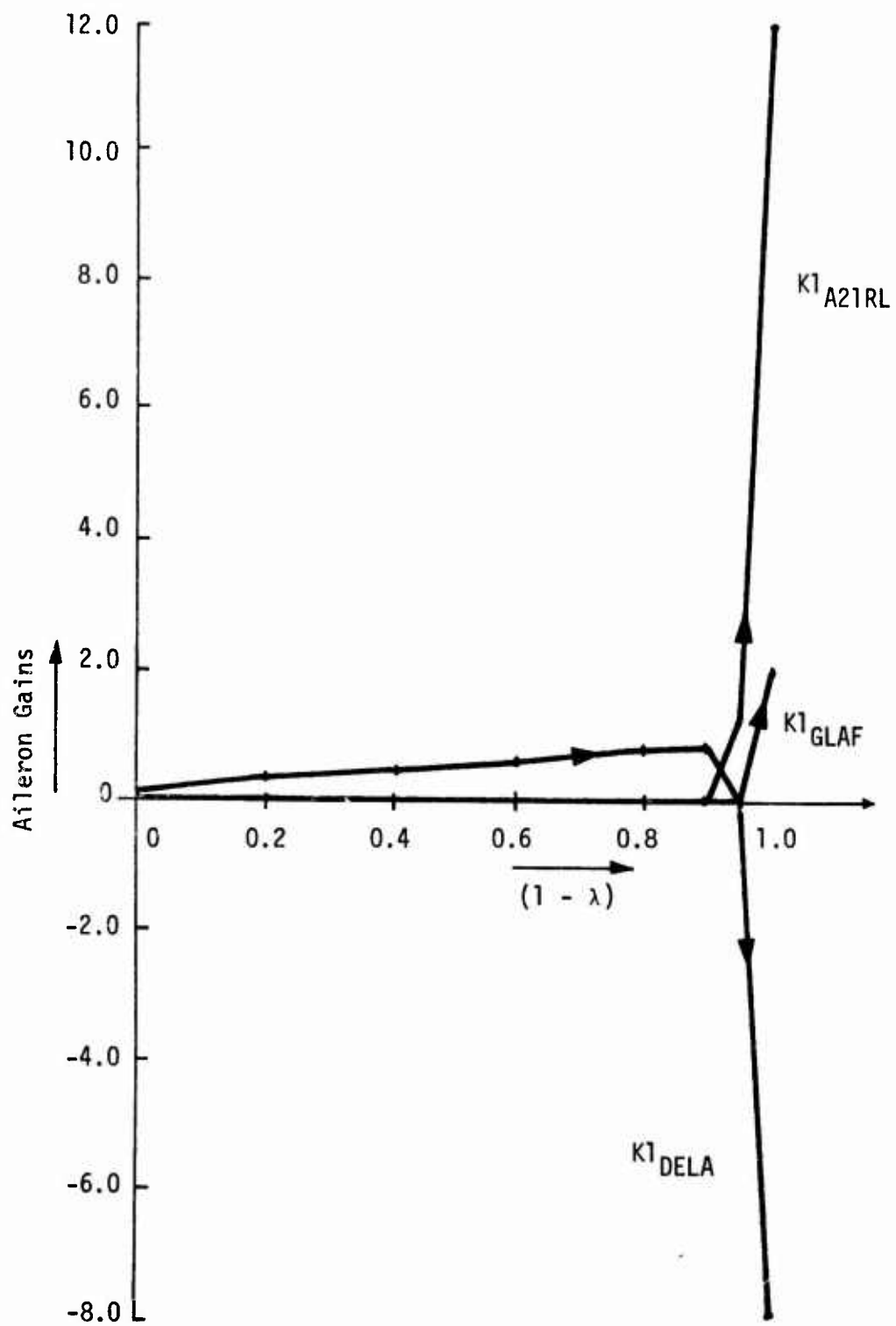
Figure 44. Variation of Aileron Feedback Gains with (1-λ)
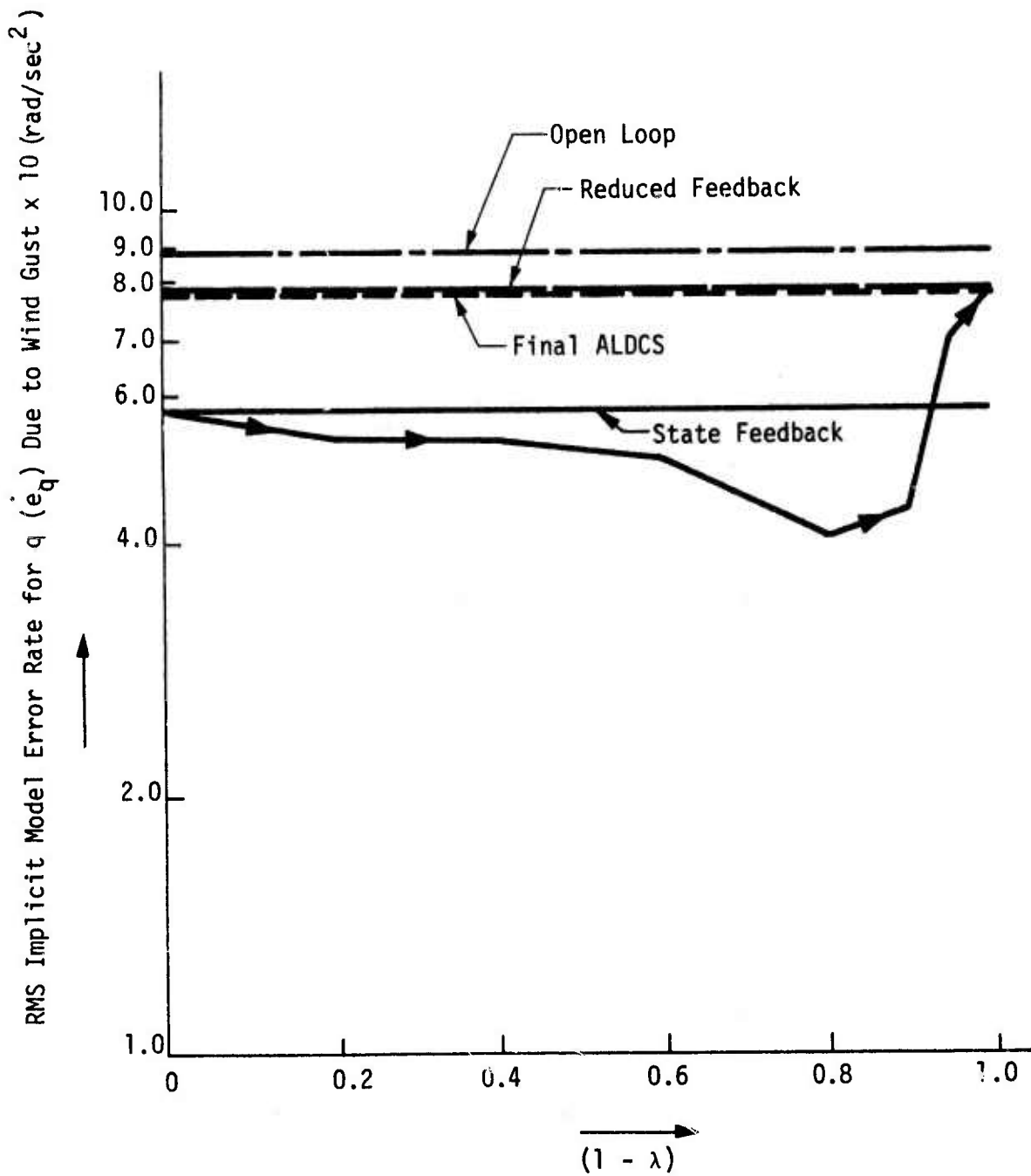
Figure 45. Variation of RMS Response (For Implicit Model Error Rate for q ($\dot{e}_q$) Due to Wind Gust) with ($1-\lambda$)
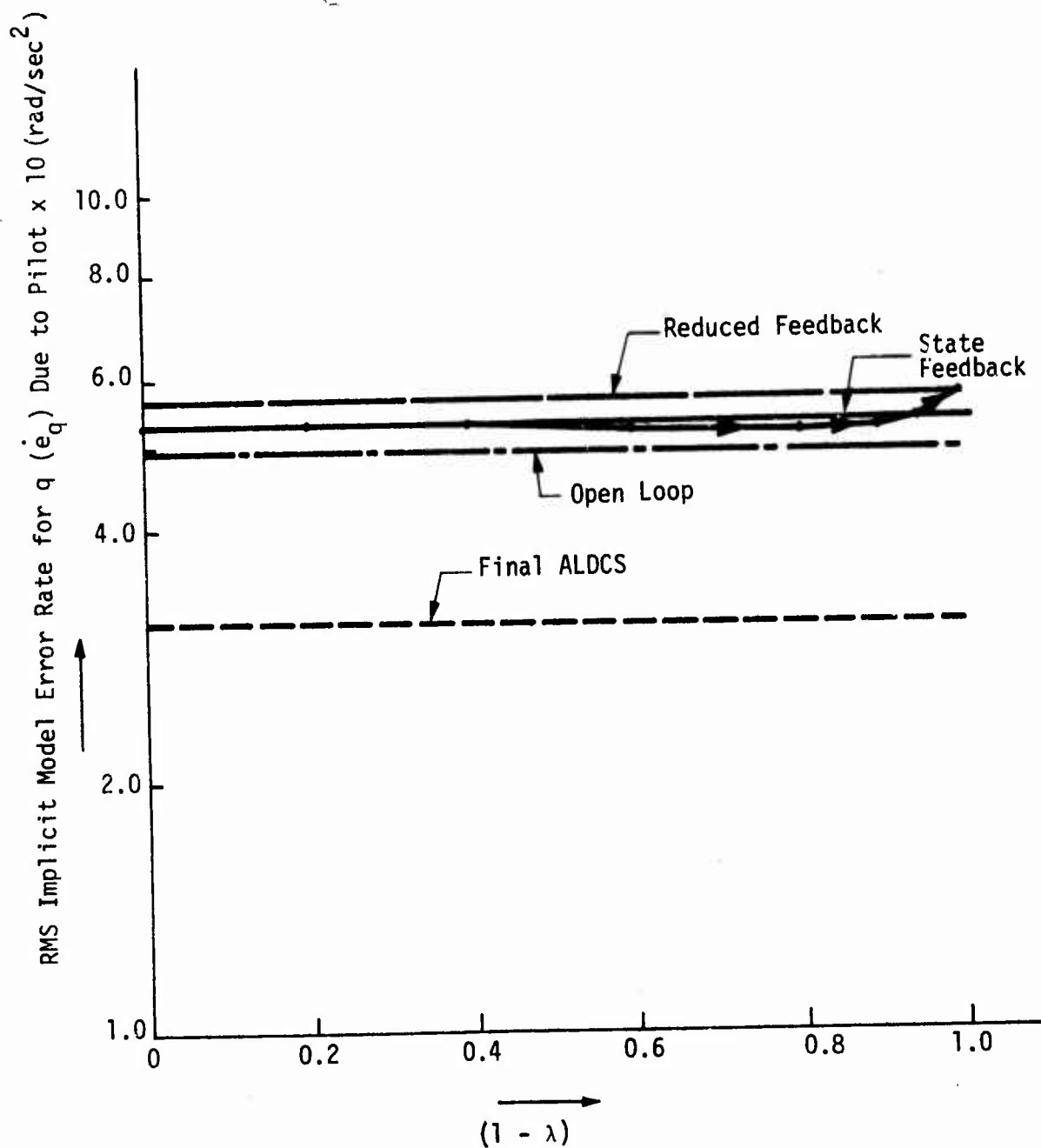
Figure 46.   Variation of RMS Response (For Implicit Model Error
Rate for q ($\dot{e}_q$) Due to Pilot) with ($1-\lambda$)

112
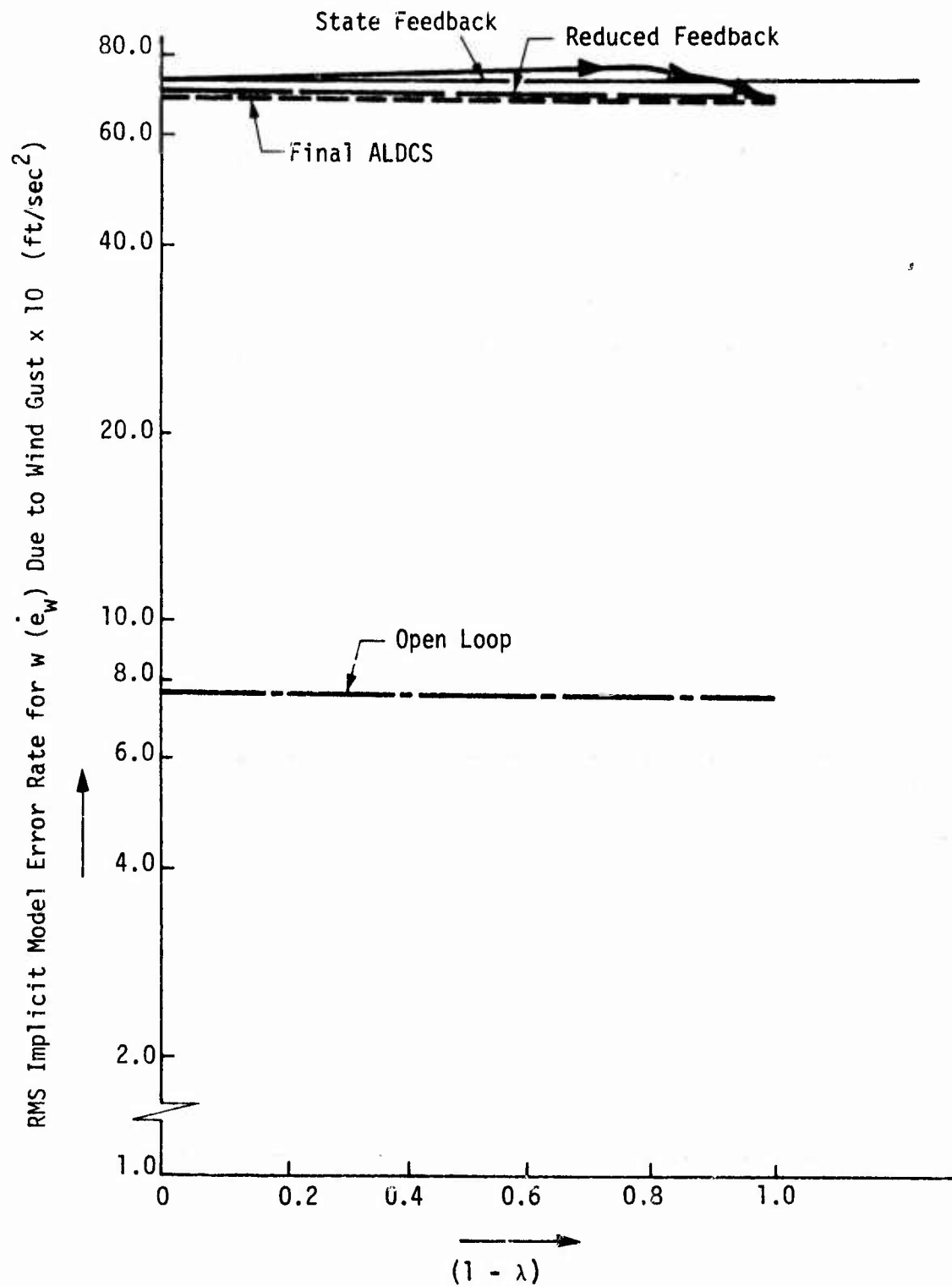
Figure 47.   Variation of RMS Response (For Implicit Model Error
Rate for w ($\dot{e}_w$) Due to Wind Gust) with (1-λ)

113
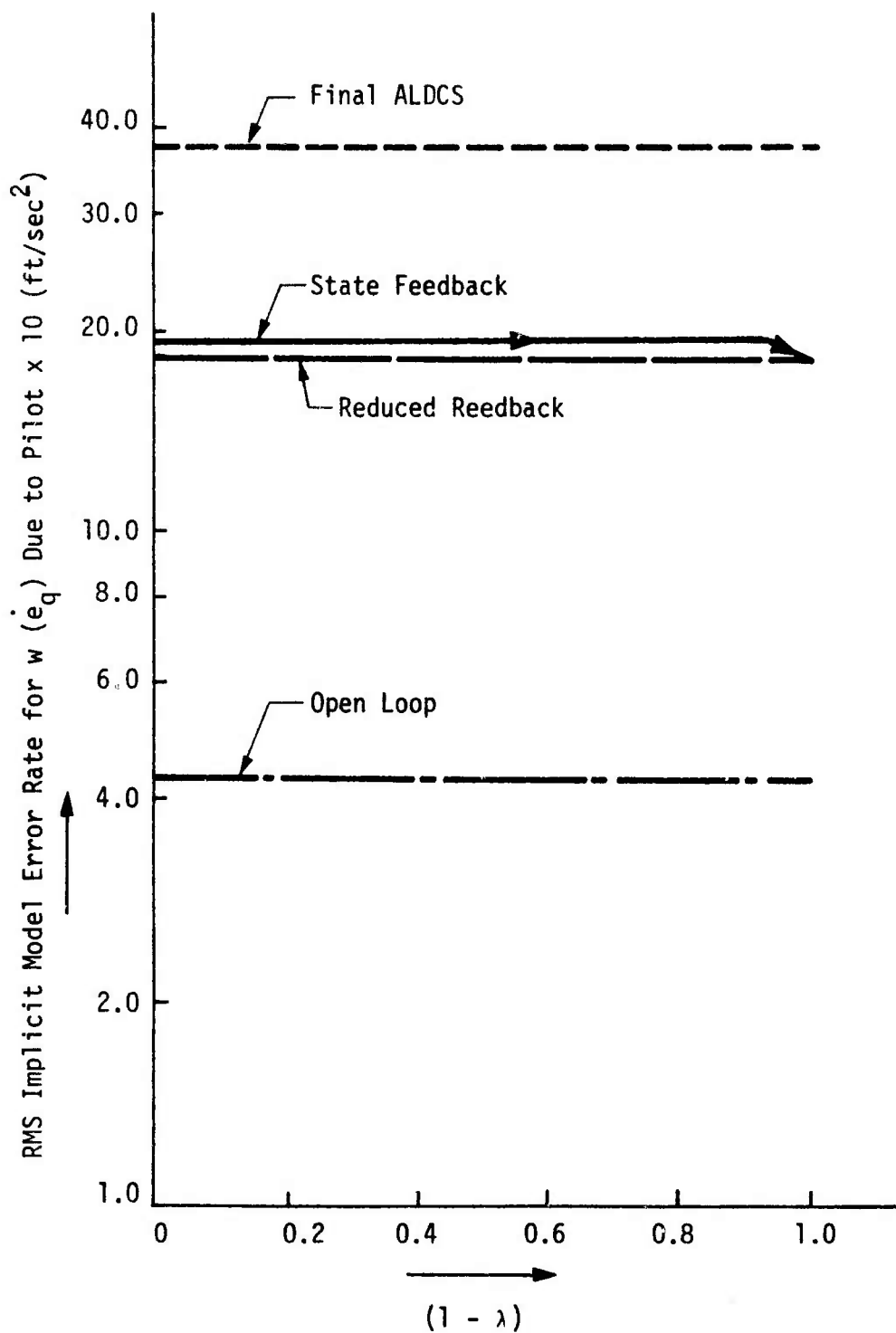
Figure 48.   Variation of RMS Response (For Implicit Model Error
Rate for w ($\dot{e}_w$) Due to Pilot) with (1-λ)

114
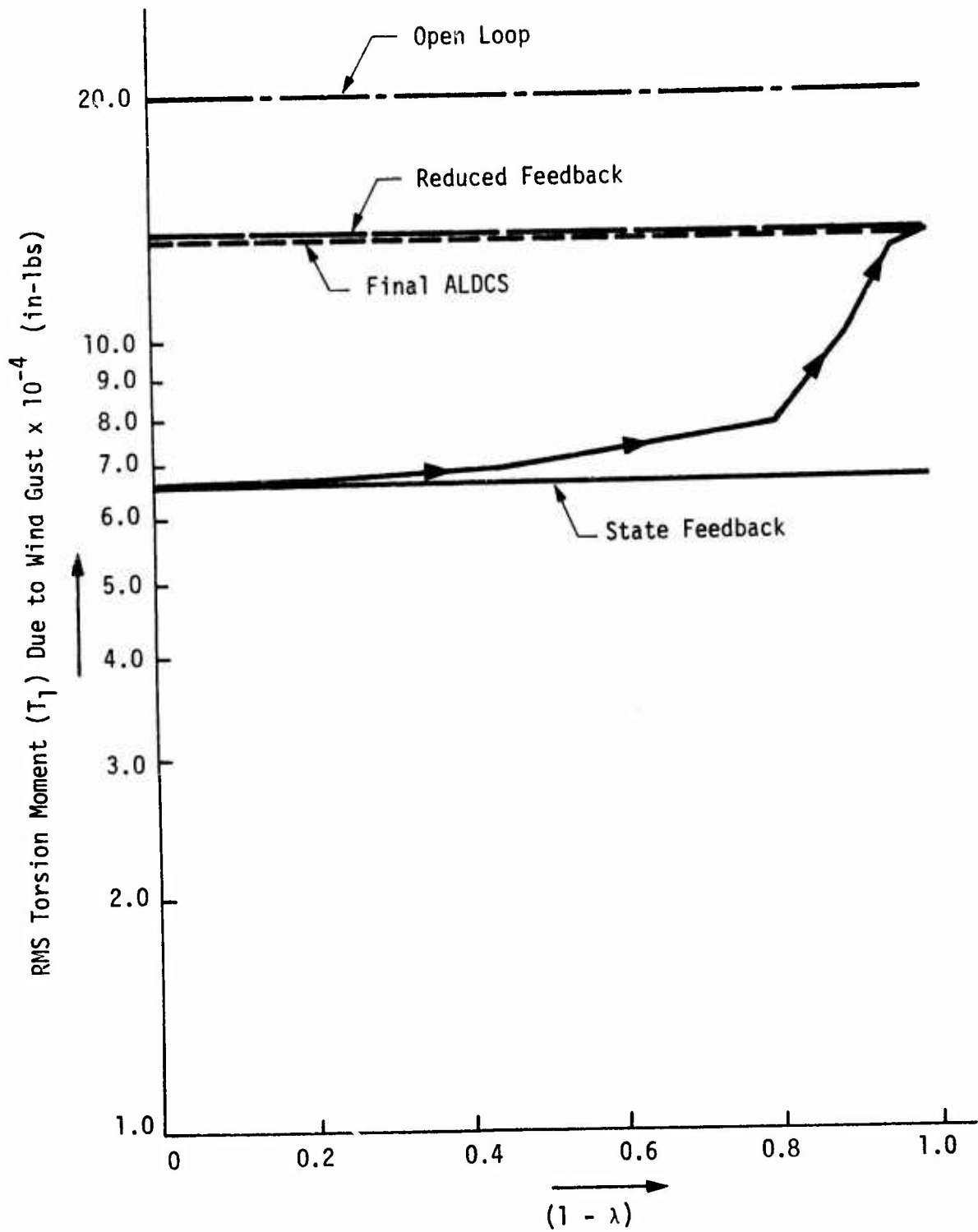
Figure 49. Variation of RMS Response (For Torsion Moment (T1) Due to Wind Gust) with (1-λ)

115
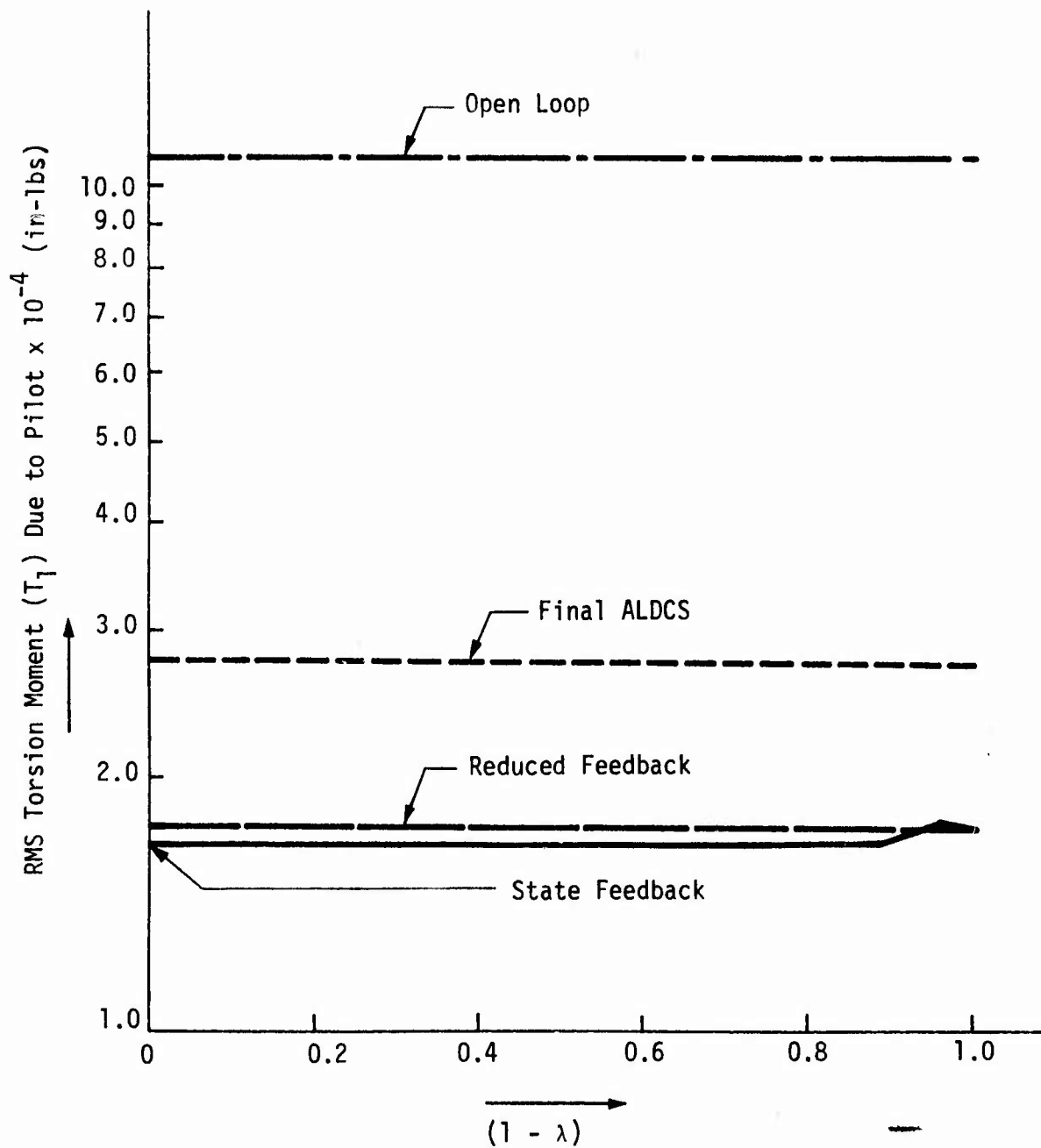
Figure 50. Variation of RMS Response (For Torsion Moment (T1) Due to Pilot) with (1-λ)
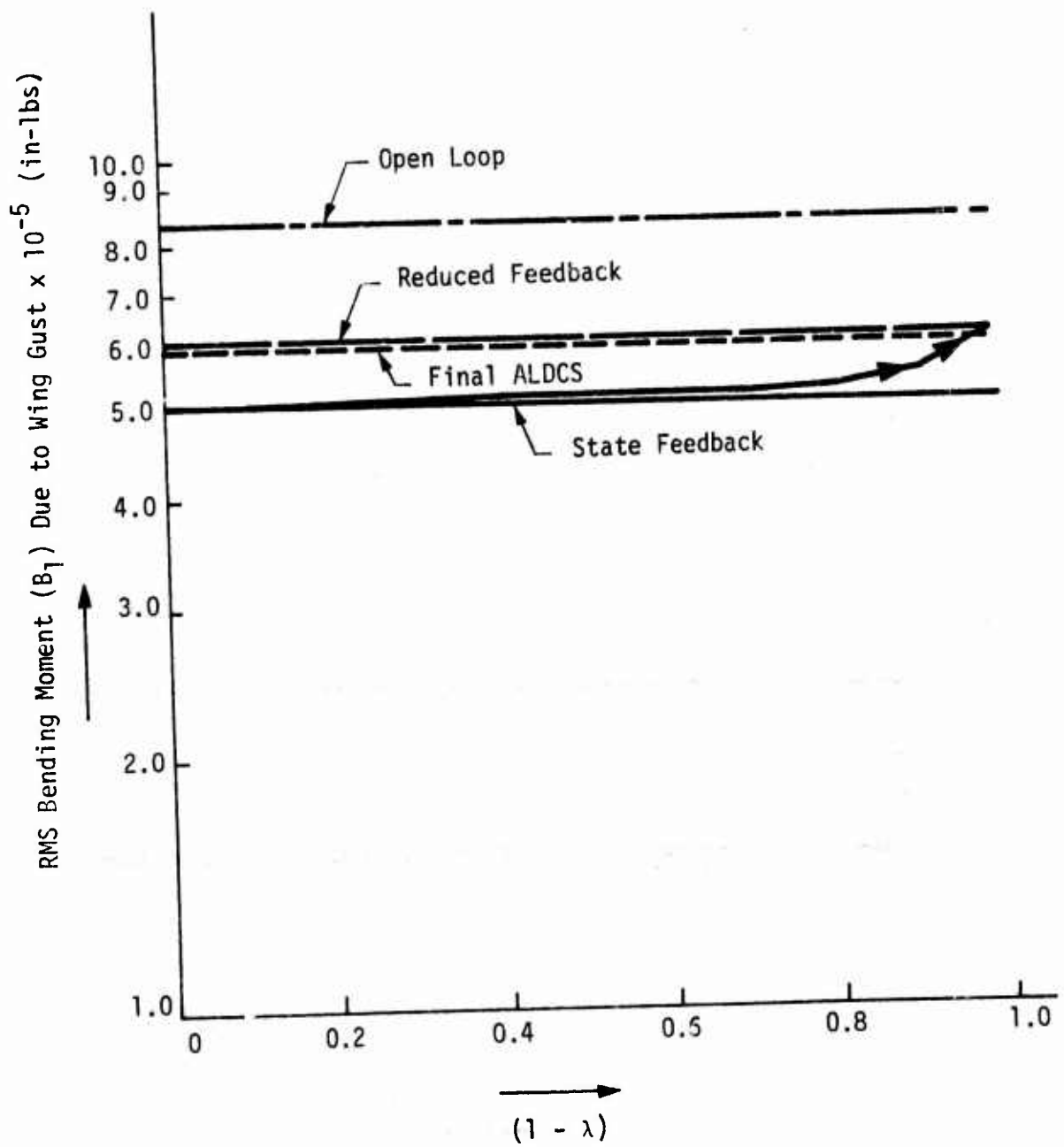
Figure 51. Variation of RMS Response (For Bending Moment (B1) Due to Wind Gust) with $(1-\lambda)$

117
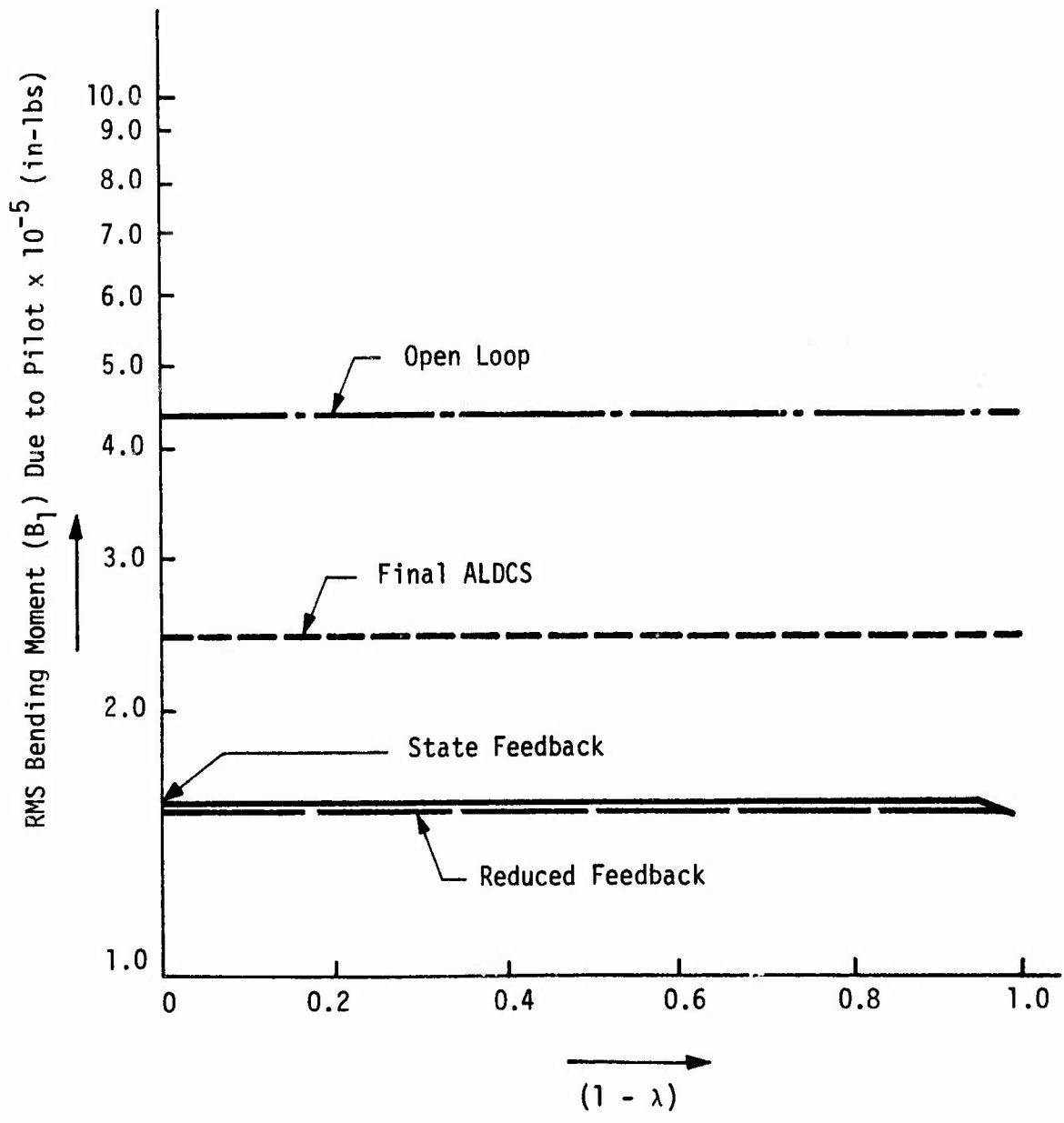
Figure 52. Variation of RMS Response (For Bending Moment (B1) Due to Pilot) with (1-λ)
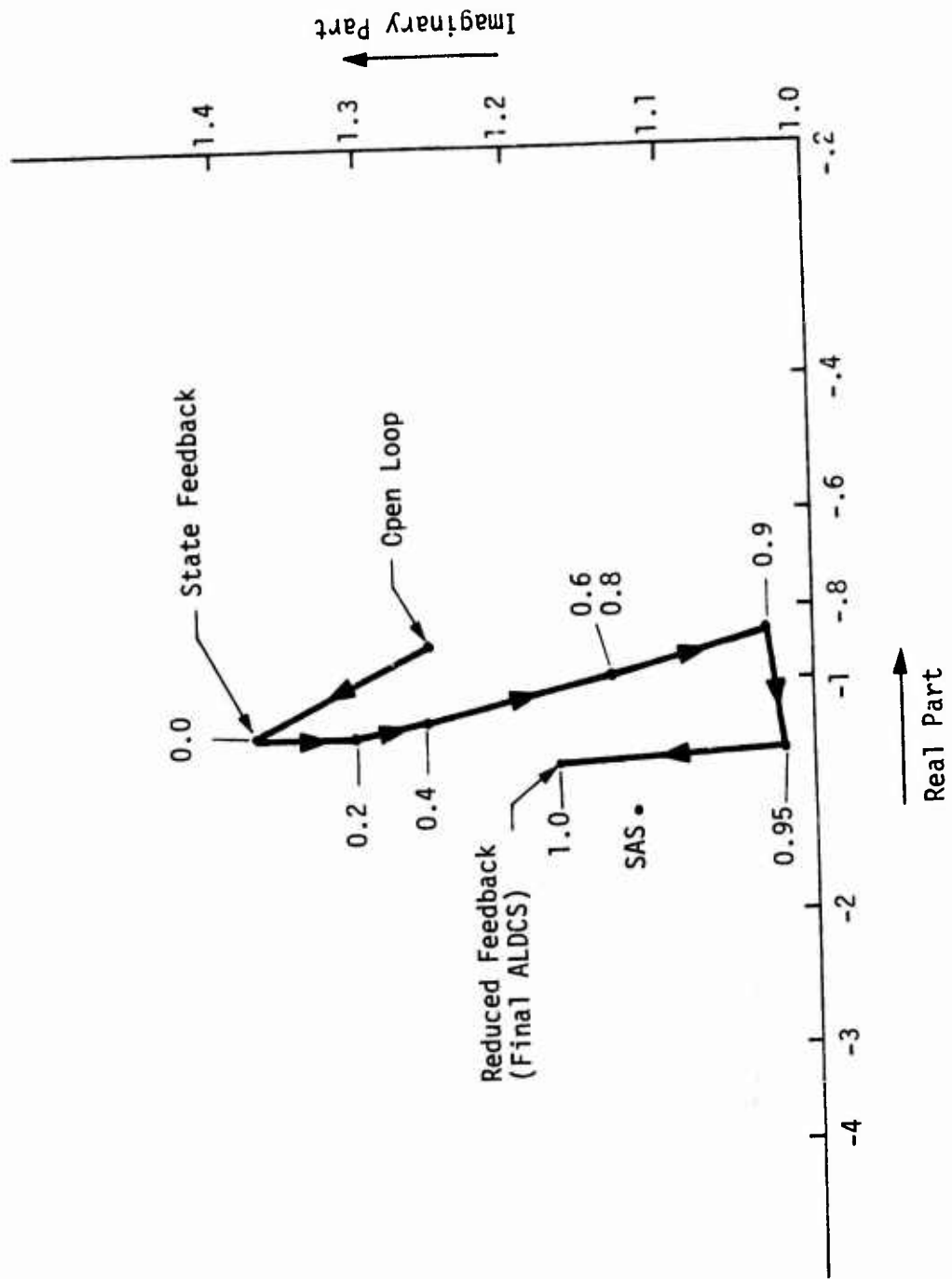
Figure 53. $(1-\lambda)$ Root Locus for Rigid Body (w, q)
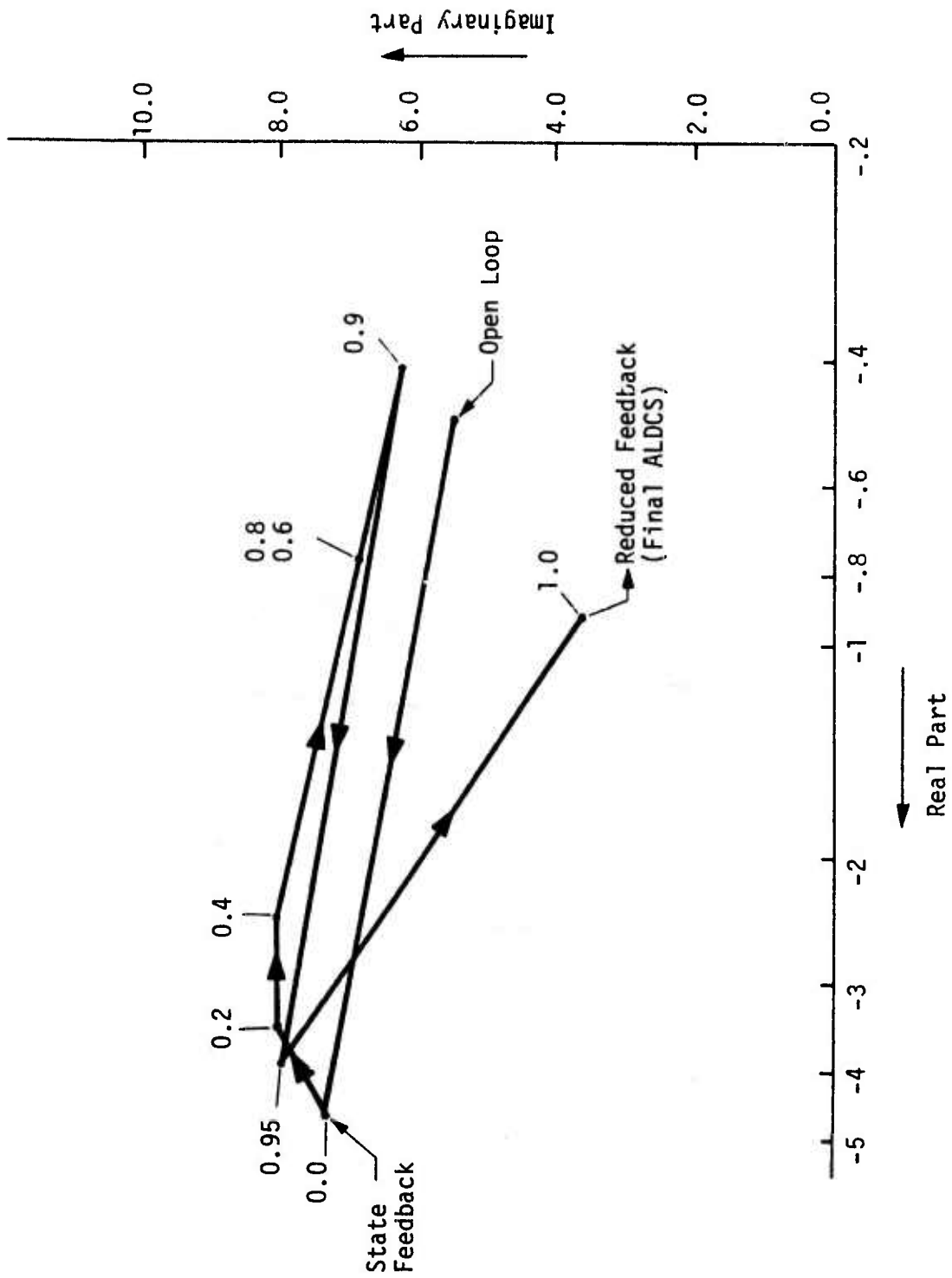
Figure 54. $(1-\lambda)$ Root Locus for First Flexure Mode (η_1)

120
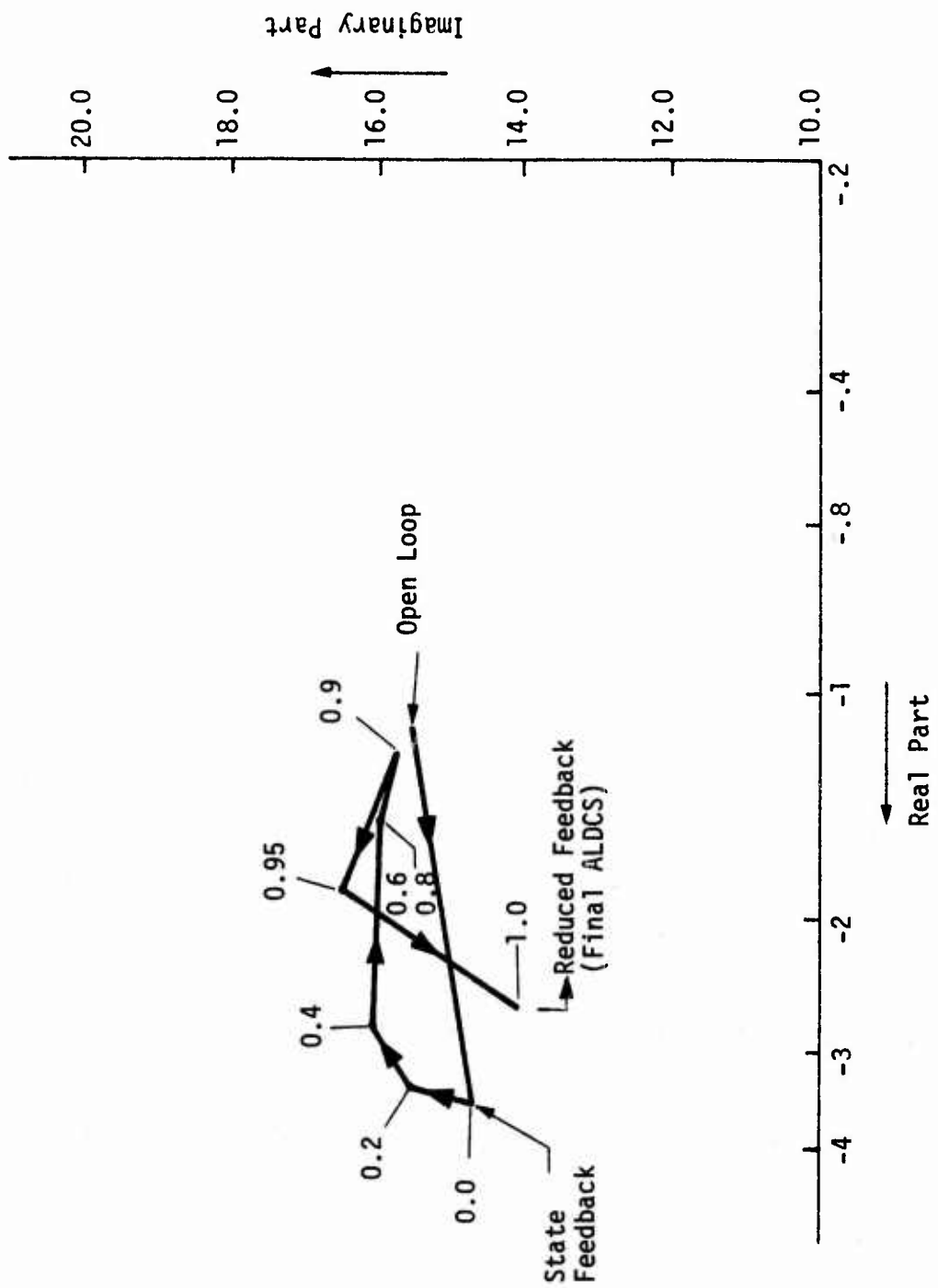
Figure 55. $(1-\lambda)$ Root Locus for Third Flexure Mode (η_3)

121

SECTION VI

IMPACT OF MODELING AND MODEL REDUCTION PROCEDURES
ON CONTROL SYSTEM DESIGN AND PERFORMANCE

Complete representations of flexible airplanes requires models of very high order (100 or more). These complete models must be used for final analysis and verification. Most control synthesis can be determined from much lower order models. The subject under discussion is how to make the best low order approximation. Best cannot be well defined. Roughly, we desire to synthesize using the low order model and hope that only minor tailoring is required to obtain comparable results on the complete model.

In the following, model reduction procedures are reviewed briefly. Then the truncation and residualization reduction procedures used in KONPACT-1 are described. This is followed by a detailed comparison of Honeywell/ GELAC and FLEXSTAB data on C-5A aircraft using the truncation and residualization operations.

REVIEW OF MODEL REDUCTION PROCEDURES

In the following, closed and open-loop approximations are discussed.

Closed-Loop

Considerable progress towards developing synthesis and analysis of the regulator problem for high order systems is presented in References 32 and 33. The plant is taken to be

$$\dot{x}_1 = A_1 x_1 + A_2 x_2 + B_1 u \tag{138}$$

$$\lambda \dot{x}_2 = A_3 x_1 + A_4 x_2 + B_2 u \tag{139}$$

where λ is a small parameter. If $\lambda = 0$, the usual residualization approximation is being made.

Synthesis and analysis are performed after invoking the quadratic performance criterion

$$J = \int_0^\infty \{y'Qy + u'Ru\} dt \tag{140}$$

where

$$y = C_1 x_1 + C_2 x_2$$

R is positive definite

Q is positive semi-definite.

Theorems and examples show continuity with respect to λ as $\lambda \to 0^+$. References 32 and 33 present the only results found on the closed-loop approximation problem. They have made considerable progress; the procedures appear to be sound, tractable, and capable of extension. These efforts should be continued toward resolving whether they can provide a better solution to control synthesis for flexible aircraft.

Open-Loop

There is a surfeit of open-loop approximation schemes to reduce the order
of large systems. Unfortunately, they have not been ranked (even for a
simple application). Promising schemes for applicability to the flexible
vehicle are discussed below.

Truncation and Residualization--With truncation, x_2 and $\dot{x}_2$ are set equal to
zero in Equation (138); Equation (139) is omitted. This approximate model
for high order systems has as its main virtue simplicity in application.
For a given reduced order model it is usually the worst.

With Schwendler and MacNeal's residualization (Reference 46), λ is set
equal to zero in Equation (139). This approximation yields exact values
with respect to the steady-state response of the large system. Further
details on these are given in Section III on Model Conditioning and in this
section.

Stable Partial-Padé Moment Matching--References 34 through 38 present rather
simple computational methods for approximating the system H(s) by an
approximate models $\hat{H}_k(s)$ where

$$X(s) = H(s)\,U(s) \tag{141}$$

$$H(s) = \frac{b_1 s^{n-1} + - - - - - - - - - - - - + b_n}{a_o s^n + a_1 s^{n-1} + - - - - - - - - - + a_n} \tag{142}$$

and

$$\hat{H}_k(s) = \frac{\hat{b}_1 s^{k-1} + - - - - - - - - - - - - - + \hat{b}_k}{\hat{a}_o s^k + \hat{a}_1 s^{n-1} + - - - - - - - - - + \hat{a}_k} \tag{143}$$

124

where

$X(s)$ = p-vector

$U(s)$ = r-vector

b_i = p x r matrices

$a_i, \hat{a}_j$ = scalars

$k < n$

The approximation $\hat{H}_k(s)$ is stable if $H(s)$ is stable.

Let the MacLaurin expansion of $H(s)$ and $\hat{H}_k(s)$ be

$$H(s) \cong \alpha_o + \alpha_1 s + \alpha_2 s^2 + - - - - \tag{144}$$

$$\hat{H}_k(s) \cong \hat{\alpha}_o + \hat{\alpha}_1 s + \hat{\alpha}_2 s^2 + - - - - - \tag{145}$$

The criteria for obtaining reduced system is to match the coefficients in (144) and (145) starting with the lower degree terms.

Another interpretation of (144) or (145) is available. For a single-input single-output system

$$\alpha_i (i!) (-1)^i = \int_o^\infty t^i h(t) \, dt \tag{146}$$

$$\triangleq \text{ the } i^{th} \text{ time-moment of } h(t)$$

where $h(t)$ is the impulse response corresponding to $H(s)$.

It is seen that this is a generalization of residualization: exact not only in the steady-state but also a good approximation at low frequencies.

Iterative Matrix Matching By Identification--Reference 39 presents an identification scheme that has been used at Honeywell to construct lower order approximations to high order models.

$$\dot{x} = Ax + Bu \tag{147}$$

$$y = Cx + Du \tag{148}$$

$$\dot{\hat{x}} = \hat{A}\hat{x} + \hat{B}u \tag{149}$$

Equation (147) is the known plant of nth order with prescribed response relationship (148). Equation (149) is an mth order approximation with $m < n$.

Both systems are forced by a prescribed u. $\hat{A}$ and $\hat{B}$ are determined to minimize quadratic cost due to error between aided and approximate response. This scheme has the advantage that it can be forced over the bandwidth over which it operates the closed-loop controls.

Single-Input Single-Output Transfer Matching--Reference 40 presents a method which has been shown to yield excellent results on particular examples. Very favorable comments have been voiced by independent users.

Given a high order transfer function

$$H(s) = K \frac{1 + a_1 s + - - - - - - - - + a_m s^m}{1 + b_1 s + - - - - - - - - + b_n s^n} \tag{150}$$

where $m < n$ which is to be approximated by

126

$$L(s) = K \frac{1 + c_1 s + - - - - - - - - - - -c_p s^p}{1 + d_1 s + - - - - - - - - - - -d_q s^q} \tag{151}$$

where

$$p < q < n$$

Define

$$\lambda(\omega) \overset{\Delta}{=} \left| \frac{H(j\omega)}{L(j\omega)} \right|^2 \tag{152}$$

The $\lambda(\omega)$ is expanded in a MacLaurin series. This leads to a set of non-linear algebraic equations for determining c_i and d_i.

Multiple-Input Multiple-Output Transfer Matching--Reference 41 presents results of a procedure that could be used for developing low order matrix transfer function or state equation approximations. The user specifies (by the data input) the bandpass over which the approximations are to be made.

Reduced Models from Noisy Data--References 42 through 44 discuss open-loop low order approximations in a noisy environment. They approximate with respect to noise in a manner analogous to frequency domain approximations.

Hierarchal Control--Hierarchal control is concerned with control of large systems. The flexible aircraft is certainly represented as a large system. Hierarchal control makes synthesis tractable, in part, by special

127

decomposition techniques. Recently, two treatises have been published (References 48 and 49); they should be reviewed for applicability to the flexure control problem.

TRUNCATION OF LARGE MODELS CONTAINING RATES

In general, the physics of dynamical processes generate a model in the form of

$$
\begin{bmatrix} \dot{x}_1 \\ \dot{x}_2 \end{bmatrix} = \begin{bmatrix} A_{11} & A_{12} \\ A_{21} & A_{22} \end{bmatrix} \begin{bmatrix} x_1 \\ x_2 \end{bmatrix} + \begin{bmatrix} B_1 \\ B_2 \end{bmatrix} u \tag{153}
$$

$$
r = \begin{bmatrix} C_{11} & C_{12} \end{bmatrix} \begin{bmatrix} x_1 \\ x_2 \end{bmatrix} + \begin{pmatrix} C_{21} & C_{22} \end{pmatrix} \begin{bmatrix} \dot{x}_1 \\ \dot{x}_2 \end{bmatrix} + D u
$$

in which the response vector contain state rates.

In this case, care should be exercised in obtaining the truncated model. The truncated model can be obtained either before or after differentiation with different results. It is recommended that the response data matrices C_{11}, C_{12}, C_{21}, and C_{22} should not be modified before the truncation operation.

Case I: Truncation Before Differentiation

First the system described by equations (153) is truncated to obtain

$$\dot{x}_1 = A_{11} \, x_1 + B_1 \, u$$

$$r = C_{11} \, x_1 + C_{21} \, \dot{x}_1 + Du \tag{154}$$

and then substitution for $\dot{x}_1$ is made to obtain the truncated state model

$$\dot{x}_1 = A_{11} \, x_1 + B_1 u$$

$$r = (C_{11} + C_{21} \, A_{11}) \, x_1 + (C_{21} \, B_1 + D)u \tag{155}$$

Case II: Truncation After Differentiation

First the substitution of state rates into response equation is made

$$\begin{bmatrix} \dot{x}_1 \\ \dot{x}_2 \end{bmatrix} = \begin{bmatrix} A_{11} & A_{12} \\ A_{21} & A_{22} \end{bmatrix} \begin{bmatrix} x_1 \\ x_2 \end{bmatrix} + \begin{bmatrix} B_1 \\ B_2 \end{bmatrix} u$$

$$r = \left[\begin{bmatrix} (C_{11} & C_{12}) \end{bmatrix} + \begin{bmatrix} (C_{21} & C_{22}) \end{bmatrix} \begin{bmatrix} A_{11} & A_{12} \\ A_{21} & A_{22} \end{bmatrix} \right] \begin{bmatrix} x_1 \\ x_2 \end{bmatrix} \tag{156}$$

$$+ \left[\begin{bmatrix} (C_{21} & C_{22}) \end{bmatrix} \begin{bmatrix} B_1 \\ B_2 \end{bmatrix} + D \right] u$$

and then Equation (156) is truncated

$$\dot{x}_1 = A_{11} x_1 + B_1 u$$

$$r = (C_{11} + C_{21} A_{11} + C_{22} A_{21}) x_1 \tag{157}$$

$$+ (C_{21} B_1 + C_{22} B_2 + D) u$$

As can be seen, the truncated models represented by Equations (155) and (157) differ in the response equations. For good steady-state response, the differentiation of response must follow the reduction process as presented in Case I. In the residualization, models obtained by either methods are identical.

In Reference 4, truncated models were obtained as described in Case I, before differentiation because of the availability of C-5A model generating program, generating data in the form of (153). In the present study the response data in the form of (156) was available only. For this reason, the responses containing state rates are in error in steady-state for truncated models.

Effect of Truncation on Response Rates

Consider the system described by

$$\begin{bmatrix} \dot{x}_1 \\ \dot{x}_2 \end{bmatrix} = \begin{bmatrix} A_{11} & A_{12} \\ A_{21} & A_{22} \end{bmatrix} \begin{bmatrix} x_1 \\ x_2 \end{bmatrix} + \begin{bmatrix} B_1 \\ B_2 \end{bmatrix} u \tag{158}$$

$$r = \begin{bmatrix} (C_{11} & C_{12}) \end{bmatrix} \begin{bmatrix} x_1 \\ x_2 \end{bmatrix}$$

where r is the set of responses whose rates are required as design responses. The response rates can be obtained either before or after truncation.

Response Rates Before Truncation--Response equation is differentiated first.

$$\dot{r} = \begin{bmatrix} (C_{11} & C_{12}) \end{bmatrix} \begin{bmatrix} \dot{x}_1 \\ \dot{x}_2 \end{bmatrix} \tag{159}$$

Then the state rates are substituted from (158) and the resulting equations are truncated.

This yields

$$\dot{x}_1 = A_{11} x_1 + B_1 u \tag{160}$$

$$\dot{r} = (C_{11} A_{11} + C_{12} A_{21}) x_1 + (C_{11} B_1 + C_{12} B_2) u$$

Response Rates After Truncation--The model is truncated first yielding

$$\dot{x}_1 = A_{11} \, x_1 + B_1 u$$

$$r = C_{11} \, x_1 \tag{161}$$

Then the truncated response equation is differentiated and the truncated
state rates are substituted from (161) yielding

$$\dot{r} = C_{11} \, \dot{x}_1 = (C_{11} \quad A_{11}) \, x_1 + (C_{11} \, B_1) \, u \tag{162}$$

If the steady-state value of the response rate of the reduced system is
required to be zero, then the truncated model represented by Equations
(161) and (162) should be used. This means that one should obtain the
response rates after obtaining the reduced model. In the present study,
response rates were obtained before truncation. Because of this some of
the response rates in the truncated model do not satisfy steady-state
requirements.

Wind Simplification

All previous discussion has been concerned with simplifying the flexible
body representation. This is the primary concern. However, time and
money could also be saved by using the simplest wind (and wind distribution)
filter that met requirements. For FLEXSTAB C-5A ALDCS effort, a 7th
order filter was used for both synthesis and analysis. It is believed a much
lower order would have been adequate for the relatively expensive synthesis
effort.

132

In summary, a cursory survey made in this study indicates that there is a dearth of closed-loop and a surfeit of open-loop methods for model reduction. We recommend that an attempt be made to extend the closed-loop scheme presented in Reference 32 into an engineering tool to reduce design computation time. Furthermore, the open-loop methods should be ranked for potential applicability and the more promising refined and incorporated into KONPACT.

C-5A MODEL COMPARISON (FLEXSTAB AND HONEYWELL/GELAC)

The Honeywell/GELAC 79th order model (HG79) for the cruise flight condition was made available at Honeywell for this program. The 42nd order model (HG42) is obtained by truncation of the Wagner dynamics. Because of the way the unsteady effects were modeled in the 79th order model, the 42nd order reduced model had slight errors with respect to the original Honeywell/GELAC 42nd order model. Table 15 shows an eigenvalue comparison between these two models for the bending modes. Note that HG42 used in this study has less damping than the original model. This required more iterations on the reduced optimal course design.

Table 15. Root Comparison of Free A/C with HG42
and Original HG42 Models

Association	HG42 (used in this study)		HG42 (used in Ref. 4)	
	ωn	ζ	ωn	ζ
$\eta 1$, $\dot{\eta}1$	5.9	.086	5.9	.147
$\eta 2$, $\dot{\eta}2$	11.4	.021	11.4	.021
$\eta 3$, $\dot{\eta}3$	14.5	.028	14.5	.034
$\eta 4$, $\dot{\eta}4$	16.1	.044	16.0	.066
$\eta 5$, $\dot{\eta}5$	17.5	.023	17.5	.024

Air Force supplies C-5A data for the cruise flight condition in the form of cards (simulator deck data) (Reference 2, 5, and 6). This data was converted to state space data and augmented by the gust model and actuators (used in the Honeywell/Gelac HG42 model). The resulting system was scaled and shuffled to bring it to correspondence with Honeywell/GELAC data. This FLEXSTAB model (F42) is then compared and correlated to the Honeywell/GELAC model (HG42).

In the following the open-loop comparisons are made.

- Steady-state values
- rms values due to wind gust
- Roots (Eigenvalues)
- PSD plots due to wind gust and white noise
  inputs to aileron and inboard elevator

For these comparisons the FLEXSTAB inboard load axis system (see Figure 4) was rotated 18.6° right wing tip aft to be comparable to the HG42 model. This rotation was performed at the completion of this study. This correction is reflected in Tables 16, 17, 27b, 29 only and Figures 57, 59, 61, 63, 65, and 67 only.

Table 16 compares the steady-state 1G maneuver responses for the HG42 and F42 models. The rigid body responses (w, q, α) compare very favorably between the two models. Elevator deflection requirements for the HG42 model are 50 percent larger than those for the F42 model; this is to be expected since the HG42 model data have been corrected for the disc effects. The bending and torsion moment data also agree reasonably closely. The numerical comparisons between the bending moments and torsion moments are very good, with an exception being that of T1 and T2. A magnitude difference is to be expected.

134

Table 16. Steady-State Comparison of Free A/C with HG42 and F42 Models for 1G Maneuver

VARIABLE	DESCRIPTION	UNIT	HG42	F42
X(1)	HEAVE VELOCITY	INCH/SEC	.6364E+00	.5130E+13
X(2)	PITCH RATE	INCH/SEC	.7215E+02	.7212E+02
X(3)	ETA1DOT BENDING MODE VELOCITY	INCH/SEC	-.6134E-11	0.
X(4)	ETA2DOT BENDING MODE VELOCITY	INCH/SEC	0.	-.1147E-10
X(5)	ETA3DOT BENDING MODE VELOCITY	INCH/SEC	.2765E-11	.2855E-10
X(6)	ETA4DOT BENDING MODE VELOCITY	INCH/SEC	0.	0.
X(7)	ETA5DOT BENDING MODE VELOCITY	INCH/SEC	0.	0.
X(8)	ETA6DOT BENDING MODE VELOCITY	INCH/SEC	0.	.5077E-11
X(9)	ETA7DOT BENDING MODE VELOCITY	INCH/SEC	.1731E-11	.4537E-11
X(10)	ETA8DOT BENDING MODE VELOCITY	INCH/SEC	.1373E-11	.1219E-10
X(11)	ETA9DOT BENDING MODE VELOCITY	INCH/SEC	0.	-.2220E-11
X(12)	ETA10DOT BENDING MODE VELOCITY	INCH/SEC	.5364E-12	.1553E-10
X(13)	ETA11DOT BENDING MODE VELOCITY	INCH/SEC	.4597E-12	-.5773E-12
X(14)	ETA12DOT BENDING MODE VELOCITY	INCH/SEC	-.7199E-15	.6572E-11
X(15)	ETA13DOT BENDING MODE VELOCITY	INCH/SEC	-.1467E-11	-.1280E-10
X(16)	ETA14DOT BENDING MODE VELOCITY	INCH/SEC	-.2715E-11	.5155E-12
X(17)	ETA15DOT BENDING MODE VELOCITY	INCH/SEC	.2195E-11	-.2035E-11
X(18)	ETA1 BENDING MODE DEFLECTION	INCH	-.3532E+02	-.2637E+03
X(19)	ETA2 BENDING MODE DEFLECTION	INCH	-.4967E+00	-.1455E+02
X(20)	ETA3 BENDING MODE DEFLECTION	INCH	.2375E+01	-.7805E+01
X(21)	ETA4 BENDING MODE DEFLECTION	INCH	-.4271E+01	.4513E+01
X(22)	ETA5 BENDING MODE DEFLECTION	INCH	-.2564E+00	-.4707E+01
X(23)	ETA6 BENDING MODE DEFLECTION	INCH	.9363E+00	.3869E+01
X(24)	ETA7 BENDING MODE DEFLECTION	INCH	.3939E+00	.3561E+00
X(25)	ETA8 BENDING MODE DEFLECTION	INCH	-.2436E+00	-.2202E+01
X(26)	ETA9 BENDING MODE DEFLECTION	INCH	-.5249E+00	-.5279E+00
X(27)	ETA10 BENDING MODE DEFLECTION	INCH	.1470E+00	-.3135E+01
X(28)	ETA11 BENDING MODE DEFLECTION	INCH	.5525E+00	-.5513E+00
X(29)	ETA12 BENDING MODE DEFLECTION	INCH	-.1746E-03	.2011E+01
X(30)	ETA13 BENDING MODE DEFLECTION	INCH	-.1752E+00	.1947E+01
X(31)	ETA14 BENDING MODE DEFLECTION	INCH	.3515E+00	-.1341E+00
X(32)	ETA15 BENDING MODE DEFLECTION	INCH	-.3276E+00	-.2168E+00
X(33)	DELA AILERON POSITION	RADIAN	0.	0.
X(34)	DELEI INBOARD ELEVATOR POSITION	RADIAN	-.1163E+00	-.7370E-01
X(35)	DELEO OUTBOARD ELEVATOR POSITION	RADIAN	-.1163E+00	-.7370E-01
X(36)	P1 KUSSNER STATE (NT)	FEET/SEC	0.	0.
X(37)	P2 TRANSPORT DELAY STATE (H)	FEET/SEC	0.	0.
X(38)	P3 TRANSPORT DELAY STATE (T)	FEET/SEC	0.	0.
X(39)	P4 TRANSPORT DELAY STATE (T)		0.	0.
X(40)	P5 KUSSNER STATE (H)		0.	0.
X(41)	P5 WIND FILTER STATE		0.	0.
X(42)	W5 WIND GUST STATE		0.	0.

135

Table 16. Steady-State Comparison of Free A/C with HG42 and F42 Models for 1G Maneuver (Concluded)

VARIABLE	DESCRIPTION	UNIT	HG42	F42
RE 1)	BENDING MOMENT (122.4)	INCH-LB	.4975E+03	.6651E+08
RE 2)	TORSION MOMENT (121.4)	INCH-LB	.7931E+07	.5501E+07
RE 3)	BENDING MOMENT (323.4)	INCH-LB	.4272E+08	.4073E+18
RE 4)	TORSION MOMENT (329.5)	INCH-LB	.3814E+07	.1596E+07
RE 5)	BENDING MOMENT (577.3)	INCH-LB	.2945E+08	.1982E+08
RE 6)	TORSION MOMENT (577.3)	INCH-LB	.1738E+07	.1734E+07
RE 7)	BENDING MOMENT (748.3)	INCH-LB	.1043E+08	.1069E+08
RE 8)	TORSION MOMENT (748.3)	INCH-LB	.2963E+07	.2289E+07
RE 9)	BENDING MOMENT (923.5)	INCH-LB	.4205E+07	.4413E+07
RE ?)	TORSION MOMENT (923.5)	INCH-LB	.153RE+07	.1195E+07
RE(11)	D/DT OF Q1 BENDING MOMENT	INCH-LB /SEC	-.2167E-04	-.5289E-05
RE(12)	D/DT OF T1 TORSION MOMENT	INCH-LB /SEC	.5502E-05	-.1122E-04
RE(13)	D/DT OF Q2 BENDING MOMENT	INCH-LB /SEC	-.1451E-04	-.1700E-04
RE(14)	D/DT OF T2 TORSION MOMENT	INCH-LB /SEC	-.4853E-05	-.4822E-05
RE(15)	D/DT OF Q3 BENDING MOMENT	INCH-LB /SEC	-.6251E-05	.4254E-05
RE(16)	D/DT OF T3 TORSION MOMENT	INCH-LB /SEC	-.1344E-04	-.1027E-04
RE(17)	D/DT OF Q4 BENDING MOMENT	INCH-LB /SEC	-.1434E-05	-.4983E-07
RE(18)	D/DT OF T4 TORSION MOMENT	INCH-LB /SEC	-.2290E-04	-.1243E-04
RE(19)	D/DT OF Q5 BENDING MOMENT	INCH-LB /SEC	.3845E-05	.3592E-05
RE(2)	D/DT OF T5 TORSION MOMENT	INCH-LB /SEC	-.1574E-04	-.1455E-04
RE(21)	ALPHA ANGLE OF ATTACK	RADIAN	.6983E-01	.6950E-01
RE(22)	QCG PITCH RATE AT CG	RADIAN/SEC	.4377E-01	.4375E-01
RE(23)	DELA AILERON POSITION	RADIAN	0.	0.
RE(24)	DFLEI INBOARD ELEVATOR POSITION	RADIAN	-.1195E+00	-.7370E-01
RE(25)	DELEO OUTBOARD ELEVATOR POSITION	RADIAN	-.1195E+00	-.7370E-01
RE(26)	W HEAVE VELOCITY	INCH/SEC	.6139E+03	.6139E+03
RE(27)	D/DT OF W HEAVE VELOCITY	INCH/SEC /SEC	-.3439E-11	-.1300E-11
RE(28)	A21F ACCELEROMETER OUTPUT (21)	1G	-.1003E+01	-.1001E+01
RE(29)	A21R ACCELEROMETER OUTPUT (21)	1G	-.1000E+01	-.1001E+01
RE(30)	AFUS FUSELAGE ACCELEROMETER OUTPUT	1G	-.1001E+01	-.1001E+01
RE(31)	TFUS PITCH RATE GYRO OUTPUT	RADIAN/SEC	.4377E-01	.4377E-01
UI 1)	UDELA AILERON CONTROL INPUT	RADIAN	0.	0.
UI 2)	UDELEI INBOARD ELEVATOR CONTROL INPUT	RADIAN	-.1195E+00	-.7370E-01
UI 3)	UDELEO OUTBOARD ELEVATOR CONTROL INPUT	RADIAN	-.1195E+00	-.7370E-01
UI 4)	ETAG WHITE NOISE INPUT TO GUST MODEL	INCH/SEC	0.	0.

The torsional moments are about an axis parallel to the wing elastic axis. The magnitudes of the torsional moments are extremely dependent on the chordwise location of the net load center of pressure and therefore are extremely math model dependent. Sensors outputs (A21F, A21R, AFUS, and TFUS) are exactly the same as should be expected. The first hint that there are major differences between the two models comes in viewing the bending mode selection data. Magnitudes and signs just simply do not agree any place. This indicates (but does not prove) that there may be significant difference between the two models.

HG42 and F42 model free aircraft rms responses due to wind gust are compared in Table 17. Generally, the comparisons indicate that the F42 model is matching the HG42 model well. There are two significant discrepancies: the HG42 T2 torsion moment and the accelerometer outputs A21F and A21R are larger than the F42 data. Since exactly the same gust field is "striking" each model, data indicate that the HG42 model is more responsive to gust. Other than that, the comparisons are very good. This would indicate that the F model is a good approximation to the HG model for the wind gust inputs.

Table 17. RMS Comparison of Free A/C with HG42 and F42 Models for 1 FPS Disturbance on η_g

VARIABLE	DESCRIPTION	UNIT	HG42	F42
R(1)	B1 BENDING MOMENT (127.4)	INCH-LB	.1145E+07	.8042E+06
R(2)	T1 TORSION MOMENT (127.4)	INCH-LB	.1372E+06	.4906E+05
R(3)	B2 BENDING MOMENT (523.8)	INCH-LB	.7267E+06	.5333E+06
R(4)	T2 TORSION MOMENT (523.8)	INCH-LB	.7517E+05	.2635E+05
R(5)	B3 BENDING MOMENT (577.8)	INCH-LB	.3722E+06	.2642E+06
R(6)	T3 TORSION MOMENT (577.8)	INCH-LB	.4454E+05	.2564E+05
R(7)	B4 BENDING MOMENT (748.3)	INCH-LB	.2047E+06	.1442E+06
R(8)	T4 TORSION MOMENT (748.3)	INCH-LB	.4954E+05	.3198E+05
R(9)	B5 BENDING MOMENT (323.5)	INCH-LB	.9079E+05	.6035E+05
R(10)	T5 TORSION MOMENT (323.5)	INCH-LB	.2777E+05	.1659E+05
R(11)	D/DT OF (B1 BENDING MOMENT)	INCH-LB /SEC	.2769E+07	.2037E+07
R(12)	D/DT OF (T1 TORSION MOMENT)	INCH-LB /SEC	.5395E+06	.5231E+06
R(13)	D/DT OF (B2 BENDING MOMENT)	INCH-LB /SEC	.1937E+07	.1317E+07
R(14)	D/DT OF (T2 TORSION MOMENT)	INCH-LB /SEC	.4812E+06	.5613E+05
R(15)	D/DT OF (B3 BENDING MOMENT)	INCH-LB /SEC	.1136E+07	.6641E+06
R(16)	D/DT OF (T3 TORSION MOMENT)	INCH-LB /SEC	.3589E+06	.5779E+05
R(17)	D/DT OF (B4 BENDING MOMENT)	INCH-LB /SEC	.7981E+06	.3548E+06
R(18)	D/DT OF (T4 TORSION MOMENT)	INCH-LB /SEC	.1507E+06	.7215E+05
R(19)	D/DT OF (B5 BENDING MOMENT)	INCH-LB /SEC	.4235E+06	.1535E+06
R(20)	D/DT OF (T5 TORSION MOMENT)	INCH-LB /SEC	.1020E+05	.3858E+05
R(21)	ALPHA ANGLE OF ATTACK	RADIAN	.1905E-02	.1654E-02
R(22)	DSS PITCH RATE AT 25	RADIAN/SEC	.1175E-02	.6583E-03
R(23)	DELA AILERON POSITION	RADIAN	.5855E-14	.5855E-15
R(24)	DELEI INBOARD ELEVATOR POSITION	RADIAN	.2024E-15	.7915E-15
R(25)	DELEO OUTBOARD ELEVATOR POSITION	RADIAN	.2012E-15	.1443E-14
R(26)	W HEAVE VELOCITY	INCH/SEC	.1762E+02	.1379E+02
R(27)	D/DT OF (W HEAVE VELOCITY)	INCH/SEC /SEC	.1159E+02	.8261E+01
R(28)	A21F ACCELEROMETER OUTPUT (21)	G	.2450E-01	.1249E-01
R(29)	A21R ACCELEROMETER OUTPUT (21)	G	.2725E-01	.1267E-01
R(30)	AFUS FUSELAGE ACCELEROMETER OUTPUT	G	.1431E-01	.1141E-01
R(31)	TFUS PITCH RATE GYRO OUTPUT	RADIAN/SEC	.1239E-02	.7041E-03

Table 18. Root Comparison of Free A/C with HG79, HG42 and F42 Models

Association	HG79		HG42		F42	
	Real ω_n	ζ	Real ω_n	ζ	Real ω_n	ζ
$\dot{\theta}$, α	1.7070	0.4617	1.667	0.4976	1.550	0.5775
η_1, $\dot{\eta}_1$	5.9350	0.0803	5.932	0.0861	5.528	0.0893
η_2, $\dot{\eta}_2$	11.4639	0.0211	11.460	0.0207		
η_3, $\dot{\eta}_3$	14.7083	0.0390	14.490	0.0277	15.600	0.0693
η_4, $\dot{\eta}_4$	16.0974	0.0439	16.060	0.0438	17.230	0.0471
η_5, $\dot{\eta}_5$	17.4729	0.0233	17.470	0.0234	18.370	0.0241
η_6, $\dot{\eta}_6$	19.2202	0.0265	19.110	0.0231	19.35	0.0313
η_7, $\dot{\eta}_7$	21.4329	0.0308	21.510	0.0328	22.140	0.0482
η_8, $\dot{\eta}_8$	27.3576	0.0206	27.340	0.0205	29.490	0.0219
η_9, $\dot{\eta}_9$	35.3109	0.0285	35.340	0.0283	33.510	0.0284
η_{10}, $\dot{\eta}_{10}$	37.3090	0.0232	37.350	0.0234	34.300	0.0375
η_{11}, $\dot{\eta}_{11}$	40.9267	0.0539	41.140	0.0574	38.590	0.0289
η_{12}, $\dot{\eta}_{12}$	41.6351	0.0193	41.610	0.0193	43.740	0.0891
η_{13}, $\dot{\eta}_{13}$	44.9485	0.0246	44.780	0.0221	48.140	0.0464
η_{14}, $\dot{\eta}_{14}$	45.9438	0.0185	45.250	0.0167	51.240	0.0242
η_{15}, $\dot{\eta}_{15}$	52.7879	0.0203	52.370	0.0199	75.320	0.0461
η_{16}, $\dot{\eta}_{16}$					80.010	0.0211

Table 18. Root Comparison of Free A/C with HG79, HG42 and F42 Models (Concluded)

Association	HG79		HG42		F42	
	Real ω_n	ζ	Real ω_n	ζ	Real ω_n	ζ
δ_a	-6.0000		-6.000		-6.000	
δ_{ei}	-7.5000		-7.500		-7.500	
δ_{eo}	-7.5000		-7.500		-7.500	
Gust Filter	-0.2100		-0.210		-0.210	
Gust Filter	-0.2100		-0.210		-0.210	
Wing Kussner	-9.1560		-9.156		-9.156	
1st Order Delay	-13.4270		-13.427		-13.427	
2nd Order Delay	9.8020	0.8165	9.802	0.8165	9.802	0.8165
Tail Kussner	-18.4930		-18.493		-18.493	
Wing Wagner (19)	-9.1560					
Tail Wagner (20)	-18.493					

140

In Table 18 the roots of HG79, HG42 and F42 aircraft models are compared. The root values are quite close. They are good enough so that based on these data alone, one would expect that there were only small differences between the HG and F model.

Figures 56 through 79[*]present the power density plots for HG42 model and F42 model. The rms values as obtained from PSD plots are different from those obtained from covariance analysis. This difference is due to frequency factor in the rms values computed by integrating the PSD plots as given below.

$$\text{rms}_{\text{PSD}} = \sqrt{2\pi} \ \text{rms}_{\text{COV}}$$

The PSD plots provide two valuable services. First, they are an excellent means of checking models to ascertain that errors have not been caused by the data handling procedures. Second, the qualitative nature of the plots provide a good indication of where the problem areas are.

The PSD plots for HG42 model, as presented here, compare very well with the previous PSD plots obtained during previous ALDCS work (Reference 4). This shows that the data handling in KONPACT with the HG42 model is accurate.

The first comparison to note between FLEXSTAB and Honeywell/GELAC models is to compare Figures 56 and 57 for the bending moment due to wind gusts. For the HG42 model resonant peaks occur at rigid body near 0.2 cps and also at the first mode, at somewhat less than 1 cps.

---

[*] Figures 56 through 151 appear behind the main text of this section.

The data for the F42 model show a lot of resonance for only the rigid body. Similarly, the bending moment due to the elevator shows for the HG42 airplane (in Figure 58) has resonant peaks at the rigid body first and third bending modes. The F42 model in Figure 59 shows a majority of the resonance at the rigid body, a neglectable amount for the first mode, and then apparently picks up a fourth mode. Figures 60 and 61 show that the HG42 model has significant first and third mode energy; the F42 model has significant resonant peaks for the first flexture mode only. Torsional plots, due to gusts for the HG42 and F42 models in Figures 62 and 63, show that the HG42 aircraft has rigid body, first and third flexure resonant peaks; the F42 model has resonant peaks in the rigid body area only. Torsion, due to the elevator, is shown in Figures 64 and 65. For the HG42 model there are resonant peaks for the rigid body, the first mode, second mode, third mode, fourth, sixth, seventh and eighth mode; for the F42 model, there are resonant peaks for the rigid body, first mode, fourth mode, and seventh mode; these latter frequencies are very low relative to the values that we see on the HG42 model. Torsion due to aileron is shown in Figures 66 and 67. For the HG42 model, there are resonant peaks for the rigid body, first, second, third, sixth, seventh, and thirteenth mode; for the F42 model, there is also an additional resonant peak for the fifth mode.

The third flexure mode response due to gusts is shown in Figures 68 and 69. The HG42 model has resonant peaks for rigid body, first, third, and fourth modes; the F42 model has resonant peaks for the rigid body only. The third flexure mode due to elevator are shown in Figures 70 and 71. For the HG42 model, there are resonant peaks for rigid body, third and fourth modes; and the F42 model has it for the rigid body, first and third modes. For the

142

third flexure mode bending due to aileron, plots are shown in Figures 72 and 73. There is qualitative agreement between the two sets of data, except that the rms values differ by a factor of $\sqrt{2\pi}$. Pitch rate responses due to gusts are shown in Figures 74 and 75. The comparisons show that the only responses due to the rigid body are quite good. Pitch rate due to the inboard elevator are shown in Figures 76 and 77. The comparisons are very good. Pitch rate due to ailerons are shown in Figures 78 and 79 and again the comparisons are quite good, although there is a little more first and third mode response in the HG42 data.

Further open-loop comparison on the reduced (residualized) models for FLEXSTAB and Honeywell/GELAC is given in the next subsection.

RESIDUALIZATION AND TRUNCATION STUDY ON FLEXSTAB MODEL

The 42nd order FLEXSTAB model is used to obtain three different models of 24th order for residualization and truncation study. The names of the models and the procedure to obtain them are shown in Table 19.

Table 19. Models for Residualization and Truncation Study
Obtained from the F42 Model

Model	Procedure
*F24RR	Residualize states, responses and sensors.
*F24RT	Residualize states and responses and truncate sensors.
*F24TT	Truncate states, responses and sensors.

*Note the inboard bending moments (B1, T1) (for the F24RR, F24RT and F24TT models) are about the axis system shown in Figure 4.

143

In addition, these models are also compared with HG24RR obtained from HG42 model. First, open-loop (free aircraft) results are presented and then the closed-loop (ALDCS) results are presented.

The following performance measures are used for comparison:

- Steady-state values

- rms values due to wind and pilot

- Roots (Eigenvalues)

- Time response plots.

Open-Loop Results

Table 20 compares the steady-state free aircraft 1G maneuver responses for the F24RR, F24RT, and F24TT models. The quantities w, α, q, flexure modes, and bending moments compare favorably among all models. Table 21 illustrates the effect of residualization and truncation on the steady-state value of sensors. (Note that truncation here means truncation after differentiation.) In Reference 4, there was much closer correspondence among the RR, RT, and TT models. (There, truncation was done before differentiation.) Also note that the steady-state value of T5 for the F24TT model is about 20 times lower than that for the other models. (This again is due to truncation after differentiation operation.) This fact was not known before this study was undertaken.

One other significant thing to note is that the steady-state values of the bending and torsion moment rates for F24TT model are not zero as should be expected. For this reason the response rates should be obtained after the reduced

144

Table 20. Steady-State Comparison of Free A/C with F24RR, F24RT
and F24TT Models for 1G Maneuver

VARIABLE	DESCRIPTION	UNIT	F24RR	F24RT	F24TT
X(1)	W	HEAVE VELOCITY	INCH/SEC	.6130E+03	.6130E+03	.5768E+03
X(2)	Q	PITCH RATE	INCH/SEC	.7212E+02	.7212E+02	.7125E+02
X(3)	ETA1DOT	BENDING MODE VELOCITY	INCH/SEC	.1135E-10	.1135E-10	0.
X(4)	ETA2DOT	BENDING MODE VELOCITY	INCH/SEC	-.8499E-11	-.8499E-11	-.8581E-11
X(5)	ETA3DOT	BENDING MODE VELOCITY	INCH/SEC	.2116E-10	.2116E-10	.3138E-10
X(6)	ETA4DOT	BENDING MODE VELOCITY	INCH/SEC	0.	0.	0.
X(7)	ETA5DOT	BENDING MODE VELOCITY	INCH/SEC	-.7306E-11	-.7306E-11	-.3677E-11
X(8)	ETA6DOT	BENDING MODE VELOCITY	INCH/SEC	-.2437E+03	-.2437E+03	-.2444E+03
X(9)	ETA1	BENDING MODE DEFLECTION	INCH	-.1416E+02	-.1416E+02	-.1423E+02
X(10)	ETA2	BENDING MODE DEFLECTION	INCH	-.7806E+01	-.7806E+01	-.7745E+01
X(11)	ETA3	BENDING MODE DEFLECTION	INCH	.4618E+01	.4618E+01	.4532E+01
X(12)	ETA4	BENDING MODE DEFLECTION	INCH	.4727E+01	.4727E+01	.4485E+01
X(13)	ETA5	BENDING MODE DEFLECTION	INCH	.3869E+01	.3869E+01	.3611E+01
X(14)	ETA6	BENDING MODE DEFLECTION	INCH	.167E-14	.5475E-14	.5855E-14
X(15)	DFLA	AILERON POSITION	RADIAN	-.7170E-01	-.7373E-01	-.7370E-01
X(16)	DELEI	INBOARD ELEVATOR POSITION	RADIAN	-.1669E+00	-.6527E+00	-.6110E+00
X(17)	A21RL	LAGGED NORMAL ACCELERATION	1G	-.3859E+05	-.3859E+05	-.7812E+05
X(18)	MLC1	FWL STATE MLC FOR AILERON		-.826E+02	-.3231E+03	-.2975E+03
X(19)	GLAF	GUST LOAD ALLEVIATION FILTER		-.7371E-01	-.7375E-01	-.7375E-01
X(20)	DELEO	OUTBOARD ELEVATOR POSITION	RADIAN			
X(21)	B	PILOT FILTER		-.7371E-01	-.7376E-01	-.737 E-01
X(22)	P1	KJSSVER STATE (NT)	FEET/SEC	0.	0.	0.
X(23)	P2	TRANSPORT DELAY STATE (W)	FEET/SEC	0.	0.	0.
X(24)	P3	TRANSPORT DELAY STATE (T)	FEET/SEC	0.	0.	0.
X(25)	P4	TRANSPORT DELAY STATE (T)		0.	0.	0.
X(26)	P5	KJSSVER STATE (W)		0.	0.	0.
X(27)	P6	WIND FILTER STATE		0.	0.	0.
X(28)	WG	WIND GUST STATE		0.	0.	0.

145

Table 20. Steady-State Comparison of Free A/C with F24RR, F24RT and F24TT Models for 1G Maneuver (Continued)

VARIABLE	DESCRIPTION		UNIT		F24RR	F24RT	F24TT
RC 1)	MLC1	FUL STATE MLC FOR AILERON	IN2-LB		-.3859E-05	-.3859E-05	-.3812E-05
RC 2)	B1	BENDING MOMENT (120.4)	IN2-LB		.6479E-08	.6479E-08	.6475E-08
RC 3)	T1	TORSION MOMENT (120.4)	IN2-LB		-.1600E+08	-.1600E-08	-.1355E+08
RC 4)	TFUS	PITCH RATE GYRO OUTPUT	RADIAN/SEC		.4377E-01	.4378E-01	.4326E-01
RC 5)	B2	BENDING MOMENT (323.5)	IN2-LB		.4173E+08	.4173E+08	.4281E+08
RC 6)	T2	TORSION MOMENT (329.5)	IN2-LB		.1596E+07	.1596E+07	.2529E+07
RC 7)	D/DT OF (DELA AILERON POSITION)		RADIAN	/SEC	-.1002E-13	-.3004E-13	-.3513E-13
RC 8)	B3	BENDING MOMENT (577.3)	IN2-L3		.1982E+08	.1982E+08	.2276E+08
RC 9)	T3	TORSION MOMENT (577.3)	IN2-LB		.1734E+07	.1734E+07	.3571E+07
RC(10)	D/DT OF (DELE INBOARD ELEVATOR)		RADIAN	/SEC	-.1666E-13	-.1666E-13	-.7105E-14
RC(11)	B4	BENDING MOMENT (748.3)	IN2-LB		.1069E+08	.1069E+08	.1152E+09
RC(12)	T4	TORSION MOMENT (748.3)	IN2-LB		.2289E+07	.2289E+07	.1328E+07
RC(13)	DELA	AILERON POSITION	RADIAN		.1677E-14	.5607E-14	.5855E-14
RC(14)	I5	BENDING MOMENT (323.5)	IN2-LA		.4414E+07	.4414E+07	.3446E+07
RC(16)	T5	TORSION MOMENT (323.5)	IN2-LB		.1195E+07	.1195E+07	.4478E+05
RC(17)	DELEI	INBOARD ELEVATOR POSITION	RADIAN		-.7374E-01	-.7370E-01	-.7370E-01
RC(18)	D/DT OF (B1 BENDING MOMENT)		INC4-LB	/SEC	.9164E-05	.9369E-05	.7599E-07
RC(19)	D/DT OF (T1 TORSION MOMENT)		IN2-LB	/SEC	-.9645E-05	-.9641E-05	-.2847E-06
RC(20)	ETA1DOT BENDING MODE VELOCITY		IN2-L3	-/SEC	-.1135E-10	-.1135E-10	0.
RC(21)	D/DT OF (B2 TORSION MOMENT)		IN2-L3	/SEC	.1416E-04	-.1407E-04	-.4306E-07
RC(22)	ETA2DOT BENDING MODE VELOCITY		IN24/SEC		-.5901E-05	-.5991E-05	-.1361E-07
RC(23)	D/DT OF (B3 BENDING MOMENT)		INC4-LB	/SEC	-.849RE-11	-.849RE-11	.850RE-11
RC(24)	D/DT OF (T3 TORSION MOMENT)		INC4-L3	/SEC	-.1302E-04	-.1302E-04	-.5507E-07
RC(25)	ETA3DOT BENDING MODE VELOCITY		IN24/SEC		-.7962E-05	-.7964E-05	-.1802E-07
RC(26)	D/DT OF (B4 BENDING MOMENT)		IN24-LB	/SEC	.2116E-10	.2116E-10	.1134E-10
RC(27)	D/DT OF (T4 TORSION MOMENT)		IN24-LB	/SEC	-.4862E-04	-.5627E-05	-.1645E+07
RC(28)	ETA4DOT BENDING MODE VELOCITY		IN24/SEC		.6594E-05	.6474E-05	.3289E+07
RC(30)	D/DT OF (B5 BENDING MOMENT)		IN2-LB		0.	0.	0.
RC(31)	D/DT OF (T5 TORSION MOMENT)		IN24-LB	/SEC	.6053E-05	.6037E-05	.1616E+07
RC(32)	ETA5DOT BENDING MODE VELOCITY		IN24-LR	-/SEC	.7875E-05	.7896E-05	.2221E+07
RC(31)	ETA5DOT BENDING MODE VELOCITY		IN2-VSEC		0.	0.	0.
RC(32)	ETA6DOT BENDING MODE VELOCITY		IN2-1/SEC		-.7306E-11	-.7306E-11	-.3677E-11

Table 20. Steady-State Comparison of Free A/C with F24RR, F24RT and F24TT Models for 1G Maneuver (Concluded)

VARIABLE		DESCRIPTION	UNIT	F24RR	F24RT	F24TT
R(33)	E4DOT	IMP MODEL ERROR RATE FOR W		.5625E-01	.5625E-01	.4966E-01
R(34)	EQDOT	IMP MODEL ERROR RATE FOR Q		.5812E-02	.5812E-02	.5742E-02
R(35)	ALPHA	ANGLE OF ATTACK	RADIAN	.6950E-01	.6950E-01	.6549E-01
R(36)	U1	AILERON OPTIMAL CONTROL INPUT		0.	0.	0.
R(37)	U2	INBOARD ELEV OPTIMAL CONTROL INP		0.	0.	0.
R(38)	P	PILOT FILTER		-.7370E-01	-.7370E-01	-.7370E-01
R(39)	P1	KJSMER STATE (W)	FEET/SEC	0.	0.	0.
R(40)	P2	TRANSPORT DELAY STATE (W)	FEET/SEC	0.	0.	0.
R(41)	P3	TRANSPORT DELAY STATE (T)	FEET/SEC	0.	0.	0.
R(42)	P4	TRANSPORT DELAY STATE (T)		0.	0.	0.
R(43)	P5	KJSMER STATE (W)		0.	0.	0.
R(44)	P6	WIND FILTER STATE		0.	0.	0.
R(45)	W6	WIND GUST STATE		0.	0.	0.
R(46)	W	WE-WE VELOCITY	IN./SEC	.6135E-03	.6135E-03	.5768E-03
R(47)	ETA1	BENDING MODE DEFLECTION	IN.	-.2437E-03	-.2437E-03	-.2446E-03
R(48)	DELA	AILERON POSITION	RADIAN	.1670E-14	.5007E-14	.5855E-14
R(49)	DELEI	INBOARD ELEVATOR POSITION	RADIAN	-.7370E-01	-.7370E-01	-.7370E-01
R(50)	DELEO	OUTBOARD ELEVATOR POSITION	RADIAN	-.7370E-01	-.7370E-01	-.7370E-01
R(51)	ETA1DOT	BENDING MODE VELOCITY	IN./SEC	.1135E-15	.1135E-16	0.
R(52)	ETA2DOT	BENDING MODE VELOCITY	IN./SEC	-.8496E-11	-.8496E-11	-.8581E-11
R(53)	ETA3DOT	BENDING MODE VELOCITY	IN./SEC	.2116E-10	.2116E-10	.3138E-10
R(54)	A212	ACCELEROMETER OUTPUT (21)	1.S	-.1691E-01	-.3916E-01	-.3596E-01
R(55)	ETANDOT	BENDING MODE VELOCITY	IN./SEC	0.	0.	0.
R(56)	ETA5DOT	BENDING MODE VELOCITY	IN./SEC	-.7366E-11	-.7306E-11	-.3677E-11
R(57)	ETA6DOT	BENDING MODE VELOCITY	IN./SEC	-.1501E-01	-.7412E-30	-.7551E-06
R(58)	AFUS	FUSELAGE ACCELEROMETER OUTPUT	1.S	.4377E-01	.4374E-01	.4326E-01
R(59)	TFUS	PITCH RATE GYRO OUTPUT	RADIAN/SEC	.1416E-02	.1416E-02	.1413E-02
R(60)	ETA2	BENDING MODE DEFLECTION	IN.	.4618E-01	.4618E-01	.4532E-01
R(61)	ETA4	BENDING MODE DEFLECTION	IN.	.3669E-01	.3669E-01	.3641E-01
R(62)	ETA6	BENDING MODE DEFLECTION	IN.	-.1669E-30	-.6527E-30	-.6310E-00
R(63)	A21RL	LAGGED NORMAL ACCELERATION		-.3859E-05	-.3859E-05	-.3812E-05
R(64)	MLC1	FULL STATE MLC FOR AILERON		-.8264E-32	-.3231E-03	-.2945E-03
R(65)	GLAF	GUST LOAD ALLEVIATION FILTER				
JI(1)	U1	AILERON OPTIMAL CONTROL INPUT		0.	0.	0.
JI(2)	U2	INBOARD ELEV OPTIMAL CONTROL INP		0.	0.	0.
JI(3)	ETAG	WHITE NOISE INPUT TO GUST MODEL		0.	0.	0.
JI(4)	ETAP	WHITE NOISE INPUT TO PILOT FILTER	FEET/SEC	-.3296E-02	-.3296E-02	-.3296E-02

model is obtained. (In this study the response rates were obtained for the F42 model and then the reduced models were obtained.)

Table 21. Free A/C 1G Responses

Models Sensors	F42	F24RR	F24RT	F24TT
TFUS, rad/sec	0.04377	0.04377	0.04378	0.04326
AFUS, g's	-1.00000	-1.00000	-0.78000	-0.75000
A21R, g's	-1.00000	-1.00000	-3.90000	-3.60000

Table 22 shows the comparison of free aircraft rms responses due to gust input for HG24RR, F24RR, F24RT, and F24TT models. As indicated by the rms comparisons between HG42 and F42 models, the rms comparisons between HG24RR and F24RR are also very good. This means that the different reduction procedures do not affect the rms values significantly (as they do for the steady-state values).

Similar comparisons are made for the pilot response for the HG24RR, F24RR, F24RT, and F24TT models as shown in Table 23. Again the comparisons among the models would indicate that the FLEXSTAB model is good for design of controllers to take care of the rms disturbances (i.e., to handle the control problem, at least at low frequencies).

In Table 24, the roots of HG24RR, F24RR, and F24TT models for free A/C are compared. Again, the root values are close. The damping ratios of the F24RR model (as shown in Table 24 and in Table 18 for the F42 model)

148

Table 22. RMS Comparison of Free A/C with HG24RR, F24RR, F24RT and F24TT Models for 1 FPS Disturbance on η_g

VARIABLE	DESCRIPTION	UNIT	HG24RR	F24RR	F24RT	F24RT	F24TT
R(1)	MLC1 FULL STATE MLC FOR AILERON						
R(2)	B1------BENDING MOMENT (120.0)	INCH-LB					
R(3)	T1------TORSION MOMENT (120.0)	INCH-LB					
R(4)	TFUS----PITCH RATE GYRO OUTPUT	RADIAN/SEC					
R(5)	B2------BENDING MOMENT (329.3)	INCH-LB					
R(6)	T2------TORSION MOMENT (329.3)	INCH-LB					
R(7)	D/DT OF (DELA AILERON POSITION)	RADIAN /SEC					
R(8)	B3------BENDING MOMENT (577.3)	INCH-LB					
R(9)	T3------TORSION MOMENT (577.3)	INCH-LB					
R(10)	D/DT OF (DELEI INBOARD ELEVATOR)	RADIAN /SEC					
R(11)	B4------BENDING MOMENT (746.3)	INCH-LB					
R(12)	T4------TORSION MOMENT (746.3)	INCH-LB					
R(13)	DELA AILERON POSITION	RADIAN					
R(14)	B5------BENDING MOMENT (923.3)	INCH-LB					
R(15)	T5------TORSION MOMENT (923.3)	INCH-LB					
R(16)	DELEI INBOARD ELEVATOR POSITION	RADIAN					
R(17)	D/DT OF (B1------BENDING MOMENT)	INCH-LB /SEC					
R(18)	D/DT OF (---T1------TORSION MOMENT)	INCH-LB /SEC					
R(19)	ETA1DOT BENDING MODE VELOCITY	RADIAN /SEC					
R(20)	D/DT OF (B2------BENDING MOMENT)	INCH-LB /SEC					
R(21)	D/DT OF (T2------TORSION MOMENT)	INCH-LB /SEC					
R(22)	ETA2DOT BENDING MODE VELOCITY	RADIAN/SEC					
R(23)	D/DT OF (B3------BENDING MOMENT)	INCH-LB /SEC					
R(24)	D/DT OF (---T3------TORSION MOMENT)	INCH-LB /SEC					
R(25)	ETA3DOT BENDING MODE VELOCITY	RADIAN/SEC					
R(26)	D/DT OF (B4------BENDING MOMENT)	INCH-LB /SEC					
R(27)	D/DT OF (T4------TORSION MOMENT)	INCH-LB /SEC					
R(28)	ETA4DOT BENDING MODE VELOCITY	INCH-LB /SEC					
R(29)	D/DT OF (B5------BENDING MOMENT)	INCH-LB /SEC					
R(30)	D/DT OF (---T5------TORSION MOMENT)	INCH-LB /SEC					
R(31)	ETA5DOT BENDING MODE VELOCITY	INCH/SEC					
R(32)	ETAEDOT IMP MODEL MODE VELOCITY	INCH/SEC					
R(33)	EMDOT IMP MODEL ERROR RATE FOR M						
R(34)	EQDOT IMP MODEL ERROR RATE FOR Q						
R(35)	ALPHA ANGLE OF ATTACK	RADIAN					
R(36)	U1 AILERON OPTIMAL CONTROL INPUT						
R(37)	U2 INBOARD ELEV OPTIMAL CONTROL INP						

149

Table 23. RMS Comparison of Free A/C with HG24RR, F24RR, F24RT and F24TT Models for 1 FPS Disturbance on η_p

VARIABLE	DESCRIPTION	UNIT	HG24RR	F24RR	F24RT	F24TT
R(1)	MLC1 FULL STATE MLC FOR AILERON					
R(2)	B1 BENDING MOMENT (161***)	IN-LBS				
R(3)	T1 TORSION MOMENT (162***)	IN-LBS				
R(4)	TPUS PITCH RATE GYRO OUTPUT	RADIAN/SEC				
R(5)	B2 BENDING MOMENT (329.3)	IN-LBS				
R(6)	T2 TORSION MOMENT (329.3)	IN-LBS				
R(7)	D/DT OF ( ) DEL4 AILERON POSITION	/SEC				
R(8)	B3 BENDING MOMENT (517.3)	IN-LBS				
R(9)	T3 TORSION MOMENT (517.3)	IN-LBS				
R(10)	D/DT OF ( ) DEL1 INBOARD ELEVATOR	/SEC				
R(11)	B4 BENDING MOMENT (7..3)	IN-LBS				
R(12)	T4 TORSION MOMENT (74..3)	IN-LBS				
R(13)	DELA AILERON POSITION					
R(14)	B5 BENDING MOMENT (963.3)	IN-LBS				
R(15)	T5 TORSION MOMENT (963.3)	IN-LBS				
R(16)	DELE1 INBOARD ELEVATOR POSITION					
R(17)	D/DT OF ( ) B1 BENDING MOMENT	/SEC				
R(18)	D/DT OF ( ) T1 TORSION MOMENT	/SEC				
R(19)	ETA1DOT BENDING MODE VELOCITY	/SEC				
R(20)	D/DT OF ( ) B2 BENDING MOMENT	/SEC				
R(21)	D/DT OF ( ) T2 TORSION MOMENT	/SEC				
R(22)	ETA2DOT BENDING MODE VELOCITY	/SEC				
R(23)	D/DT OF ( ) B3 BENDING MOMENT	/SEC				
R(24)	D/DT OF ( ) T3 TORSION MOMENT	/SEC				
R(25)	ETA3DOT BENDING MODE VELOCITY	/SEC				
R(26)	D/DT OF ( ) B4 BENDING MOMENT	/SEC				
R(27)	D/DT OF ( ) T4 TORSION MOMENT	/SEC				
R(28)	ETA4DOT BENDING MODE VELOCITY	/SEC				
R(29)	D/DT OF ( ) B5 BENDING MOMENT	/SEC				
R(30)	D/DT OF ( ) T5 TORSION MOMENT	/SEC				
R(31)	ETA5DOT BENDING MODE VELOCITY	IN/SEC				
R(32)	ETA6DOT BENDING MODE VELOCITY	IN/SEC				
R(33)	LADOT IMP MODEL ERROR RATE FOR M					
R(34)	EQDOT IMP MODEL ERROR RATE FOR Q					
R(35)	ALPHA ANGLE OF ATTACK	RADIAN				
R(36)	U1 AILERON OPTIMAL CONTROL INPUT					
R(37)	U2 INBOARD ELEV OPTIMAL CONTROL INP					

Table 24. Root Comparison of Free A/C with HG24RR, F24RR and F24TT Models

Association	HG24RR Real ω_n	ζ	F24RR Real ω_n	ζ	F24TT Real ω_n	ζ
$\dot{\theta}$, α	1.6663	0.4981	1.5501	0.5785	1.6987	0.5854
η_1, $\dot{\eta}_1$	5.9309	0.0854	5.5283	0.0892	5.5501	0.0921
η_2, $\dot{\eta}_2$	11.4585	0.0207				
η_3, $\dot{\eta}_3$	14.5012	0.0286	15.5911	0.0699	15.5416	0.0707
η_4, $\dot{\eta}_4$	16.0682	0.0447	17.2662	0.0491	17.4777	0.0531
η_5, $\dot{\eta}_5$	17.4781	0.0235	18.3701	0.0245	18.3842	0.0263
η_6, $\dot{\eta}_6$	19.1533	0.0252	19.3531	0.0315	19.3590	0.0323
η_7, $\dot{\eta}_7$			22.1171	0.0487	22.0976	0.0499
δ_a	-6.0000		-6.0000		-6.0000	
δ_{ei}	-7.5000		-7.5000		-7.5000	
δ_{eo}	-7.5000		-7.5000		-7.5000	
A21RL	-6.0000		-6.0000		-6.0000	
GLAF	-0.0200		-0.0200		-0.0200	
MLC1	-0.0100		-0.0100		-0.0100	
Pilot Filter	-0.1000		-0.1000		-0.1000	
Gust Filter	-0.2100		-0.2100		-0.2100	

Table 24. Root Comparison of Free A/C with HG24RR, F24RR
and F24TT Models (Concluded)

Association	HG24RR		F24RR		F24TT	
	Real ω_n	ζ	Real ω_n	ζ	Real ω_n	ζ
Gust Filter	-0.2100		-0.2100		-0.2100	
Wing Kussner	-9.1560		-9.1560		-9.1560	
1st Order Delay	-13.4270		-13.4270		-13.4270	
2nd Order Delay	9.8020	0.8165	9.8020	0.8165	9.8020	0.8165
Tail Kussner	-18.4930		-18.4930		-18.4930	

change very little due to model reduction process. Previous experience had indicated that there would be typically about 50 percent more damping ratio on the flexture modes for the lower order residualized models than for the high order models.

Figures 80 through 99 contain the time response plots for HG24RR model and F24RR model to elevator input. The elevator input to produce this series of plots is shown in Figures 96, 97, 98, 99; this is the amount of elevator deflection required to pull a 1-g incremental maneuver. The responses (B1, T1, α, q, η_1, η_3, η_6, δ_{ei}, $\dot{\delta}_{ei}$, δ_{eo}) for the two models are all very similar.

Closed-Loop Results

Table 25 compares the steady-state ALDCS aircraft 1G maneuver responses for the F24RR, F24RT, and F24TT models. (Note: ALDCS controller is designed with F24RR model as explained in Section V and the same controller is used with the models F24RT and F24TT). The following (Table 26) illustrates the comparison of steady-state values of sensors. The different model reduction procedures seem to have less effect in closed-loop performance measures.

By comparing the data for the free aircraft from Table 20 and the data from ALDCS aircraft in Table 25 we get the data as shown in Table 27a and 27b.

The maneuver relief for the F24RR model for B1 is nearly the exact value specified (namely 0.7). The F24RT model gets a little more bending relief than required and the F24TT model shows that only about 4/5 required bending relief is achieved. Bending reliefs achieved with different models is comparable to the data that were obtained during the ALDCS design phase using the Honeywell/GELAC model, (Reference 4).

The second line presents comparable data for torsion. Here it is seen that the relative torsion values for the F24RR, F24RT, and F24TT models are 0.2983, 0.3116, and 0.0761. These torsional moment ratios were produced relative to the axis system shown in Figure 4. If the SS loads of Tables 20 and 25 are rotated 18.6° to agree with the Honeywell/GELAC model, then Table 27b results. These data agree very favorably with the Honeywell/GELAC in that the torsional moments increase with the ALDCS aircraft.

153

Table 25. Steady-State Comparison of ALDCS A/C with F24RR, F24RT and F24TT Models for 1G Maneuver

VARIABLE	DESCRIPTION	UNIT	F24RR	F24RT	F24TT
XI 1)	W HEAVE VELOCITY	IN./SEC			
XI 2)	2 PITCH RATE	IN./SEC			
XI 3)	ETA1DOT BENDING MODE VELOCITY	IN./SEC			
XI 4)	ETA2DOT BENDING MODE VELOCITY	IN./SEC			
XI 5)	ETA3DOT BENDING MODE VELOCITY	IN./SEC			
XI 6)	ETA4DOT BENDING MODE VELOCITY	IN./SEC			
XI 7)	ETA5DOT BENDING MODE VELOCITY	IN./SEC			
XI 8)	ETA6DOT BENDING MODE VELOCITY	IN./SEC			
XI 9)	ETA1 BENDING MODE DEFLECTION	IN.			
XI10)	ETA2 BENDING MODE DEFLECTION	IN.			
XI11)	ETA3 BENDING MODE DEFLECTION	IN.			
XI12)	ETA4 BENDING MODE DEFLECTION	IN.			
XI13)	ETA5 BENDING MODE DEFLECTION	IN.			
XI14)	ETA6 BENDING MODE DEFLECTION	IN.			
XI15)	DELA AILERON POSITION	RADIAN			
XI16)	DELEI INBOARD ELEVATOR POSITION	RADIAN			
XI17)	AZIRL LAGGED NORMAL ACCELERATION	G			
XI18)	WLC1 FULL STATE MLS FOR AILERON				
XI19)	GLAF GUST LOAD ALLEVIATION FILTER				
XI20)	DELEO OUTBOARD ELEVATOR POSITION	RADIAN			
XI21)	P PILOT FILTER				
XI22)	P1 GUSSNER STATE (NT)	FEET/SEC			
XI23)	P2 TRANSPORT DELAY STATE (W)	FEET/SEC			
XI24)	P3 TRANSPORT DELAY STATE (T)	FEET/SEC			
XI25)	P4 TRANSPORT DELAY STATE (T)				
XI26)	P5 GUSSNER STATE (W)				
XI27)	P5 WIND FILTER STATE				
XI28)	WG WIND GUST STATE				

154

Table 25. Steady-State Comparison of ALDCS A/C with F24RR, F24RT and F24TT Models for 1G Maneuver (Continued)

VARIABLE	DESCRIPTION	UNIT	F24RR	F24RT	F24TT
RE(1)	MLC1 FULL STATE MLC FOR AILERON	IN-LB	.6520E+02	.1636E+04	-.1959E+03
RE(2)	B1 BENDING MOMENT (120.6)	IN-LB	.6531E+08	.4947E+08	.4751E+08
RE(3)	T1 TORSION MOMENT (120.6)	IN-LB	-.4774E+07	-.4935E+07	-.1032E+07
RE(4)	TFUS PITCH RATE GYRO OUTPUT	RAD/IN/SEC	-.4375E-01	-.4324E-01	-.4316E-01
RE(5)	B2 BENDING MOMENT (329.3)	IN-LB	.2125E+08	.2239E+08	.2364E+0...
RE(7)	T2 TORSION MOMENT (329.3)	IN-LB	-.5374E+07	.6955E+07	-.4225E+07
RE(8)	D/DT OF (DELA) AILERON POSITION	RADIAN /SEC	-.8527E-13	-.7125E-13	-.2942E-13
RE(9)	B3 BENDING MOMENT (577.3)	IN-LB	.4321E+07	-.3145E+07	.6825E+07
RE(10)	T3 TORSION MOMENT (577.3)	IN-LB	.4453E+07	.4932E+07	.7309E+07
RE(11)	D/DT OF (DELE) INBOARD ELEVATOR	RADIAN /SEC	-.4245E-13	-.965E-13	-.1421E-13
RE(11)	B4 BENDING MOMENT (745.3)	IN-LB	-.7940E+06	-.1149E+07	-.7730E+06
RE(12)	T4 TORSION MOMENT (748.3)	IN-LB	.5357E+07	.5044E+07	.3127E+07
RE(13)	DELA AILERON POSITION	RADIAN	-.2755E+00	-.313E+00	-.3077E+08
RE(14)	B5 BENDING MOMENT (323.5)	IN-LB	-.2133E+07	-.2515E+07	-.2907E+07
RE(15)	T5 TORSION MOMENT (323.5)	IN-LB	.3523E+07	.4036E+07	.1027E+07
RE(16)	DELEL INBOARD ELEVATOR POSITION	RADIAN	-.2257E-01	-.2723E-01	-.2705E-01
RE(17)	D/DT OF (B1) BENDING MOMENT	IN-LB /SEC	-.3971E-05	-.2416E-05	.6265E+07
RE(18)	D/DT OF (T1) TORSION MOMENT	IN-LB /SEC	-.1174E-04	-.1336E-04	-.3295E+07
RE(19)	ETA12DOT BENDING MODE VELOCITY	IN-LB/SEC	-.3747E-11	-.1674E-10	0.
RE(20)	D/DT OF (B2) BENDING MOMENT	IN-LB /SEC	-.1713E-05	-.1317E-04	-.7551E+07
RE(21)	D/DT OF (T2) TORSION MOMENT	IN-LB /SEC	-.8520E-05	-.9570E-05	-.3645E+07
RE(22)	ETA12DOT BENDING MODE VELOCITY	IN-LB/SEC	-.1800E-10	-.2322E-10	-.1549E-10
RE(23)	D/DT OF (B3) BENDING MOMENT	IN-LB /SEC	-.1350E-04	-.4930E-04	-.6732E+07
RE(24)	D/DT OF (T3) TORSION MOMENT,	IN-LB /SEC	-.5505E-05	-.5934E-05	-.1945E+07
RE(25)	ETA3DOT BENDING MODE VELOCITY	IN-LB/SEC	-.1590E-10	.1716E-11	-.1905E-10
RE(26)	D/DT OF (B4) BENDING MOMENT	IN-LB /SEC	-.1732E-05	-.2015E-05	-.6962E+06
RE(27)	D/DT OF (T4) TORSION MOMENT	IN-LB /SEC	-.1339E-04	-.1436E-04	.5147E+07
RE(28)	ETA4DOT BENDING MODE VELOCITY	IN-LB/SEC	0.	0.	0.
RE(29)	D/DT OF (B5) BENDING MOMENT	IN-LB /SEC	.3203E-05	.3672E-05	.1562E+06
RE(30)	D/DT OF (T5) TORSION MOMENT	IN-LB /SEC	-.1505E-04	.1604E-04	.4812E+07
RE(31)	ETA5DOT BENDING MODE VELOCITY	IN-LB/SEC	0.	0.	0.
RE(32)	ETA6DOT BENDING MODE VELOCITY	IN-LB/SEC	-.1203E-10	-.1340E-10	-.1848E-10

155

Table 25. Steady-State Comparison of ALDCS A/C with F24RR, F24RT and F24TT Models for 1G Maneuver (Concluded)

VARIABLE		DESCRIPTION	UNIT	F24RR	F24RT	F24TT
R(33)	EMDOT	IMP MODEL ERROR RATE FOR 4		.6955E+02	.3926E+02	.7942E+02
R(34)	E2DOT	IMP MODEL ERROR RATE FOR 2		.4501E+02	.5508E+02	.8442E+02
R(35)	ALPHA	ANGLE OF ATTACK	RADIAN	.7603E-01	.6176E-01	.7961E-01
R(36)	U1	AILERON OPTIMAL CONTROL INPUT		-.2752E+00	-.3133E+00	-.3073E+00
R(37)	U2	INBOARD ELEV OPTIMAL CONTROL INP		.5701E-01	.6239E-01	.6253E-01
R(38)	P	PILOT FILTER		-.8957E-01	-.8957E-01	-.8957E-01
R(39)	P1	GUSSNER STATE (WT)	FEET/SEC	0.	0.	0.
R(40)	P2	TRANSPORT DELAY STATE (W)	FEET/SEC	0.	0.	0.
R(41)	P3	TRANSPORT DELAY STATE (T)	FEET/SEC	0.	0.	0.
2(42)	P4	TRANSPORT DELAY STATE (T)		0.	0.	0.
2(43)	P5	GUSSNER STATE (W)		0.	0.	0.
2(44)	P5	WIND FILTER STATE		0.	0.	0.
2(45)	W5	WIND GUST STATE		0.	0.	0.
R(46)	W	WAVE VELOCITY	INCH/SEC	.6534E+03	.7213E+03	.7006E+03
R(47)	ETA1	BENDING MODE DEFLECTION	INCH	-.1005E+03	-.1073E+03	-.1004E+03
R(48)	DELA	AILERON POSITION	RADIAN	-.2752E+00	-.3163E+00	-.3373E+00
R(49)	DELEI	INBOARD ELEVATOR POSITION	RADIAN	-.2257E-01	-.2723E-01	-.2705E-01
R(50)	DELEO	OUTBOARD ELEVATOR POSITION	RADIAN	-.8957E-01	-.8957E-01	-.8957E-01
R(51)	ETA1DOT	BENDING MODE VELOCITY	INCH/SEC	-.3747E-11	-.2032E-10	-.1549E-10
R(52)	ETA2DOT	BENDING MODE VELOCITY	INCH/SEC	-.1400E-10	-.2032E-10	-.1005E-10
R(53)	ETA3DOT	BENDING MODE VELOCITY	INCH/SEC	.1590E-10	-.1765E-10	.1117E-01
R(54)	A213	ACCELEROMETER OUTPUT (2Y)	G	-.1001E+01	-.1128E+01	-.1117E+01
R(55)	ETA4DOT	BENDING MODE VELOCITY	INCH/SEC	0.	0.	0.
R(56)	ETA5DOT	BENDING MODE VELOCITY	INCH/SEC	-.1203E-10	-.1340E-10	-.1040E-10
R(57)	ETA6DOT	BENDING MODE VELOCITY	INCH/SEC	-.1001E+01	-.8930E+00	-.8940E+00
R(58)	AFUS	FUSELAGE ACCELEROMETER OUTPUT	G	.4375E-01	.4324E-01	.4915E-01
R(59)	TFUS	PITCH RATE GYRO OUTPUT	RADIAN/SEC	-.2259E+02	-.2567E+02	-.2567E+02
R(50)	ETA2	BENDING MODE DEFLECTION	INCH	.5651E+01	.7621E-01	.7761E+01
R(61)	ETA4	BENDING MODE DEFLECTION	INCH	.5401E+01	.6502E+01	.6235E+01
R(62)	ETA6	BENDING MODE DEFLECTION	INCH	.1660E+00	.1802E+00	.1602E+00
R(63)	A21RL	LAGGED NORMAL ACCELERATION	G	.6520E+02	.1362E+02	.1954E+03
R(64)	MLC1	FULL STATE MLC FOR AILERON		-.2222E+00	-.2433E+00	-.2459E+00
R(65)	GLAF	GUST LOAD ALLEVIATION FILTER				
U1 1)	U1	AILERON OPTIMAL CONTROL INPUT		0.	0.	0.
JI 2)	U2	INBOARD ELEV OPTIMAL CONTROL INP		0.	0.	0.
JI 3)	ETAG	WHITE NOISE INPUT TO GUST MODEL				
JI 4)	ETAP	WHITE NOISE INPUT TO PILOT FILTE	FEET/SEC	-.4005E+02	-.4006E+02	-.4005E+02

Table 26. Closed-Loop 1G Responses

Models Sensors	F24RR	F24RT	F24TT
TFUS rad/sec	0.04375	0.04824	0.04916
AFUS, g's	-1.00100	-0.89800	-0.89400
A21R, g's	-1.00100	-1.12800	-1.11700

Table 27a. Steady-State Maneuver Load Relief Ratio
(Moment ALDCS/Moment Free)
(Figure 4 Load Axis System)

	F24RR	F24RT	F24TT
B1	0.6991	0.7635	0.7821
T1	0.2983	0.3116	0.0761

Table 27b. Steady-State Maneuver Load Relief
(Moment ALDCS/Moment Free)
(Figure 3 Load Axis System)

	F24RR	F24RT	F24TT
B1	0.6686	0.7289	0.7328
T1	1.8046	2.009	2.1702

In Table 28 steady-states are compared for the free and ALDCS aircraft using the HG24RR and F24RR models. Table 29 compares bending and torsion data relief for the F24RR and HG24RR models. It is seen that

157

Table 28. Steady-State Comparison of Free A/C and ALDCS A/C with F24RR and HG24RR Models for 1G Maneuver

VARIABLE	DESCRIPTION	UNIT	F24RR(FREE)	HG24RR(FREE)	HG24RR(ALDCS)	F24RR(ALDCS)
X(1)	W HEAVE VELOCITY	INCH/SEC	.6139E+03	-.6162E+03	.5411E+03	.5534E+03
X(2)	Q PITCH RATE	INCH/SEC	.7212E+02	.7213E+02	-.7215E+02	.7209E+02
X(3)	ETA4DOT BENDING MODE VELOCITY	INCH/SEC	.1135E-10	0.	0.	.9747E-11
X(4)	ETA DOT BENDING MODE VELOCITY	INCH/SEC	-.8499E-11	0.	0.	-.1475E-10
X(5)	ETA3DOT BENDING MODE VELOCITY	INCH/SEC	.2116E-10	.2690E-11	.9435E-11	-.1500E-10
X(6)	ETA4DOT BENDING MODE VELOCITY	INCH/SEC	0.	.6955E-11	0.	0.
X(7)	ETA5DOT BENDING MODE VELOCITY	INCH/SEC	0.	0.	0.	0.
X(8)	ETA6DOT BENDING MODE VELOCITY	INCH/SEC	-.7306E-11	-.6949E-12	-.2371E-11	-.1203E-10
X(9)	ETA1 BENDING MODE DEFLECTION	INCH	-.2437E+03	-.3633E+02	-.1464E+02	-.1035E+03
X(10)	ETA2 BENDING MODE DEFLECTION	INCH	-.1416E+02	.4956E+00	.7463E+00	-.2253E+02
X(11)	ETA3 BENDING MODE DEFLECTION	INCH	-.7496E+01	.2376E+01	.3555E+01	-.1777E+02
X(12)	ETA4 BENDING MODE DEFLECTION	INCH	.4614E+01	-.1971E+01	-.2634E+01	.6851E+01
X(13)	ETA5 BENDING MODE DEFLECTION	INCH	.4727E+01	-.2663E+00	-.2865E+00	-.9353E+01
X(14)	ETA6 BENDING MODE DEFLECTION	INCH	.3469E+01	.9366E+00	.1528E+01	.5416E+01
X(15)	DFLA AILERON POSITION	RADIAN	.167E-14	.3791E-14	-.2650E-14	-.2752E+00
X(16)	DELEI INBOARD ELEVATOR POSITION	RADIAN	-.7377E-01	-.1105E+00	-.5593E-01	-.2237E-01
X(17)	A21RL LAGGED NORMAL ACCELERATION	G	-.1669E+00	-.1666E+00	-.1657E+00	-.1659E+00
X(18)	MLC1 FWD STATE MLC FOR AILERON		-.3659E+05	-.3859E+05	-.2063E+03	.6522E+02
X(19)	GLAF GUST LOAD ALLEVIATION FILTER		-.826E+02	-.7797E+02	-.1234E+00	-.2272E+03
X(20)	DELEO OUTBOARD ELEVATOR POSITION	RADIAN	-.7372E-01	-.1105E+00	-.1234E+00	-.8397E-01
X(21)	P PILOT FILTER		0.	0.	.6236E+05	.9357E-31
X(22)	P1 KUSSNER STATE (NT)	FEET/SEC	0.	0.	0.	0.
X(23)	P2 TRANSPORT DELAY STATE (W)	FEET/SEC	0.	0.	0.	0.
X(24)	P3 TRANSPORT DELAY STATE (T)	FEET/SEC	0.	0.	0.	0.
X(25)	P4 TRANSPORT DELAY STATE (T)		0.	0.	0.	0.
X(26)	P5 KUSSNER STATE (W)		0.	0.	0.	0.
X(27)	P6 WIND FILTER STATE		0.	0.	0.	0.
X(28)	WG WIND GUST STATE		0.	0.	0.	0.

158

VARIABLE	DESCRIPTION	UNIT	F24RR(FRFE)	HG24RR(FREE)	HG24RR(ALDCS)	F24RR(ALDCS)
RC 1)	MLC1 FJL_ STATE MLC FOR AILERON	INCH-LB	-.3859E+05	-.3859E+05	-.2063E+33	.6520E+02
RC 2)	R1 BENDING MOMENT (120.4)	INCH-LB	-.5479E+08	.6932E+08	.4554E+08	.4531E+08
RC 3)	T1 TORSION MOMENT (120.4)	INCH-LB	-.1600E+08	.7989E+07	.1392E+03	-.4774E+07
RC 4)	TFUS PITCH RATE GYRO OUTPUT	RADIAN/SEC	-.4377E-01	-.4375E-01	-.4377E-01	-.4375E-01
RC 5)	B2 BENDING MOMENT (329.3)	INCH-LB	.4173E+08	-.4270E+08	.2393E+03	-.2120E+08
RC 6)	T2 TORSION MOMENT (329.3)	INCH-LB	-.1596E+07	.3812E+07	.9532E+07	.5874E+07
RC 7)	D/DT OF (DELA AILERON POSITION)	RADIAN /SEC	-.1602E-13	-.2275E-13	-.3553E-14	-.8527E-13
RC 8)	R3 BENDING MOMENT (577.3)	INCH-LB	-.1942E+08	.2044E+08	.5121E+07	.4321E+07
RC 9)	T3 TORSION MOMENT (577.3)	INCH-LB	-.1734E+07	.1737E+07	.7120E+07	.4453E+07
RC 10)	D/DT OF (DELE INBOARD ELEVATOR)	RADIAN	-.1566E-13	-.7105E-14	.1461E-13	-.6263E-13
RC(11)	B4 BENDING MOMENT (748.3)	INCH-LB	-.1669E+08	.1042E+08	-.1524E+07	-.7936E+06
RC(12)	T4 TORSION MOMENT (748.3)	INCH-LB	.2889E+07	.2962E+07	.6545E+07	.5057E+07
RC(13)	DELA AILERON POSITION	RADIAN	.1677E-14	.3791E-14	.2693E+00	-.2759E+00
RC(14)	B5 BENDING MOMENT (323.5)	INCH-LB	.4414E+07	.4204E+07	.2721E+07	-.2433E+07
RC(15)	T5 TORSION MOMENT (323.5)	INCH-LB	.1195E+07	.1638E+07	.4573E+07	.3623E+07
RC(16)	DELEI INBOARD ELEVATOR POSITION	RADIAN	-.7374E-01	-.7185E+00	-.5543E-01	-.2257E-01
RC(17)	D/DT OF (B1 BENDING MOMENT)	INCH-LB /SEC	.9168E-05	.4990E-05	-.2193E-05	.3971E-05
RC(18)	D/DT OF (T1 TORSION MOMENT)	INCH-LB /SEC	.9645E-05	.1566E-05	-.1297E-04	-.1174E-04
RC(19)	ETA1DOT BENDING MODE VELOCITY	INCH-LB/SEC	-.1135E-10	0.	0.	.9747E-11
RC(20)	D/DT OF (B2 BENDING MOMENT)	INCH-LB /SEC	-.1415E-04	.8122E-05	.6375E-05	-.1719E-05
RC(21)	D/DT OF (T2 TORSION MOMENT)	INCH-LB /SEC	-.5591E-05	.2437E-05	-.1120E-05	-.8520E-05
RC(22)	ETA2DOT BENDING MODE VELOCITY	INCH-LB/SEC	.1301E-04	0.	0.	-.1800E-10
RC(23)	D/DT OF (B3 BENDING MOMENT)	INCH-LB /SEC	-.1301E-04	.3999E-05	.3815E-05	-.1355E-04
RC(24)	D/DT OF (T3 TORSION MOMENT)	INCH-LB /SEC	-.7942E-05	-.2119E-07	-.1612E-04	-.5505E-05
RC(25)	ETA3DOT BENDING MODE VELOCITY	INCH-LB/SEC	-.2116E-10	.2690E-11	.1480E-11	-.1590E-10
RC(26)	D/DT OF (B4 BENDING MOMENT)	INCH-LB /SEC	-.4467E-04	-.1174E-04	-.7347E-05	-.1732E-05
RC(27)	D/DT OF (T4 TORSION MOMENT)	INCH-LB /SEC	.6564E-05	-.2134E-04	-.5215E-04	.1339E-04
RC(28)	ETA4DOT BENDING MODE VELOCITY	INCH-LB/SEC	0.	-.6955E-11	.3545E-11	0.
RC(29)	D/DT OF (B5 BENDING MOMENT)	INCH-LB /SEC	.6.50E-05	-.7205E-05	-.1365E-05	.3203E-05
RC(30)	D/DT OF (T5 TORSION MOMENT)	INCH-LB /SEC	.7875E-05	.1569E-04	-.3747E-04	.1596E-04
RC(31)	ETA5DOT BENDING MODE VELOCITY	INCH/SEC	0.	0.	0.	0.
RC(32)	ETA6DOT BENDING MODE VELOCITY	INCH/SEC	-.7336E-11	-.6949E-12	-.2371E-11	-.1203E-10

Table 28. Steady-State Comparison of Free A/C and ALDCS A/C with F24RR and HG24RR Models for 1G Maneuver (Concluded)

VARIABLE		DESCRIPTION	UNIT	F24RR(FREE)	HG24RR(FREE)	HG24RR(ALDCS)	F24RR(ALDCS)
R(33)	E4DOT	IMP MODEL ERROR RATE FOR 4		.5025E-01	.5025E-01	.6294E+02	.6855E+02
R(34)	EQDOT	IMP MODEL ERROR RATE FOR 2		.5812E+02	.5813E+02	.2225E+02	.4501E+02
R(35)	ALPHA	ANGLE OF ATTACK	RADIAN	.6905E-01	.6986E-01	.7264E-01	.7403E-01
R(36)	U1	AILERON OPTIMAL CONTROL INPUT		0.	0.	.2500E+00	-.2750E+00
R(37)	U2	INBOARD ELEV OPTIMAL CONTROL INP		-.7370E-01	-.1105E+00	-.7251E-11	.5701E-01
R(38)	P	PILOT FILTER		0.	0.	-.1284E+00	-.6957E-01
R(39)	P1	KUSSNER STATE (NT)	FEET/SEC	0.	0.	0.	0.
R(40)	P2	TRANSPORT DELAY STATE (M)	FEET/SEC	0.	0.	0.	0.
R(41)	P3	TRANSPORT DELAY STATE (T)	FEET/SEC	0.	0.	0.	0.
R(42)	P4	TRANSPORT DELAY STATE (T)		0.	0.	0.	0.
R(43)	P5	KUSSNER STATE (M)		0.	0.	0.	0.
R(44)	P5	WIND FILTER STATE		0.	0.	0.	0.
R(45)	W5	WIND GUST STATE		0.	0.	0.	0.
R(46)	W	HEAVE VELOCITY	INS/SEC	.6130E-01	.6162E-03	.6411E+03	.6534E+03
R(47)	ETA1	BENDING MODE DEFLECTION	INS	-.2437E+03	-.7633E+02	-.1146E+02	-.1003E+03
R(48)	DELA	AILERON POSITION	RADIAN	.1670E-14	.3791E-14	.2500E+00	.2752E+00
R(49)	DELEI	INBOARD ELEVATOR POSITION	RADIAN	-.737E-01	-.1105E+00	-.5533E-01	-.2257E-01
R(50)	DELEO	OUTBOARD ELEVATOR POSITION	RADIAN	.737E-01	-.1105E+00	.1284E+00	-.5957E-01
R(51)	ETA1DOT	BENDING MODE VELOCITY	INS/SEC	.1135E-10	0.	0.	.3747E-11
R(52)	ETA2DOT	BENDING MODE VELOCITY	INS/SEC	-.7849E-11	0.	0.	-.1805E-10
R(53)	ETA3DOT	BENDING MODE VELOCITY	INS/SEC	-.2116E-10	.2690E-11	.4480E-11	.1590E-10
R(54)	A2IR	ACCELEROMETER OUTPUT (21)	LS	-.1 51E-01	-.9996E+00	-.1000E+01	-.1001E+01
R(55)	ETA4DOT	BENDING MODE VELOCITY	INS/SEC	0.	.6955E-11	.3345E-11	0.
R(56)	ETA5DOT	BENDING MODE VELOCITY	INS/SEC	-.736E-11	0.	0.	0.
R(57)	E5A5DOT	BENDING MODE VELOCITY	INS/SEC	-.1001E-01	-.6949E-12	-.2371E-11	-.1205E-10
R(58)	AFUS	FUSELAGE ACCELERATION OUTPUT	LS	-.4377E-01	-.9997E+00	-.1000E+01	-.1001E+01
R(59)	YFUS	PITCH RATE GYRO OUTPUT	RADIAN/SEC	.1412E-02	.4375E-01	.4377E-01	.4375E-01
R(60)	ETA2	BENDING MODE DEFLECTION	INS	.4612E-01	.4956E-20	.7463E+00	-.2259E+02
R(61)	ETA4	BENDING MODE DEFLECTION	INS	.3860E+01	-.1071E+01	-.2504E+01	.6901E+01
R(62)	ETA6	BENDING MODE DEFLECTION	INS	-.1660E+30	-.9366E+00	-.1525E+01	.5405E+01
R(63)	A2IR1	LAGGED NORMAL ACCELERATION	LS	-.3459E+05	-.1666E+05	-.1567E+00	-.1668E+00
R(64)	MLC1	FULL STATE MLC FOR AILERON		-.826E+03	-.1859E+05	-.2063E+03	.6520E+02
R(65)	GLAF	GUST LOAD ALLEVIATION FILTER			-.7797E+02	.1204E+00	-.2202E+00
JI 11	U1	AILERON OPTIMAL CONTROL INPUT		0.	0.	0.	0.
JI 21	U2	INBOARD ELEV OPTIMAL CONTROL INP		0.	0.	0.	0.
JI 31	ETAG	WHITE NOISE INPUT TO GUST MODEL		0.	0.	0.	0.
JI 41	ETAP	WHITE NOISE INPUT TO PILOT FILTE	FEET/SEC	-.7296E+02	-.6941E+02	-.5742E+02	-.6005E+02

160

the torsion moment for the HG model has increased as was mentioned before. However, the magnitude of this increase is greater than that obtained during the past ALDCS design study. This difference might be due to the fact that the ALDCS controller designed is not a very refined one. It is seen that the η_i's are markedly different between the HG24RR and F24RR models

Table 29. Steady-State MLC for HG24RR and F24RR Models
(Figure 3 Load Axis System)

	F24RR	HG24RR
B1	0.6686	0.7002
T1	1.8046	1.7428

and this raises a question on the accuracy of the F model at higher frequencies. (The discrepancy was also observed while comparing the HG42 and F42 models.)

Table 30 shows the comparison of ALDCS aircraft rms responses due to gust input for HG24RR, F24RR, F24RT and F24TT models. Table 31 shows the relative rms relief as obtained from Tables 22 and 30.

An observation is that the different improvement obtained between the RR, RT, TT models would lead one to markedly expect the different results depending upon which of the models were used. Experience in the past during the design of the ALDCS was that the ALDCS rms relief in gust was the same regardless of the model used. This difference is because of the different truncation procedures used in this study.

161

Table 30. RMS Comparison of ALDCS A/C with HG24RR, F24RT and. F24TT Models for 1 FPS Disturbance on η_g

VARIABLE	DESCRIPTION	UNIT	MG24RR	F24RR	F24RT	F24TT
R(1)	MLC1 FULL STATE MLC FOR AILERON					
R(2)	B1 BENDING MOMENT (126...)	INCH-LB				
R(3)	T1 TORSION MOMENT (126...)	INCH-LB				
R(4)	T-FUS PITCH RATE GYRO OUTPUT	RADIAN/SEC				
R(5)	B2 BENDING MOMENT (329.3)	INCH-LB				
R(6)	T2 TORSION MOMENT (329.3)	INCH-LB				
R(7)	D/DT OF DELA AILERON POSITION	RADIAN /SEC				
R(8)	B3 BENDING MOMENT (577.3)	INCH-LB				
R(9)	T3 TORSION MOMENT (577.3)	INCH-LB				
R(10)	D/DT OF DELEI INBOARD ELEVATOR	RADIAN /SEC				
R(11)	B4 BENDING MOMENT (774.3)	INCH-LB				
R(12)	T4 TORSION MOMENT (774.3)	INCH-LB				
R(13)	DELA AILERON POSITION	RADIAN				
R(14)	B5 BENDING MOMENT (923.3)	INCH-LB				
R(15)	T5 TORSION MOMENT (923.3)	INCH-LB				
R(16)	DELEI INBOARD ELEVATOR POSITION	RADIAN				
R(17)	D/DT OF B1 BENDING MOMENT	INCH-LB /SEC				
R(18)	D/DT OF T1 TORSION MOMENT	INCH-LB /SEC				
R(19)	ETA1DOT BENDING MODE VELOCITY	INCH/SEC				
R(20)	D/DT OF B2 BENDING MOMENT	INCH-LB /SEC				
R(21)	D/DT OF T2 TORSION MOMENT	INCH/SEC				
R(22)	ETA2DOT BENDING MODE VELOCITY	INCH/SEC				
R(23)	D/DT OF B3 BENDING MOMENT	INCH-LB /SEC				
R(24)	D/DT OF T3 TORSION MOMENT	INCH-LB /SEC				
R(25)	ETA3DOT BENDING MODE VELOCITY	INCH/SEC				
R(26)	D/DT OF B4 BENDING MOMENT	INCH-LB /SEC				
R(27)	D/DT OF T4 TORSION MOMENT	INCH-LB /SEC				
R(28)	ETA4DOT BENDING MODE VELOCITY	INCH/SEC				
R(29)	D/DT OF B5 BENDING MOMENT	INCH-LB /SEC				
R(30)	D/DT OF T5 TORSION MOMENT	INCH-LB /SEC				
R(31)	ETA5DOT BENDING MODE VELOCITY	INCH/SEC				
R(32)	ENDOT BENDING MODE VELOCITY	INCH/SEC				
R(33)	EMDOT IMP MODEL ERROR RATE FOR M					
R(34)	ECDOT IMP MODEL ERROR RATE FOR G-					
R(35)	ALPHA ANGLE OF ATTACK	RADIAN				
R(36)	U1 AILERON-OPTIMAL CONTROL-INPUT					
R(37)	U2 INBOARD ELEV OPTIMAL CONTROL IMP					

162

A second observation is in regard to the torsion relief. During the ALDCS design it was observed that torsion increases could be maintained below 5 percent. The torsion reductions shown here for the FLEXSTAB models are again attributed to the rotated axis system (cf. Figures 3 and 4).

Table 31. Relative ALDCS RMS Relief in Gusts

	HG24RR	F24RR	F24RT	F24TT
B1	0.5032	0.6045	0.8757	0.7775
T1	1.3071	0.4820	0.6528	1.3451

Table 32 presents the rms comparisons for the ALDCS aircraft due to pilot disturbance, and Table 33 presents the results of a combined disturbance. Table 34 compares the rms responses for the free and ALDCS A/C with the F24RR model.

Roots for the ALDCS aircraft for all the four models (HG24RR, F24RR, F24RT, and F24TT) are compared in Table 35. Here the very low damping rate ratio is generated on the third flexure mode for the HG24RR model. To improve the damping ratio it was necessary to put low pass filter into the elevator channel. As will subsequently be shown, the elevator drives the third mode rather hard on the HG model. The table does show that the rigid body objectives for all four aircraft are as desired.

Table 36 compares the roots of the free and ALDCS aircraft with the F24RR model. The ALDCS aircraft displays better root positions than does the

163

Table 32. RMS Comparison of ALDCS A/C with HG24RR, F24RR, F24RT and F24TT Models for 1 FPS Disturbance on η_p

VARIABLE	DESCRIPTION	UNIT	HG24RR	F24RR	F24RT	F24TT
R(1)	MLC1 FULL STATE MLC FOR AILERON					
R(2)	B1 ---BENDING MOMENT (126.→)	INCM-LB				
R(3)	T1 ---TORSION MOMENT (122.4)	INCM-LB				
R(4)	-TFUS- PITCH-RATE GYRO OUTPUT	RADIAN/SEC				
R(5)	B2 BENDING MOMENT (329.3)	INCM-LB				
R(6)	T2 TORSION MOMENT (329.3)	INCM-LB				
R(7)	D/OT OF (DELA AILERON POSITION)	RADIAN/SEC				
R(8)	B3 ---BENDING MOMENT (577.3)	INCM-LB				
R(9)	T3 TORSION MOMENT (577.3)	INCM-LB				
R(10)	D/OT OF (DELEI INBOARD ELEVATOR)	RADIAN/SEC				
R(11)	B4 BENDING MOMENT (726.3)	INCM-LB				
R(12)	T4 ---TORSION MOMENT (746.3)	INCM-LB				
R(13)	DELA AILERON POSITION	RADIAN				
R(14)	B5 BENDING MOMENT (923.5)	INCM-LB				
R(15)	T5 TORSION MOMENT (923.5)	INCM-LB				
R(16)	DELEI INBOARD ELEVATOR POSITION	RADIAN				
R(17)	D/OT OF (B1 BENDING MOMENT	INCM-LB/SEC				
R(18)	D/OT-OF (T1 TORSION MOMENT	INCM-LB/SEC				
R(19)	ETA1DOT BENDING MODE VELOCITY	INCM-LB/SEC				
R(20)	D/OT OF (B2 BENDING MOMENT	INCM-LB/SEC				
R(21)	D/OT CF (T2 TORSION MOMENT	INCM-LB/SEC				
R(22)	ETA2DOT BENDING MODE VELOCITY	INCM-LB/SEC				
R(23)	D/OT OF (B3 BENDING MOMENT	INCM-LB/SEC				
R(24)	D/OT-OF (T3 TORSION MOMENT	INCM-LB/SEC				
R(25)	ETA3UDOT BENDING MODE VELOCITY	INCM-LB/SEC				
R(26)	D/OT OF (B4 BENDING MOMENT	INCM-LB/SEC				
R(27)	D/OT OF (T4 TORSION MOMENT	INCM-LB/SEC				
R(28)	ETA4OUT-BENDING MODE VELOCITY	INCM-LB/SEC				
R(30)	D/OT-OF (B5 BENDING MOMENT	INCM-LB/SEC				
R(31)	ETA5DOT BENDING MODE VELOCITY	INCM/SEC				
R(32)	ETA6DOT BENDING MODE VELOCITY	INCM/SEC				
R(33)	EDOT IMP MODEL ERROR RATE FOR W					
R(34)	EDOT IMP MODEL ERROR RATE FOR Q					
R(35)	ALPHA ANGLE OF ATTACK	RADIAN				
R(36)	U4 AILERON-OPTIMAL-CONTROL-INPUT					
R(37)	U2 INBOARD ELEV OPTIMAL CONTROL INP					

164

Table 33. RMS Comparison of ALDCS A/C with HG24RR, F24RR, F24RT and F24TT Models for 1 FPS Disturbance on η_g and η_p

VARIABLE	DESCRIPTION		UNIT	MG24RR	F24RR	F24RT	F24TT
R(1)	MLC1	FULL STATE MLC FOR AILERON	INCH-LB				
R(-2)	B1	BENDING MOMENT (120.4)	INCH-LB				
R(3)	T1	TORSION MOMENT (120.4)	IN-LB				
R(4)	TFUS	PITCH RATE GYRO OUTPUT	RADIAN/SEC				
R(5)	B2	BENDING MOMENT (329.3)	INCH-LB				
R(6)	V2	TORSION MOMENT (329.3)	INCH-LB				
R(7)	D/DT OF (B2A AILERON POSITION)		RADIAN /SEC				
R(8)	B3	BENDING MOMENT (577.3)	INCH-LB				
R(9)	T3	TORSION MOMENT (577.3)	INCH-LB				
R(10)	D/DT OF (DEL1 INBOARD ELEVATOR)		RADIAN /SEC				
R(11)	B4	BENDING MOMENT (740.3)	INCH-LB				
R(12)	T4	TORSION MOMENT (740.3)	IN-LB				
R(13)	CELA	AILERON POSITION	RADIAN				
R(14)	B5	BENDING MOMENT (923.3)	INCH-LB				
R(15)	T5	TORSION MOMENT (923.3)	IN-LB				
R(16)	DEL1	INBOARD ELEVATOR POSITION	RADIAN				
R(17)	D/DT OF (B1 BENDING MOMENT)		INCH-LB /SEC				
R(18)	D/DT OF (T1 TORSION MOMENT)		INCH-LB /SEC				
R(19)	ETA1DOT BENDING MODE VELOCITY		INCH-LB /SEC				
R(20)	D/DT OF (B2 BENDING MOMENT)		INCH-LB /SEC				
R(21)	D/DT OF (T2 TORSION MOMENT)		INCH-LB /SEC				
R(22)	ETA2DOT BENDING MODE VELOCITY		INCH-LB /SEC				
R(23)	D/DT OF (B3 TORSION MOMENT)		INCH-LB /SEC				
R(25)	ETA3DOT BENDING MODE VELOCITY		INCH-LB /SEC				
R(26)	D/DT OF (B4 BENDING MOMENT)		INCH-LB /SEC				
R(27)	D/DT OF (T4 TORSION MOMENT)		INCH-LB /SEC				
R(28)	ETA4DOT BENDING MODE VELOCITY		INCH-LB /SEC				
R(29)	D/DT OF (B5 BENDING MOMENT)		INCH-LB /SEC				
R(30)	D/DT OF (T5 TORSION MOMENT)		INCH-LB /SEC				
R(31)	ETA5DOT BENDING MODE VELOCITY		INCH/SEC				
R(32)	ETA6DOT BENDING MODE VELOCITY		INCH/SEC				
R(33)	ENDOT IMP MODEL ERROR RATE FOR W						
R(34)	ECDOT IMP MODEL ERROR RATE FOR Q						
R(35)	ALPHA ANGLE OF ATTACK		RADIAN				
R(36)	U1 AILERON OPTIMAL CONTROL INPUT						
R(37)	U2 INBOARD ELEV OPTIMAL CONTROL INP						

Table 34. RMS Comparison of Free A/C and ALDCS A/C with F24RR Model for 1 FPS Disturbance on η_g and η_p

VARIABLE	DESCRIPTION	UNIT	ETAR(FREE)	ETAG(ALDCS)	ETAP(FREE)	ETAP(ALDCS)
RC 1)	MLC1 FULL STATE MLC FOR AILERON	INCH-LB				
RC 2)	B1 BENDING MOMENT (126++)	INCH-LB				
RC 3)	T1 TORSION MOMENT (126++)	INCH-LB				
RC 4)	TFUS PITCH RATE GYRO OUTPUT	RADIAN/SEC				
RC 5)	B2 BENDING MOMENT (329.3)	INCH-LB				
RC 6)	T2 TORSION MOMENT (329.3)	INCH-LB				
RC 7)	D/DT OF (DELA AILERON POSITION)	RADIAN/SEC				
RC 8)	B3 BENDING MOMENT (577.3)	INCH-LB				
RC 9)	T3 TORSION MOMENT (577.3)	INCH-LB				
RC10)	D/DT OF (DELEL INBOARD ELEVATOR)	RADIAN/SEC				
RC11)	B4 BENDING MOMENT (760.3)	INCH-LB				
RC12)	T4 TORSION MOMENT (760.3)	INCH-LB				
RC13)	DELA AILERON POSITION	RADIAN				
RC14)	B5 BENDING MOMENT (923.3)	INCH-LB				
RC15)	T5 TORSION MOMENT (923.3)	INCH-LB				
RC16)	DELEL INBOARD ELEVATOR POSITION	RADIAN				
RC17)	D/DT OF (B1 BENDING MOMENT)	INCH-LB/SEC				
RC18)	D/DT OF (T1 TORSION MOMENT)	INCH-LB/SEC				
RC19)	ETAIDOT BENDING MODE VELOCITY	INCH-LB/SEC				
RC20)	D/DT OF (B2 BENDING MOMENT)	INCH-LB/SEC				
RC21)	D/DT OF (T2 TORSION MOMENT)	INCH-LB/SEC				
RC22)	ETA2DOT BENDING MODE VELOCITY	INCH-LB/SEC				
RC23)	D/DT OF (B3 BENDING MOMENT)	INCH-LB/SEC				
RC24)	D/DT OF (T3 - TORSION MOMENT)	INCH-LB/SEC				
RC25)	ETA3DOT BENDING MODE VELOCITY	INCH-LB/SEC				
RC26)	D/DT OF (B4 BENDING MOMENT)	INCH-LB/SEC				
RC27)	D/DT OF (T4 TORSION MOMENT)	INCH-LB/SEC				
RC28)	ETA4DOT BENDING MODE VELOCITY	INCH-LB/SEC				
RC29)	D/DT OF (B5 BENDING MOMENT)	INCH-LB/SEC				
RC30)	D/DT OF (T5 TORSION MOMENT)	INCH-LB/SEC				
RC31)	ETA5DOT BENDING MODE VELOCITY	INCH/SEC				
RC32)	ETA6DOT BENDING MODE VELOCITY	INCH/SEC				
RC33)	ENDOT IMP MODEL ERROR RATE FOR M					
RC34)	EGDOT IMP MODEL ERROR RATE FOR G					
RC35)	ALPHA ANGLE OF ATTACK	RADIAN				
RC36)	U1 AILERON OPTIMAL CONTROL INPUT					
RC37)	U2 INBOARD ELEV OPTIMAL CONTROL INP					

166

Table 35. Root Comparison of ALDCS A/C with HG24RR, F24RR, F24RT and F24TT Models

Association	HG24RR		F24RR		F24RT		F24TT	
	Real ω_n	ζ	Real ω_n	ζ	Real ω_n	ζ	Real ω_n	ζ
$\dot{\theta}, \alpha$	1.9339	0.7906	1.7393	0.7354	1.5789	0.7237	1.6881	0.7360
$\eta_1, \dot{\eta}_1$	10.4500	0.0469	3.7410	0.2501	4.5914	0.1017	4.5392	0.1071
$\eta_2, \dot{\eta}_2$	11.4915	0.0214						
$\eta_3, \dot{\eta}_3$	15.9306	0.0051	14.2402	0.1852	14.3896	0.1125	14.3315	0.1130
$\eta_4, \dot{\eta}_4$	15.7992	0.0149	17.2569	0.0169	17.2468	0.0176	17.4295	0.0212
$\eta_5, \dot{\eta}_5$	17.4698	0.0225	18.3744	0.0216	18.3751	0.0215	18.4154	0.0221
$\eta_6, \dot{\eta}_6$	19.2756	0.0193	19.1853	0.0324	19.2135	0.0302	19.2364	0.0307
$\eta_7, \dot{\eta}_7$			21.9848	0.0569	22.0080	0.0513	21.9619	0.0533
δ_a	-6.9296		-1.2552		-1.5507		-1.5425	
δ_{ei}	-7.3346		-8.0200		-8.1426		-8.2204	
δ_{eo}	-7.5000		-7.5000		-7.5000		-7.5000	
A21RL	3.4370	0.1588	30.5312	0.8669	44.7684	0.0282	44.7855	0.6274

167

Table 35. Root Comparison of ALDCS A/C with HG24RR, F24RR, F24RT and F24TT Models   (Concluded)

Association	HG24RR		F24RR		F24RT		F24TT	
	Real ω_n	ζ	Real ω_n	ζ	Real ω_n	ζ	Real ω_n	ζ
GLAF	3.4370	0.1588	30.5312	0.8669	44.7884	0.6282	44.7855	0.6274
MLC1	-0.0100		-0.0100		-0.0100		-0.0100	
Pilot Filter	-0.1000		-0.1000		-0.1000		-0.1000	
Gust Filter	-0.2100		-0.2100		-0.2100		-0.2100	
Gust Filter	-0.2100		-0.2100		-0.2100		-0.2100	
Wing Kussner	-9.1560		-9.1560		-9.1560		-9.1560	
1st Order Delay	-13.4270		-13.4270		-13.4270		-13.4270	
2nd Order Delay	9.8020	0.8165	9.8020	0.8165	9.8020	0.8165	9.8020	0.8165
Tail Kussner	-18.4930		-18.4930		-18.4930		-18.4930	

168

free aircraft. Note that the damping ratio for the F24RR, F24RT, and F24TT models in the third bending mode is increased. This is not what would have been expected from previous experience in designing the HG model.

The time response plots for the closed-loop systems are presented in Figures 100 through 151. The following closed-loop models are considered.

- SAS aircraft HG24RR

- SAS aircraft F24RR

- ALDCS aircraft HG24RR

- ALDCS aircraft F24RR

- ALDCS aircraft F24RT

- ALDCS aircraft F24TT.

It is shown in Figures 100 and 101 that the SAS improves the pitch rate response for both the HG24RR and F24RR models. The basic C-5A with SAS is considered to have very desirable handling qualities and ALDCS is designed to provide the same qualities for pitch rate.

Figures 102, 103, 104, and 105 show that the pitch rate response for the ALDCS aircraft is very close to the SAS aircraft previously displayed and show that the control design technique met their objectives. For the response shown for the ALDCS HG24RR aircraft (in Figure 102), it is apparent that there is a considerable amount of the third flexure mode appearing in the pitch rate response; during the previous ALDCS design (Reference 4), a better looking pitch rate response was obtained for the ALDCS aircraft. This mildly oscillatory portion of the responses is due to the low damping ratio of 0.0051 that was previously discussed.

Table 36. Root Comparison of Free A/C and ALDCS
A/C with F24RR Model

	Free		ALDCS	
Association	Real ω_n	ζ	Real ω_n	ζ
$\dot{\theta}$, α	1.5501	0.5785	1.7393	0.7354
η_1, $\dot{\eta}_1$	5.5283	0.0892	3.7410	0.2501
η_2, $\dot{\eta}_2$				
η_3, $\dot{\eta}_3$	15.5911	0.0699	14.2402	0.1852
η_4, $\dot{\eta}_4$	17.2662	0.0491	17.2567	0.0169
η_5, $\dot{\eta}_5$	18.3701	0.0245	18.3744	0.0216
η_6, $\dot{\eta}_6$	19.3531	0.0315	19.1853	0.0324
η_7, $\dot{\eta}_7$	22.1171	0.0487	21.9848	0.0569
δ_a	-6.0		-1.2552	
δ_{ei}	-7.5		-8.0200	
δ_{eo}	-7.5		-7.5	
A21RL	-6.0		30.5312	0.8669
GLAF	-0.02		30.5312	0.8669
MLC1	-0.01		-0.01	
Pilot Filter	-0.1		-0.1	
Gust Filter	-0.21		-0.21	
Gust Filter	-0.21		-0.21	
Wing Kussner	-9.156		-9.156	
1st Order Delay	-13.427		-13.427	
2nd Order Delay	9.802	0.8165	9.802	0.8165
Tail Kussner	-18.493		-18.493	

For the bending moment response, there are two objectives. The first is that for the steady-state value of the bending moment with the ALDCS aircraft should be 70 percent of that over the free aircraft. Second, it is very desirable that there be as little overshoot as possible in the bending moment response because each overshoot represents needless damage to the aircraft. The ALDCS designs under this contract, as shown in Figures 106, 107, 108, and 109, all display rather good bending moment response; there is little overshoot. The major objection to the response is that on the HG24 model (Figure 106) there is the third mode oscillation which would be eliminated in a more refined design; for example, the third bending mode filters could be put into attenuate the elevator effects on the third mode. HG24RR responses exhibit a little more of the third mode than would be desired.

The torsion moment responses for the ALDCS aircraft are detailed in Figures 110, 111, 112, and 113. As with the bending moment, the torsion responses should be smooth with just a little overshoot. The results for the HG24RR model are quite good except for the third mode; this effect could be eliminated in a more refined design procedure than was accomplished here. The results for the F24RR model again look surprisingly close to those for the HG model with a lot of the third bending mode appearing. The results for F24RT and F24TT models are very different from what we expected to see. The reason could be the truncation after differentiation procedure that was adopted during the study. The results for the torsional version show that the general objectives for the ALDCS are achieved.

First flexure mode responses for the ALDCS aircraft are shown in Figures 114, 115, 116, and 117. Note that the first flexure mode for the HG24RR model has very low damping. During the previous ALDCS design a higher damping was achieved. The F24RR model ALDCS results are qualitatively satisfactory although the deflections are large relative to that found on the HG24 model. The results for the F24RT and F24TT models appear again to be too different than previous experience would indicate.

The transient responses for the third bending mode for the ALDCS aircraft are shown in Figures 118, 119, 120, and 121. For the HG24RR ALDCS response, the third bending mode has little damping; this checks with the damping ratio of 0.0051 that was shown previously. This corresponds to an amplitude ratio of 0.966 per cycle. With the HG24 model as indicated previously, the third mode is very difficult to control. It takes more effort and more tailoring to suppress this mode. The other ALDCS traces also show a well damped third mode oscillation.

The sixth flexure mode results for the ALDCS aircraft are shown in Figures 122, 123, 124, and 125. The sixth flexure mode shows rather modest damping. In viewing these results, it should be noted that the amplitudes and the responses are quite small; the normalized plots that we are presenting here tend to over-emphasize the importance of these terms.

Elevator response plots for the ALDCS aircraft in Figures 126 through 137 show considerable activity which reflects the feedback from the flexure modes into the ALDCS controller. The aileron response plots are shown in Figures 138 through 145. For ALDCS, the aileron response should be compared with the bending moment response. The aileron, to a high degree

establishes bending relief. Therefore, the aileron response needs to be phased in such a manner that it prevents the overshoot in bending moment response. The ALDCS objective of getting the bending moment response to look like a second order system with a damping ratio of about 0.7 can be achieved by phasing the aileron correctly with the feedback system. For example, for the HG24RR results, it is seen that the bending moment has a flat spot between 1 and 2 seconds and then peaks at around 2.7 seconds and then backs off by about 5 percent; these are results in Figure 106. The aileron transient response is shown in Figure 138. It peaks at about 2.0 seconds and stays there until about 0.2 seconds and retrenches at about 5 percent. If the aileron response was reshaped so that the portion between 0.7 of a second and 1.6 seconds had the outer end moved from 1.6 to about 2.7, the bending moment response of Figure 106 would have been improved because of the elimination of the overshoot. In any event since the step command response is really a worse case situation, the response for normal input with the system as shown here would have very little overshoot and would be very desirable. Comparisons of the ALDCS results will show that the aileron phasing is quite close to that desired in order to prevent the bending mode excesses. (Note in Figures 126 to 130, BDEI is equal to DELEI).

The angle of attack response plots are shown in Figures 146 through 151.

In summary, it can be said that on the basis of these comparisons, the FLEXSTAB produces valid vehicle models for preliminary design of CCV control laws.

HGC5A MODEL
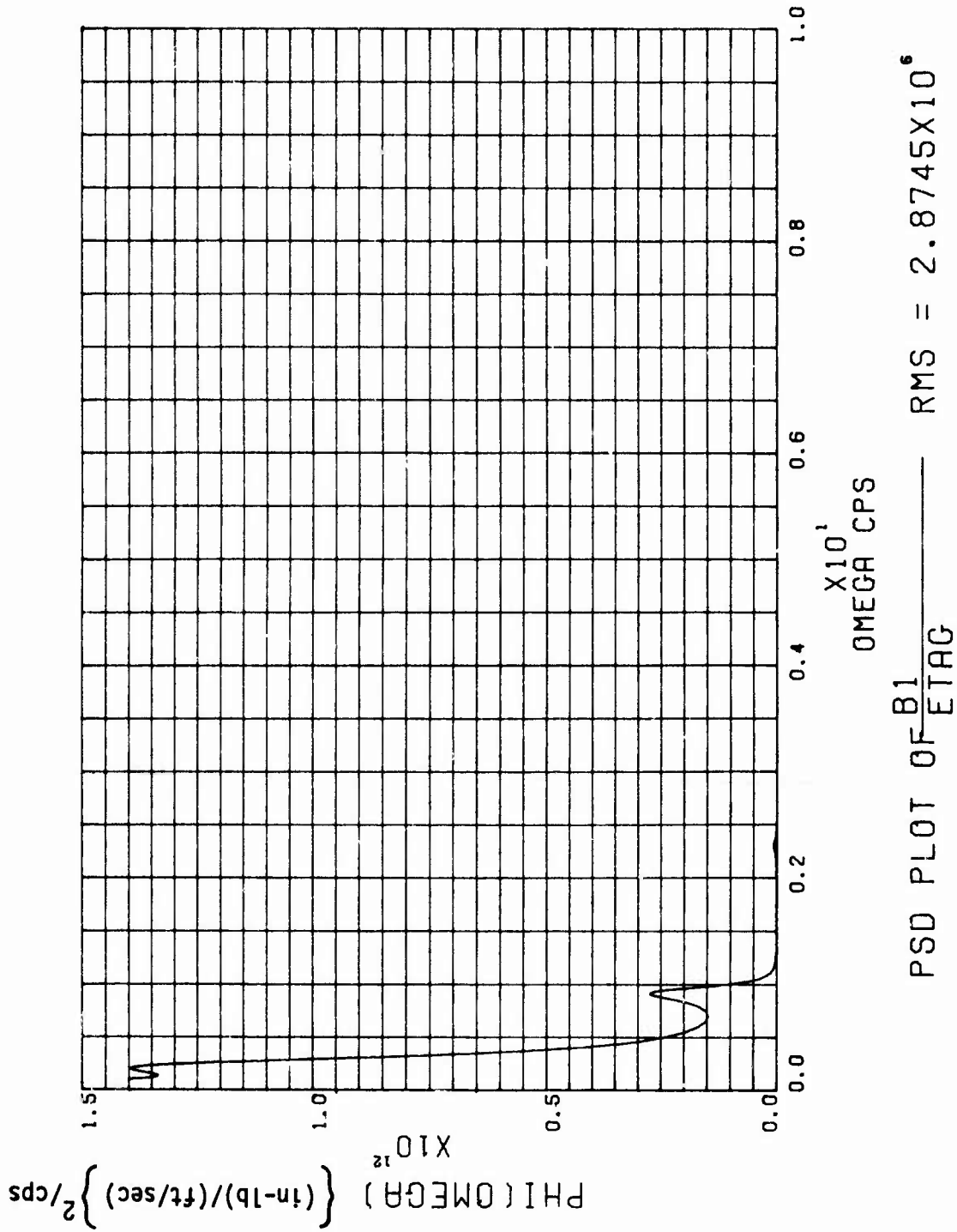
Figure 56. PSD Plot of Free A/C with HG42 Model (B1/ETAG)

174

FC5A MODEL

PSD PLOT OF $\frac{B1}{ETAG}$ ——— RMS = 2.1712X10^6
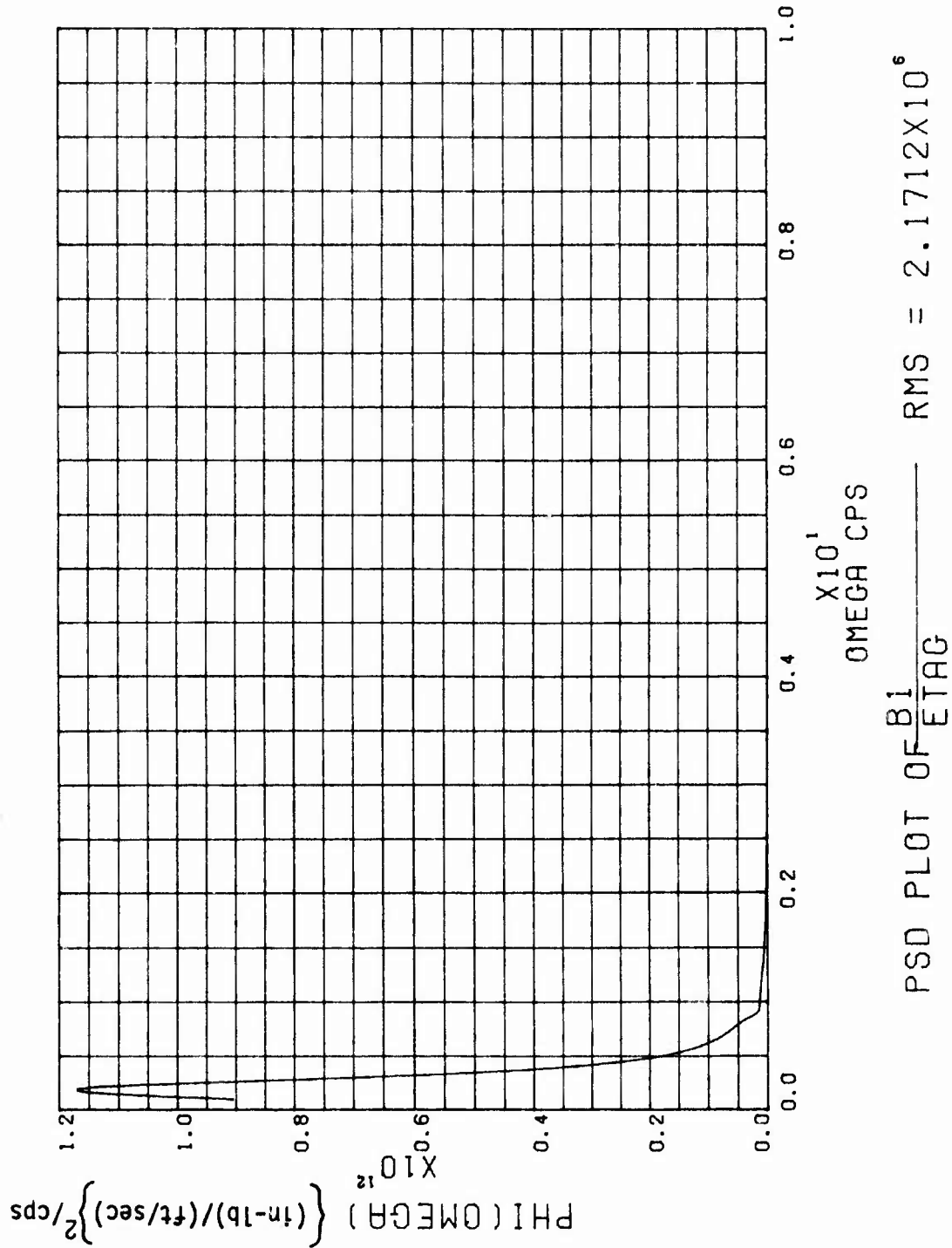
Figure 57. PSD Plot of Free A/C with F42 Model (B1/ETAG)

175
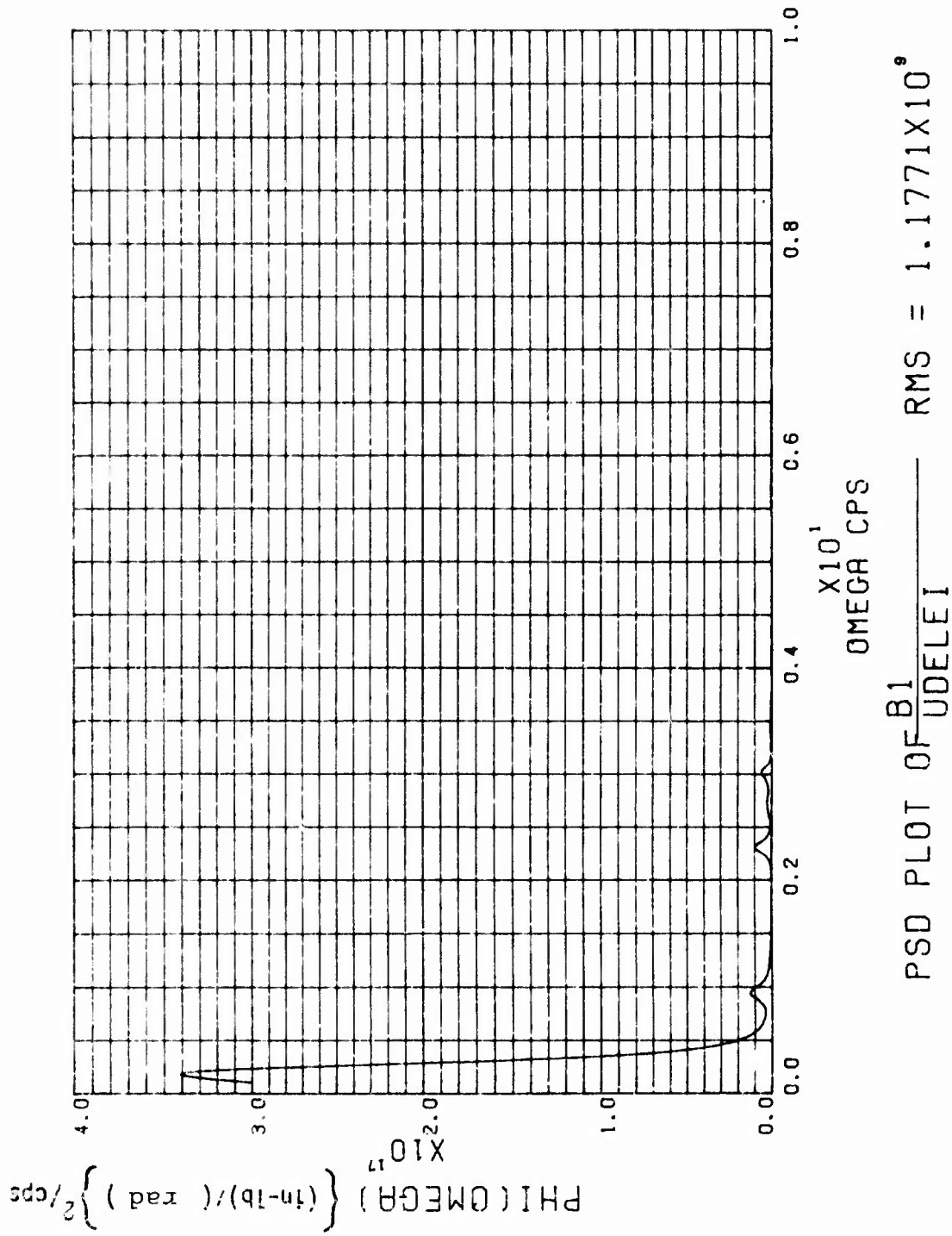
Figure 58. PSD Plot of Free A/C with HG42 Model (B1/UDELEI)

FCSA MODEL

PSD PLOT OF $\dfrac{B1}{UDELEI}$ ——— RMS = 1.3396X10^9
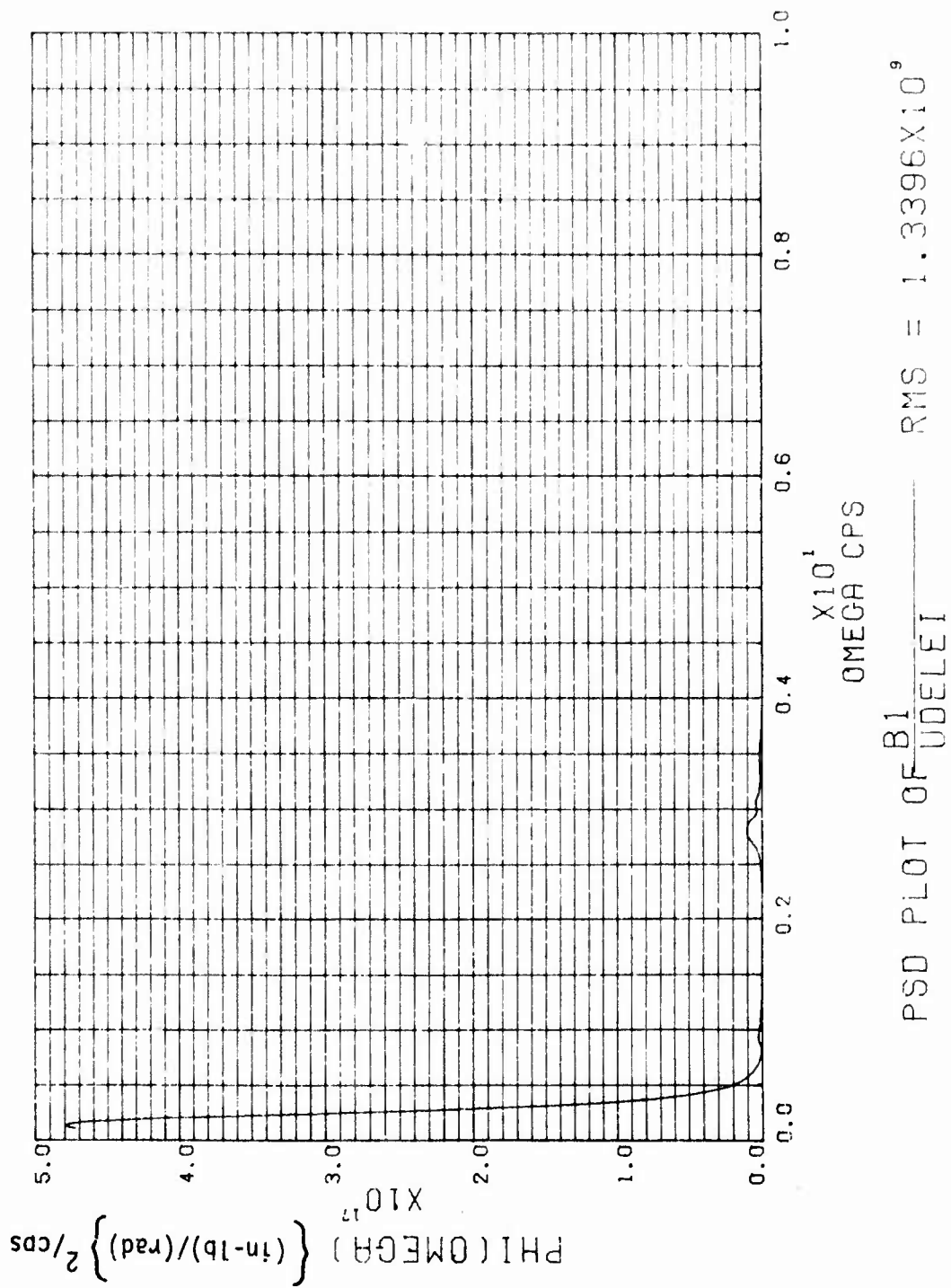
Figure 59. PSD Plot of Free A/C with F42 Model (B1/UDELEI)

HGCSA MODEL
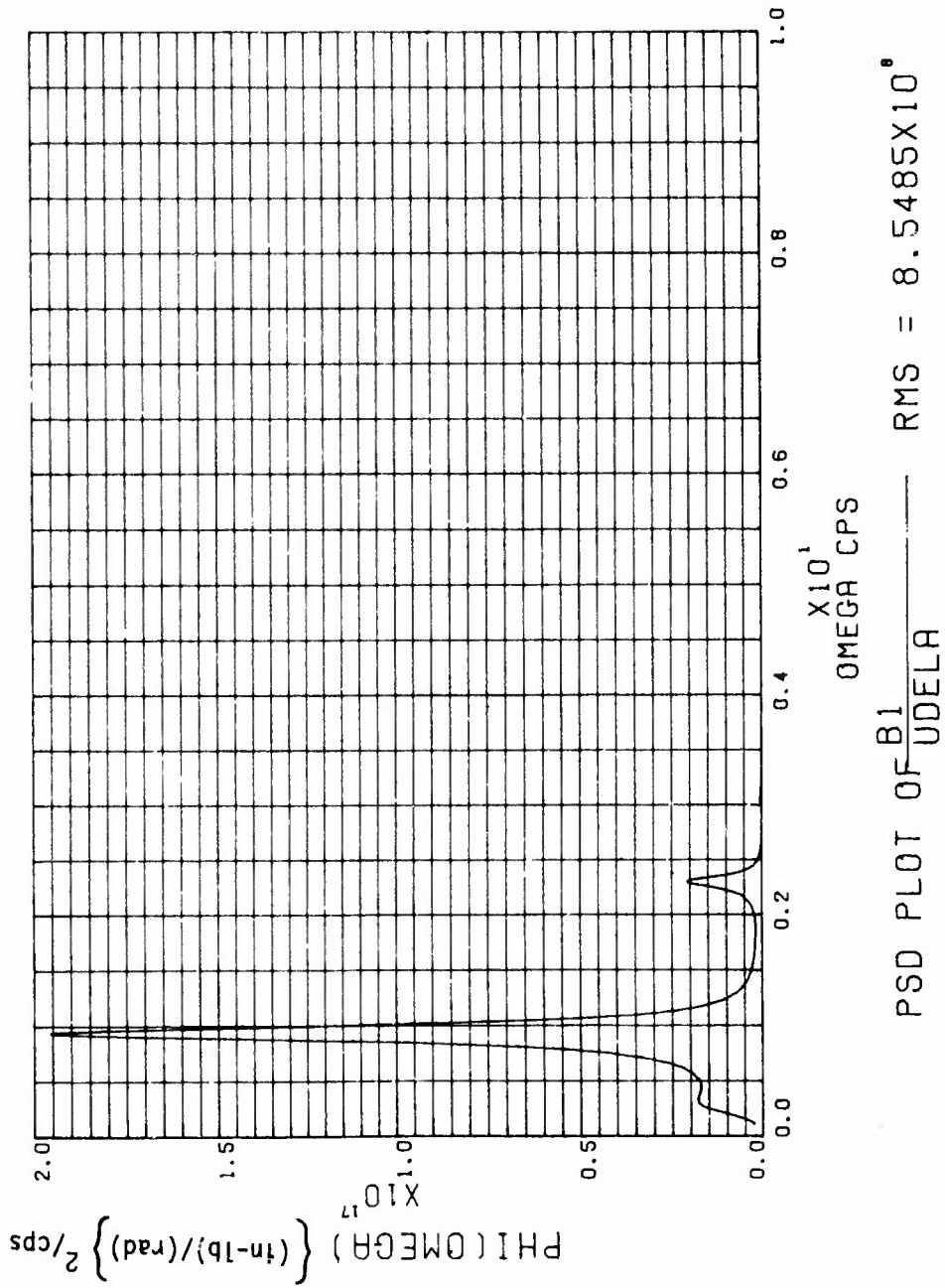
Figure 60. PSD Plot of Free A/C with HG42 Model (B1/UDELA)

FC5A MODEL
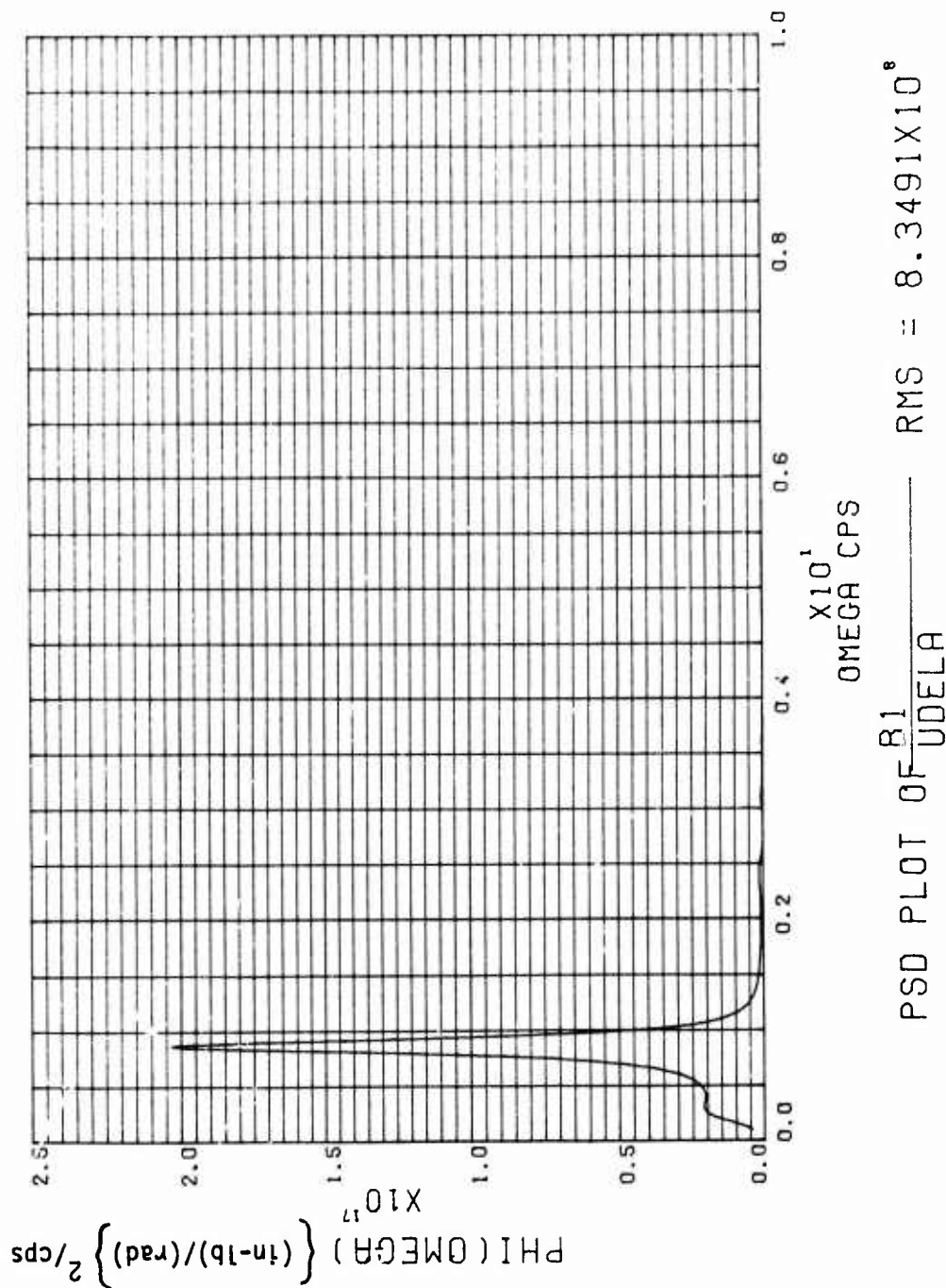
Figure 61. PSD Plot of Free A/C with F42 Model (B1/UDELA)
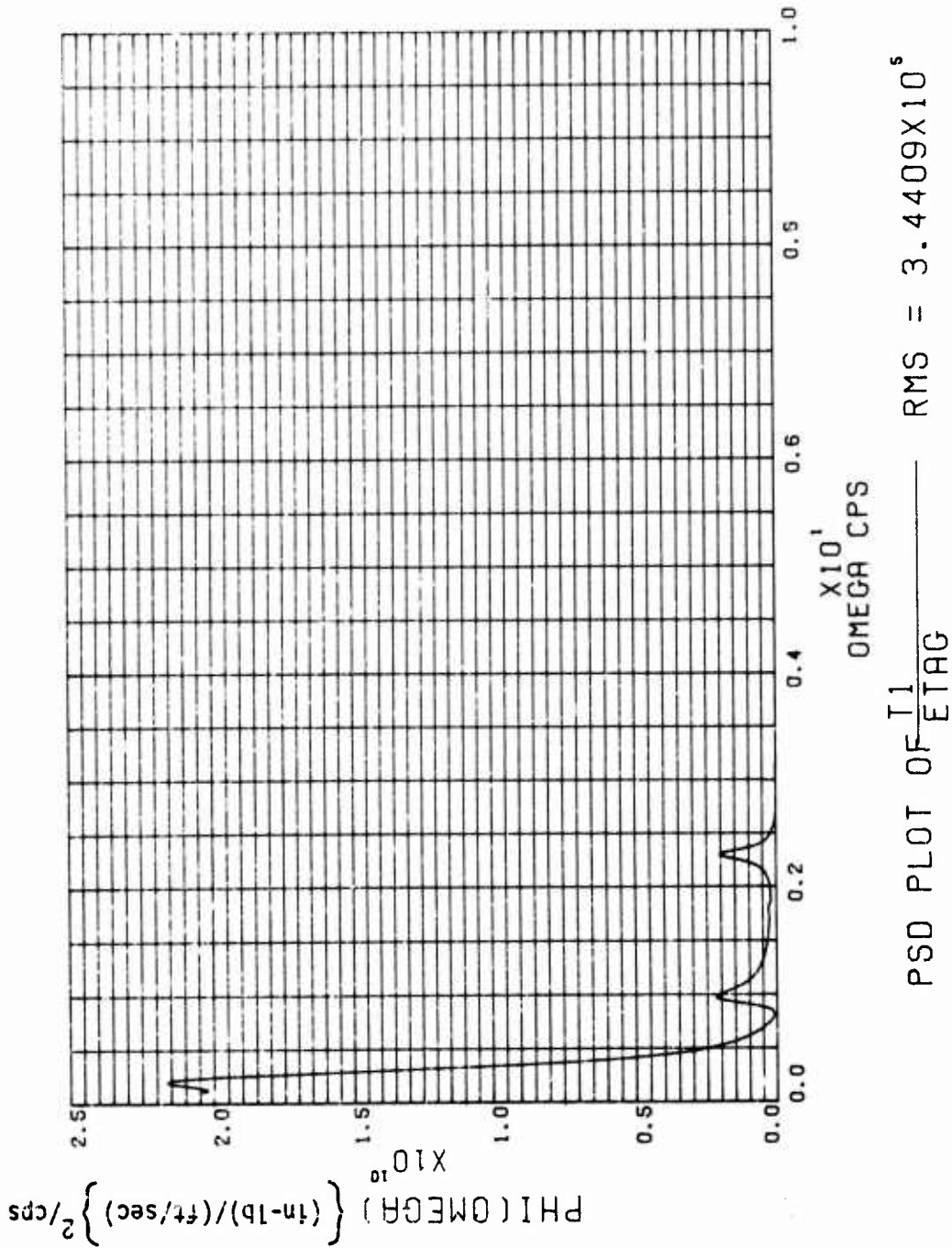
Figure 62. PSD Plot of Free A/C with HG42 Model (T1/ETAG)

FCSA MODEL
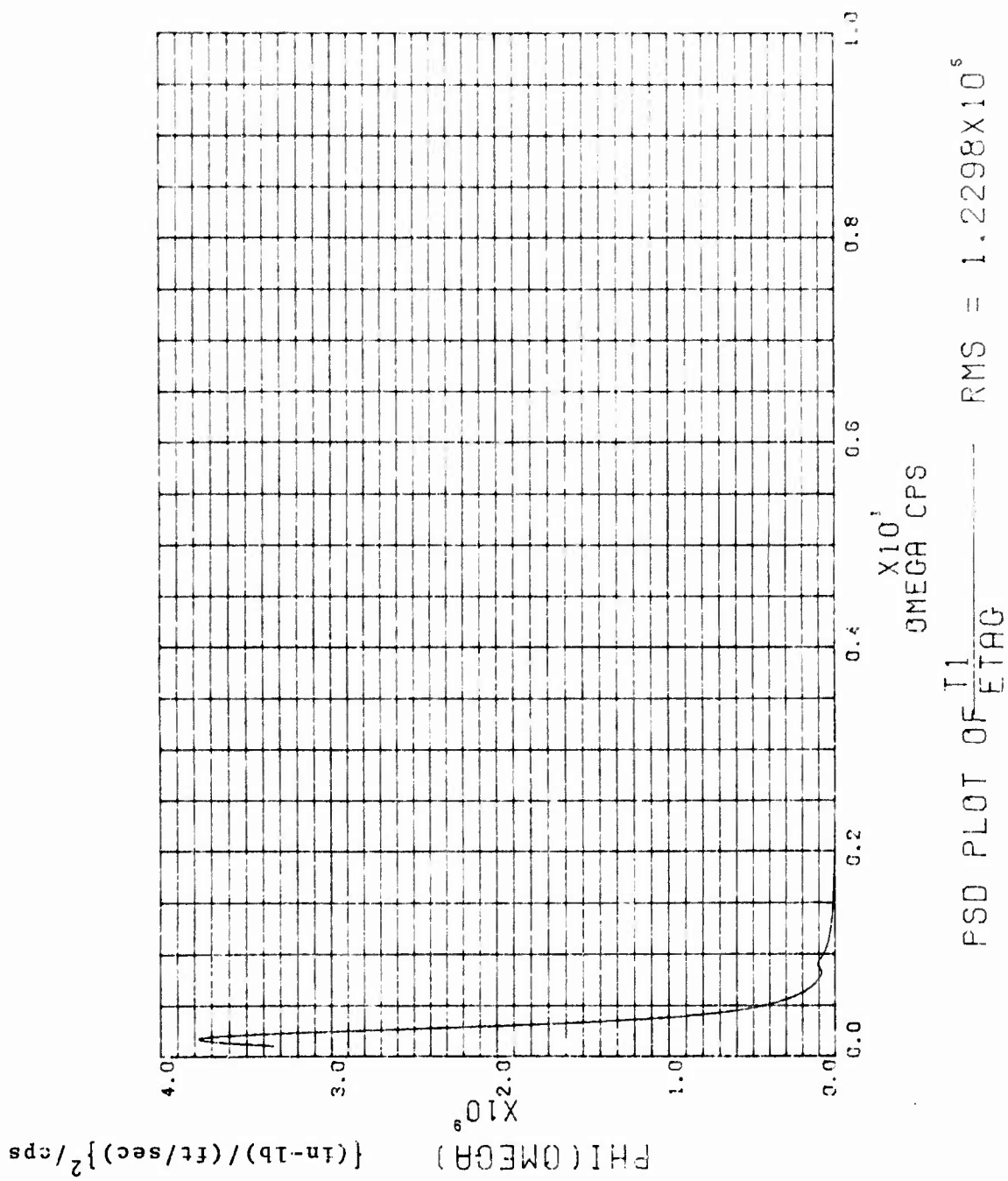
Figure 53. PSD Plot of Free A/C with F42 Model (T1/ETAG)

181
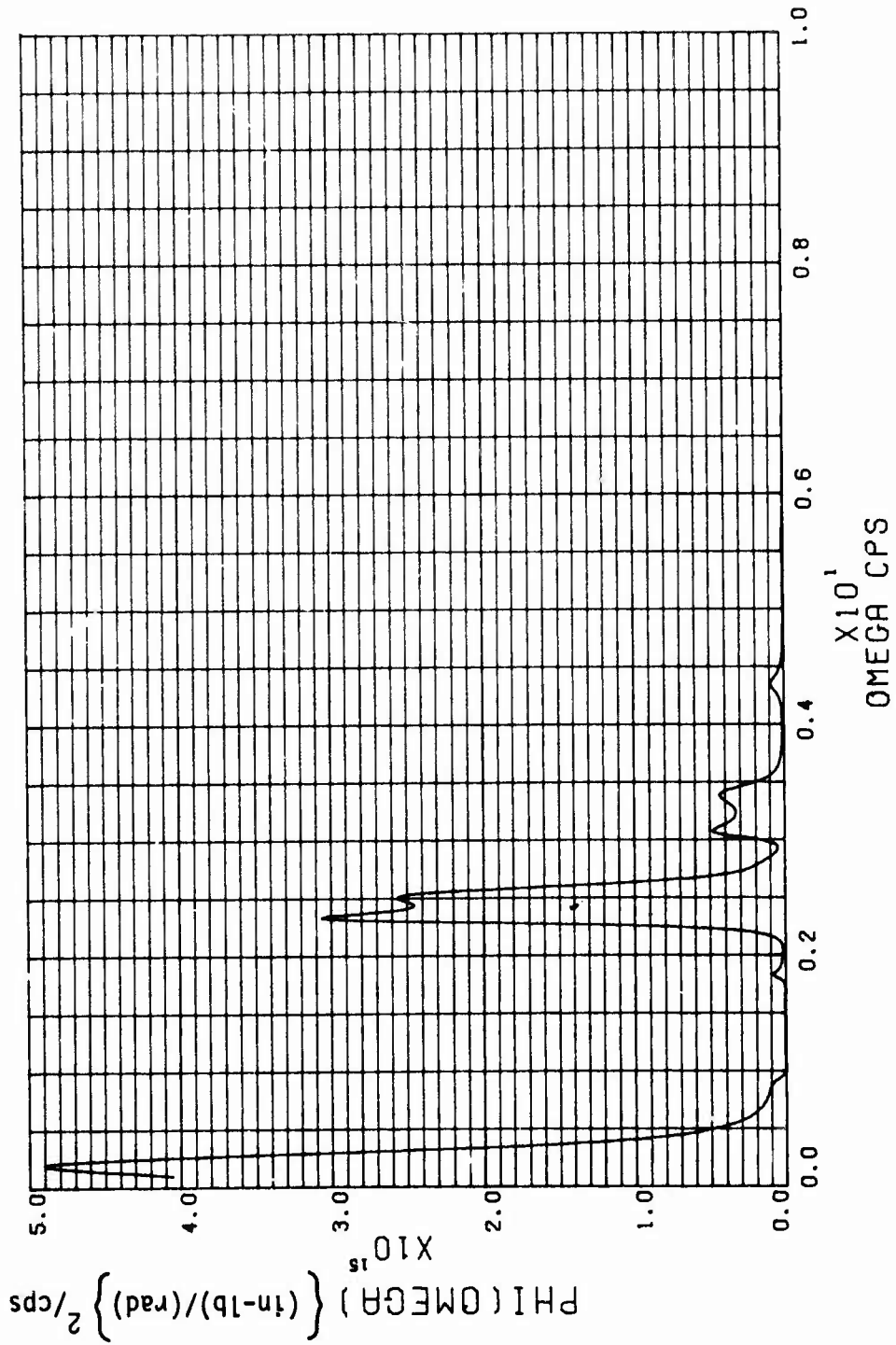
HGC5A MODEL

Figure 64. PSD Plot of Free A/C with HG4C Model (T1/UDELEI)

182

FCSA MODEL
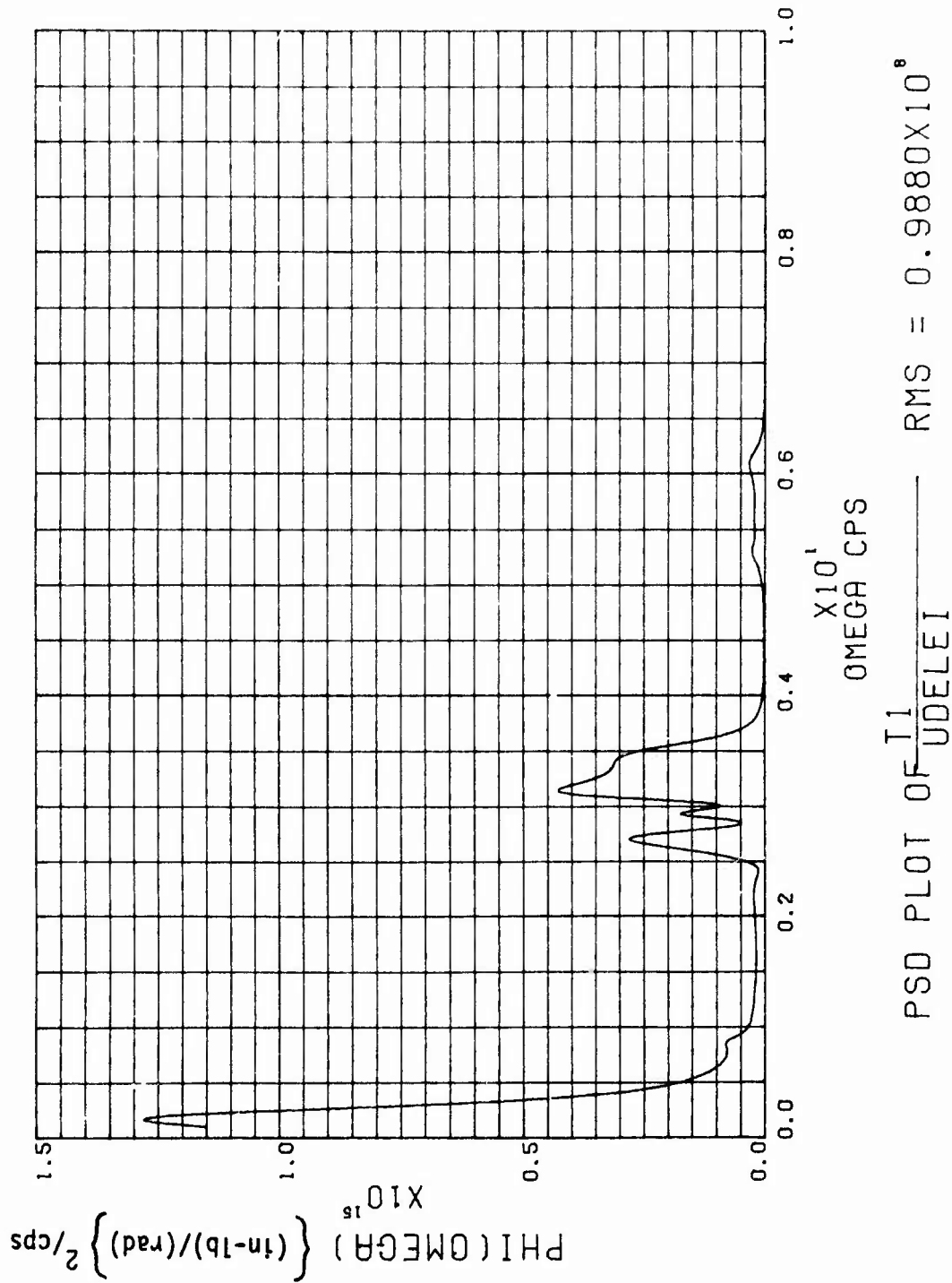
Figure 65. PSD Plot of Free A/C with F42 Model (T1/UDELEI)

$$PSD\ PLOT\ OF\ \frac{T1}{UDELA} \qquad RMS = 1.6261 \times 10^{8}$$
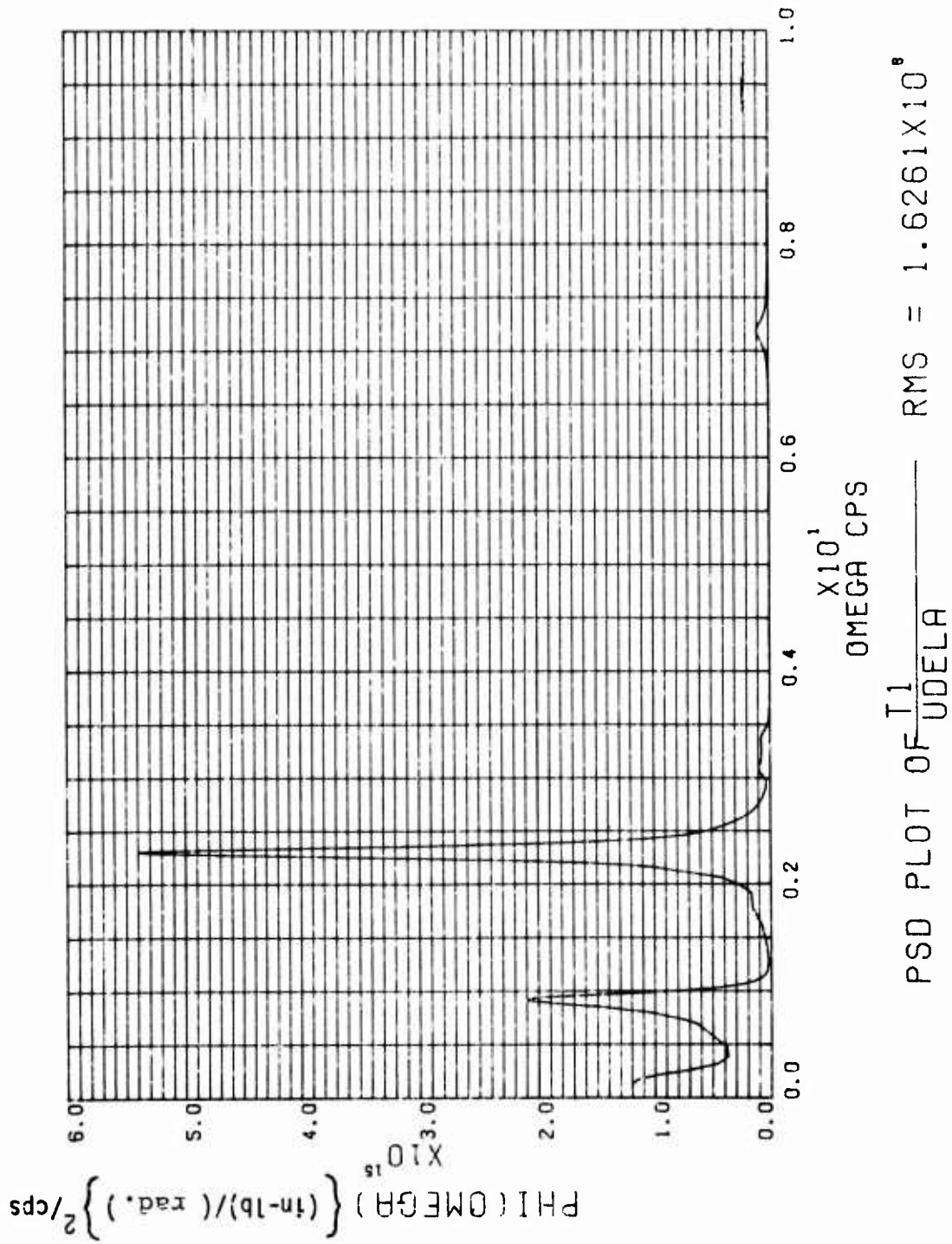
Figure 66. PSD Plot of Free A/C with HG42 Model (T1/UDELA)

FC5A MODEL

PSD PLOT OF $\frac{T1}{UDELA}$ —— RMS = 1.1446X10^8
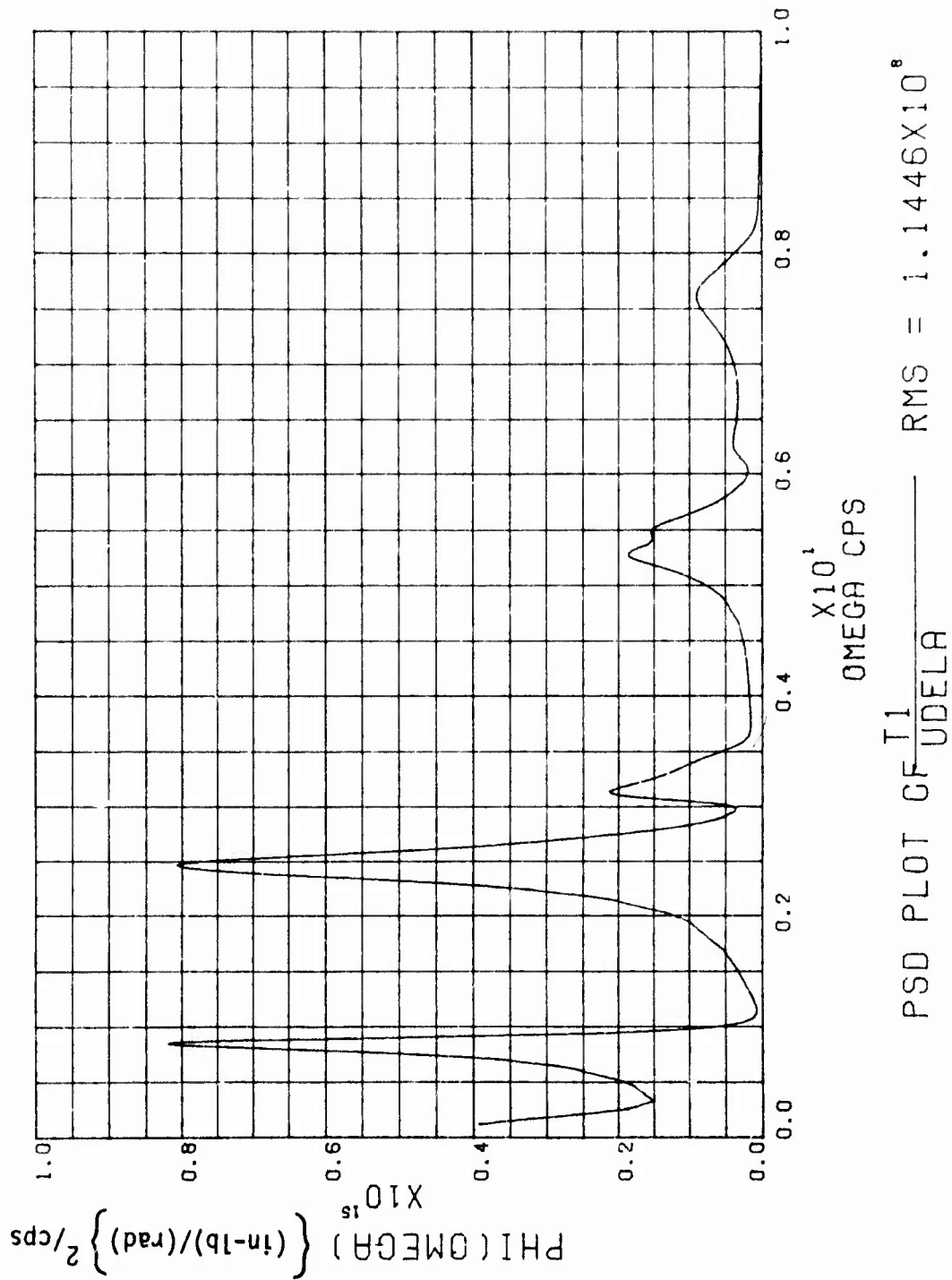
Figure 67. PSD Plot of Free A/C with F42 Model (T1/UDELA)

185

PSD PLOT OF $\frac{UE3}{ETAG}$ RMS = 6.9359×10^{-2}
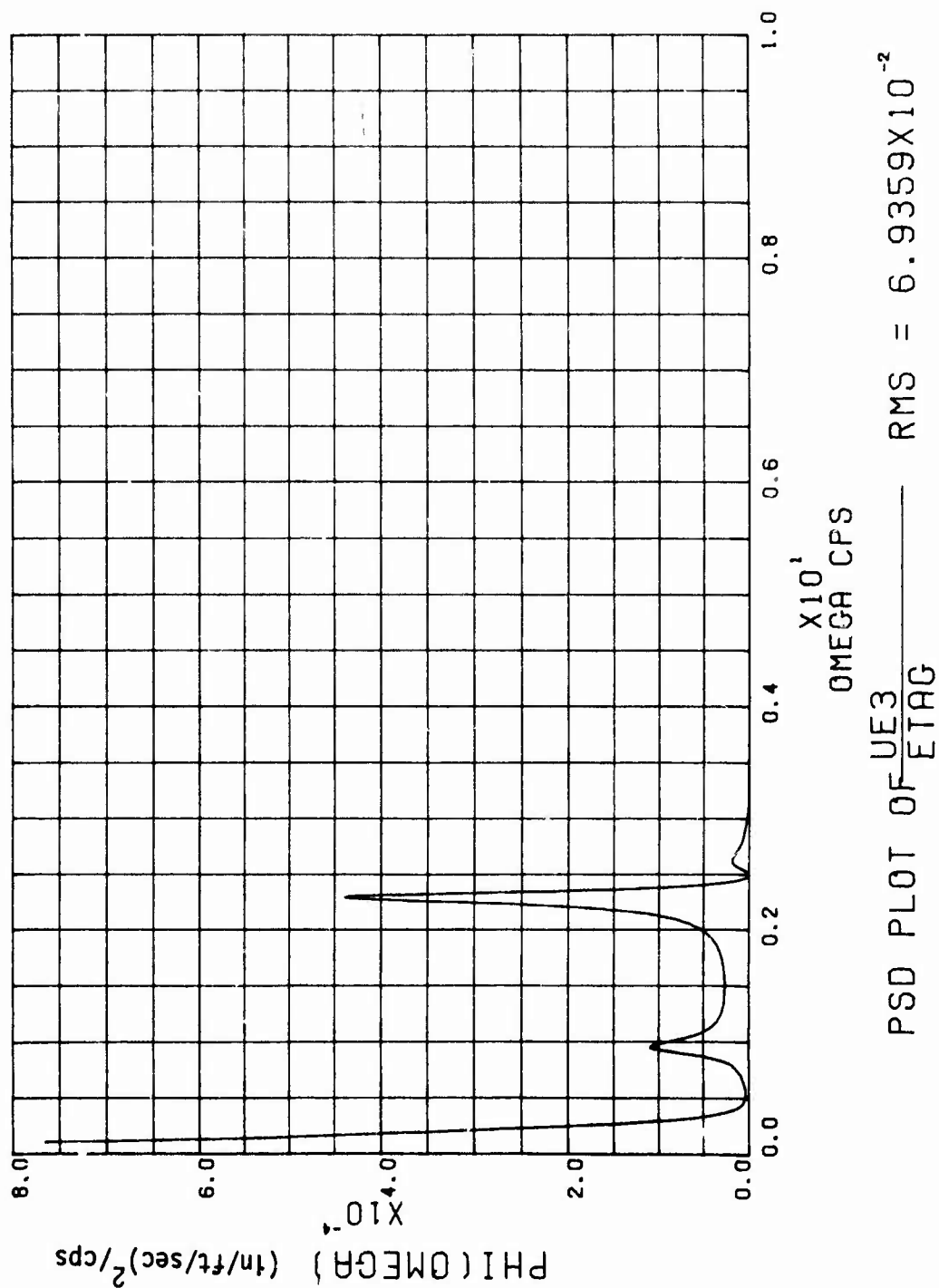
Figure 68. PSD Plot of Free A/C with HG42 Model (UE3/ETAG)

FC5A MODEL
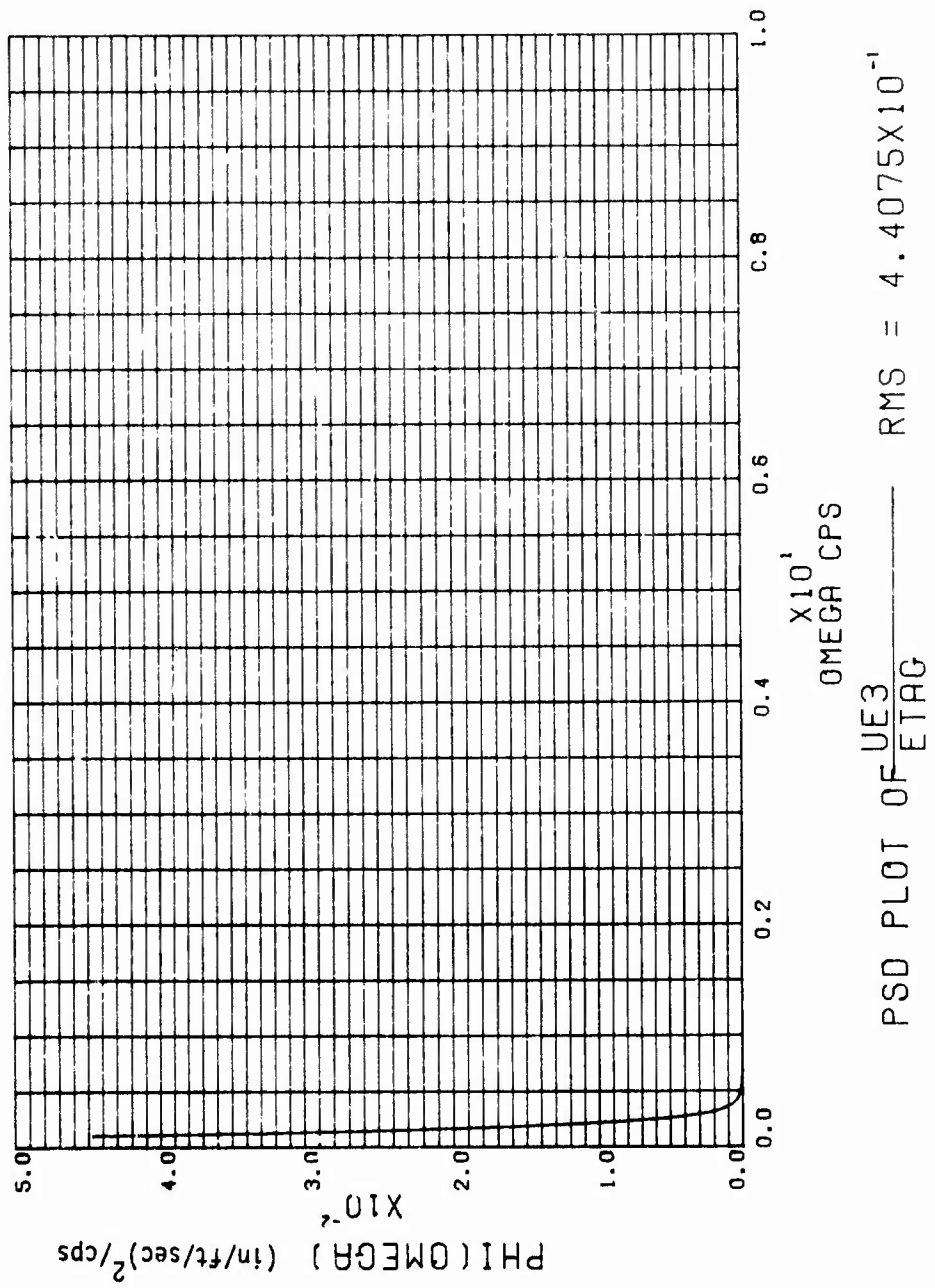
Figure 69. PSD Plot of Free A/C with F42 Model (UE3/ETAG)

HGC5A MODEL

PSD PLOT OF $\frac{UE3}{UDELEI}$ ———— RMS = 1.1509×10^2
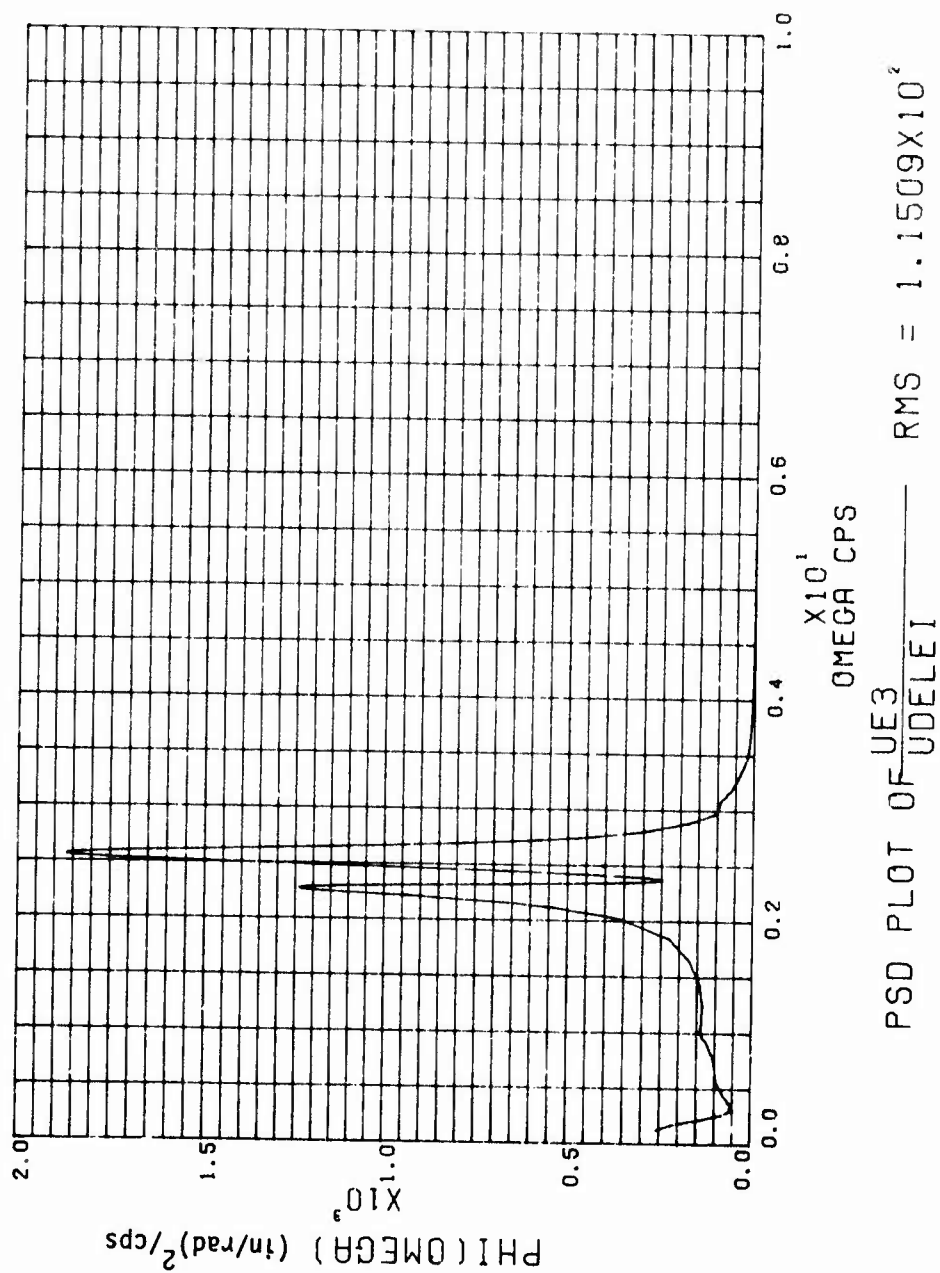
Figure 70. PSD Plot of Free A/C with HG42 Model (UE3/UDELEI)

FCSA MODEL

PSD PLOT OF $\frac{UE3}{UDELEi}$ ———— RMS = 6.9812X10²
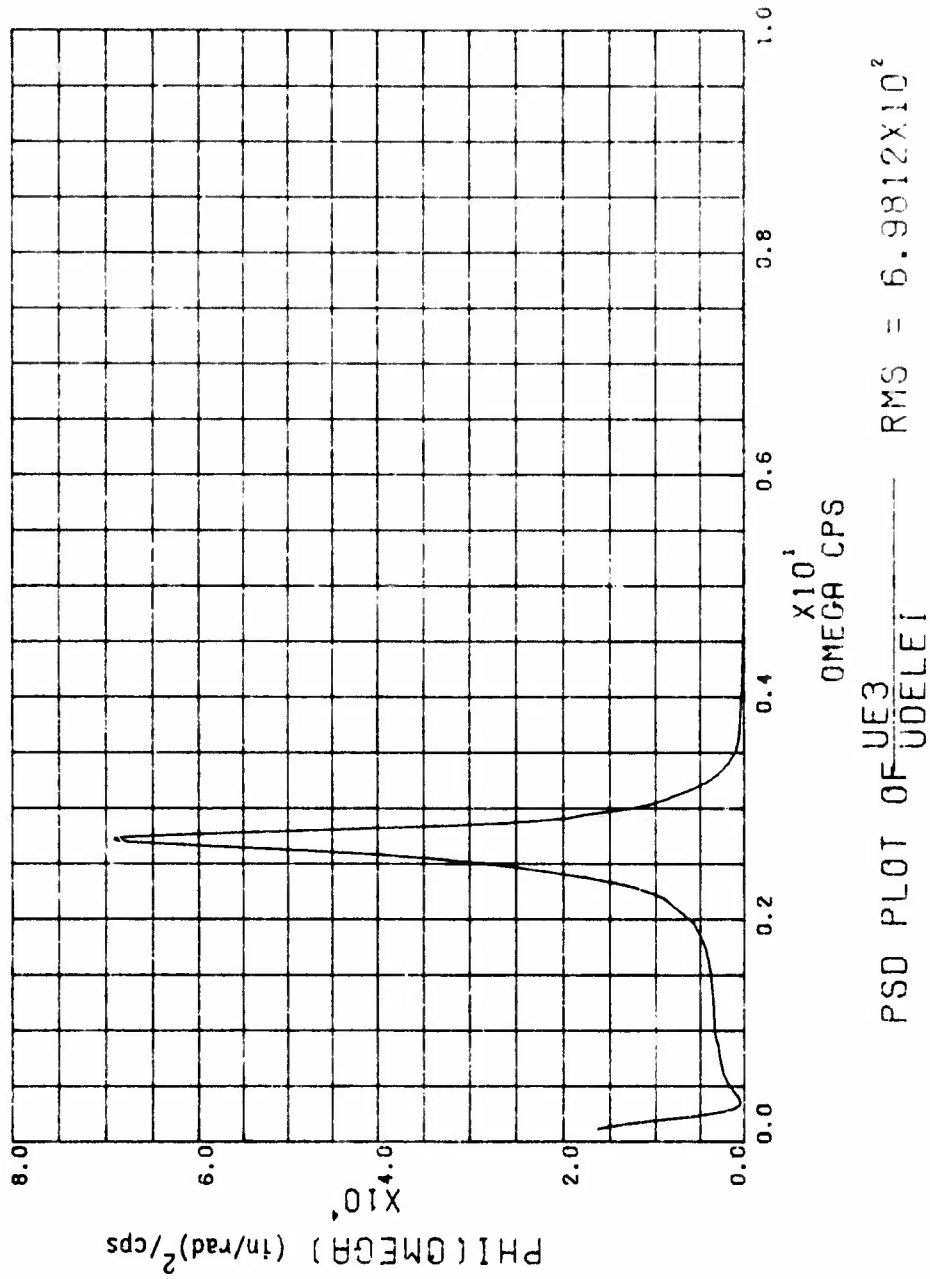
Figure 71. PSD Plot of Free A/C with F42 Model (UE3/UDELE8)

189

HGCSA MODEL

PSD PLOT OF $\dfrac{UE3}{UDELA}$ —— RMS = 6.6570X10^1
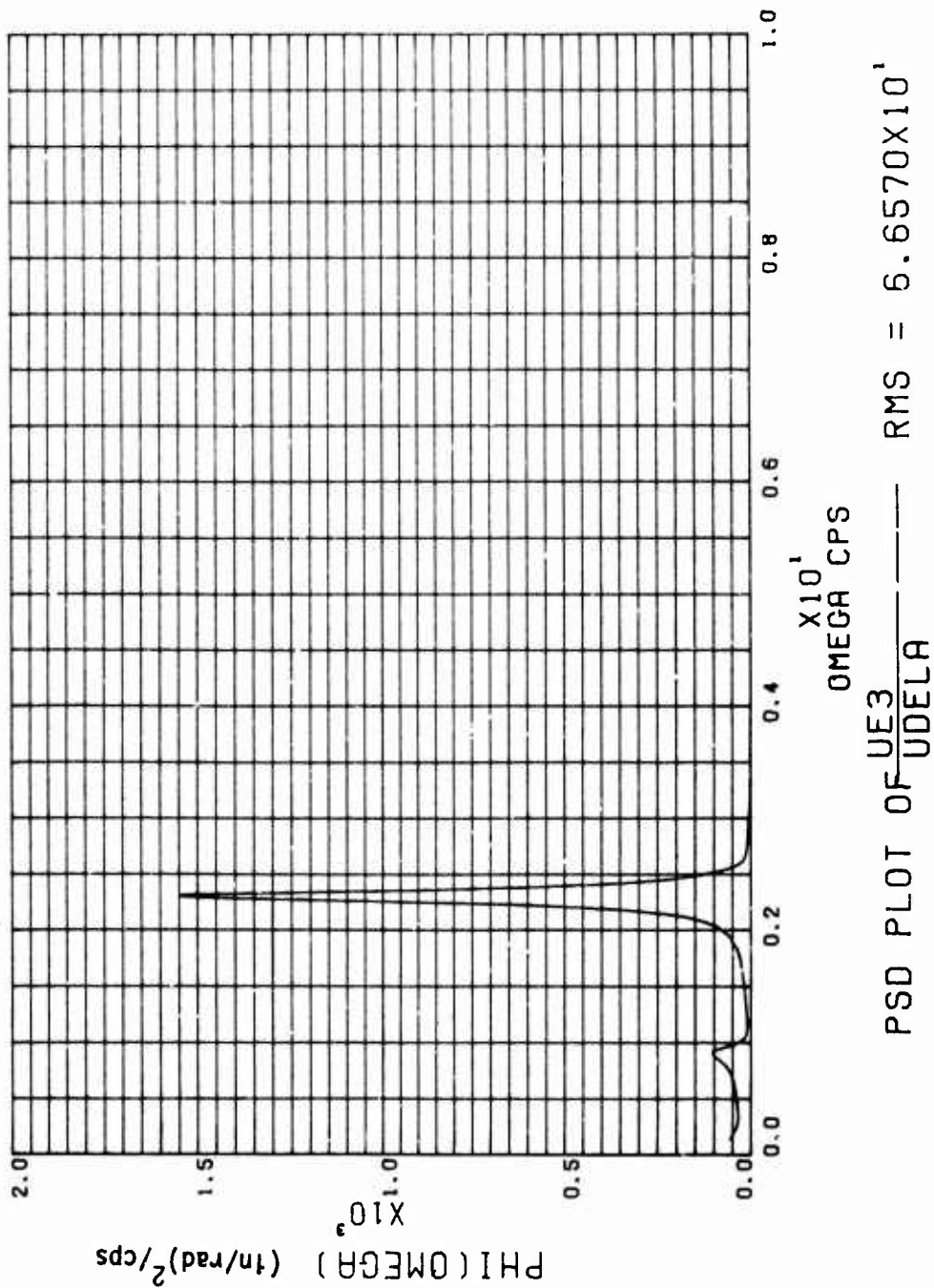
Figure 72. PSD Plot of Free A/C with HG42 Model (UE3/UDELA)

190

FC5A MODEL
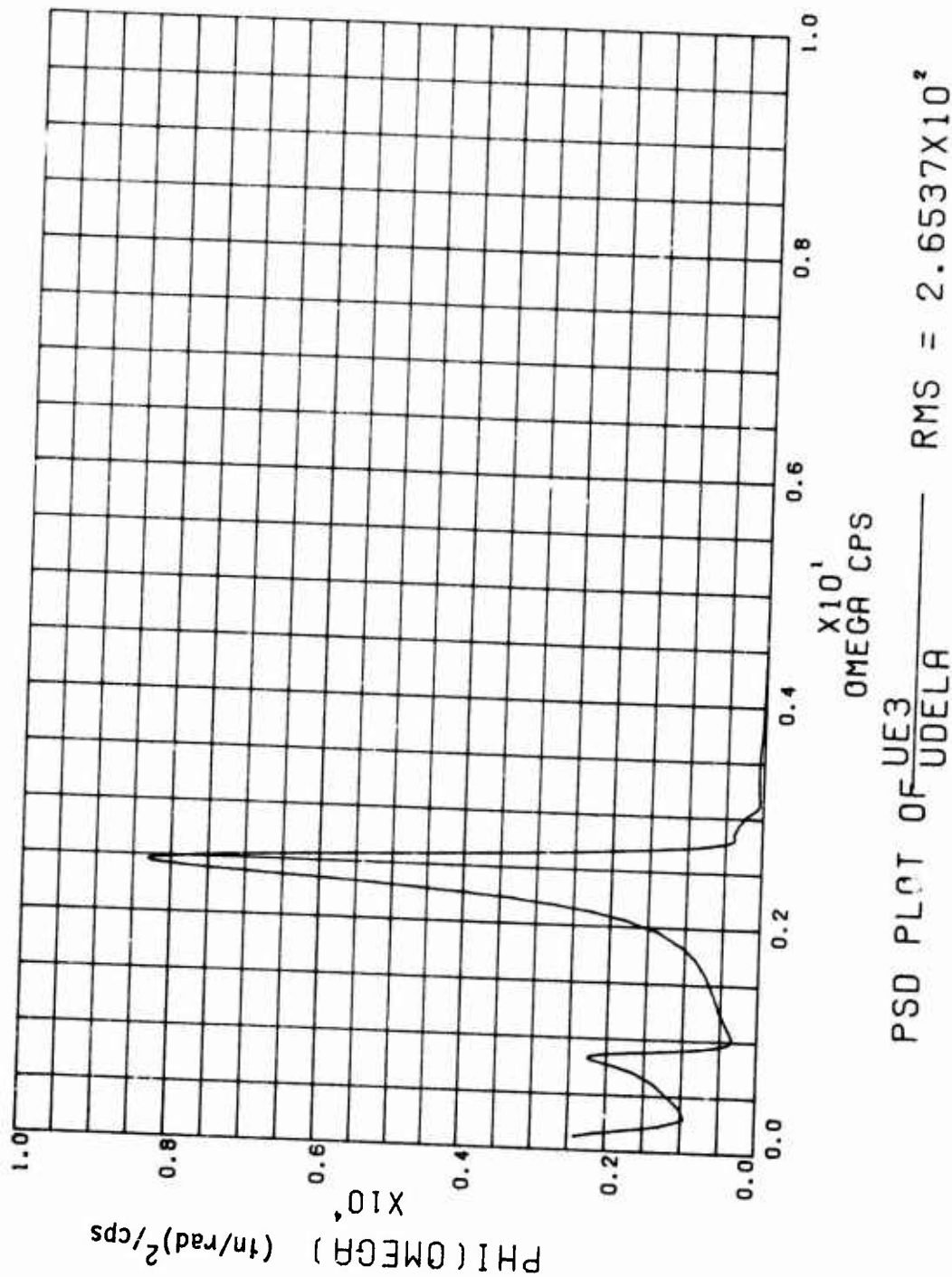
Figure 73. PSD Plot of Free A/C with F42 Model (UE3/UDELA)

191
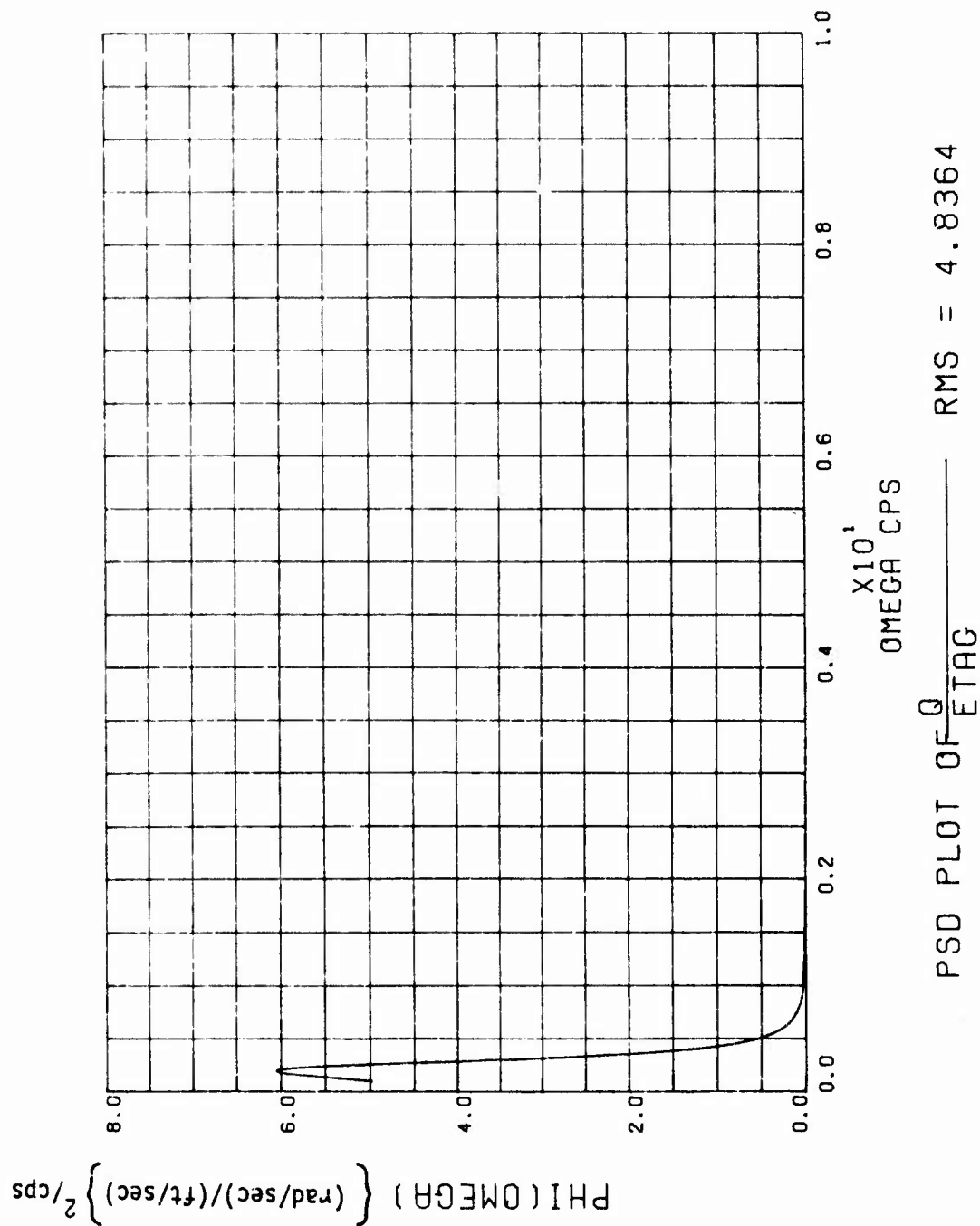
HGCSA MODEL

Figure 74. PSD Plot of Free A/C with HG42 Model (Q/ETAG)

192

FC5A MODEL

PSD PLOT OF $\frac{Q}{ETAG}$ —— RMS = 2.7643

X10¹
OMEGA CPS

PHI(OMEGA) $\left\{ (rad/sec)/(ft/sec) \right\}^2/cps$
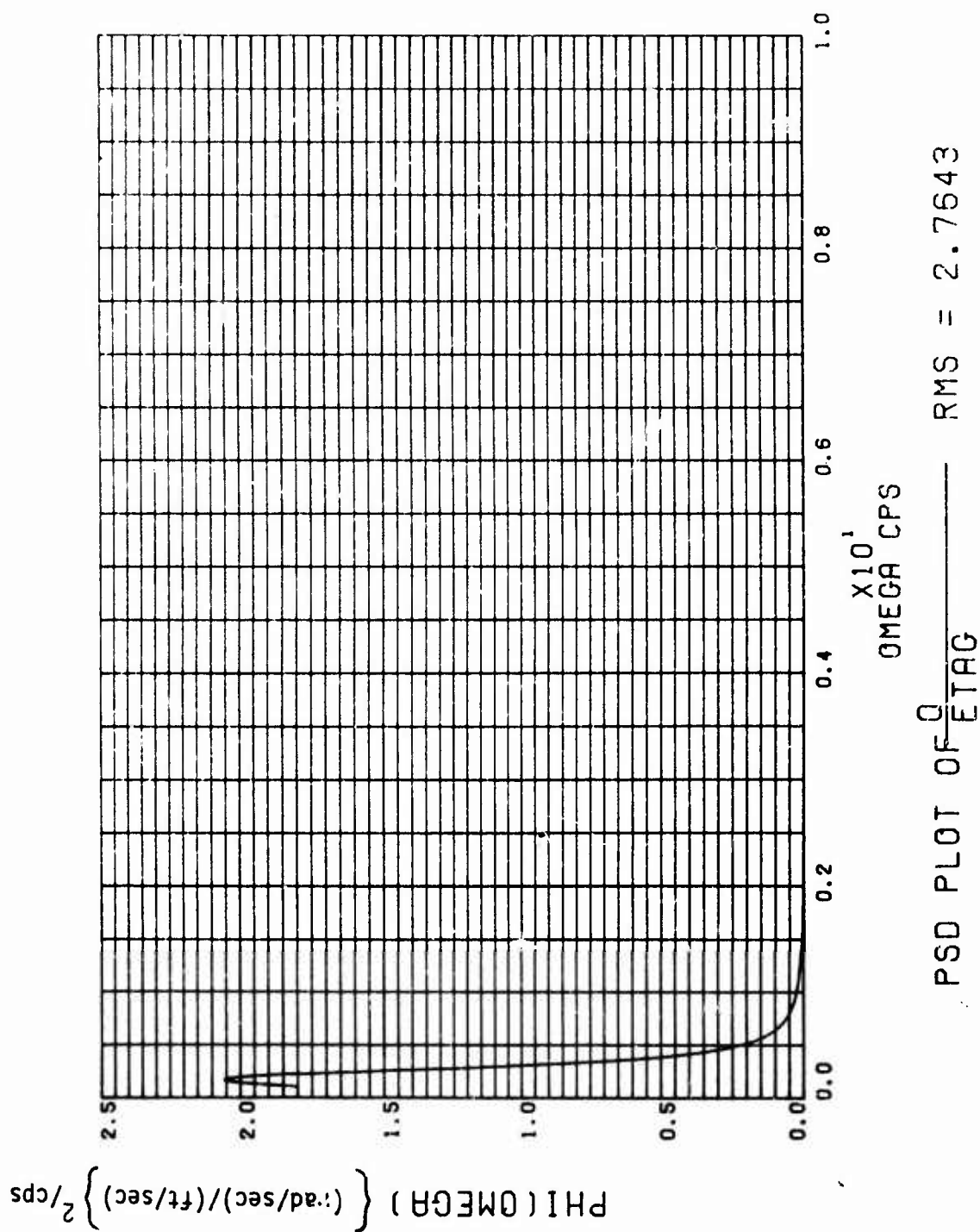
Figure 75, PSD Plot of Free A/C with F42 Model (Q/ETAG)

193
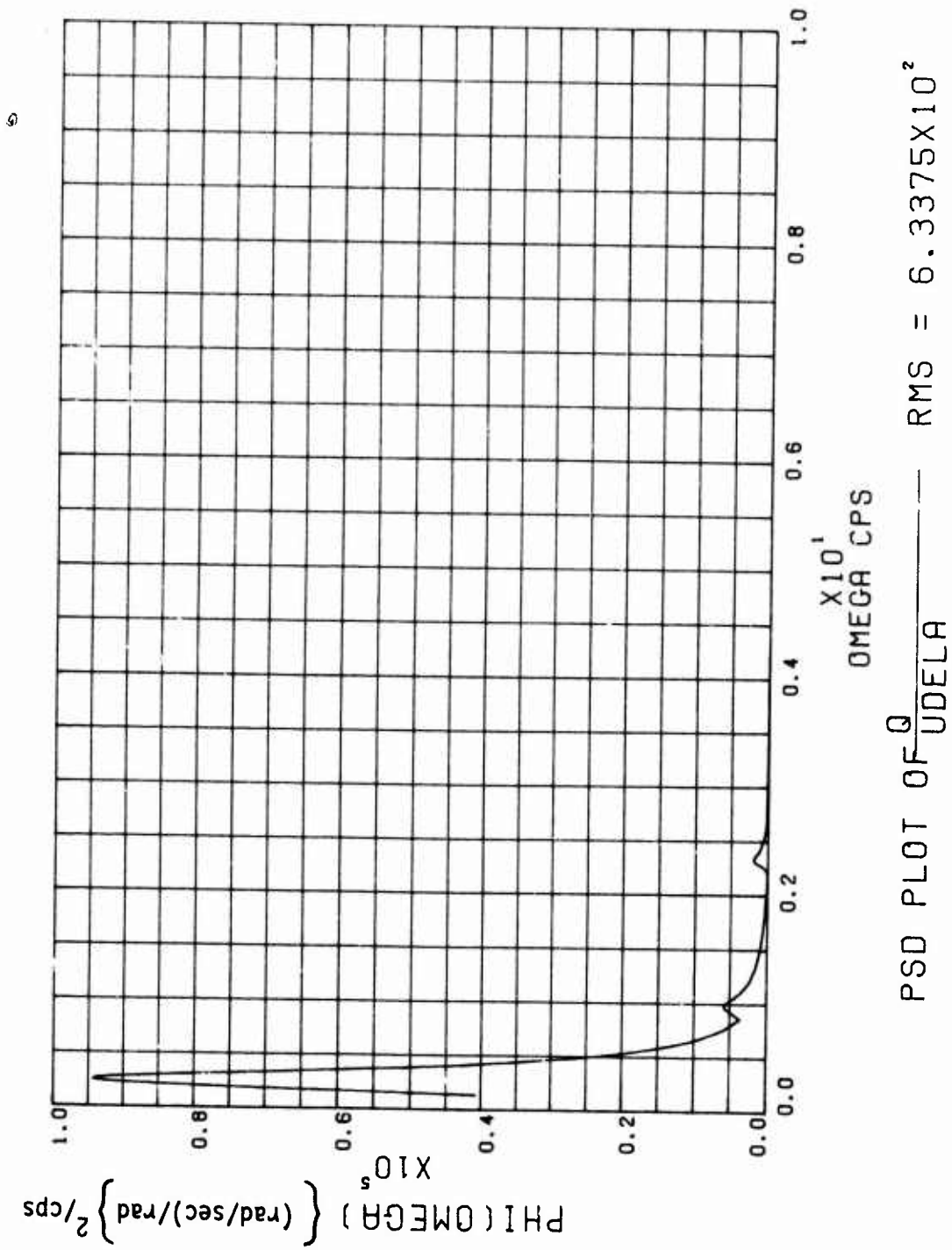
Figure 76. PSD Plot of Free A/C with HG42 Model (Q/UDELEI)

FC5A MODEL
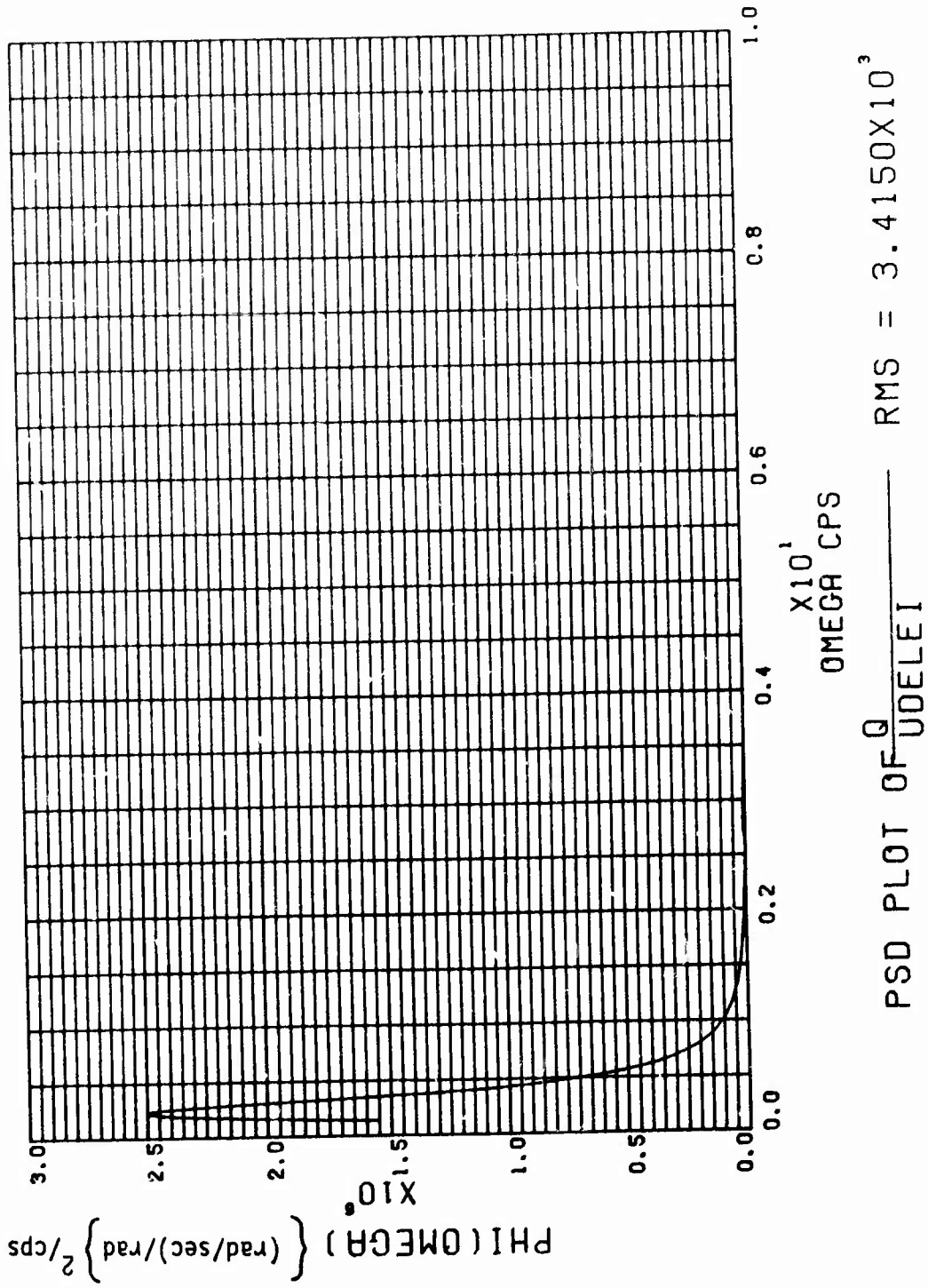
Figure 77. PSD Plot of Free A/C with F42 Model (Q/UDELEI)

195

HGC5A MODEL

PSD PLOT OF $\frac{Q}{UDELEI}$ ———— RMS = 3.1237X10³
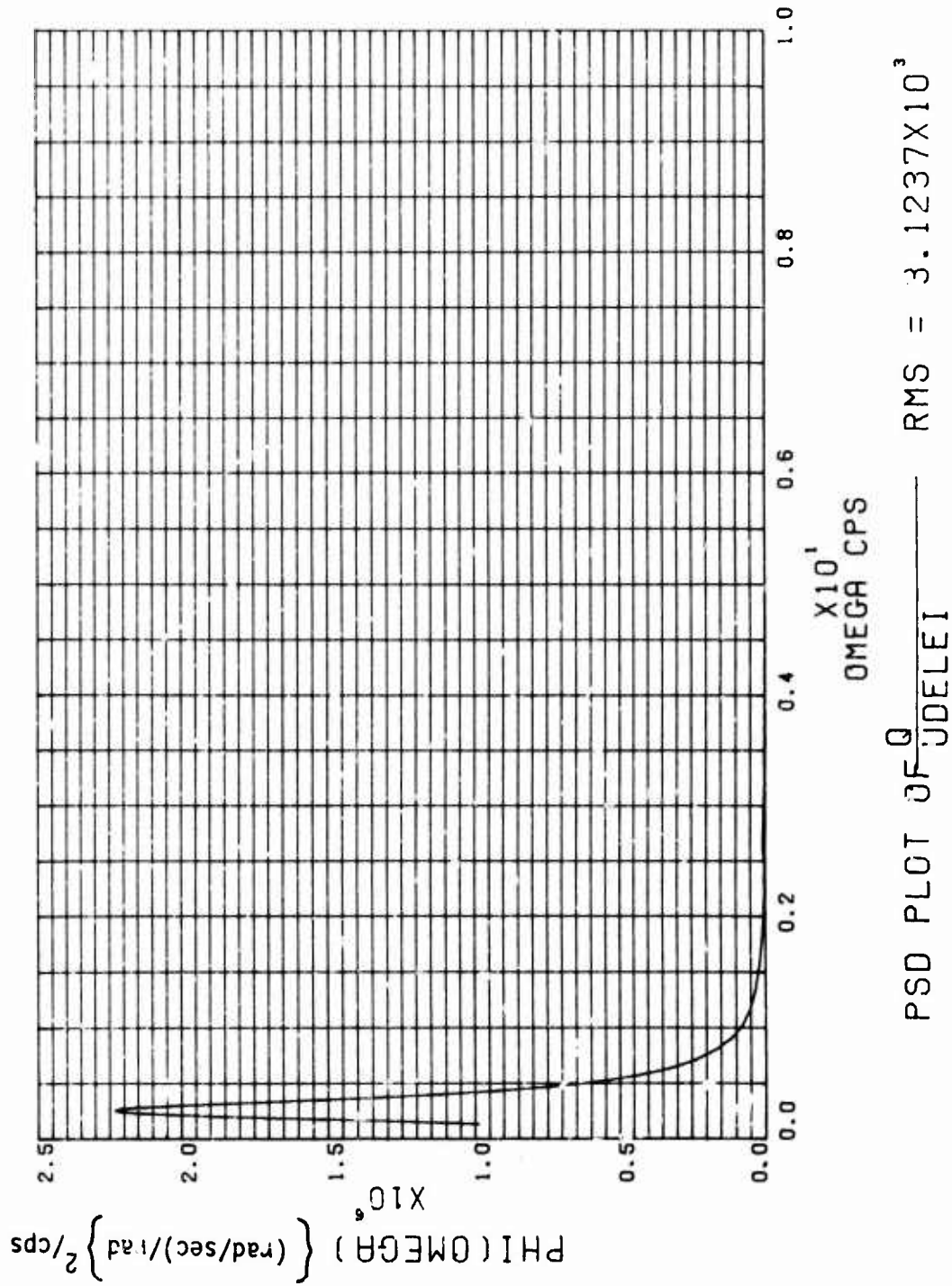
Figure 78. PSD Plot of Free A/C with HG42 Model (Q/UDELA)

196

FCSA MODEL
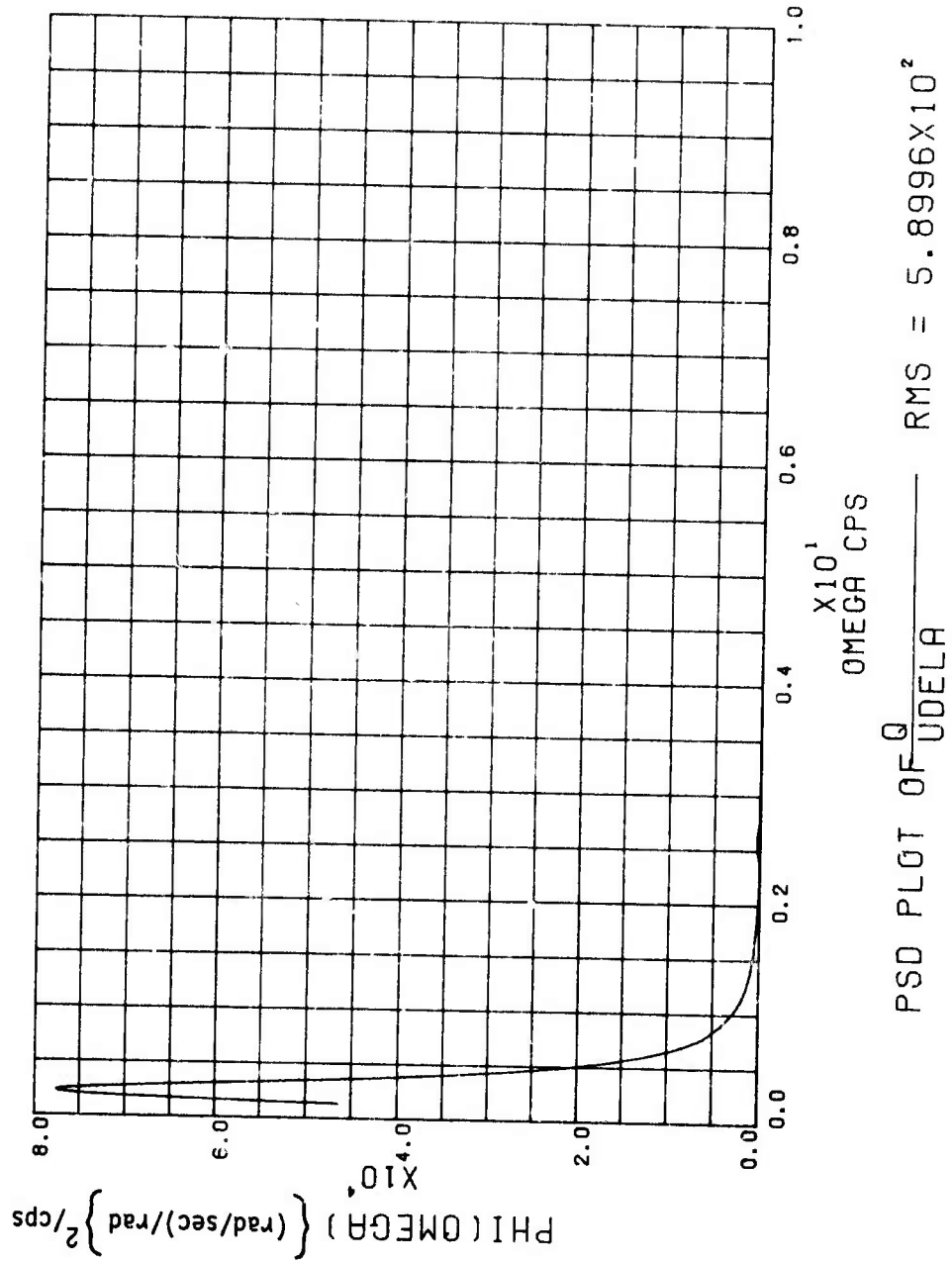
Figure 79. PSD Plot of Free A/C with F42 Model (Q/UDELA)

197
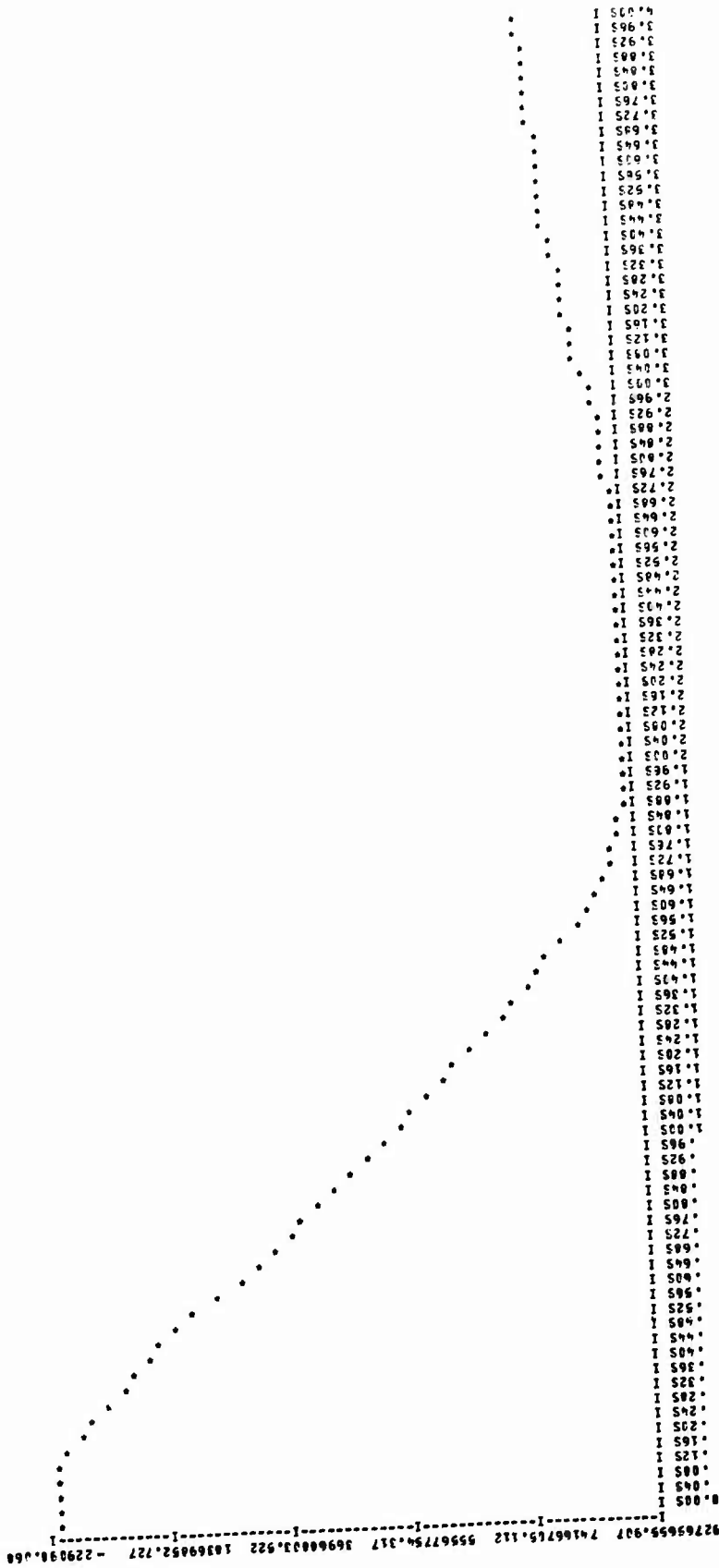
TIME (SECONDS)

Figure 80. Command Response Plot of Free A/C with HG24RR Model (B1)

(in-lbs)

198
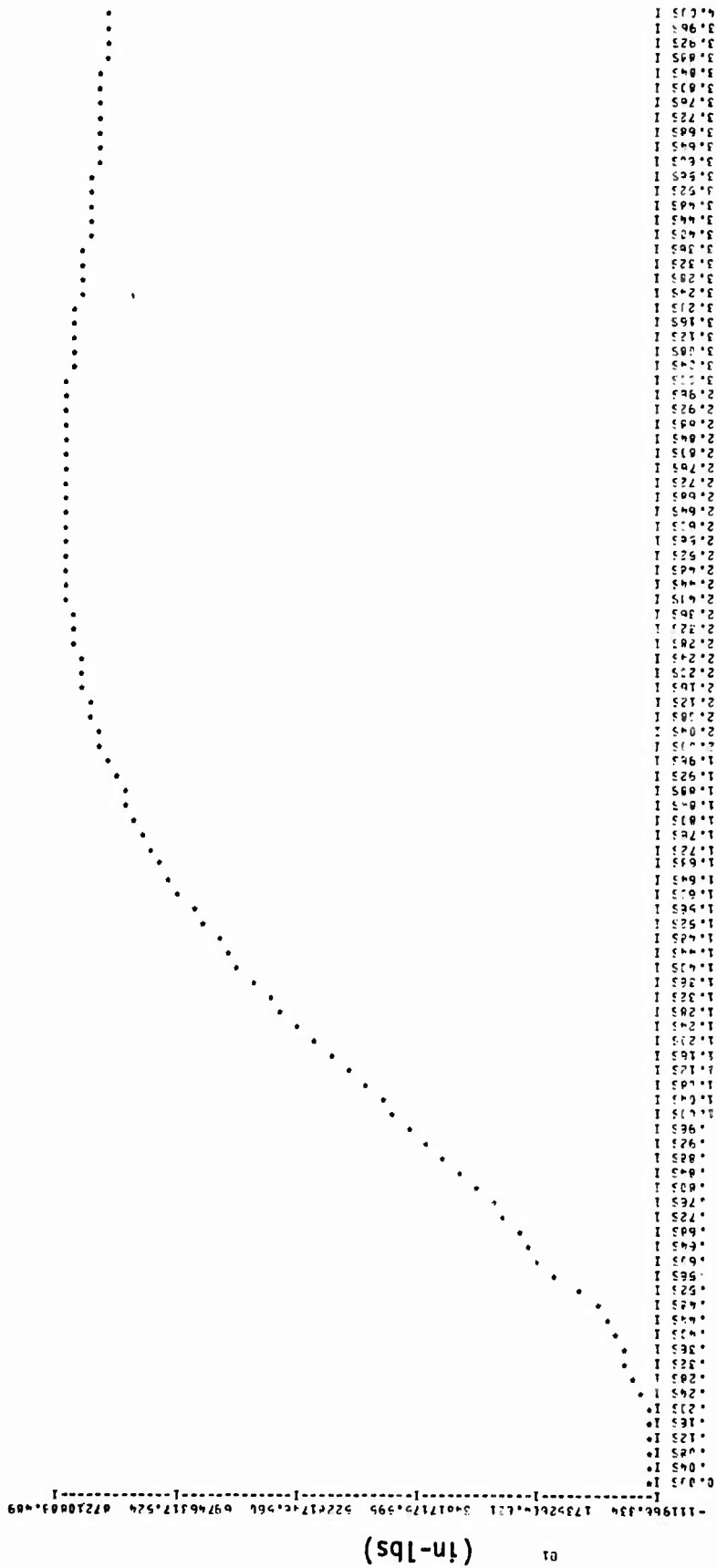
Figure 81. Command Response Plot of Free A/C with F24RR Model (B1)

TIME (SECONDS)

θ_1 (in-lbs)

TIME (SECONDS)

T1 (in-lbs)
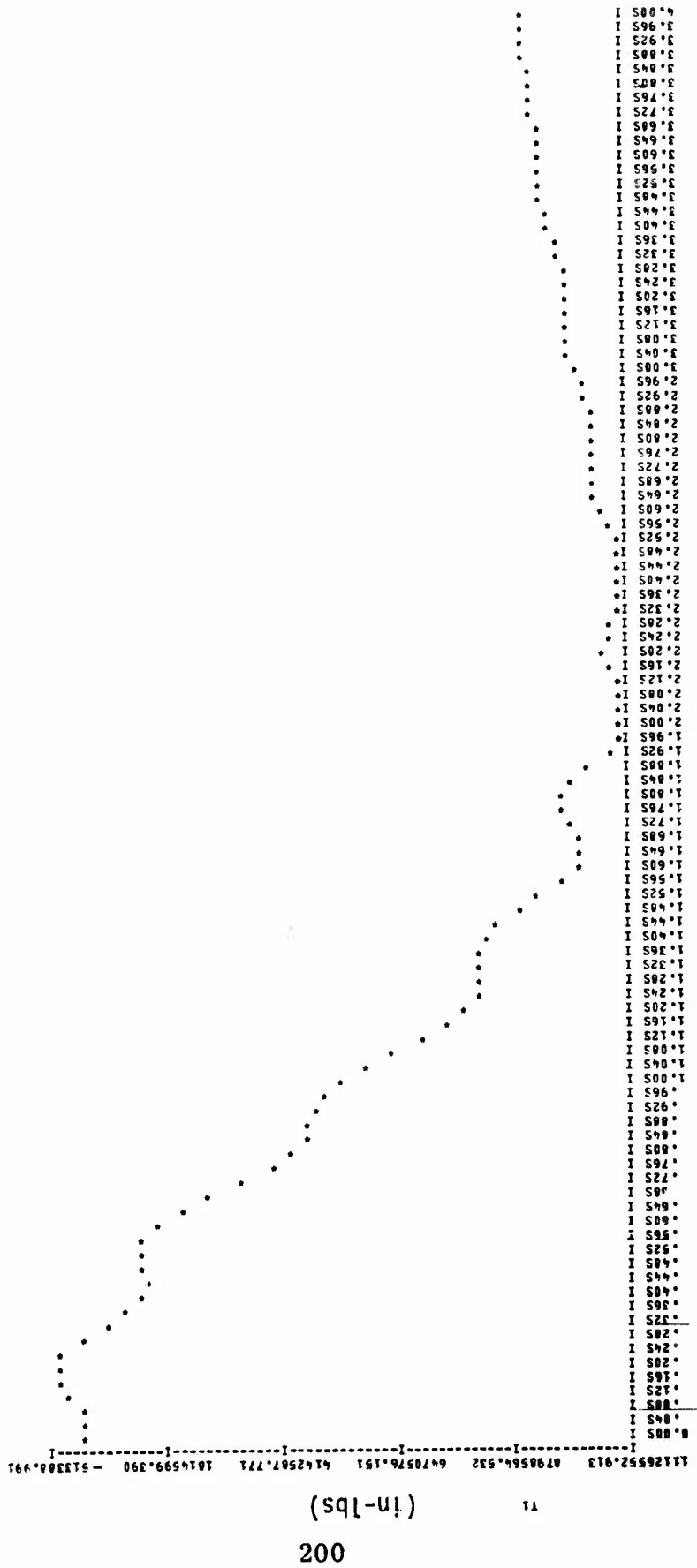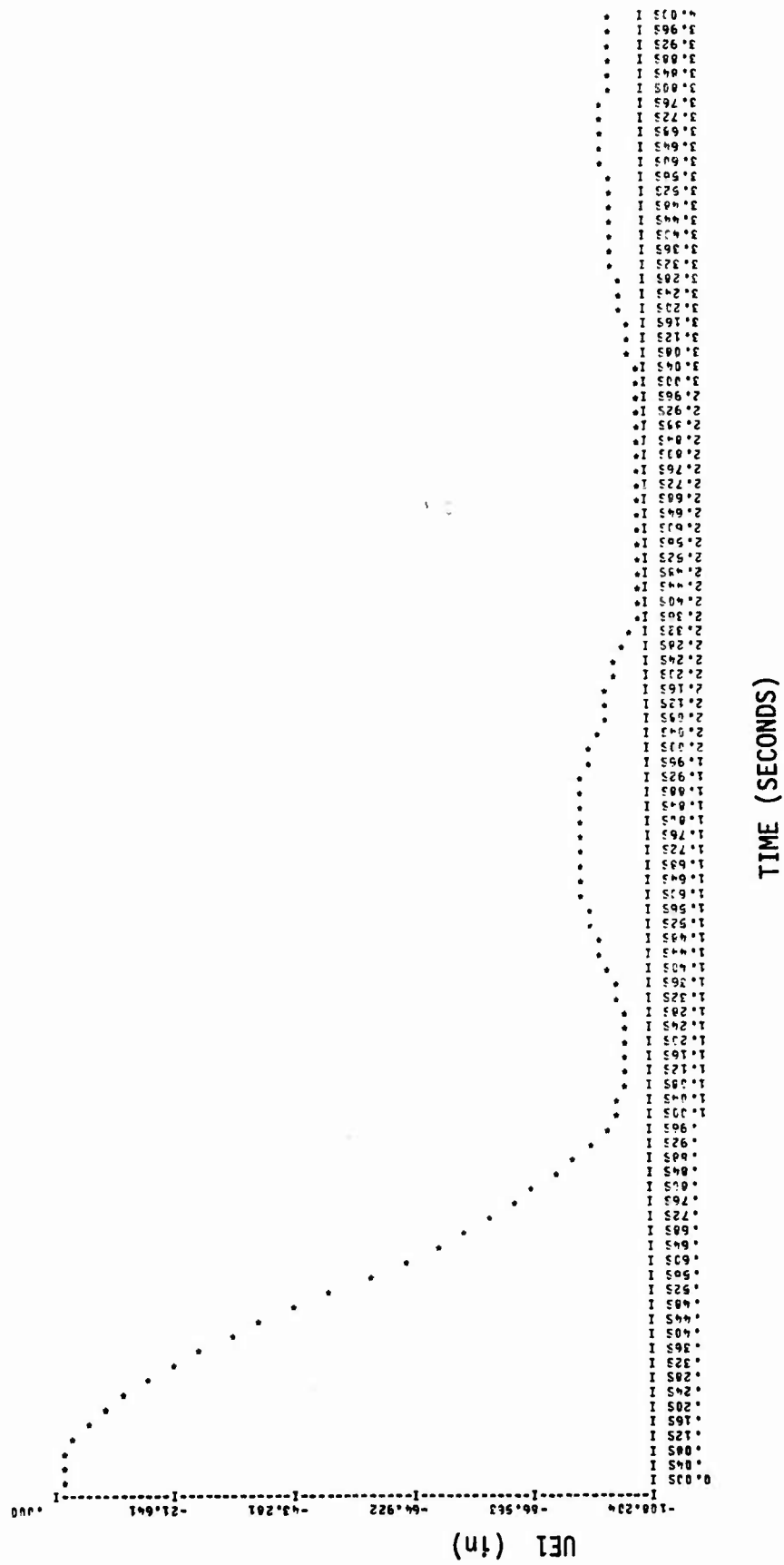
Figure 82. Command Response Plot of Free A/C with HG24RR Model (T1)
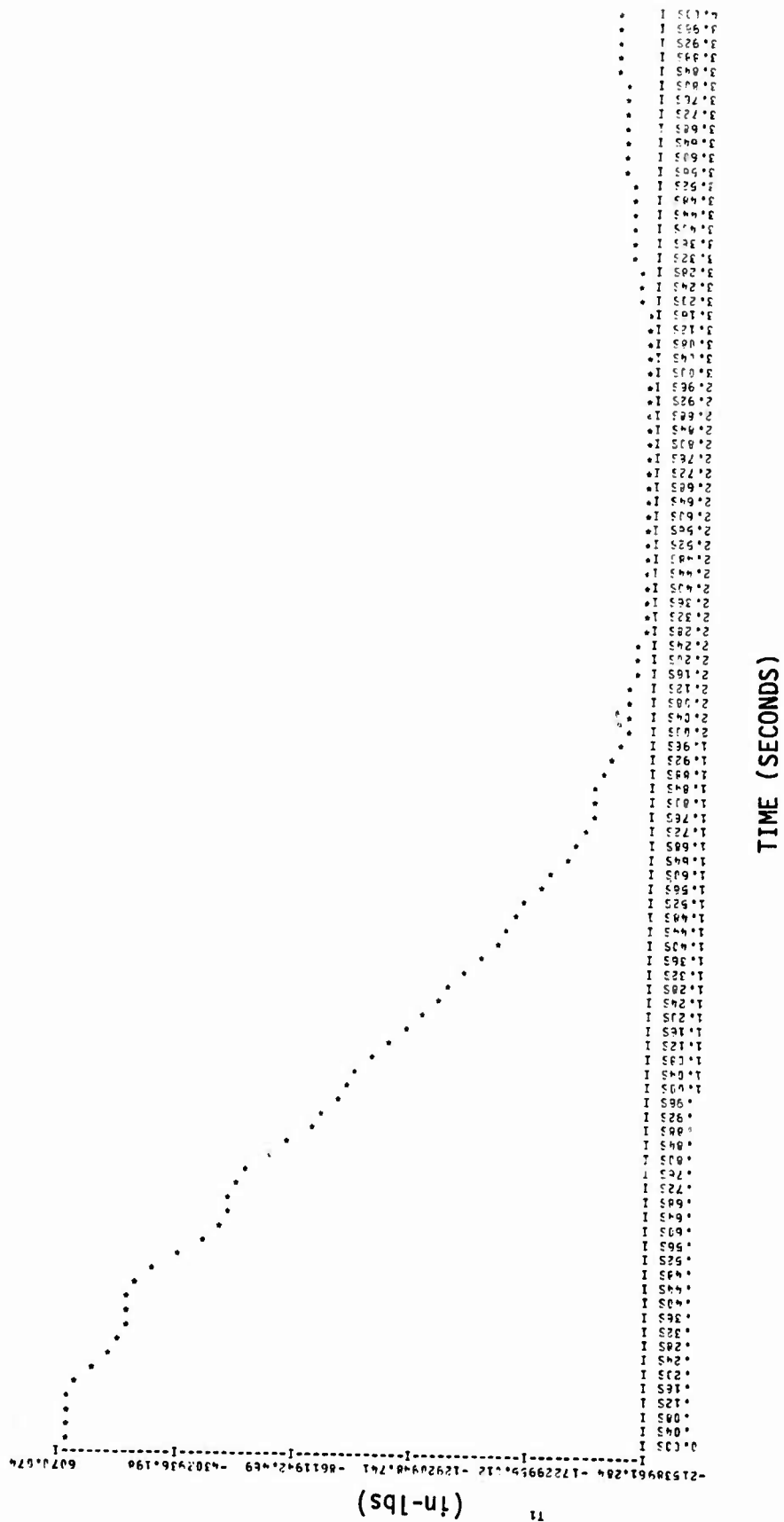
Figure 83. Command Response Plot of Free A/C with F24RR Model (T1)
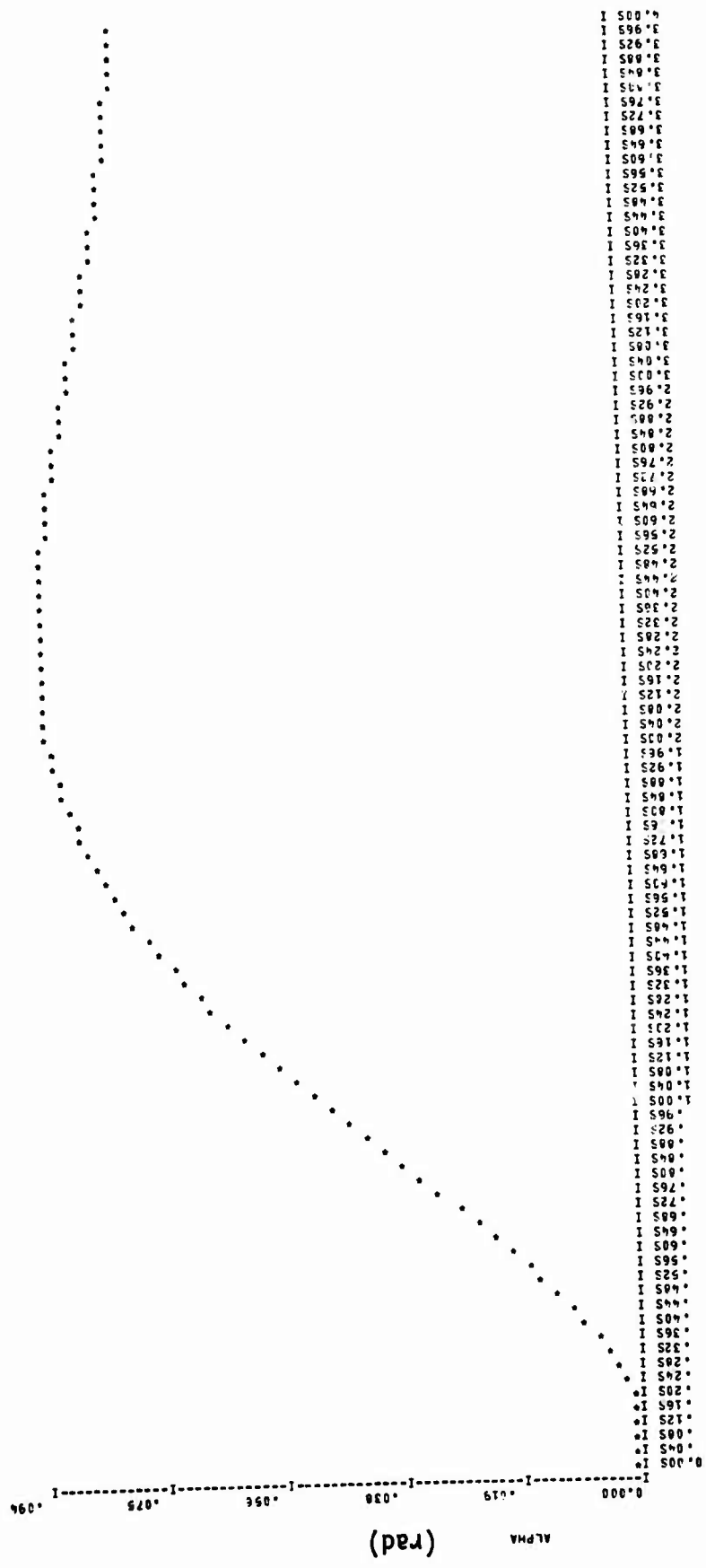
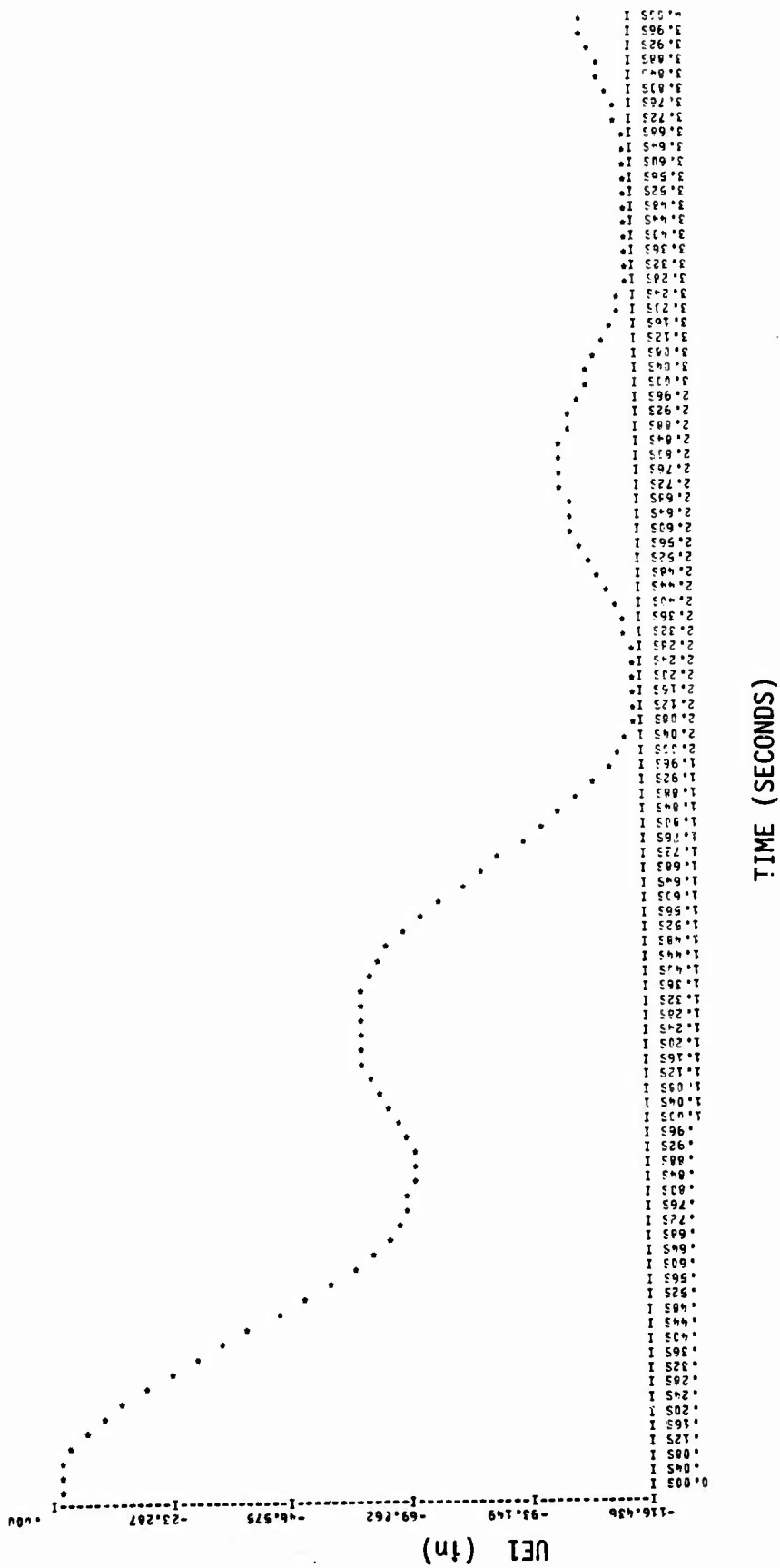Figure 84. Command Response Plot of Free A/C with HG24RR Model (ALPHA)

202

TIME (SECONDS)

ALPHA (rad)
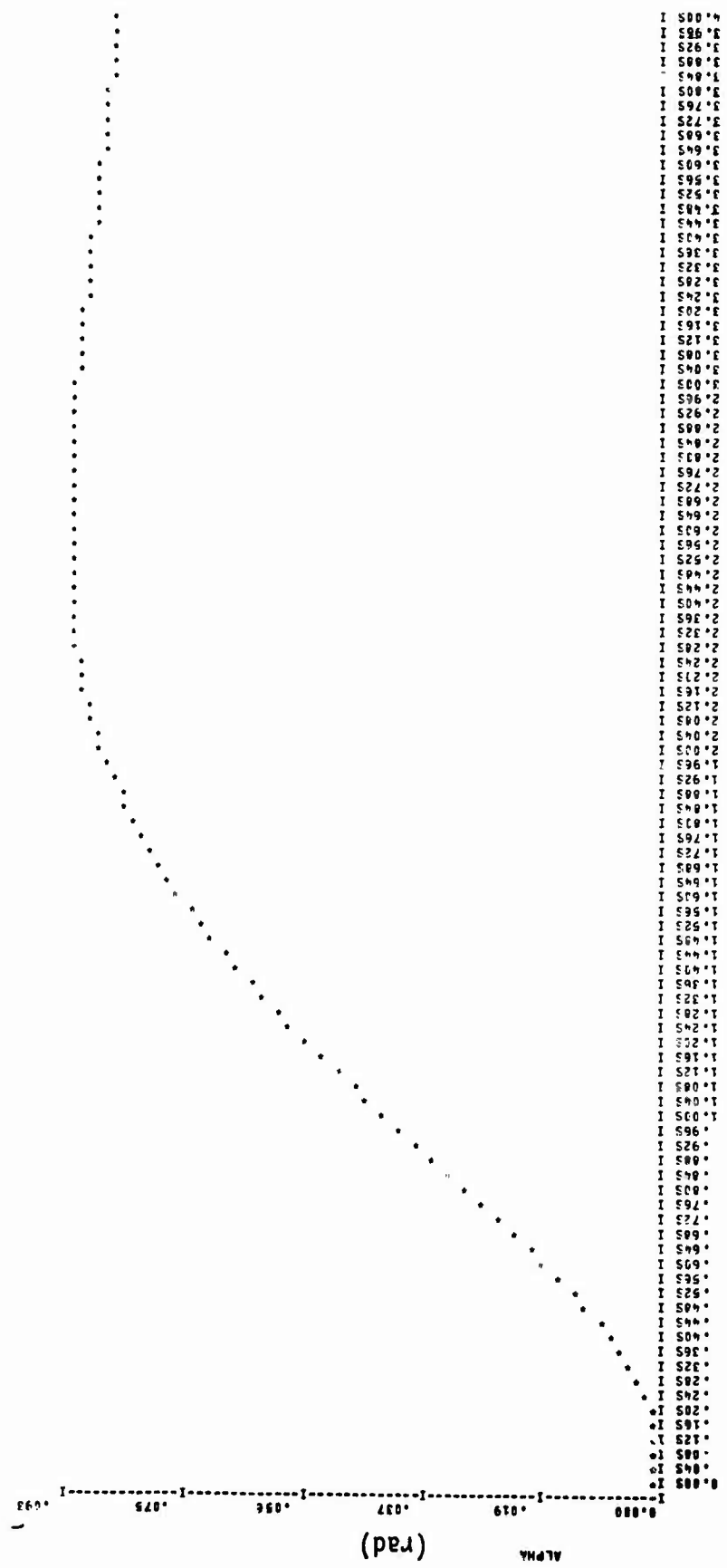
Figure 85. Command Response Plot of Free A/C with F24RR Model (ALPHA)

203
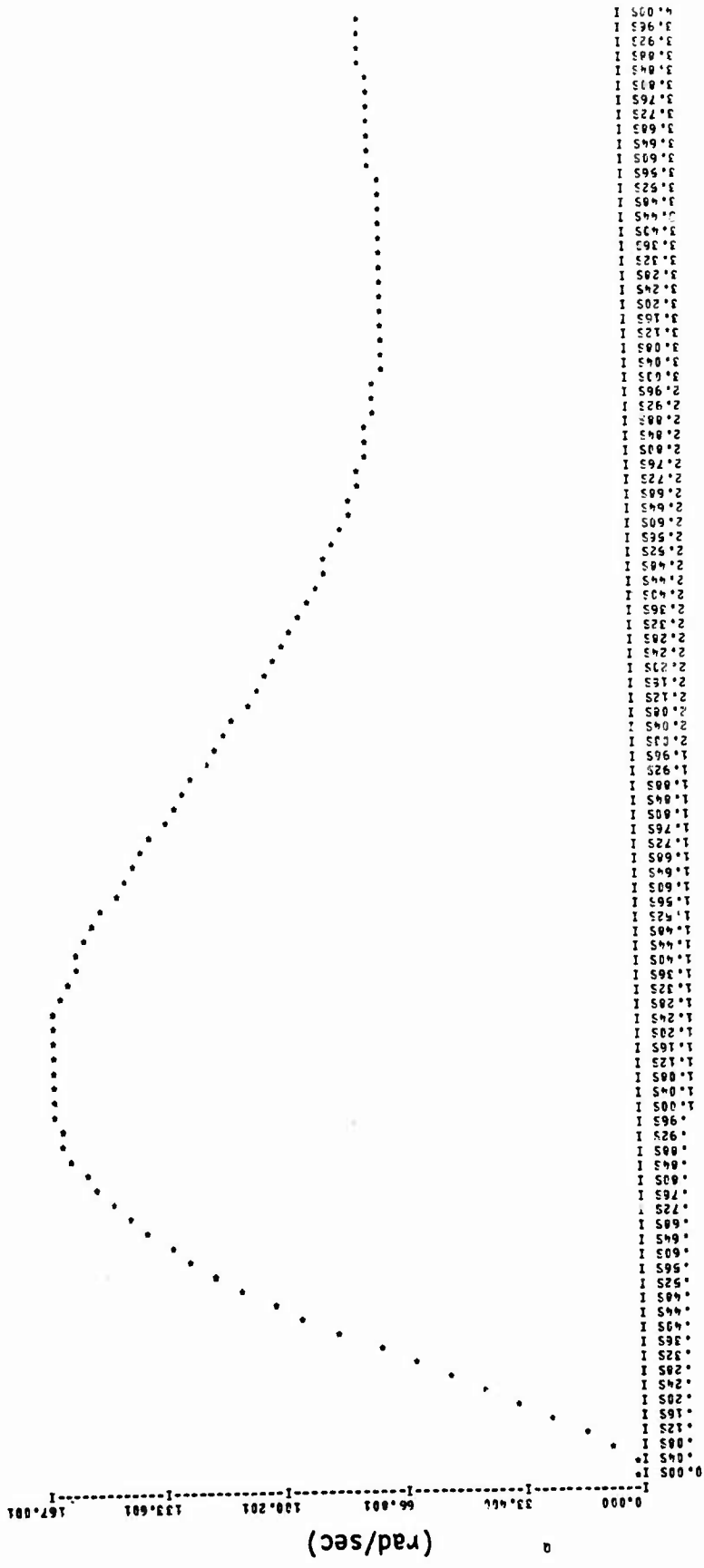
TIME (SECONDS)

Figure 86. Command Response Plot of Free A/C with HG24RR Model (Q)

204
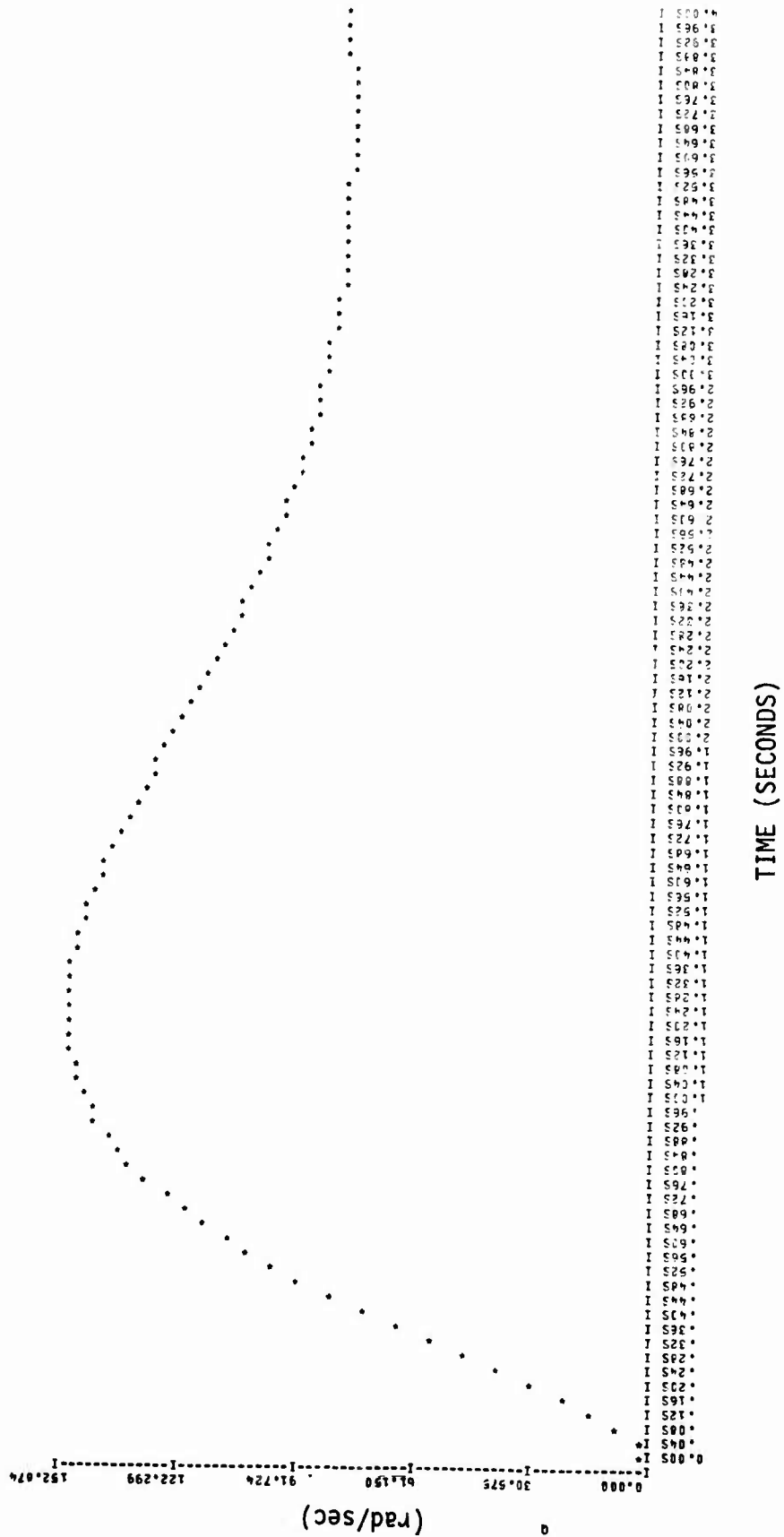
Figure 87. Command Response Plot of Free A/C with F24RR Model (Q)

205
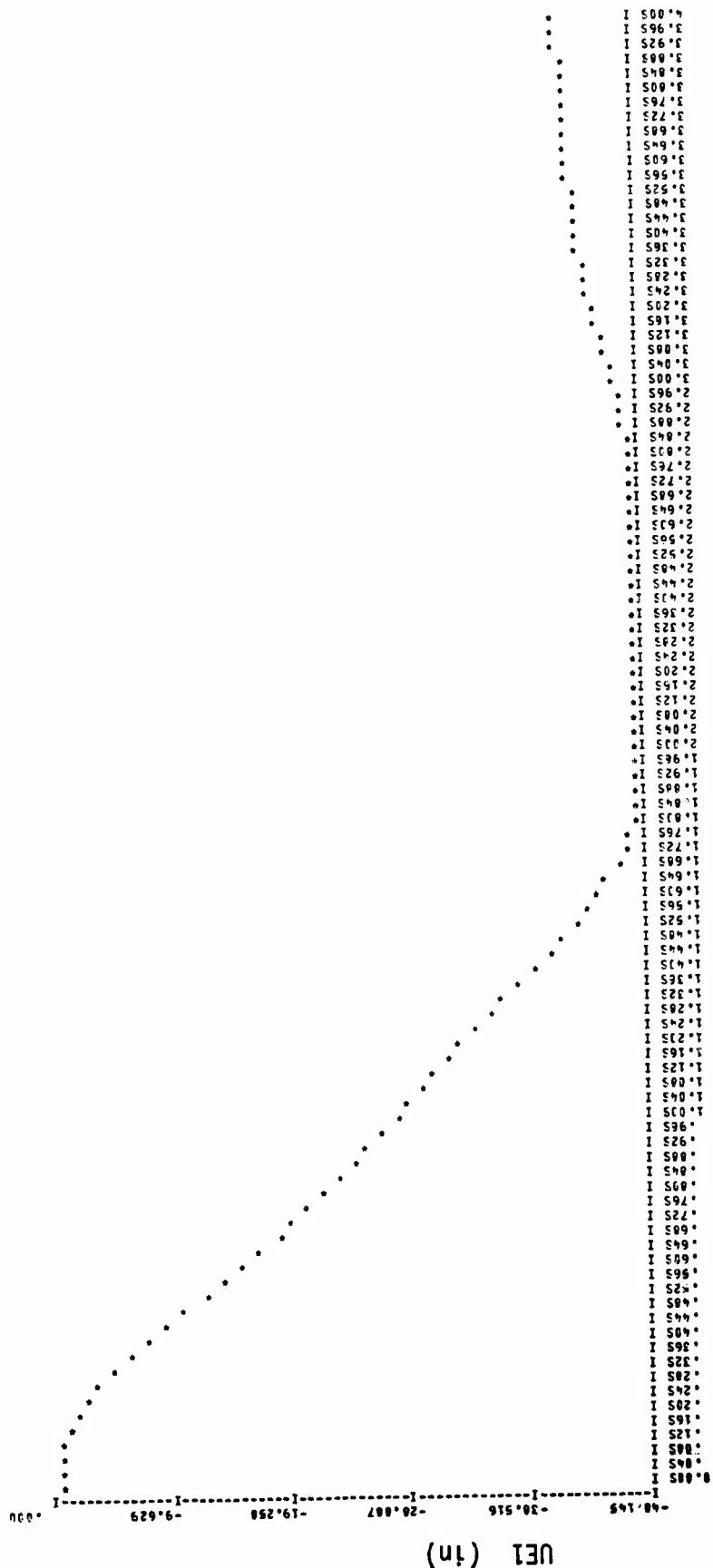
Figure 88. Command Response Plot of Free A/C with HG24RR Model (ETA1)

TIME (SECONDS)

UE1 (in)

206

TIME (SECONDS)

UE1 (in)
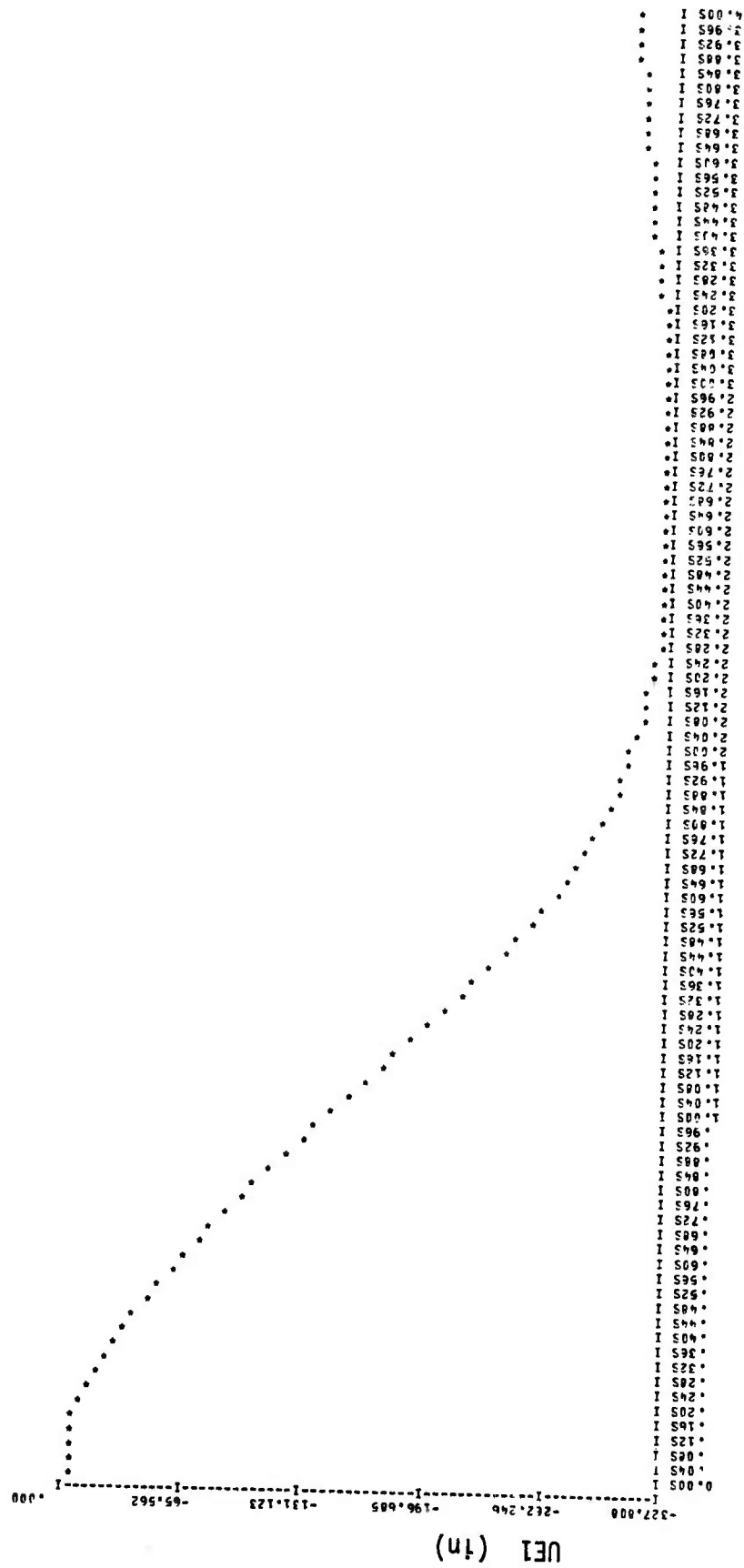
Figure 89.   Command Response Plot of Free A/C with F24RR Model (ETA1)

207
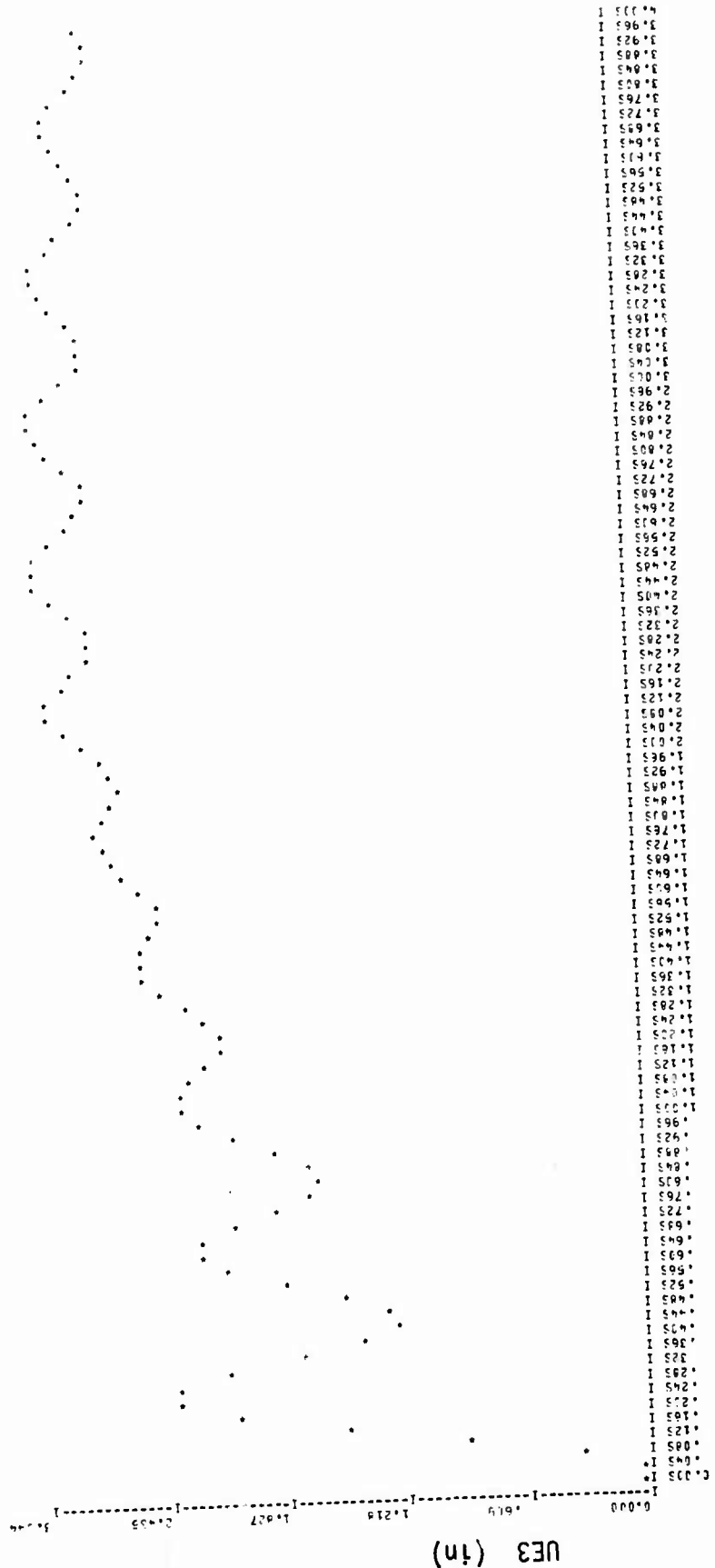
Figure 90. Command Response Plot of Free A/C with HG24RR Model (ETA3)
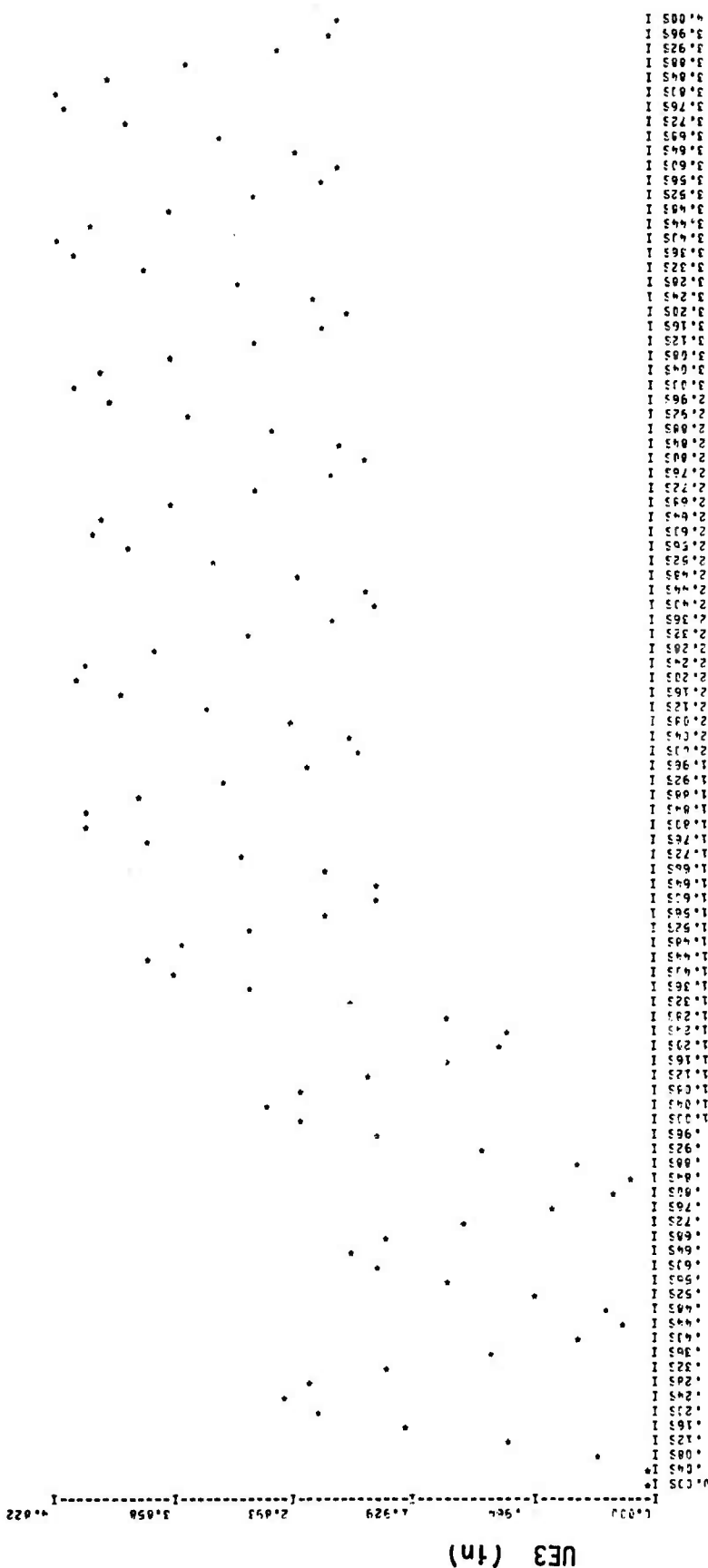
TIME (SECONDS)

UE3 (in)

TIME (SECONDS)

UE3 (in)
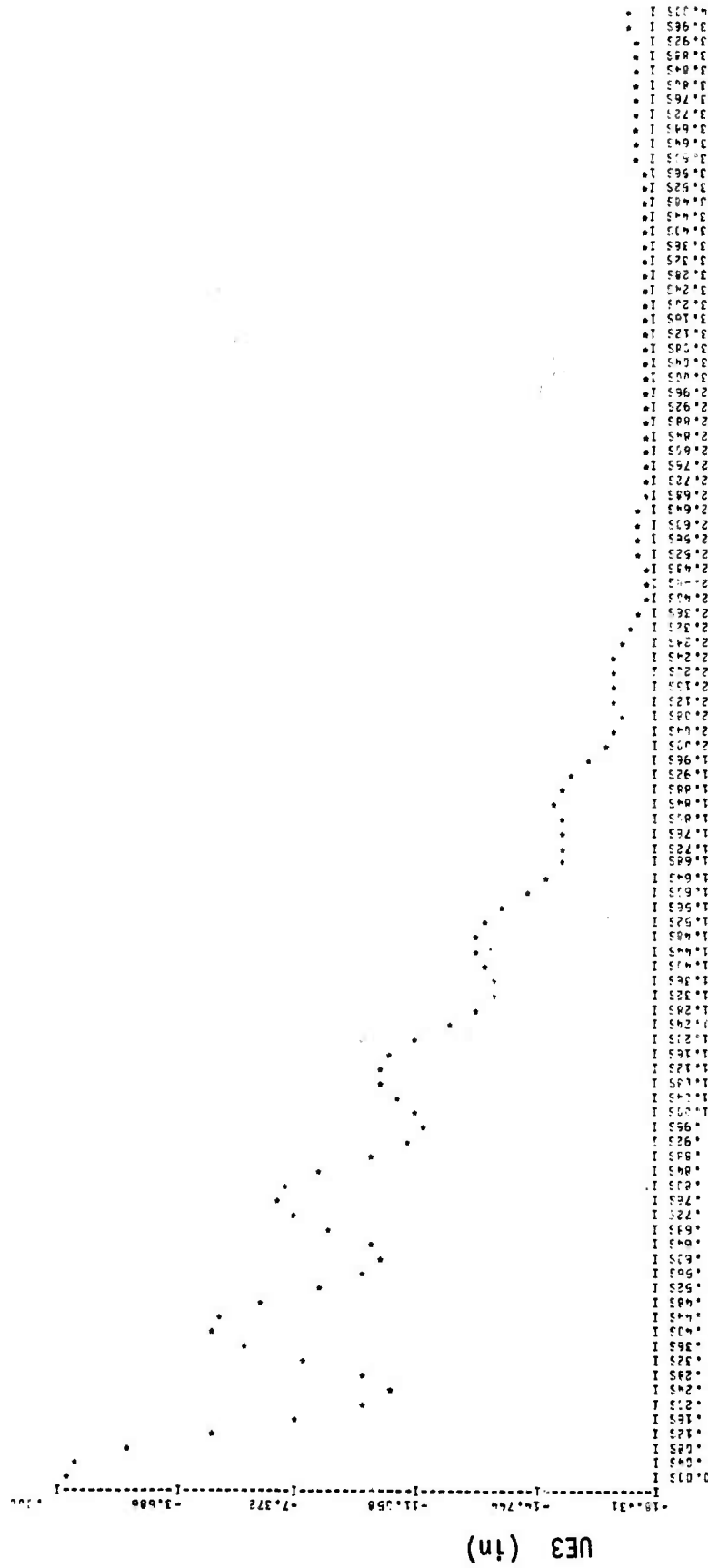
Figure 91. Command Response Plot of Free A/C with F24RR Model (ETA3)
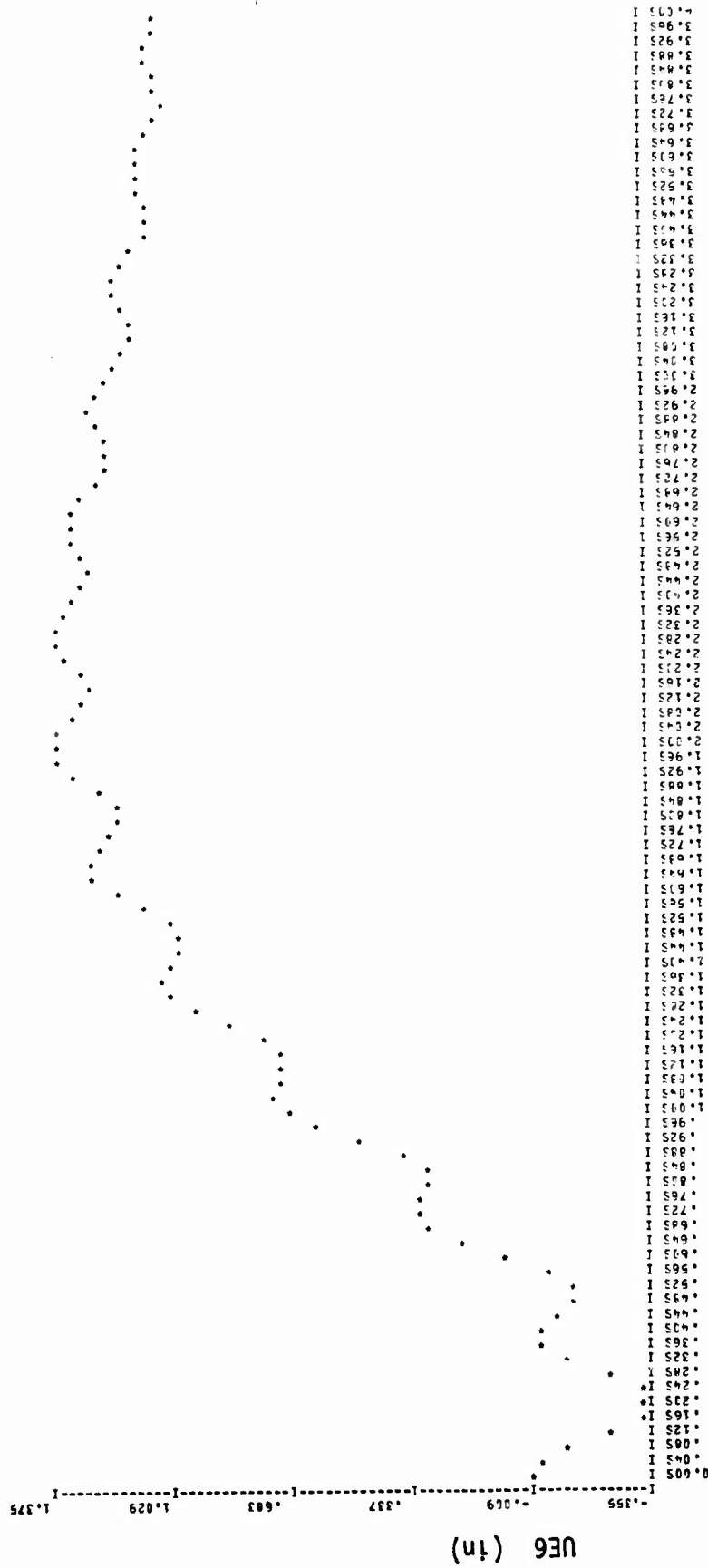
TIME (SECONDS)

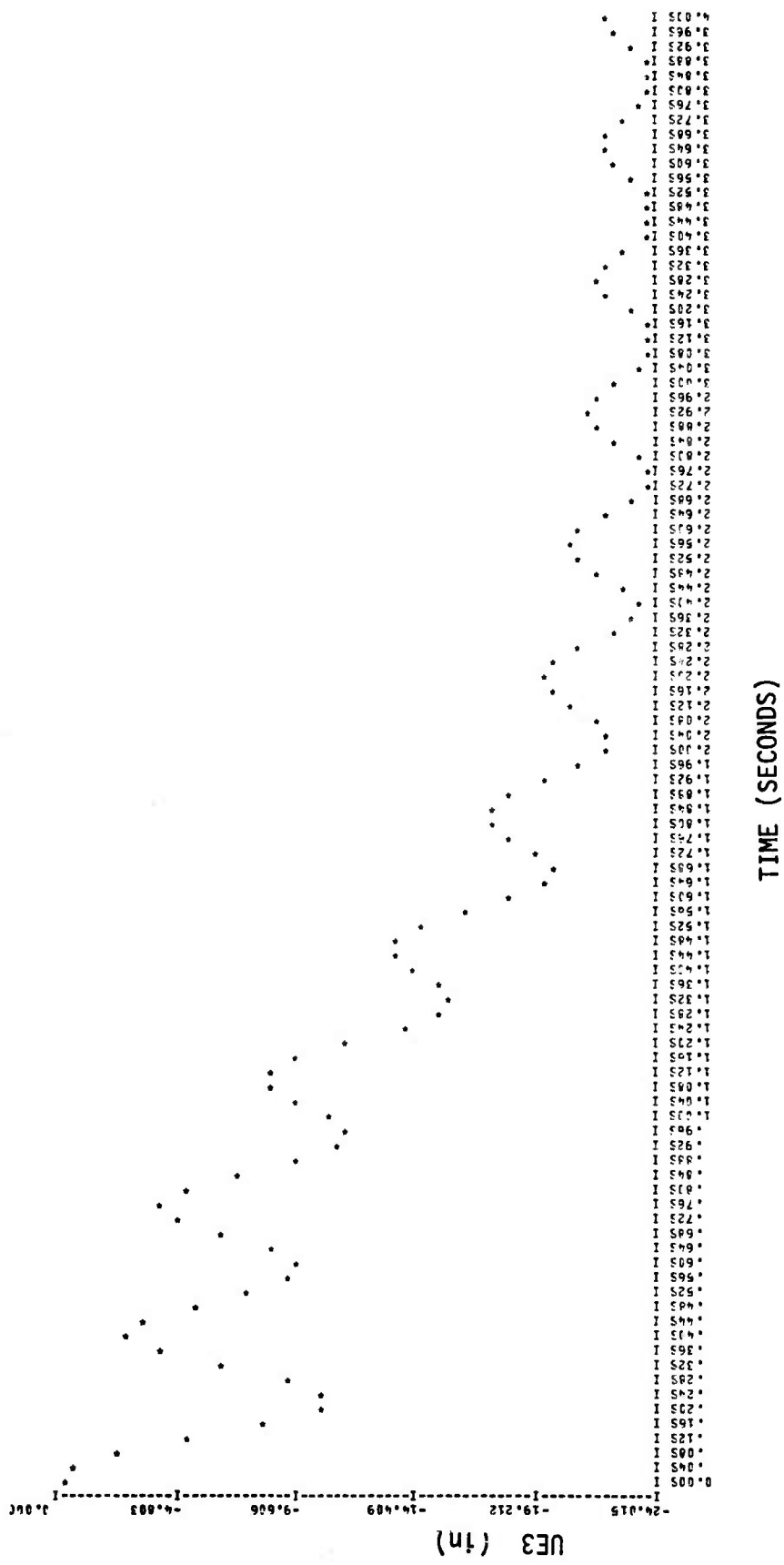Figure 92. Command Response Plot of Free A/C with HG24RR Model (ETA6)

UE6 (in)

210
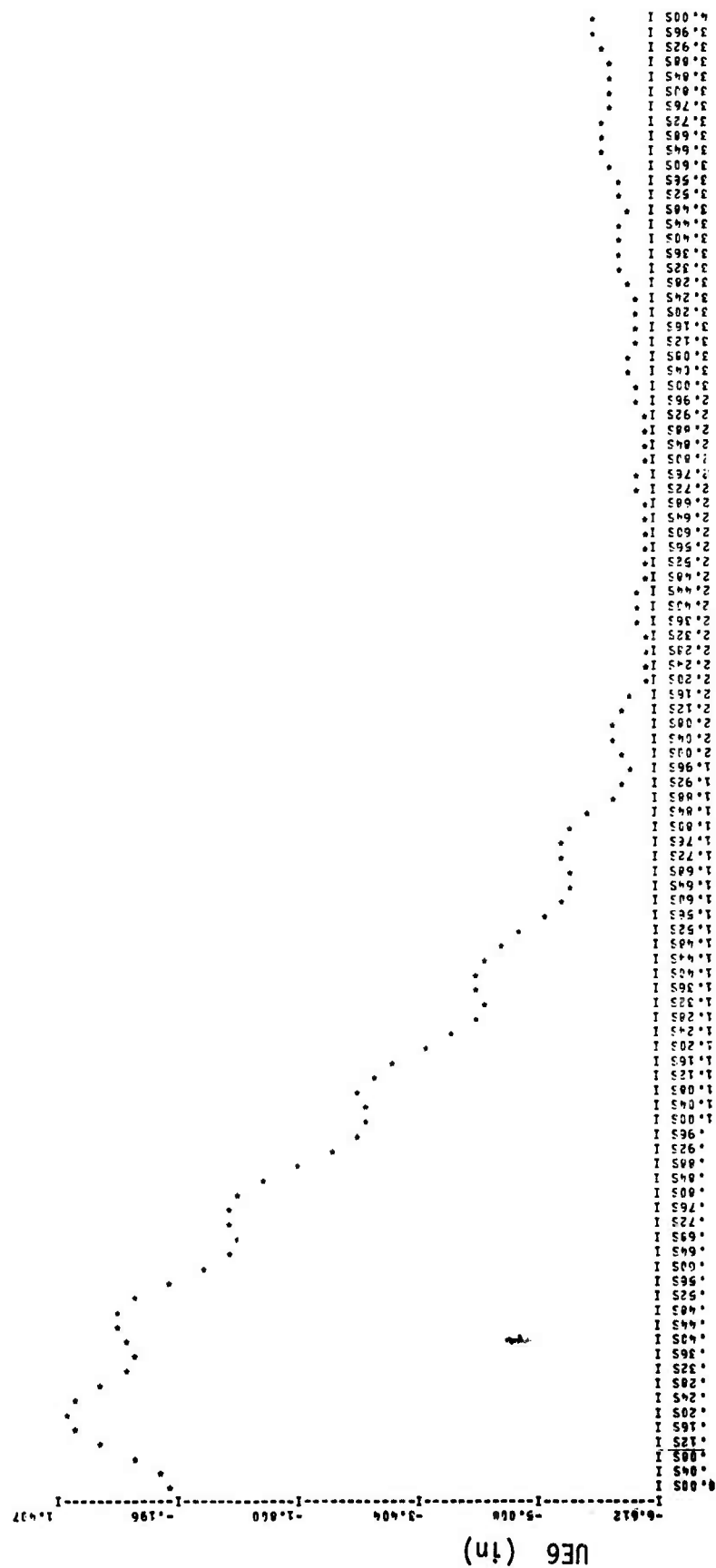
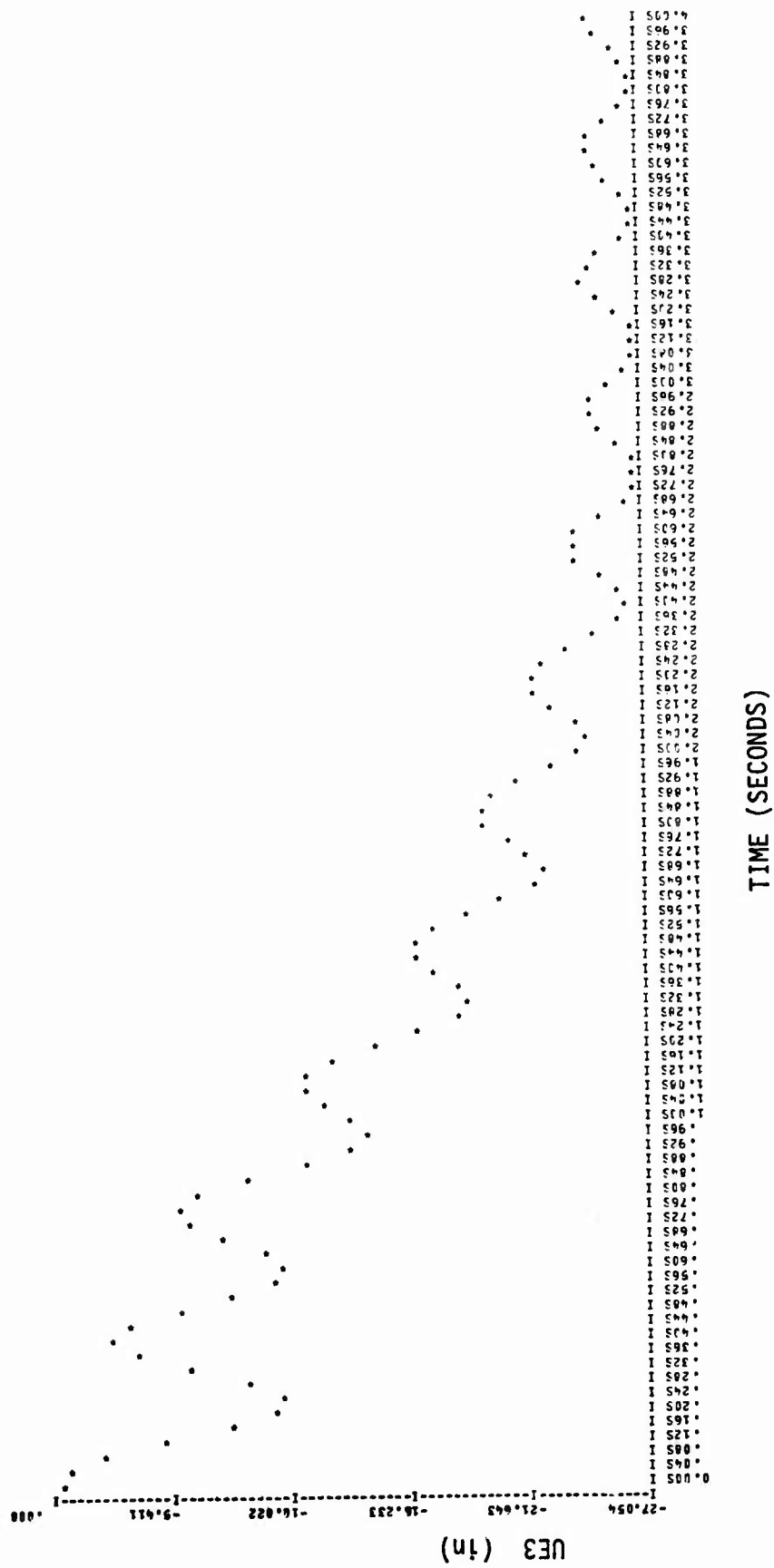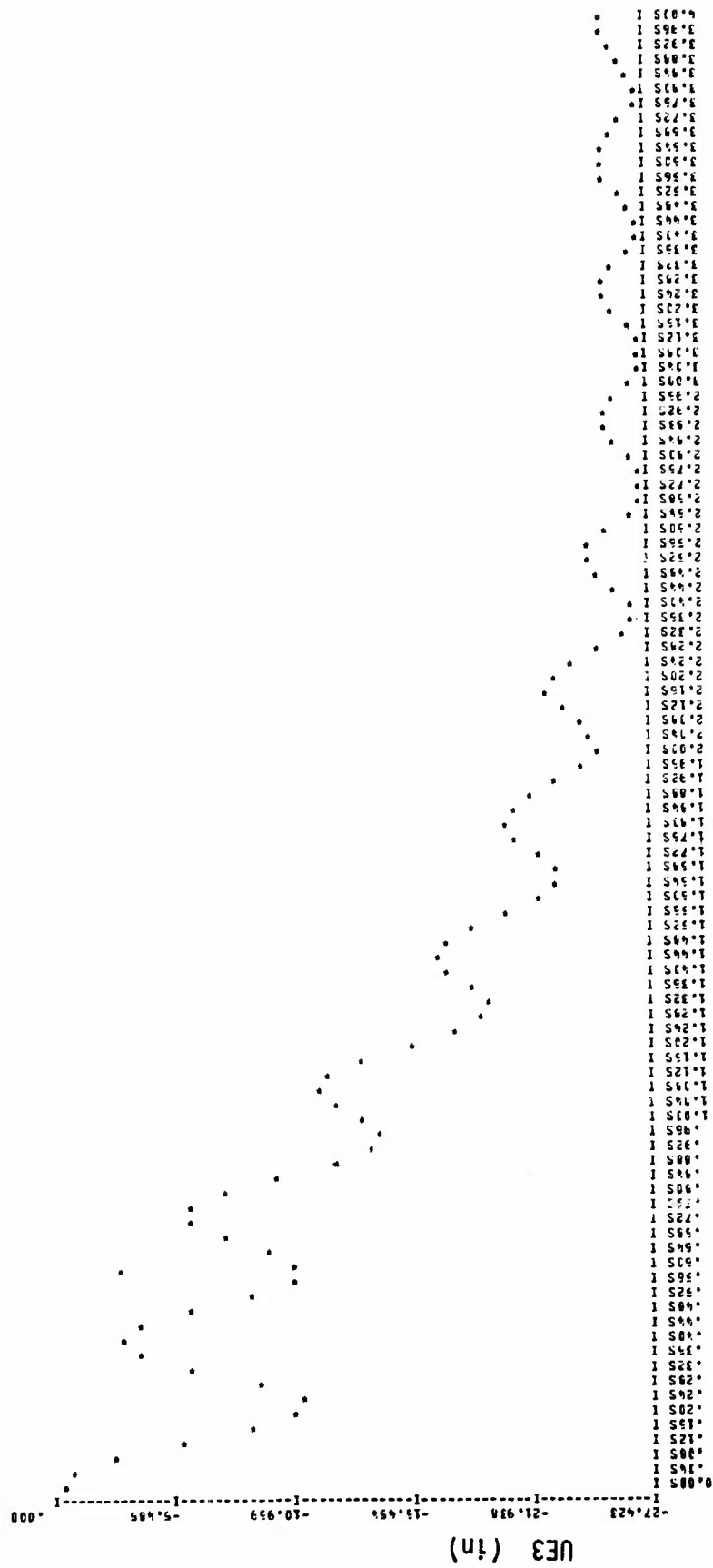Figure 93. Command Response Plot of Free A/C with F24RR Model (ETA6)

211
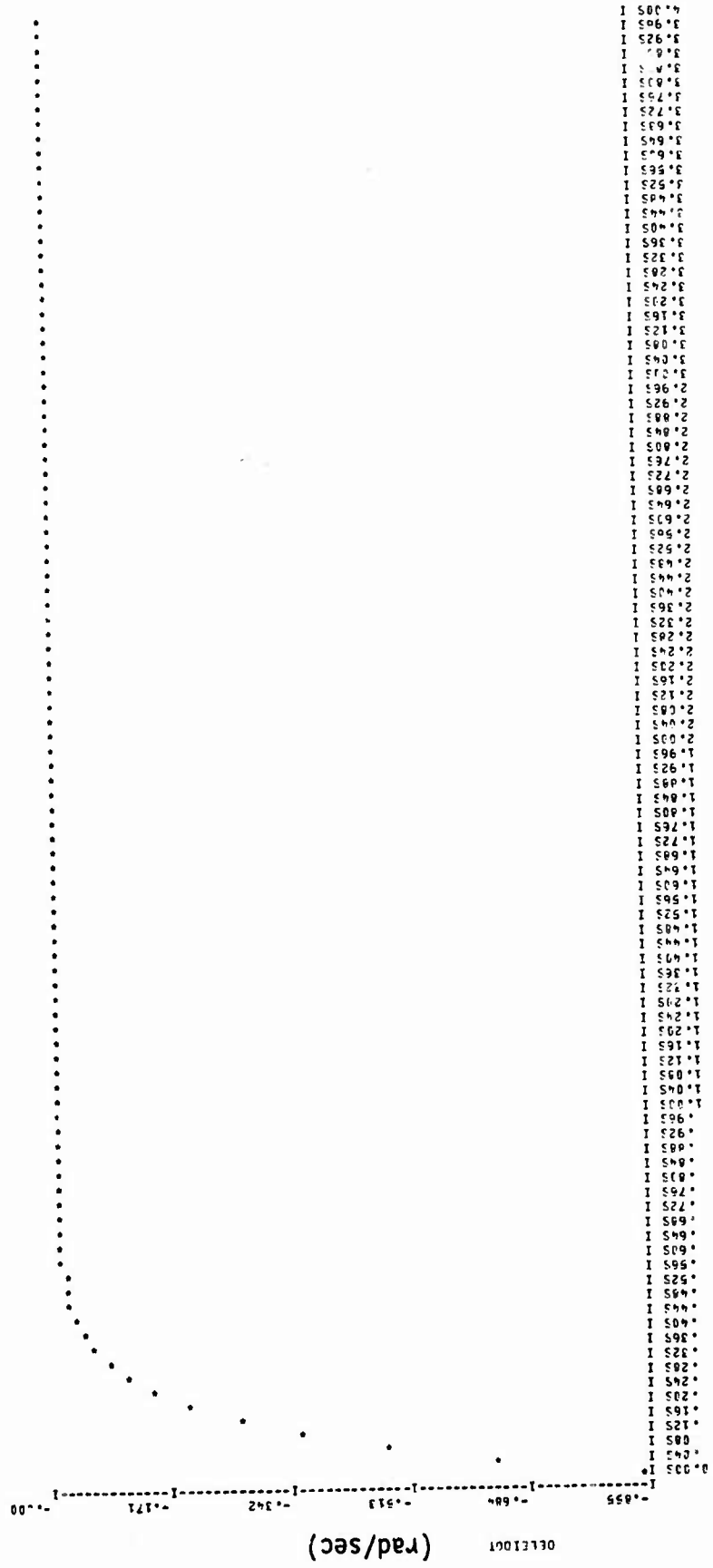
Figure 94. Command Response Plot of Free A/C with HG24RR Model (DELEIDOT)

212
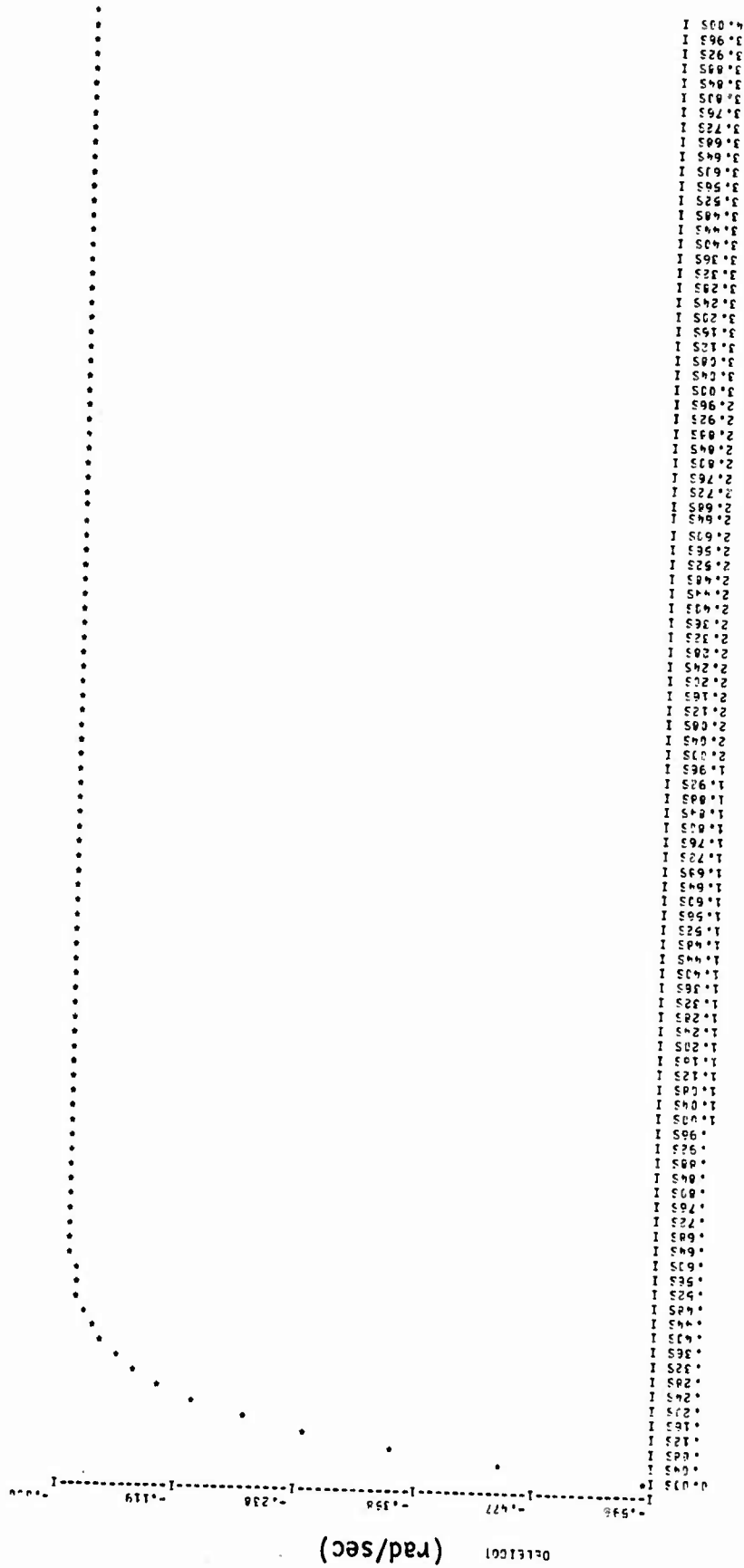
TIME (SECONDS)

Figure 95. Command Response Plot of Free A/C with F24RR Model (DELEIDOT)

213
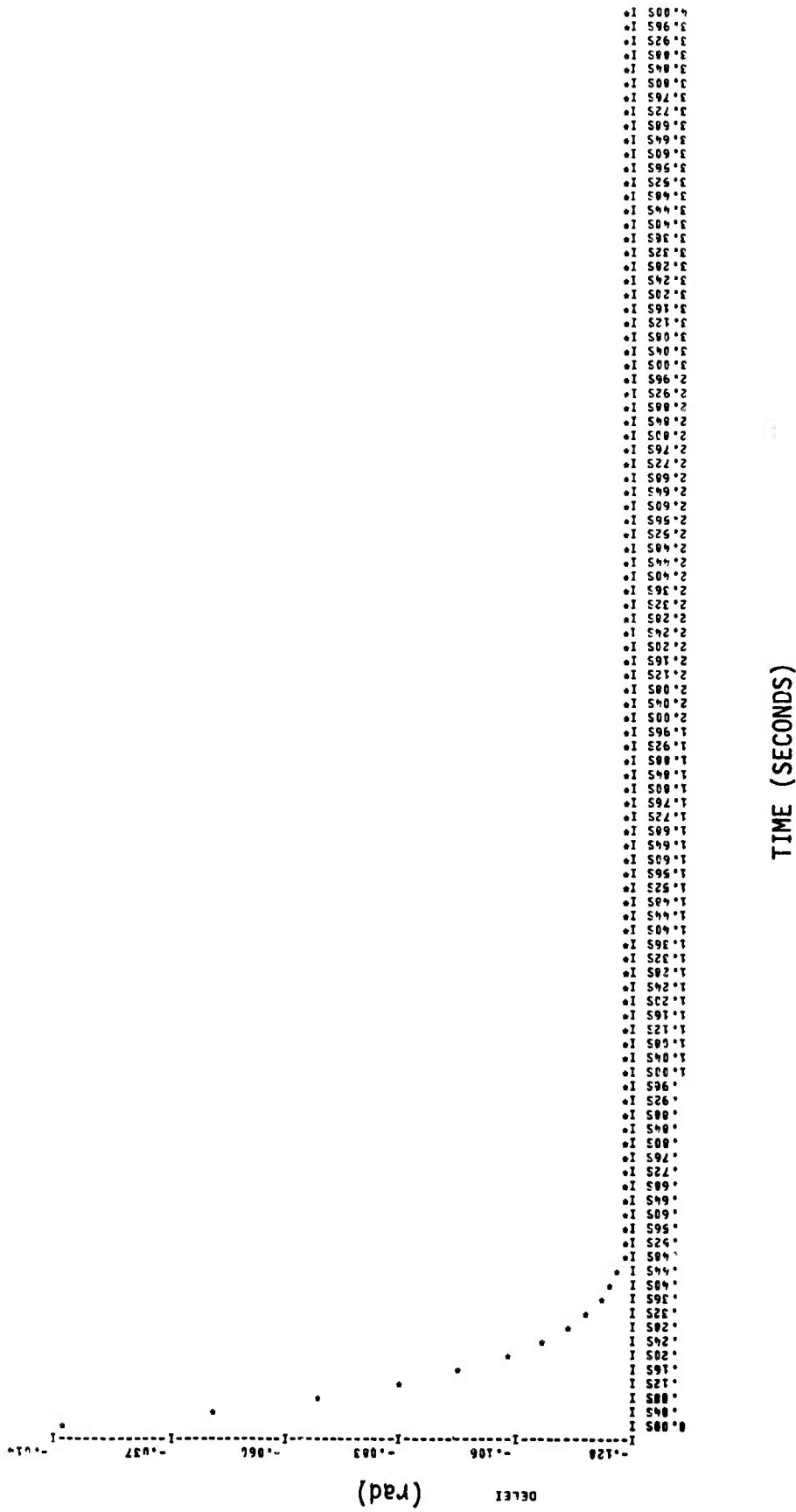
Figure 96. Command Response Plot of Free A/C with HG24RR Model (DELE1)

214
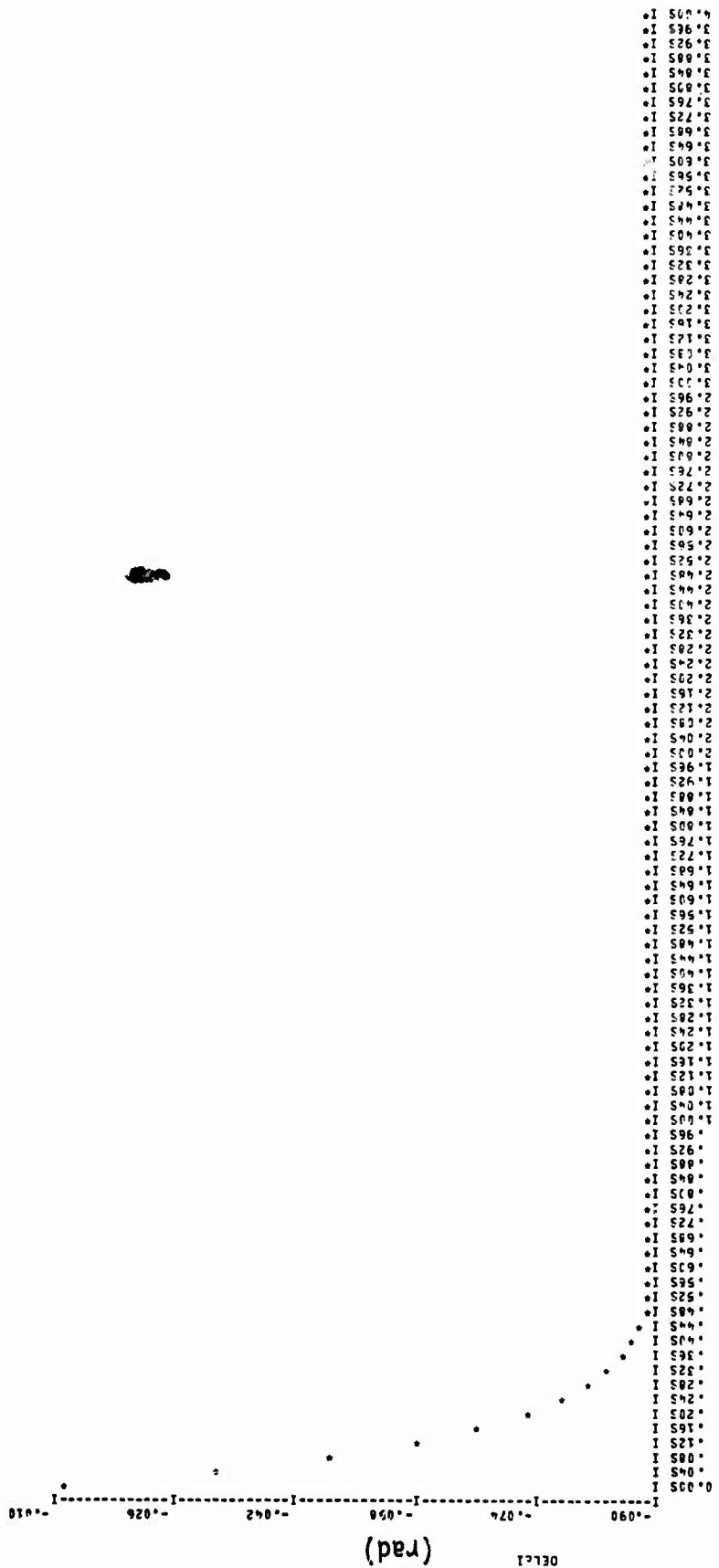
Figure 97. Command Response Plot of Free A/C with F24RR Model (DELEI)

TIME (SECONDS)

215

TIME (SECONDS)

BDEϕ (rad)
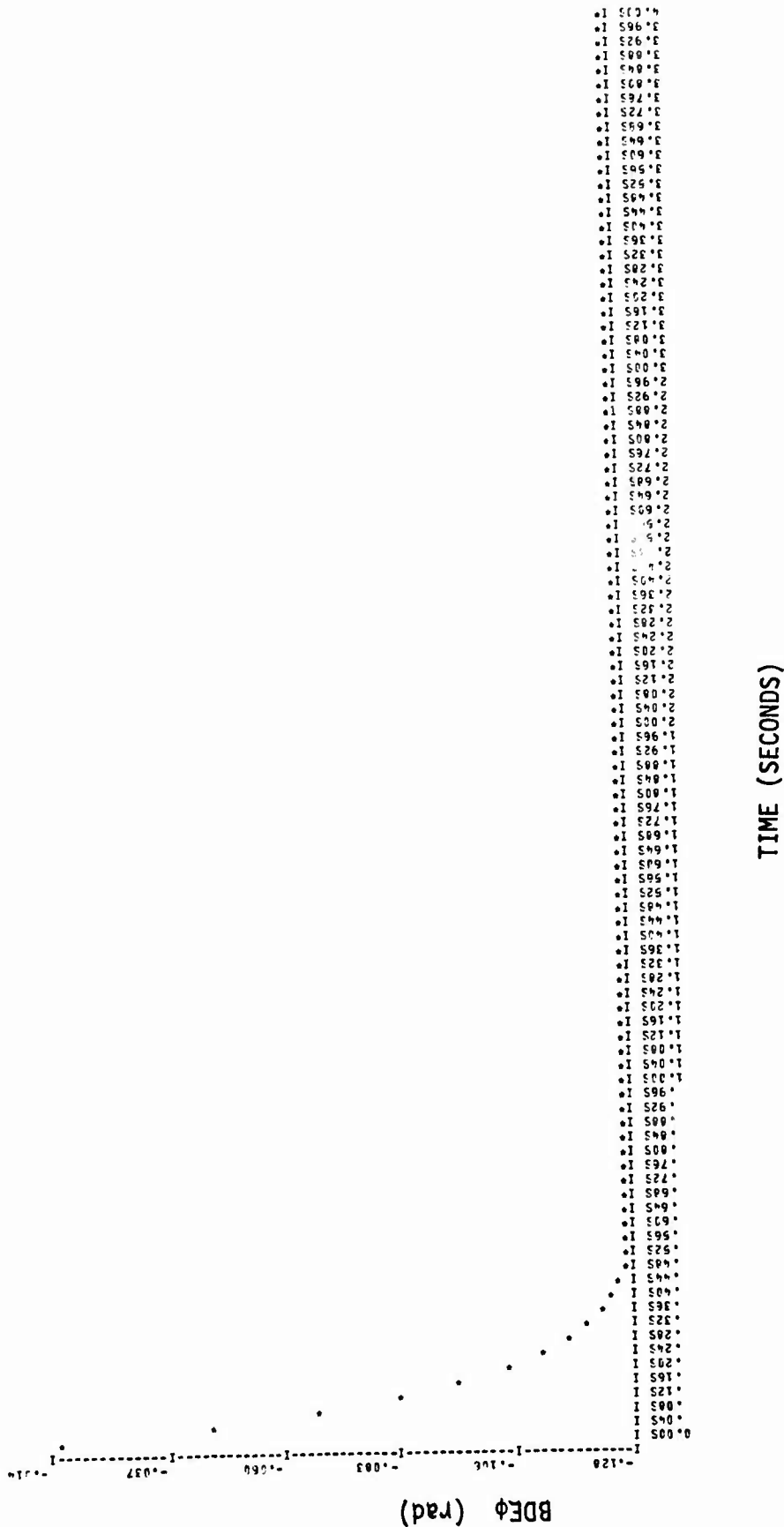
Figure 98.   Command Response Plot of Free A/C with HG24RR Model (DELEO)

216

TIME (SECONDS)
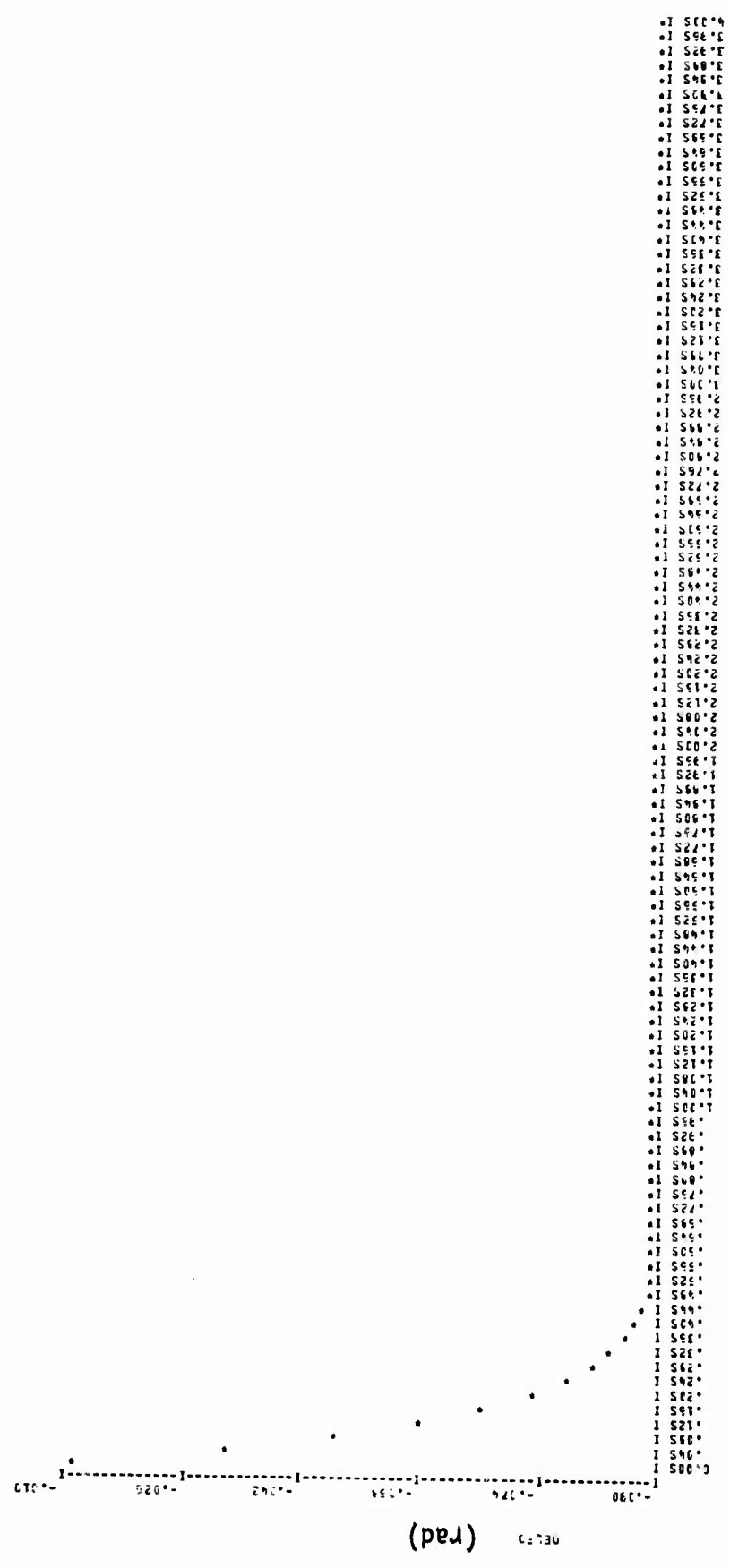
Figure 99. Command Response Plot of Free A/C with F24RR Model (DELEO)

217
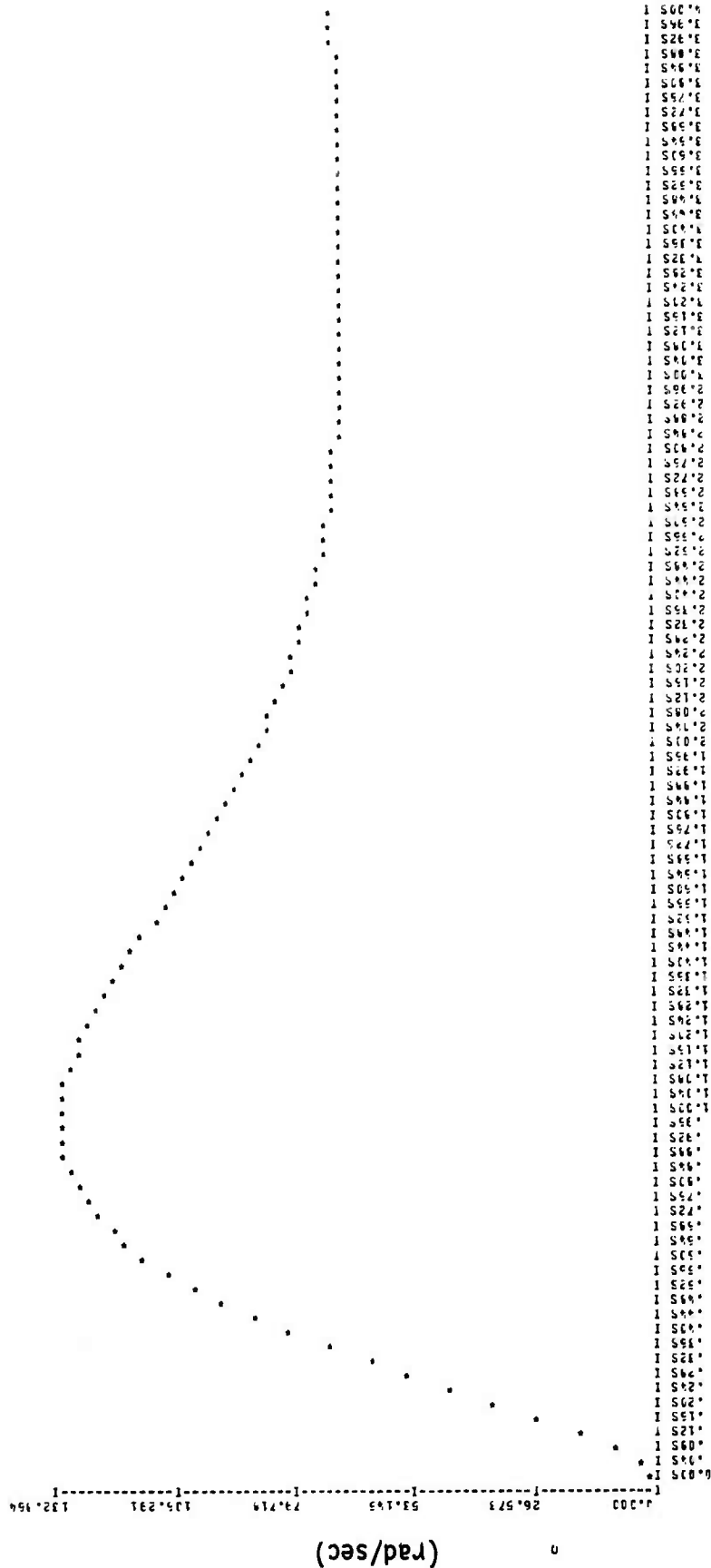
Figure 100. Command Response Plot of SAS A/C with HG24RR Model (Q)

TIME (SECONDS)

(rad/sec)

218
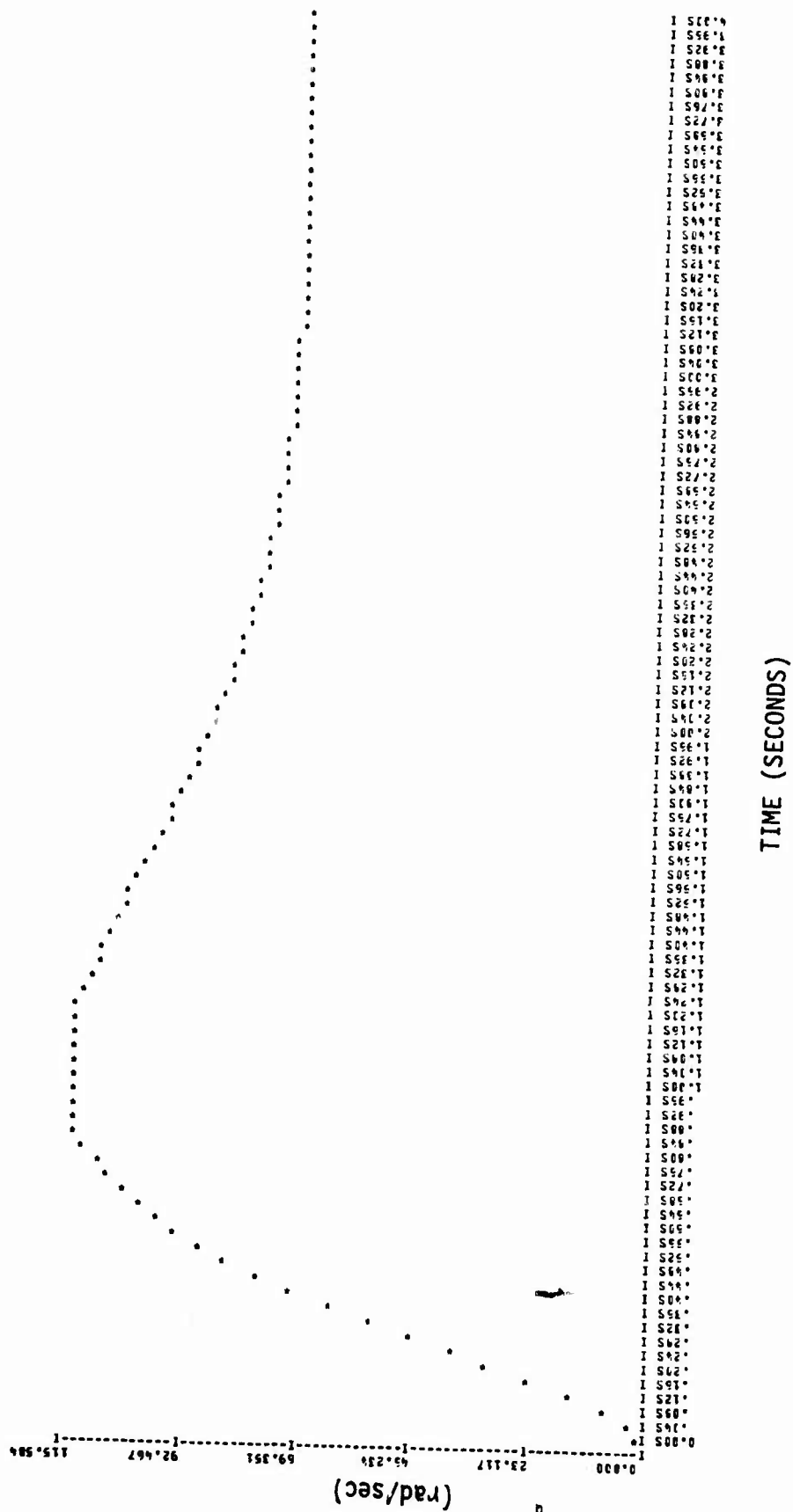
Figure 101. Command Response Plot of SAS A/C with F24RR Model (Q)

219

TIME (SECONDS)

q (rad/sec)
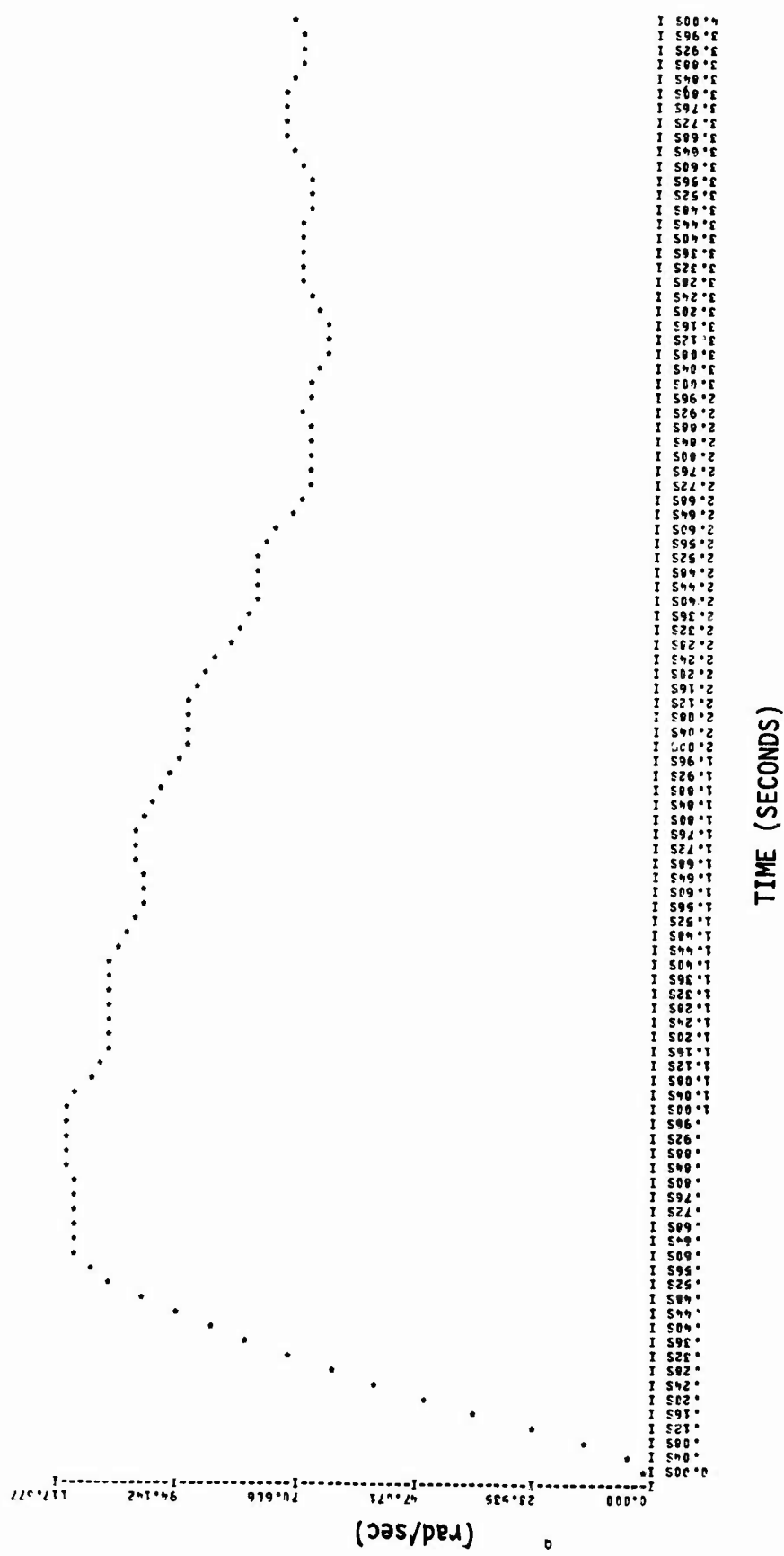
Figure 102.   Command Response Plot of ALDCS A/C with HG24RR Model (Q)

220
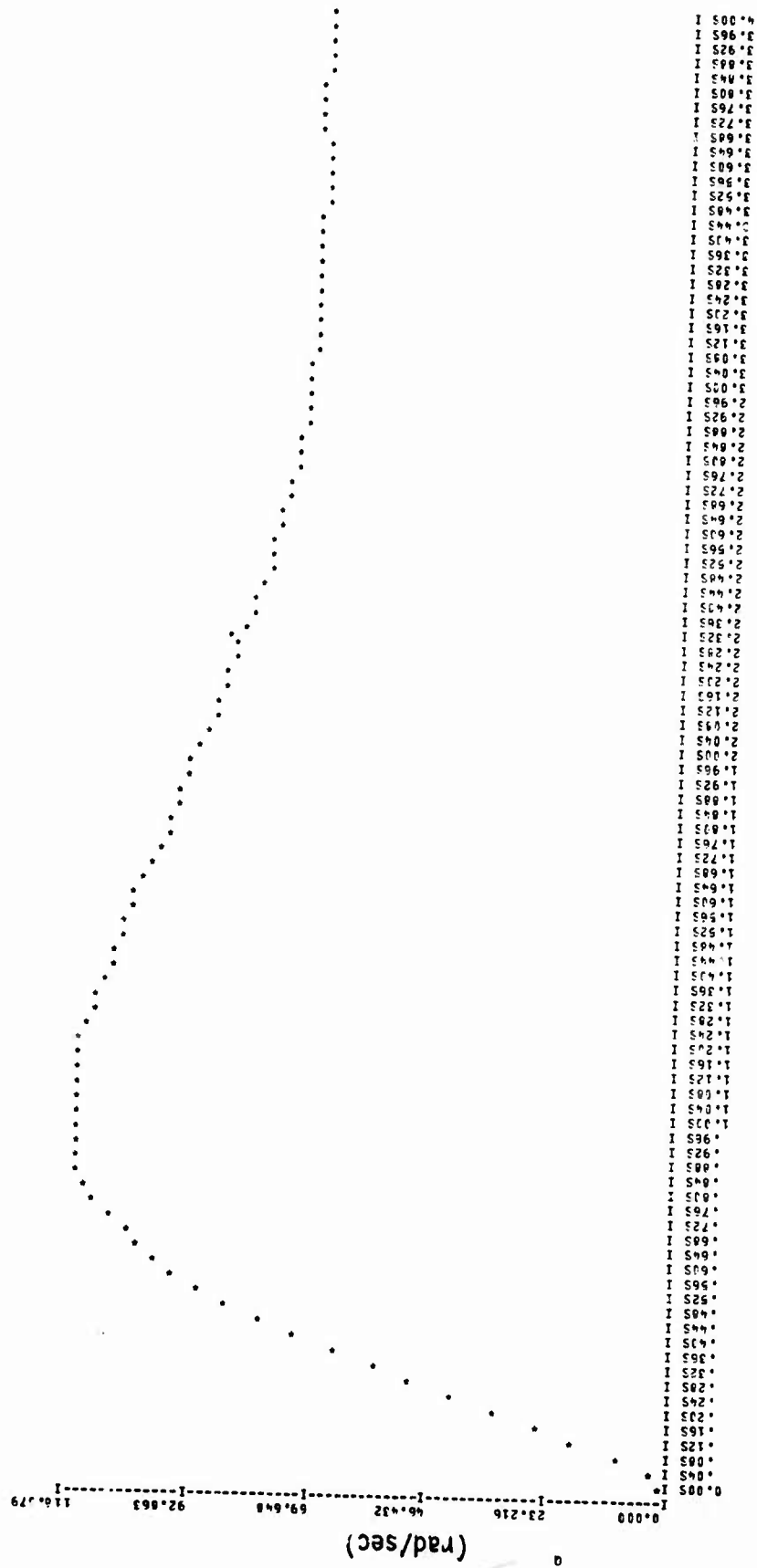
Figure 103. Command Response Plot of ALDCS A/C with F24RR Model (Q)

TIME (SECONDS)
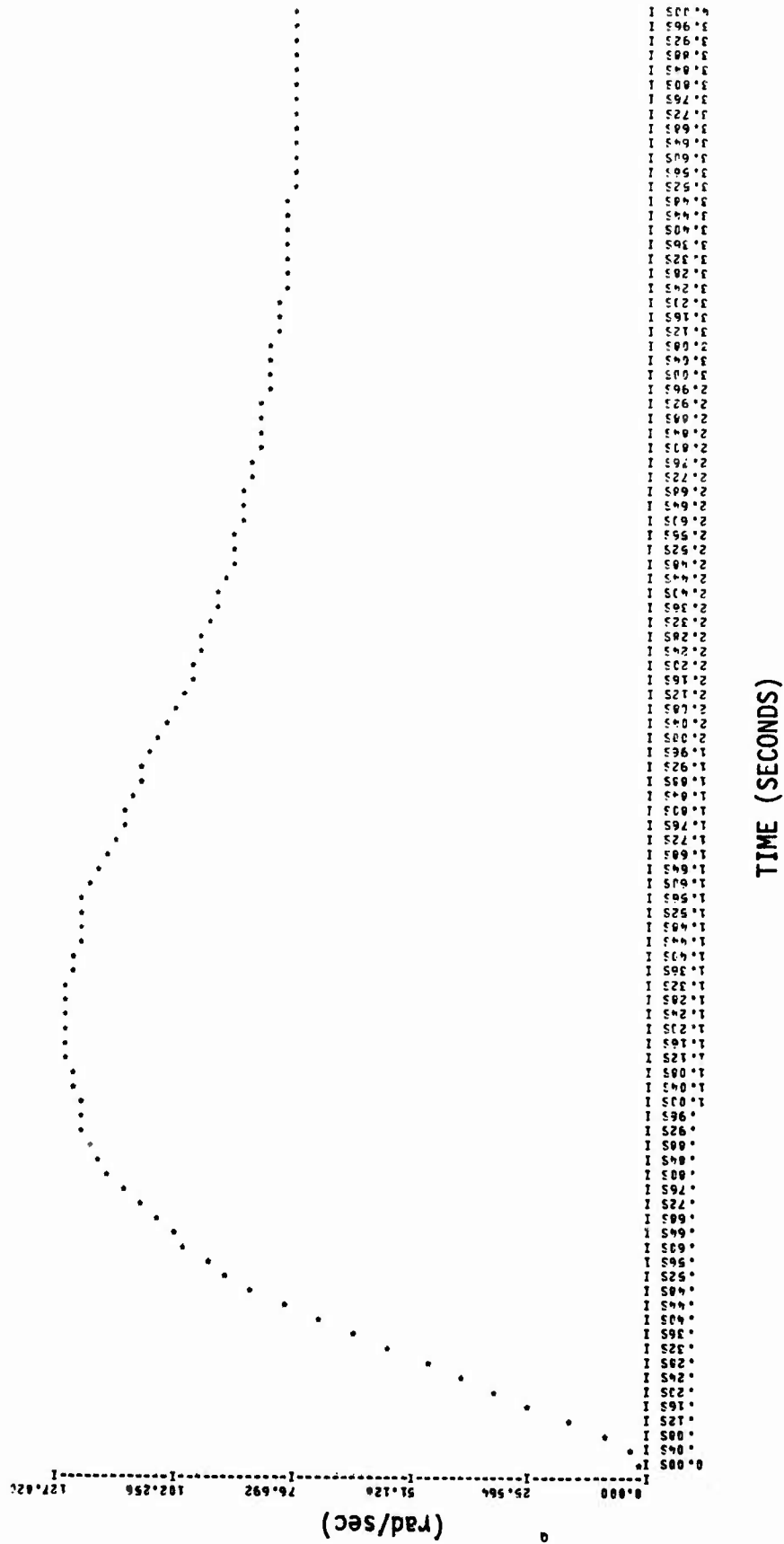
Figure 104. Command Response Plot of ALDCS A/C with F24RT Model (Q)

222
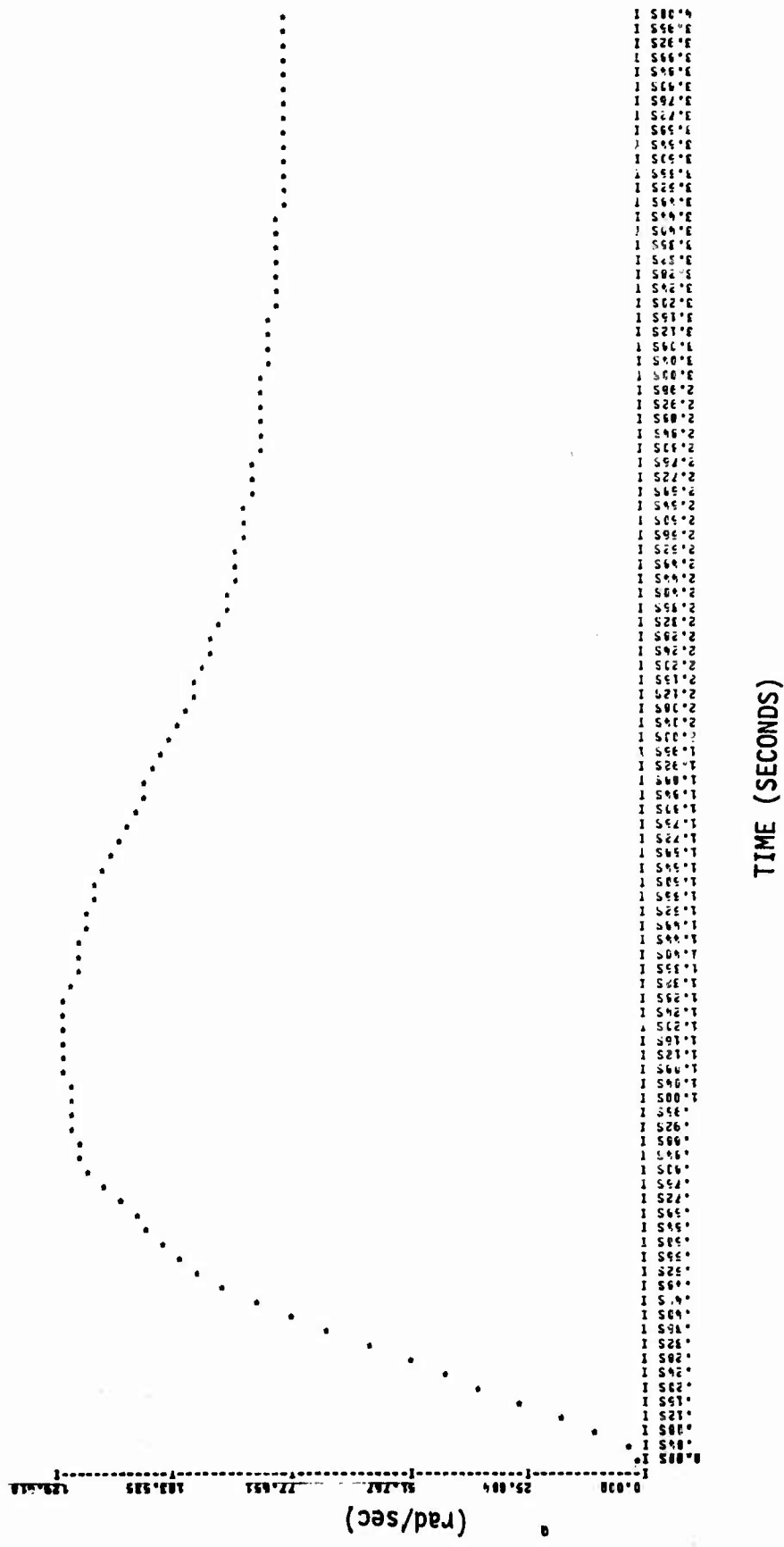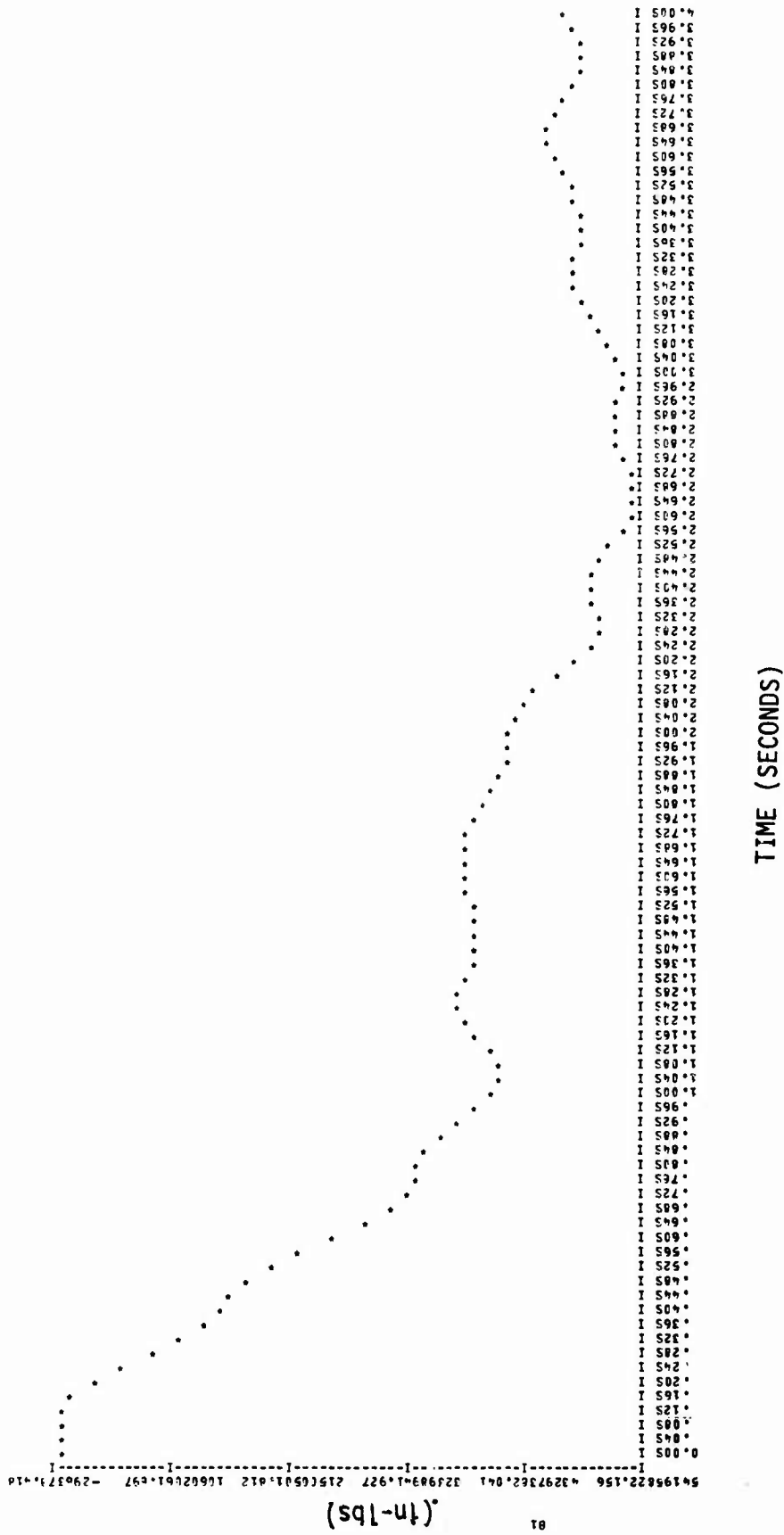
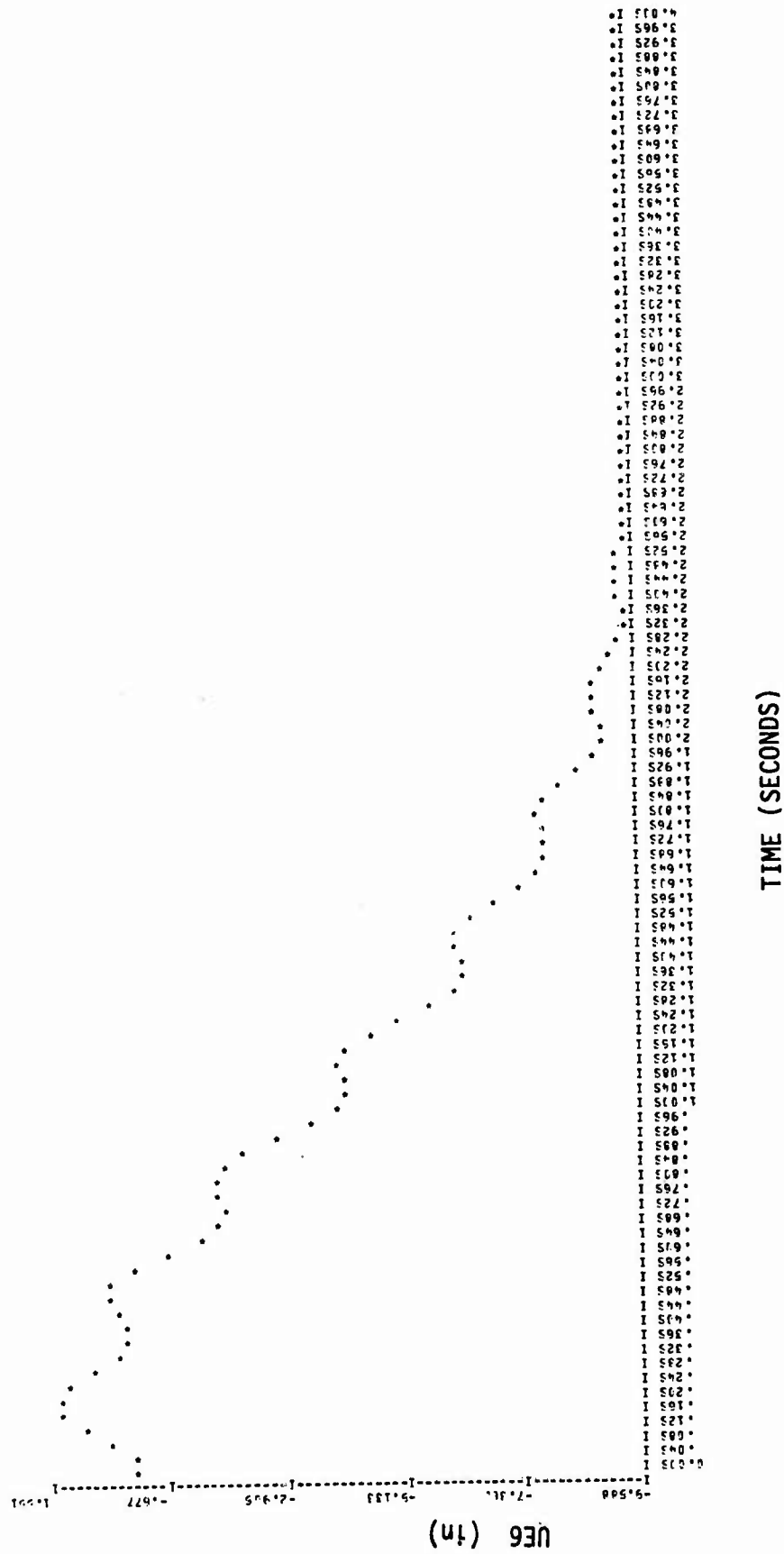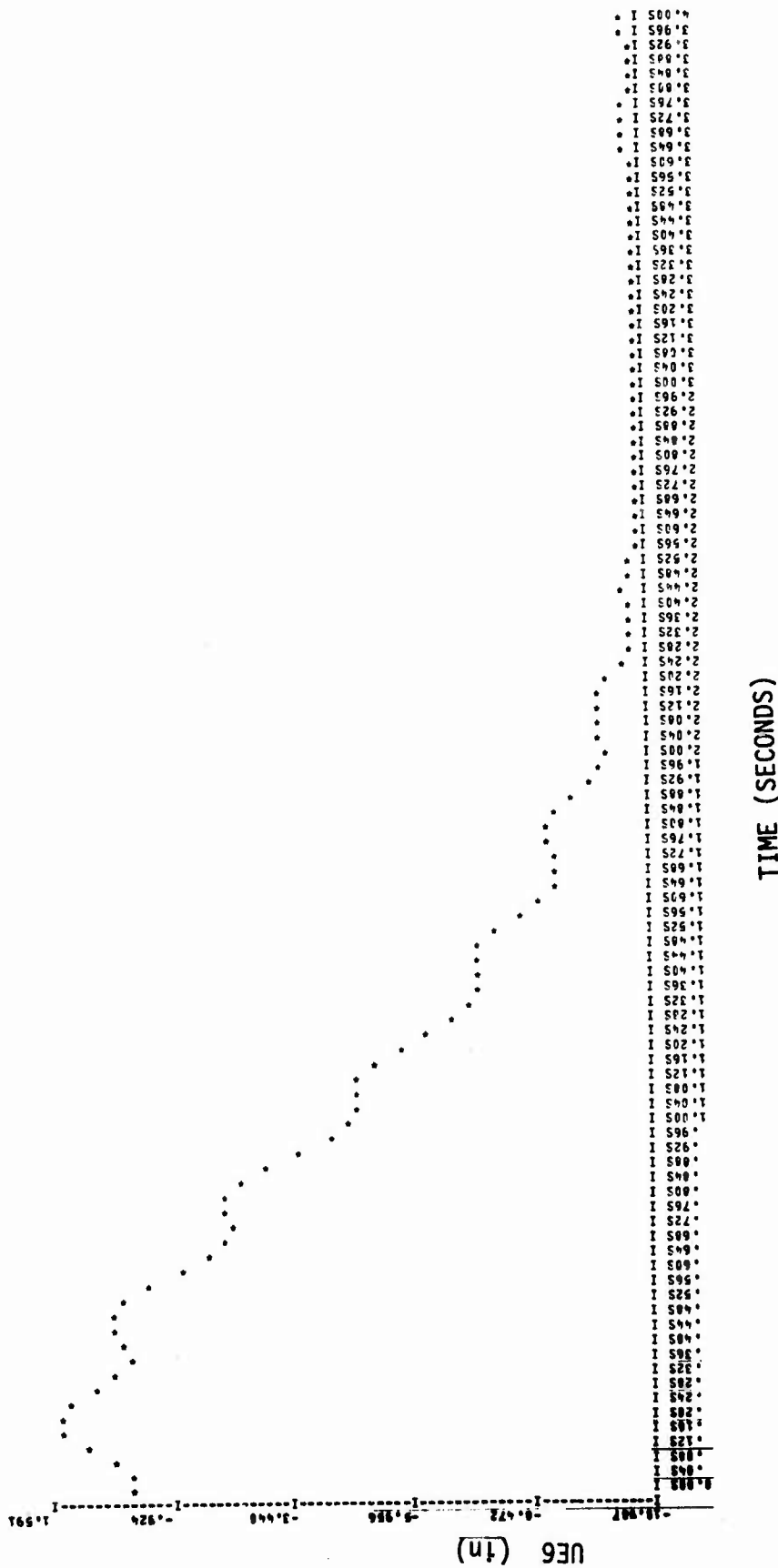Figure 106. Command Response Plot of ALDCS A/C with HG24RR Model (B1)

224
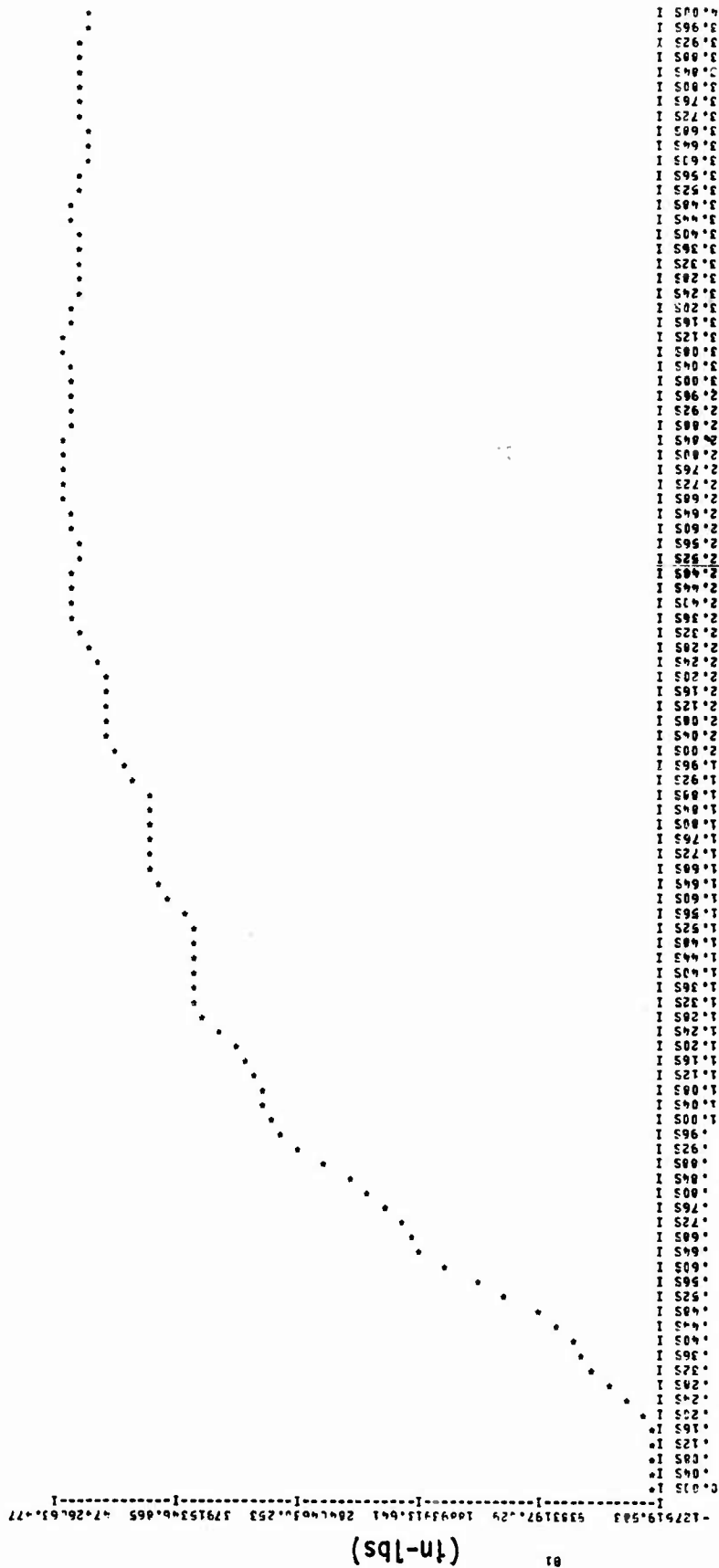
Figure 107. Command Response Plot of ALDCS A/C with F24RR Model (B1)
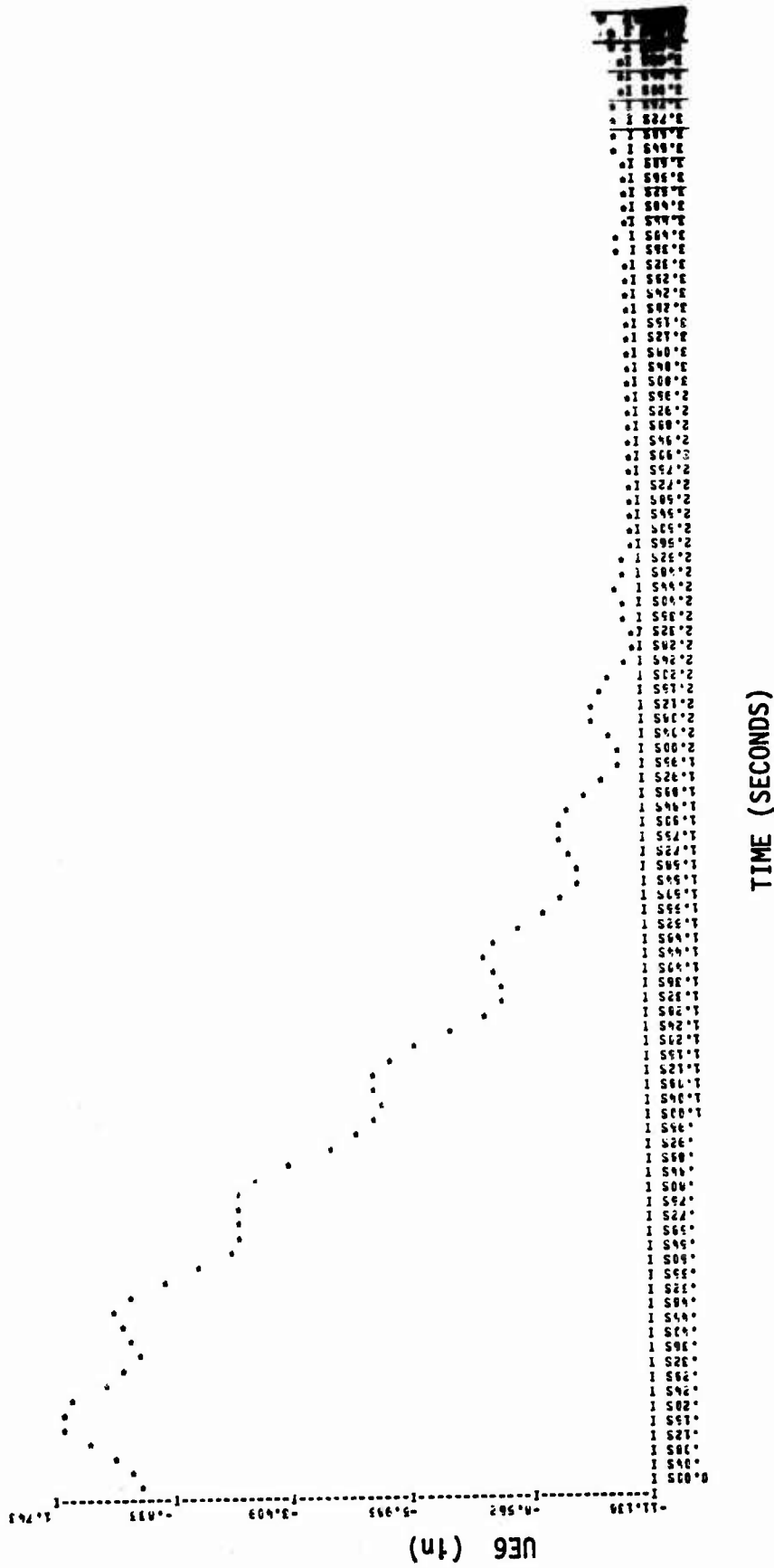
TIME (SECONDS)

(in-lbs)

225
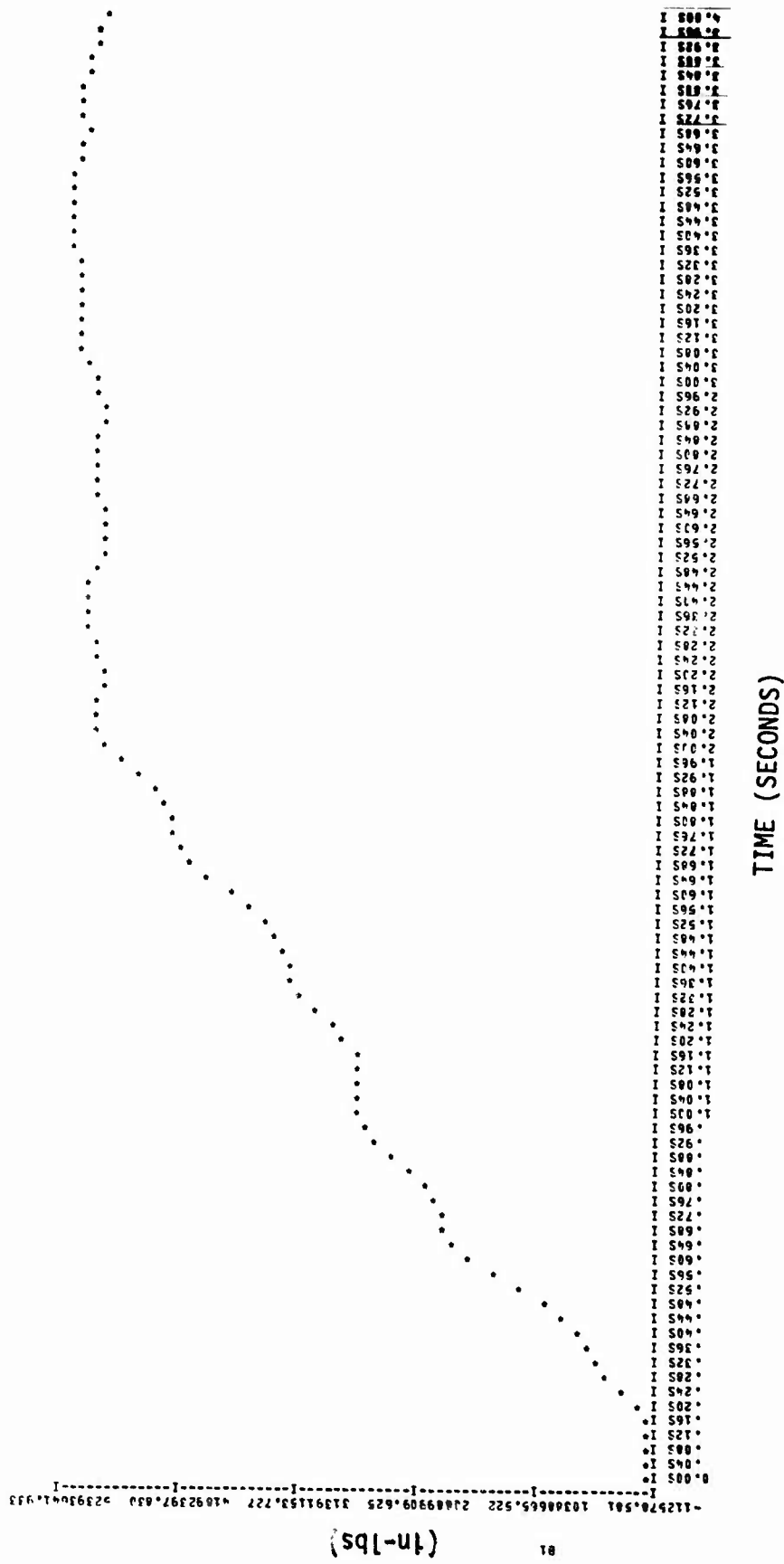
Figure 108. Command Response Plot of ALDCS A/C with F24RT Model (B1)

226
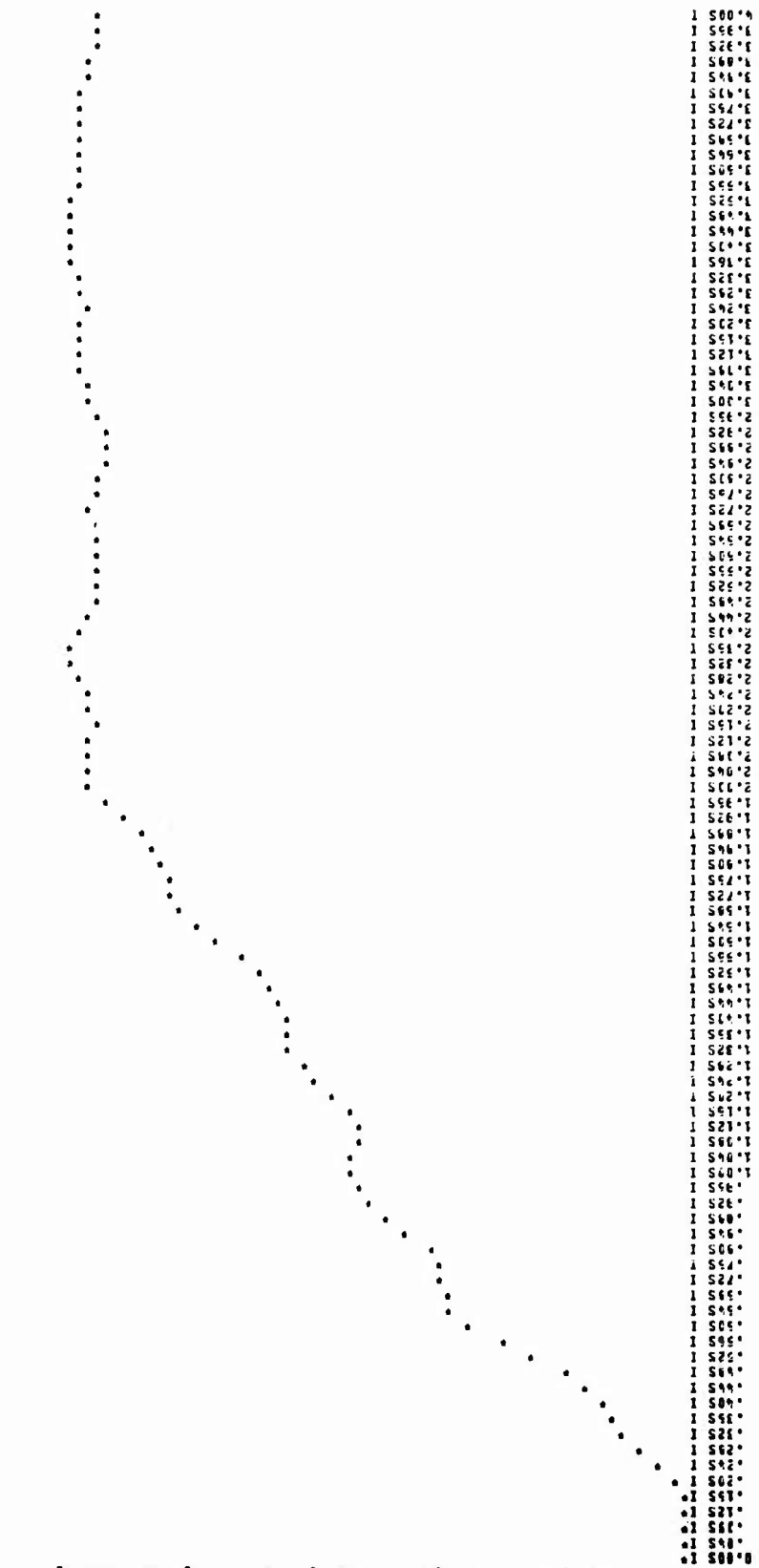
Figure 109. Command Response Plot of ALDCS A/C with F24TT Model (B1)

TIME (SECONDS)

(In-lbs)

227
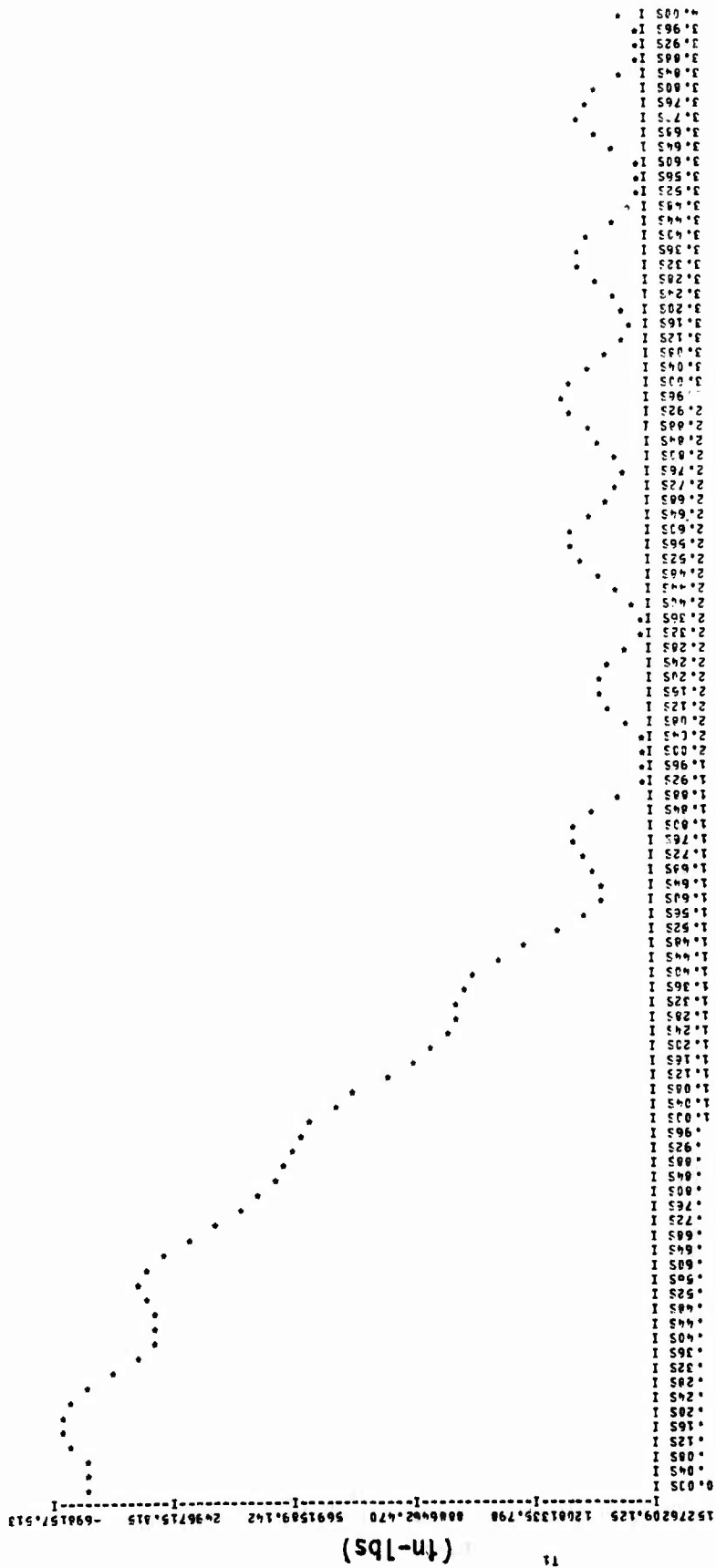
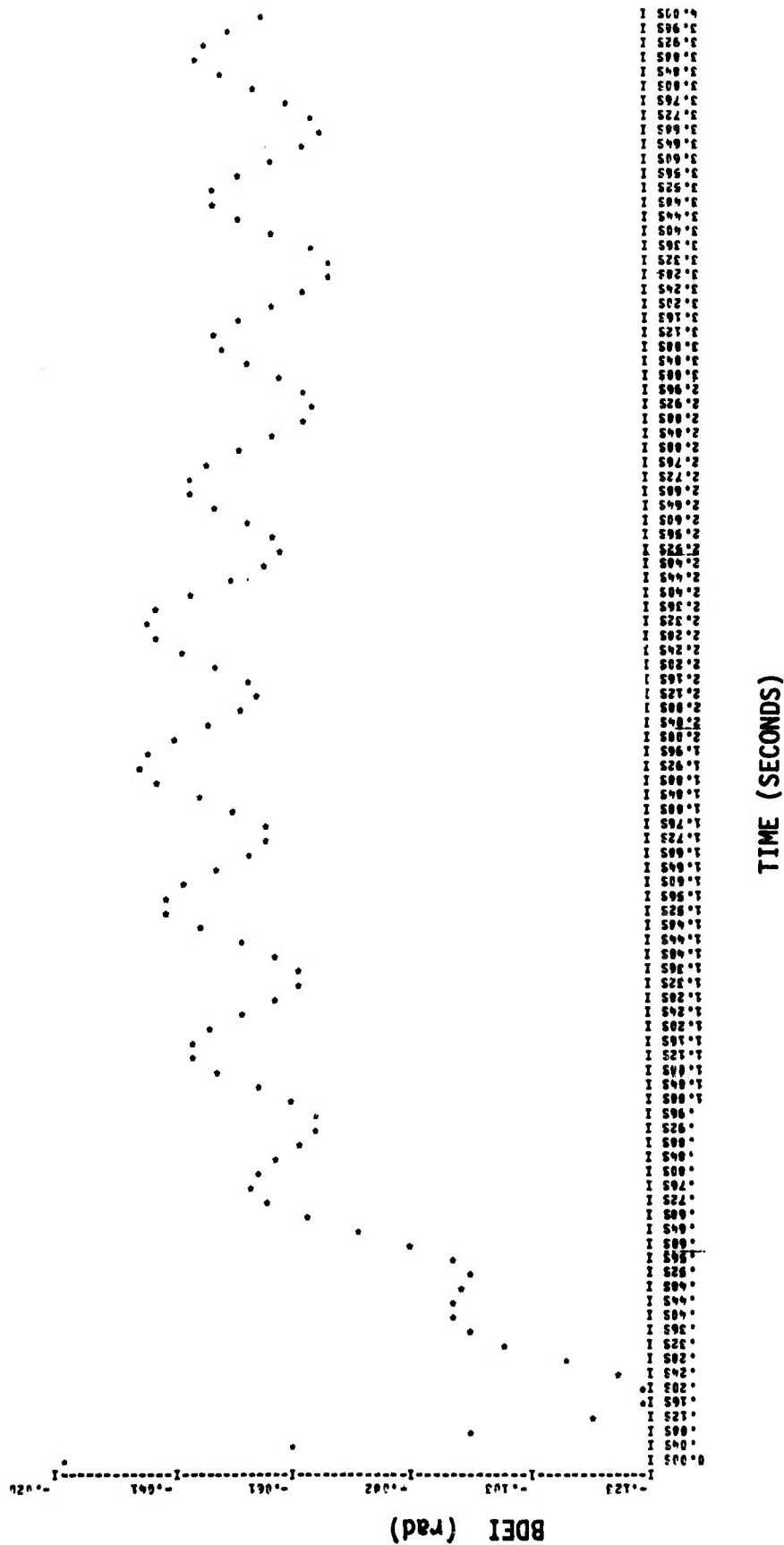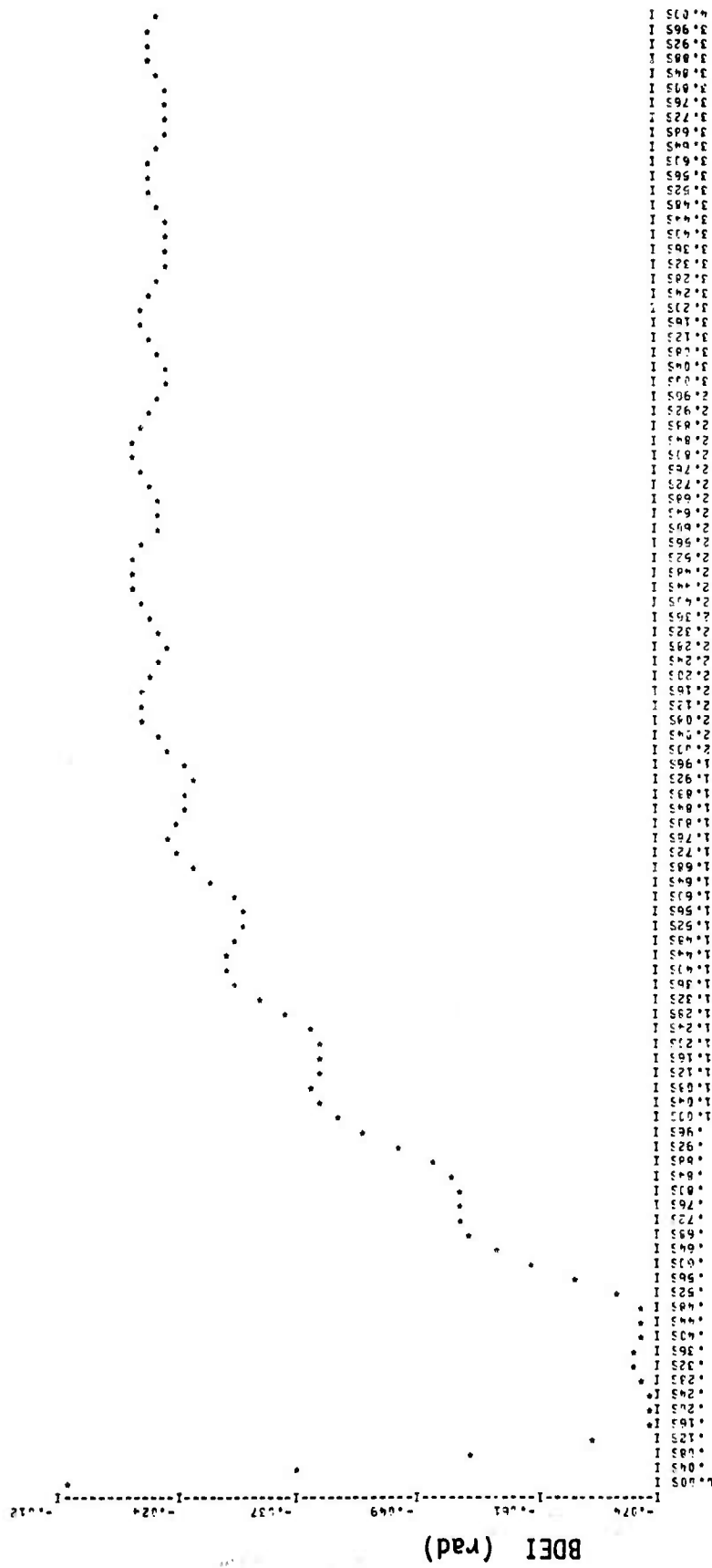Figure 110. Command Response Plot of ALDCS A/C with HG24RR Model (T1)

228
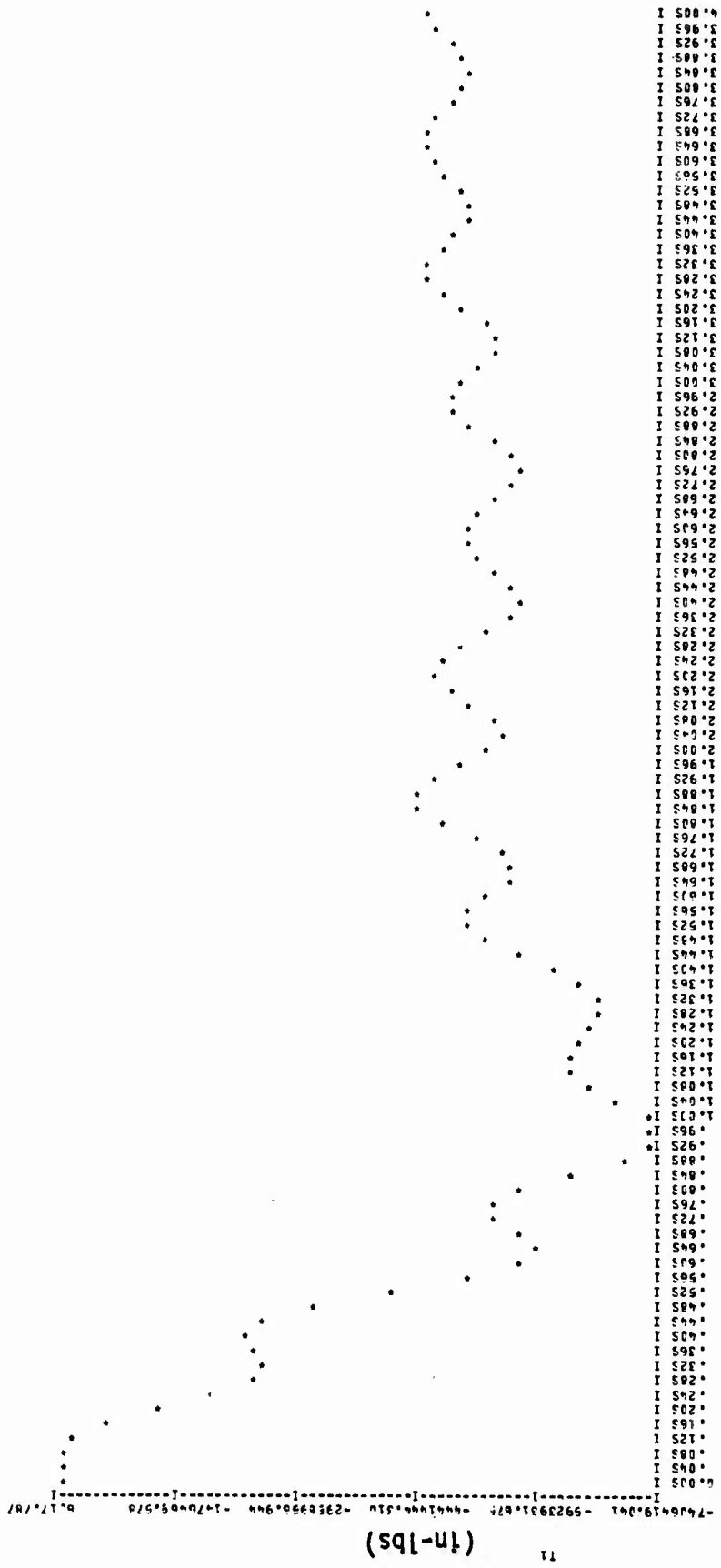
Figure 111. Command Response Plot of ALDCS A/C with F24RR Model (T1)

229
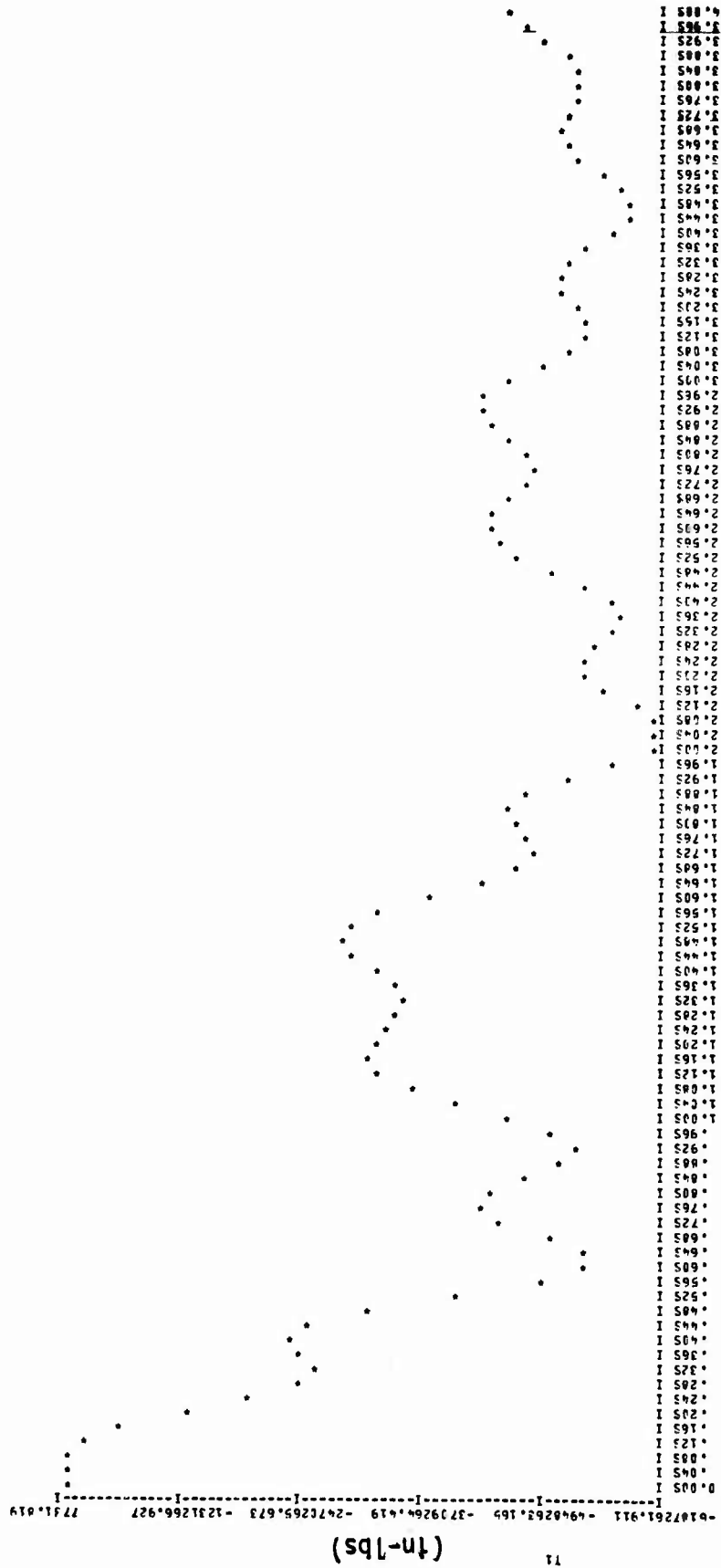
TIME (SECONDS)

Figure 112. Command Response Plot of ALDCS A/C with F24RT Model (T1)

230
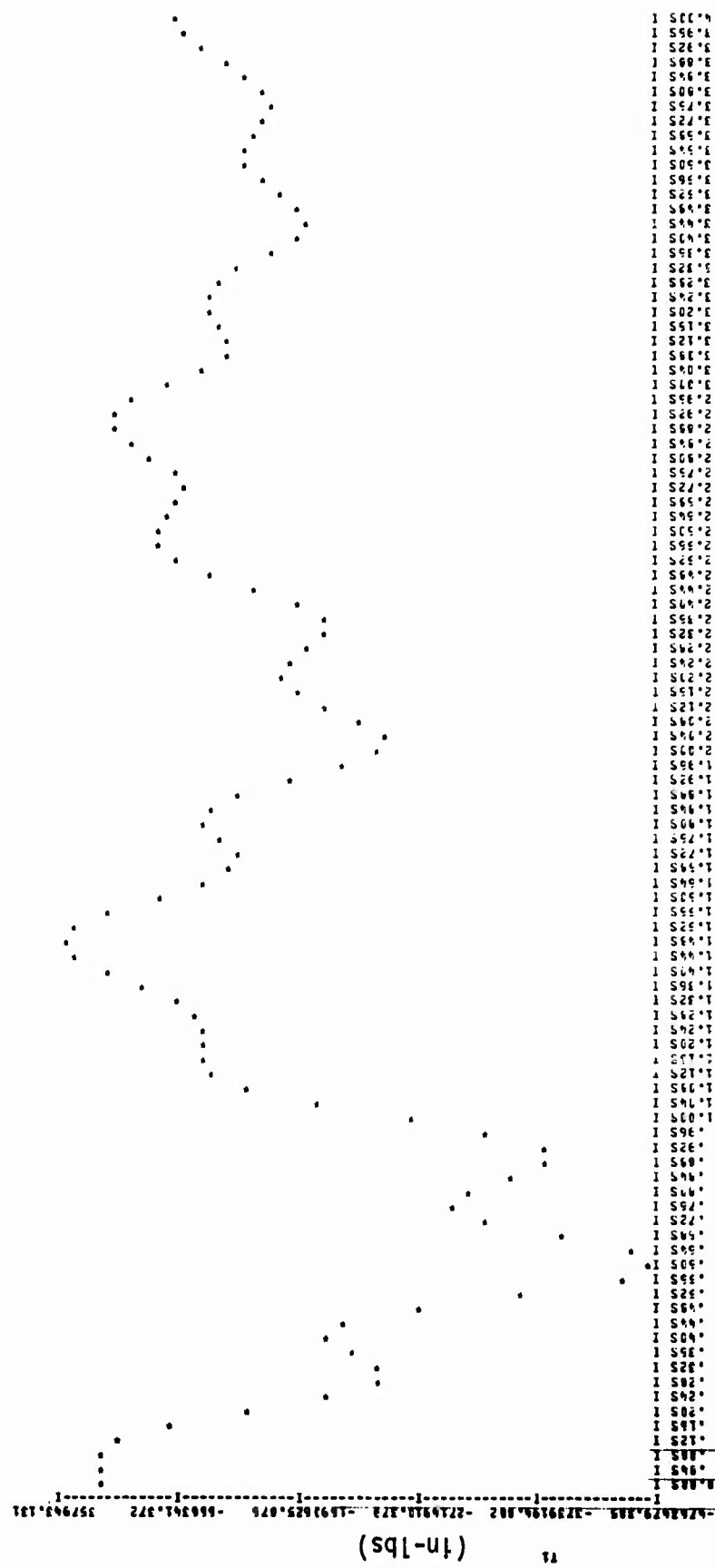
Figure 113. Command Response Plot of ALDCS A/C with F24TT Model (T1)

TIME (SECONDS)

T_1 (in-lbs)

231
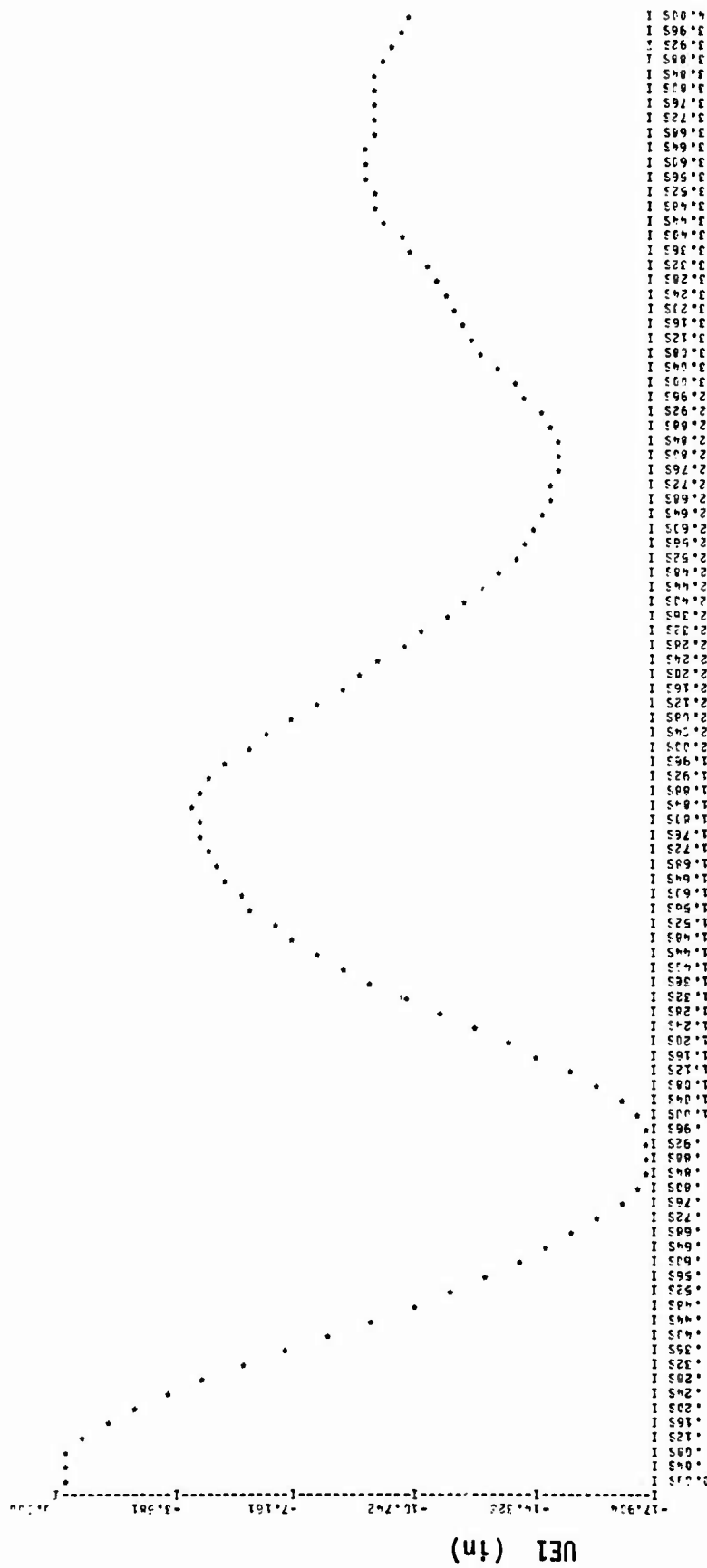
Figure 114.   Command Response Plot of ALDCS A/C with HG24RR Model (ETA1)

232

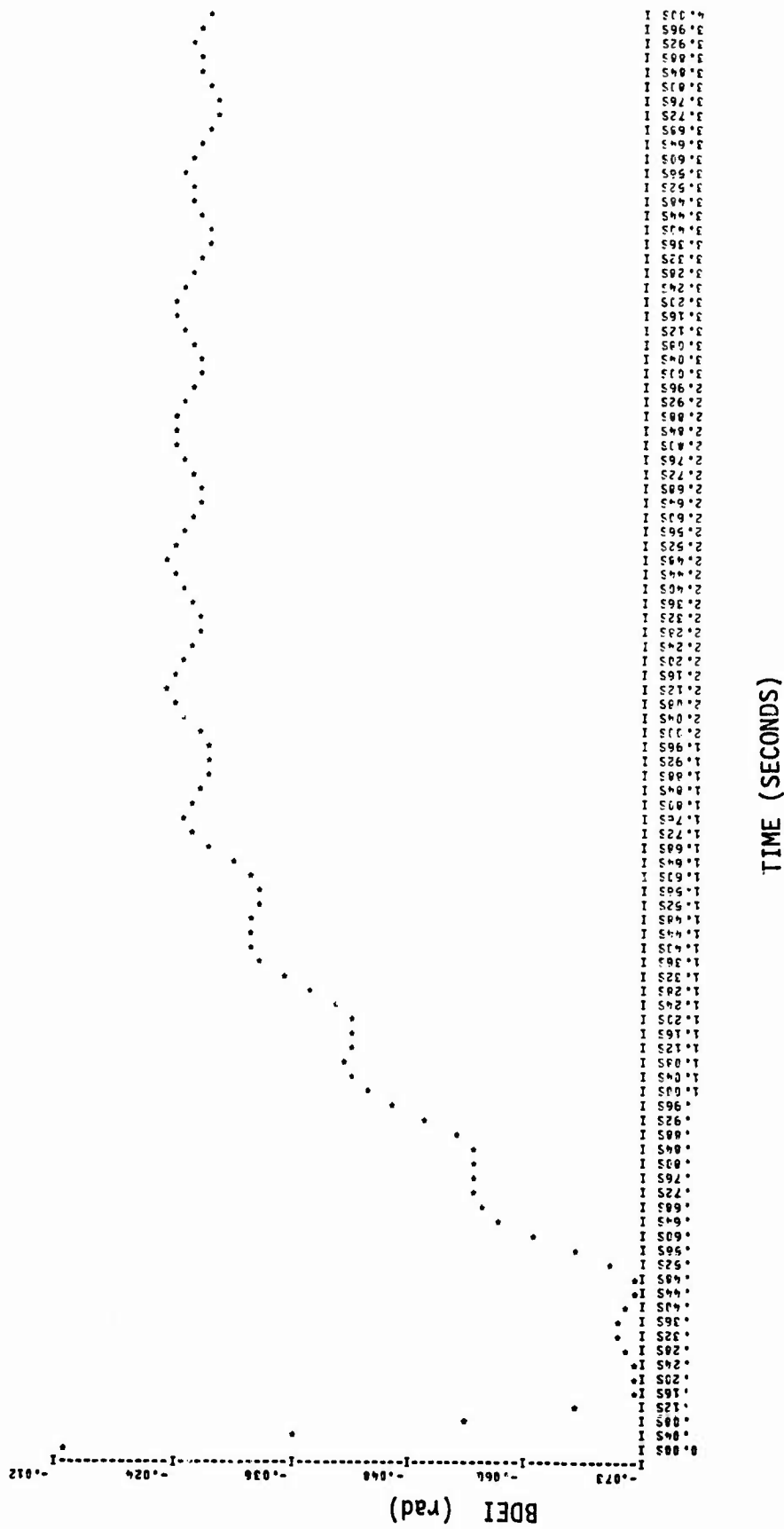Figure 115. Command Response Plot of ALDCS A/C with F24RR Model (ETA1)

233

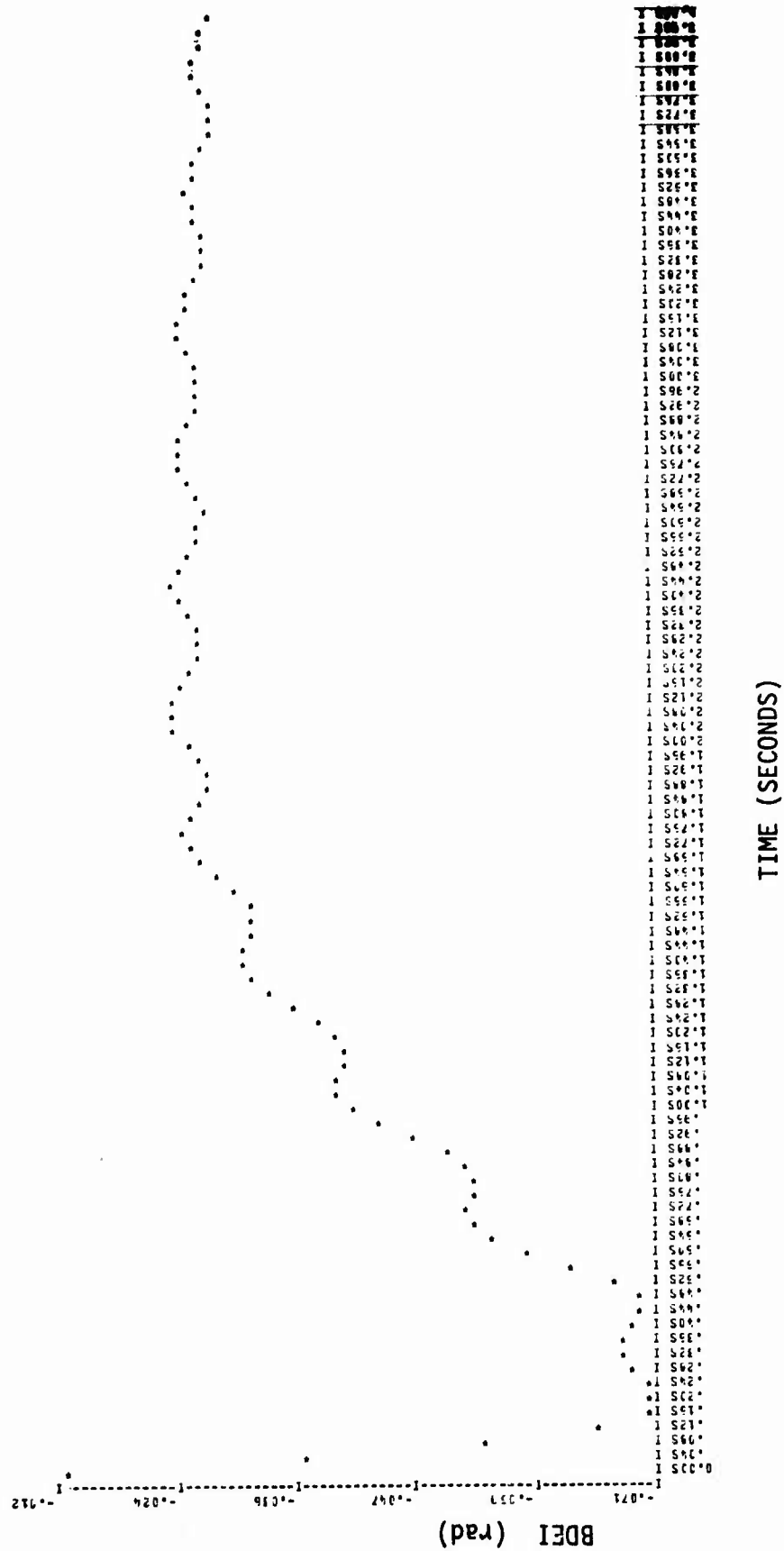Figure 116. Command Response Plot of ALDCS A/C with F24RT Model (ETA1)

234
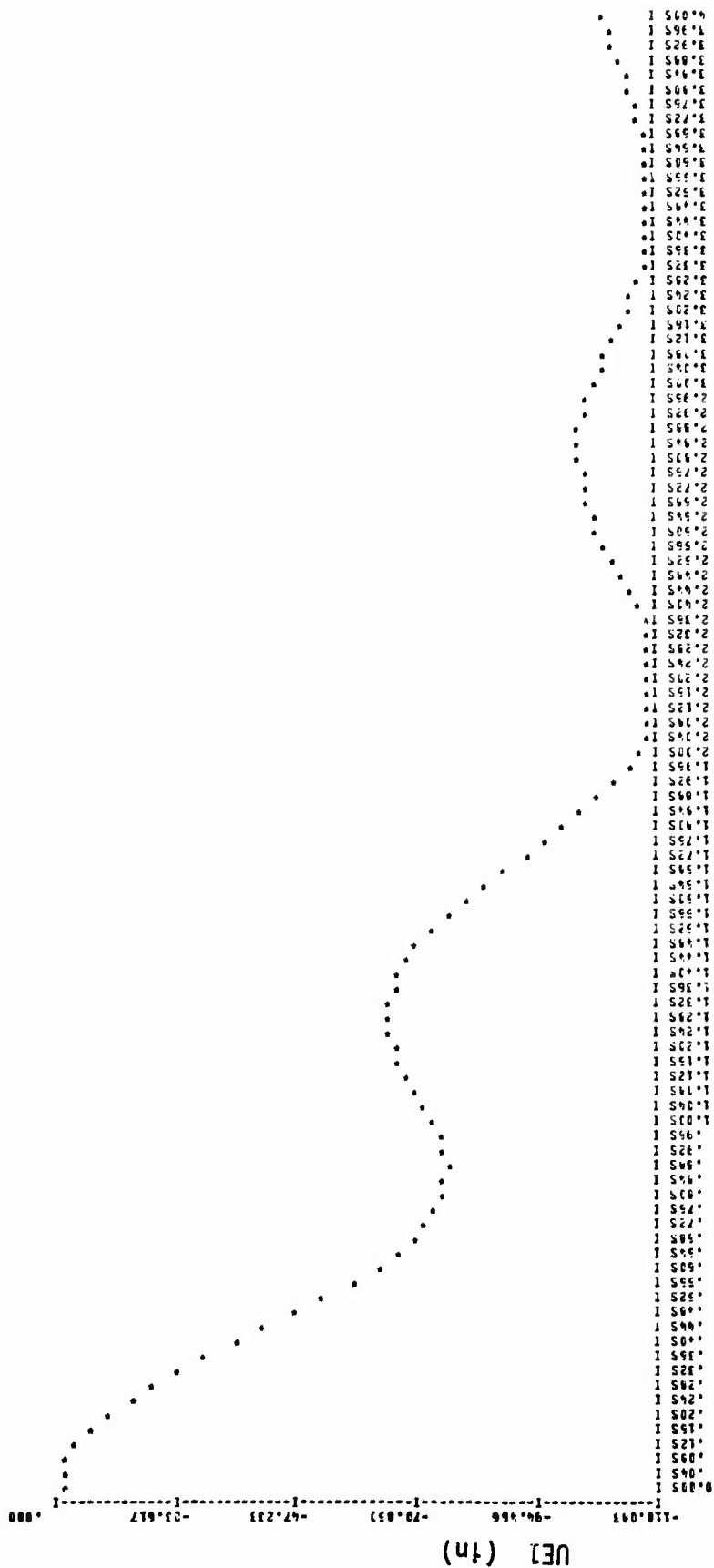
Figure 117. Command Response Plot of ALDCS A/C with F24TT Model (ETA1)

235

Figure 118. Command Response Plot of ALDCS A/C with HG24RR Model (ETA3)

236

Figure 119. Command Response Plot of ALDCS A/C with F24RR Model (ETA3)

237

Figure 120. Command Response Plot of ALDCS A/C with F24RT Model (ETA3)

238

Figure 121. Command Response Plot of ALDCS A/C with F24TT Model (ETA3)
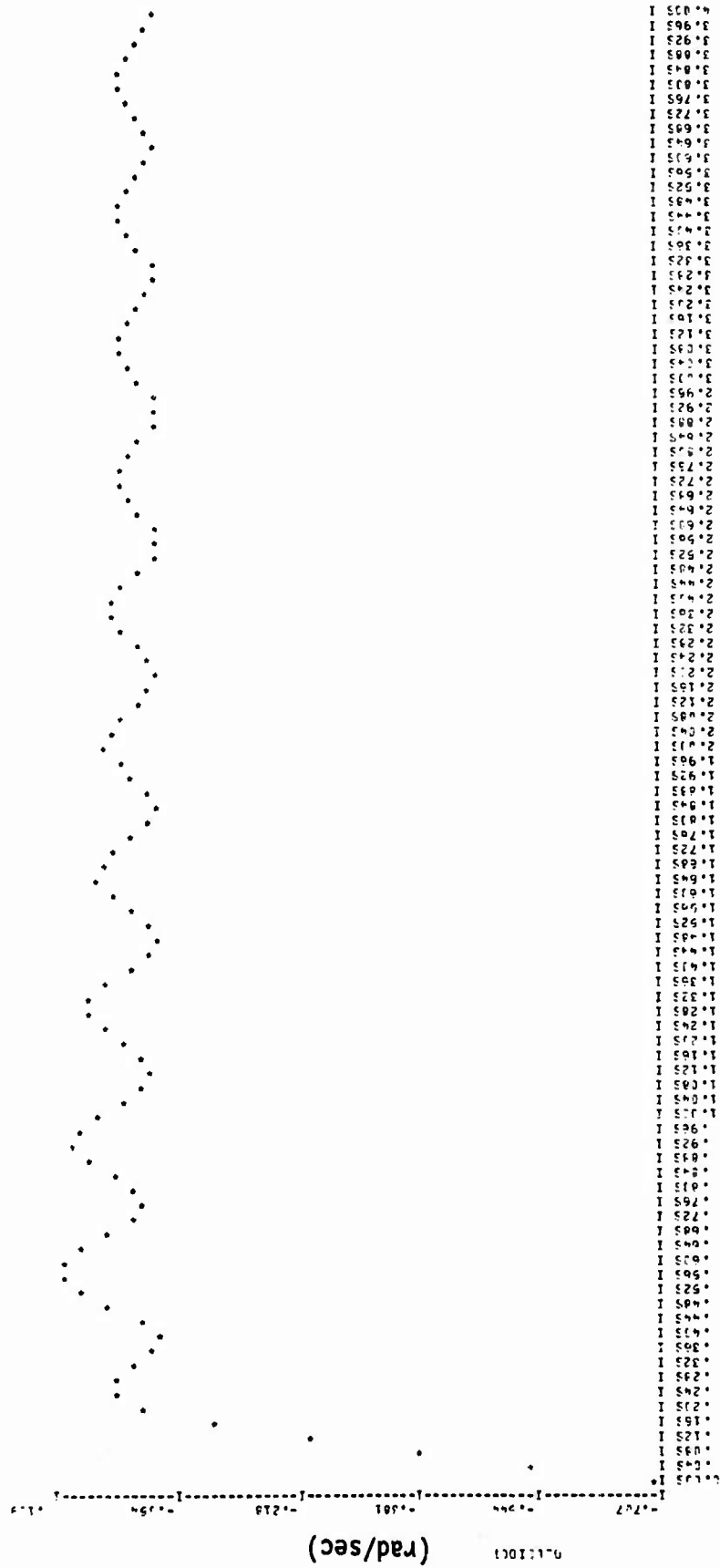
239
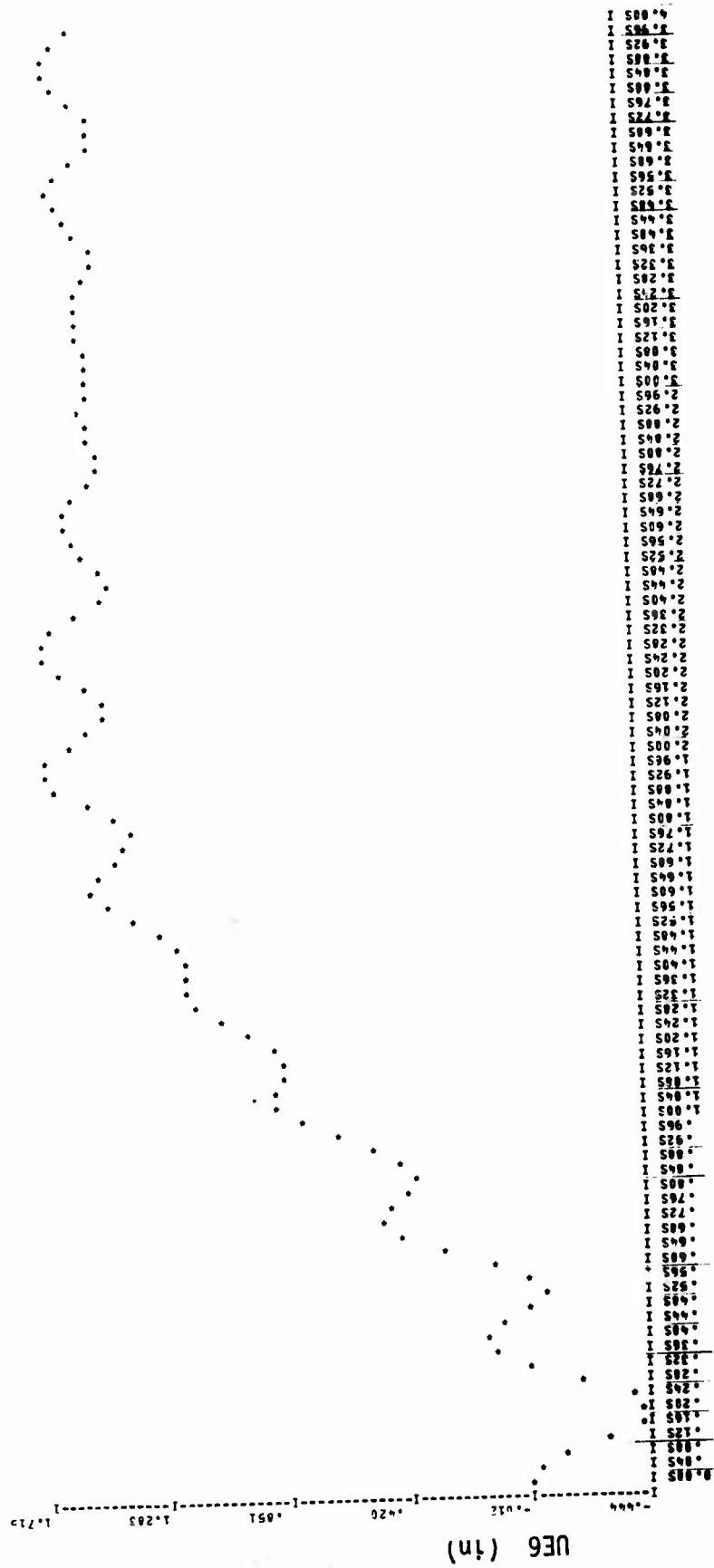
Figure 122. Command Response Plot of ALDCS A/C with HG24RR Model (ETA6)

TIME (SECONDS)

UE6 (in)

240

Figure 123. Command Response Plot of ALDCS with F24RR Model (ETA6)

TIME (SECONDS)

UE6 (in)

TIME (SECONDS)

UE6 (in)

Figure 124. Command Response Plot of ALDCS A/C with F24RT Model (ETA6)

Figure 125. Command Response Plot of ALDCS A/C with F24TT Model (ETA6)

243

Figure 126. Command Response Plot of ALDCS A/C with HG24RR Model (DELEI)

244

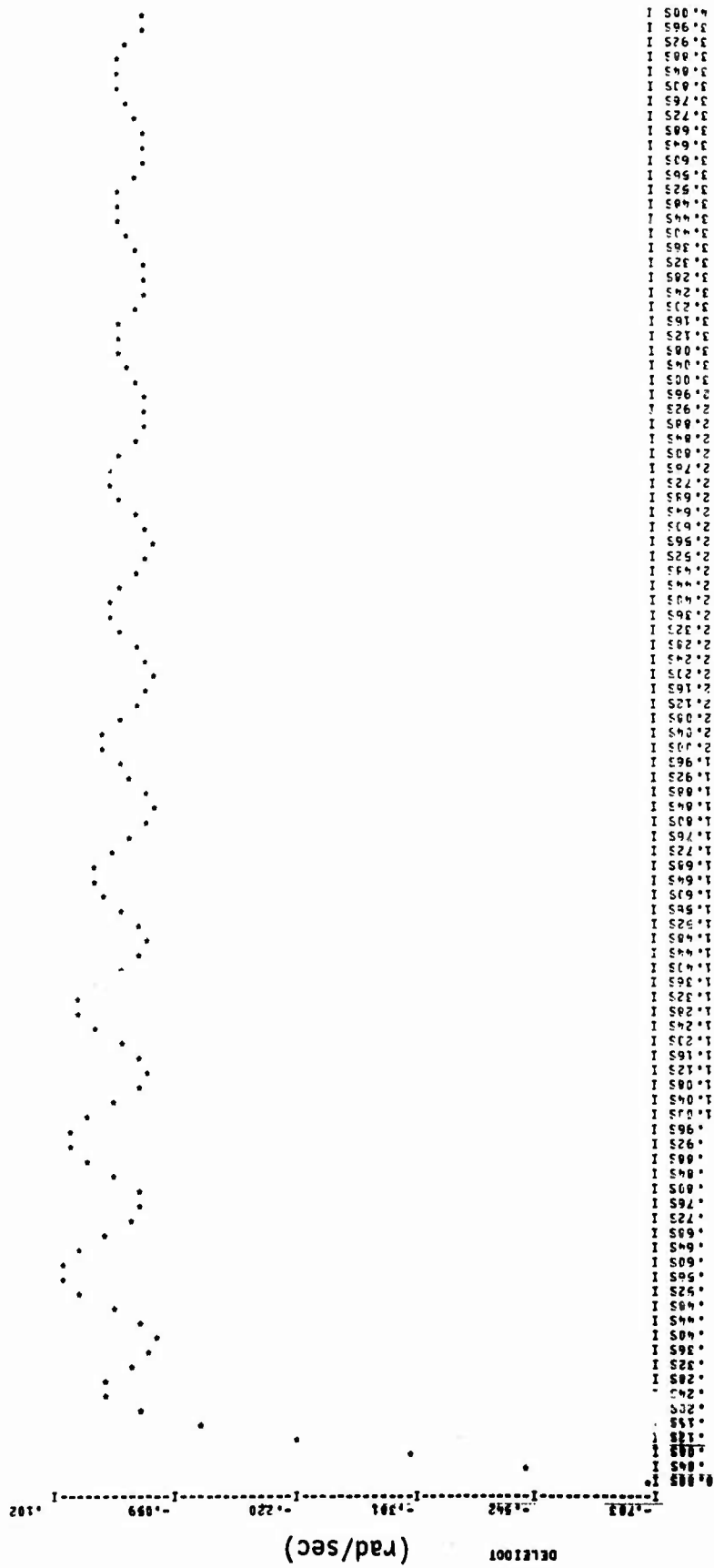Figure 127. Command Response Plot of ALDCS A/C with F24RR Model (DELEI)

245

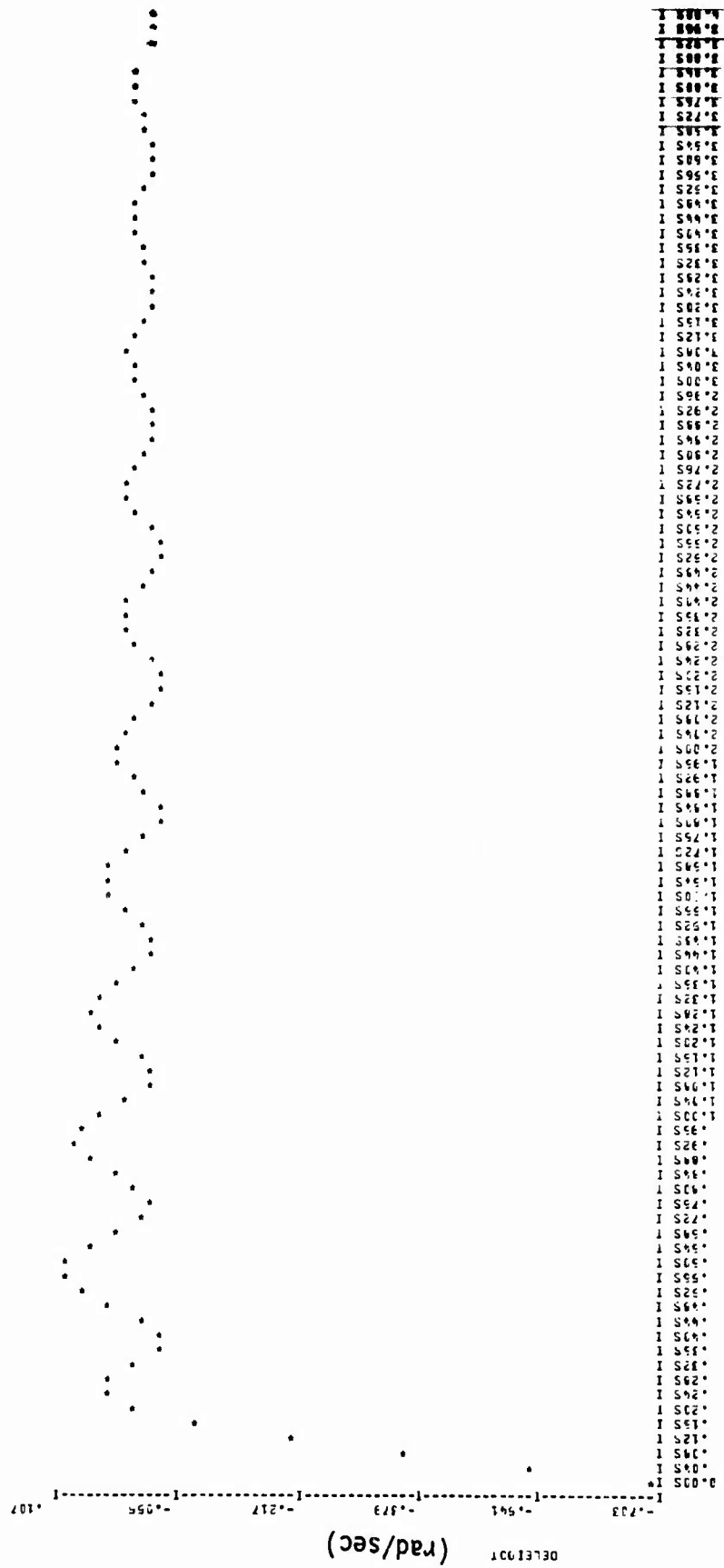Figure 128. Command Response Plot of ALDCS A/C with F24RT Model (DELEI)

246

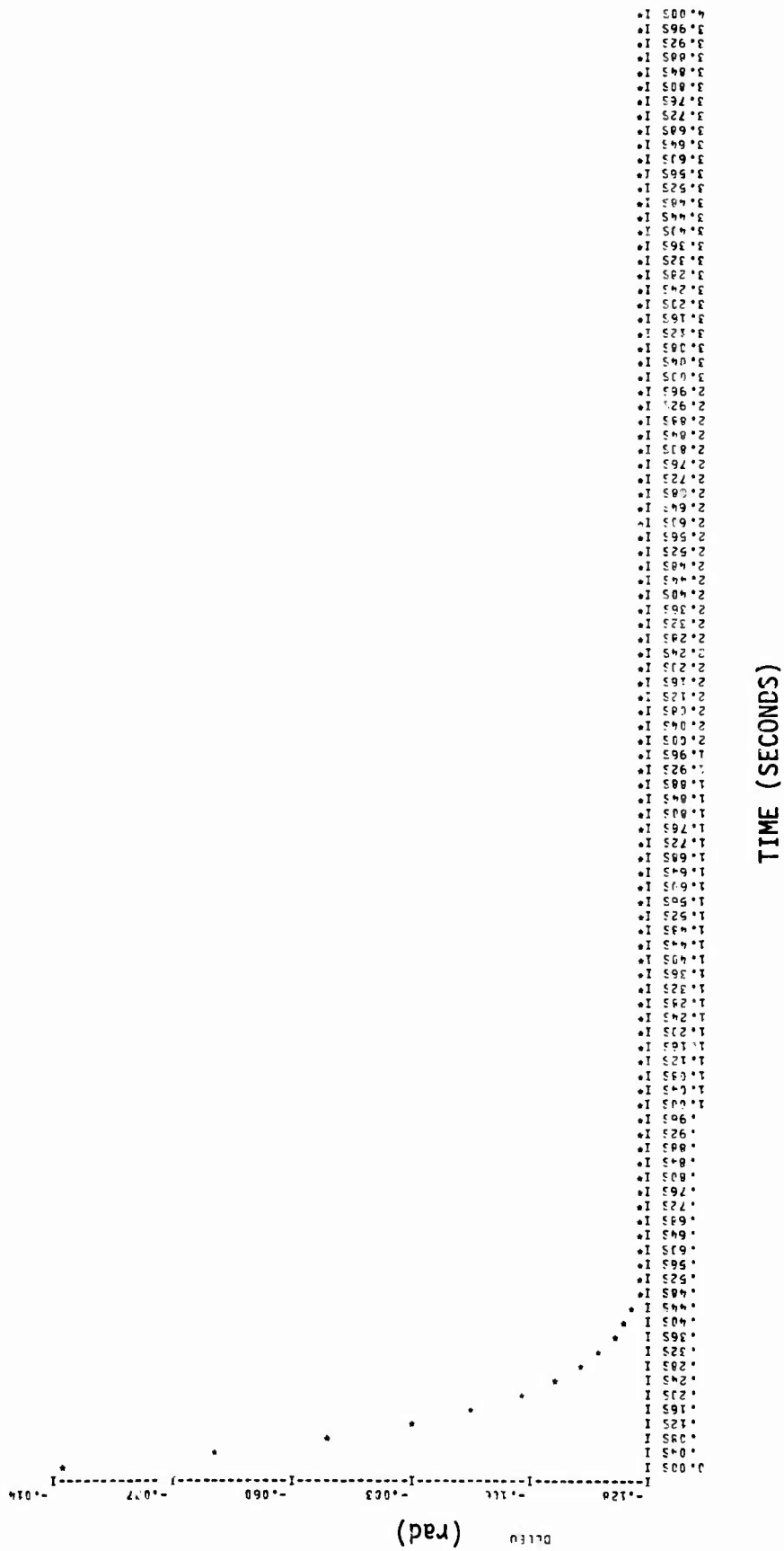Figure 129. Command Response Plot of ALDCS A/C with F24TT Model (DELEI)

247

Figure 130. Command Response Plot of ALDCS A/C with HG24RR Model (DELEIDOT)

248

Figure 131. Command Response Plot of ALDCS A/C with F24RR Model (DELEIDOT)

249

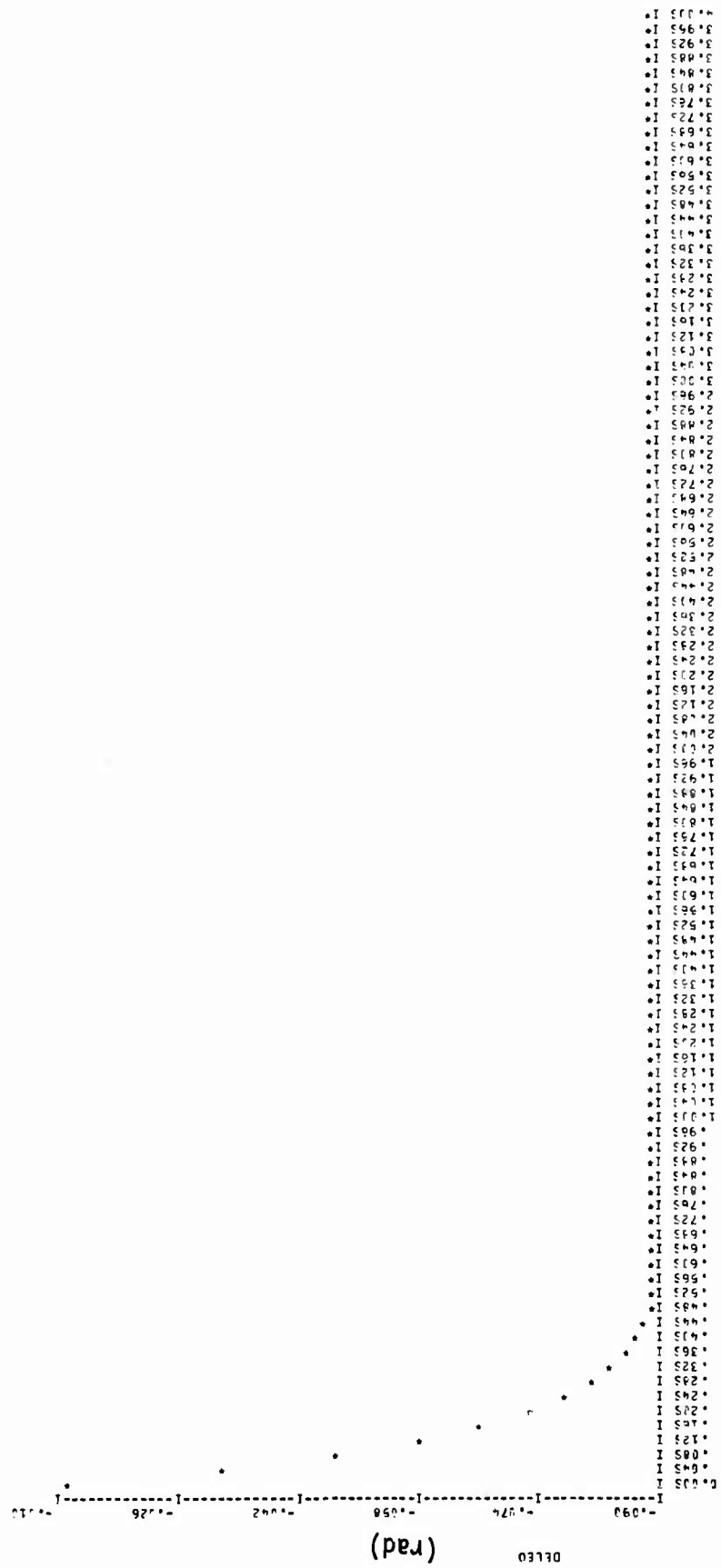Figure 132. Command Response Plot of ALDCS A/C with F24RT Model (DELEIDOT)

250

TIME (SECONDS)

Figure 133. Command Response Plot of ALDCS A/C with F24TT Model (DELEIDOT)

251

Figure 134.   Command Response Plot of ALDCS A/C with H(ω)24RR Model (DELEO)
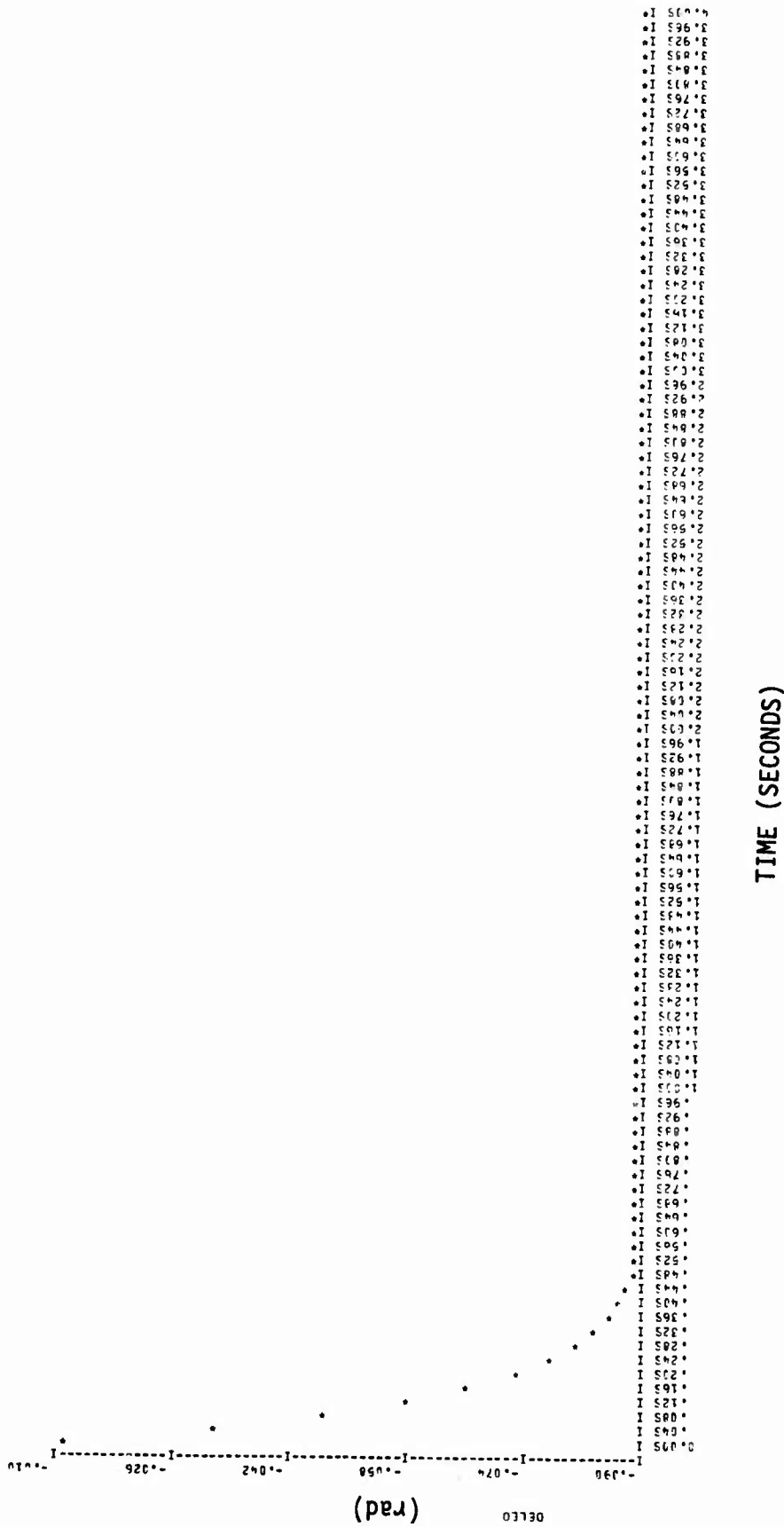
Figure 135.   Command Response Plot of ALDCS A/C with F24RR Model (DELEO)

253

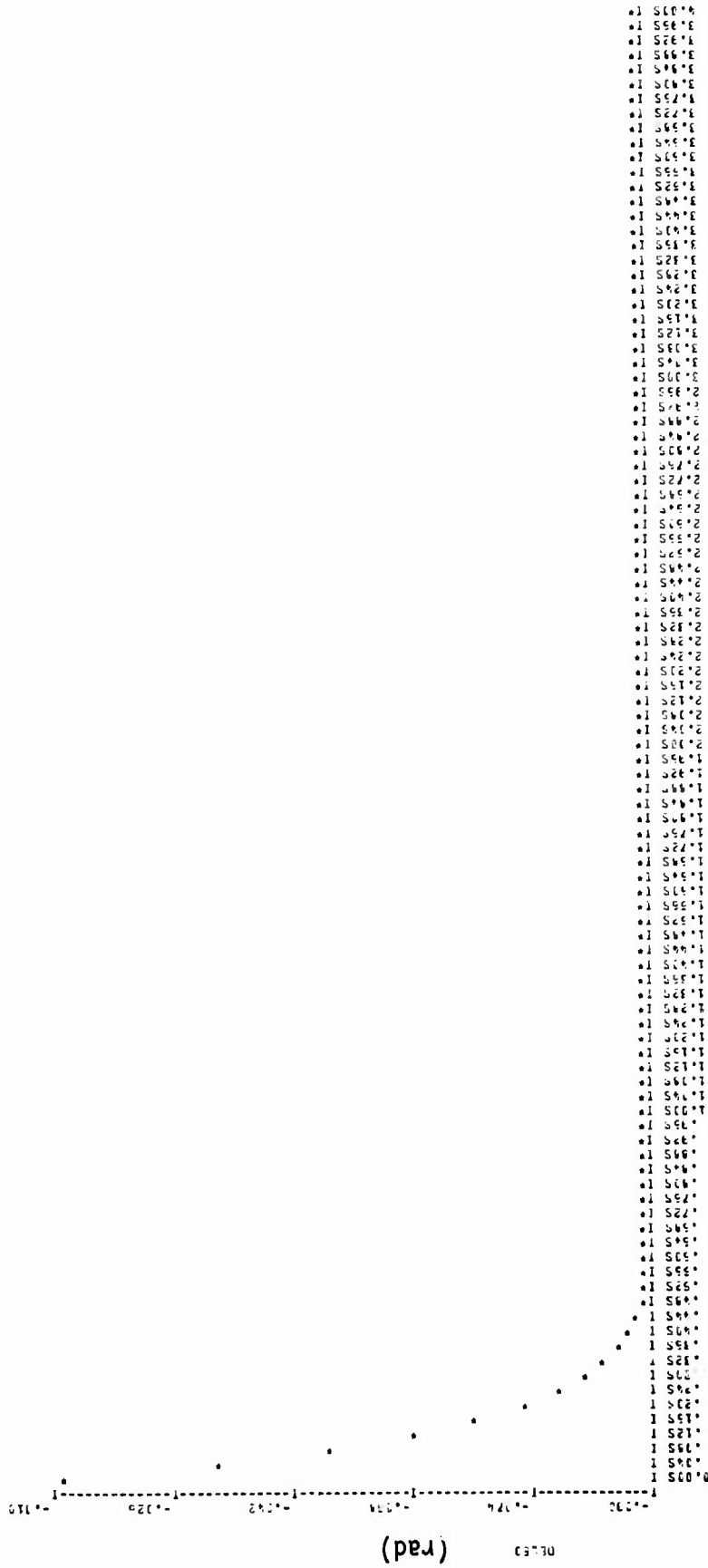Figure 136. Command Response Plot of ALDCS A/C with F24RT Model (DELEO)

TIME (SECONDS)

(rad)

DELEO

254

Figure 137. Command Response Plot of ALDCS A/C with F24TT Model (DELEO)
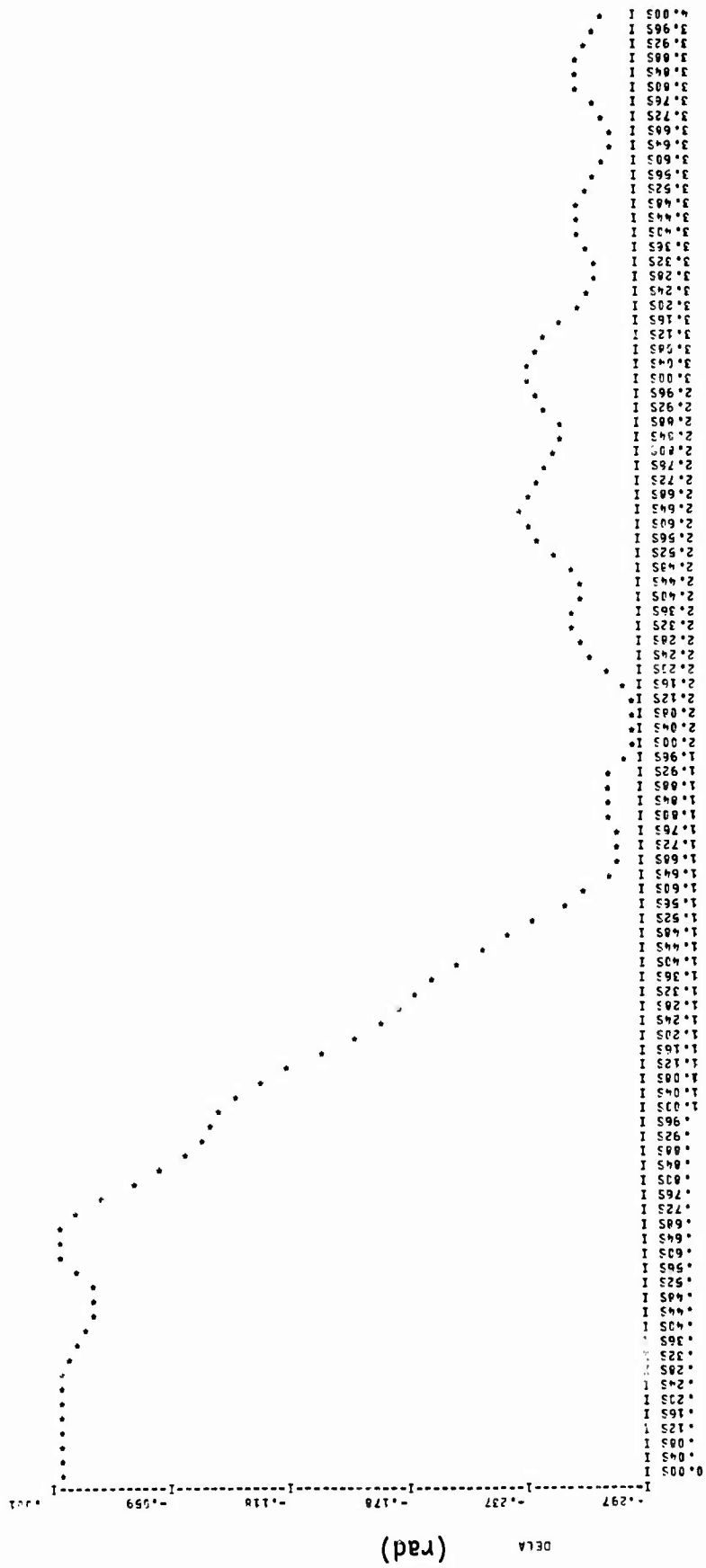
255

Figure 138. Command Response Plot of ALDCS A/C with HG24RR Model (DELA)

256

Figure 139. Command Response Plot of ALDCS A/C with F24RR Model (DELA)

Figure 140. Command Response Plot of ALDCS A/C with F24RT Model (DELA)

258

Figure 141. Command Response Plot of ALDCS A/C with F24TT Model (DELA)

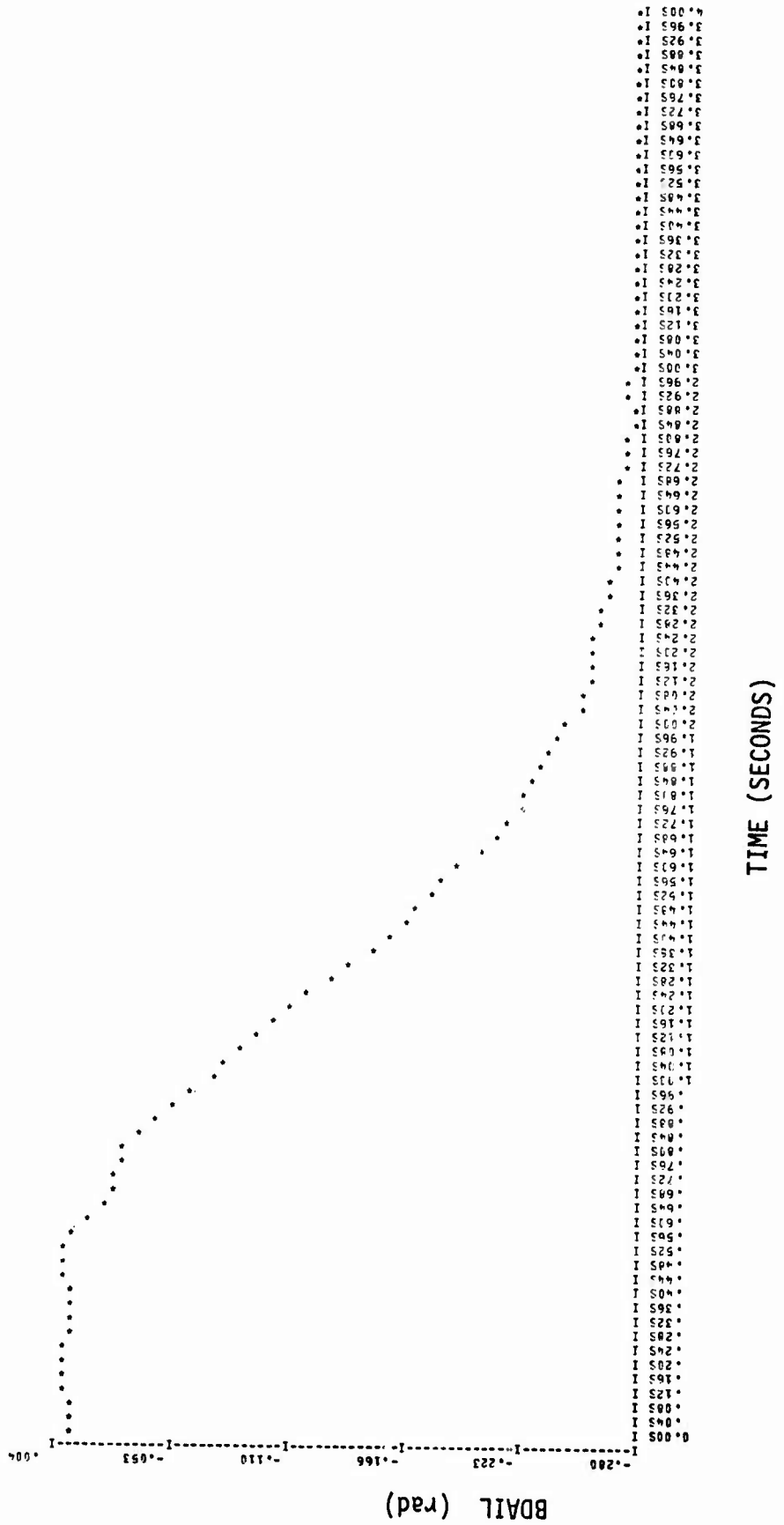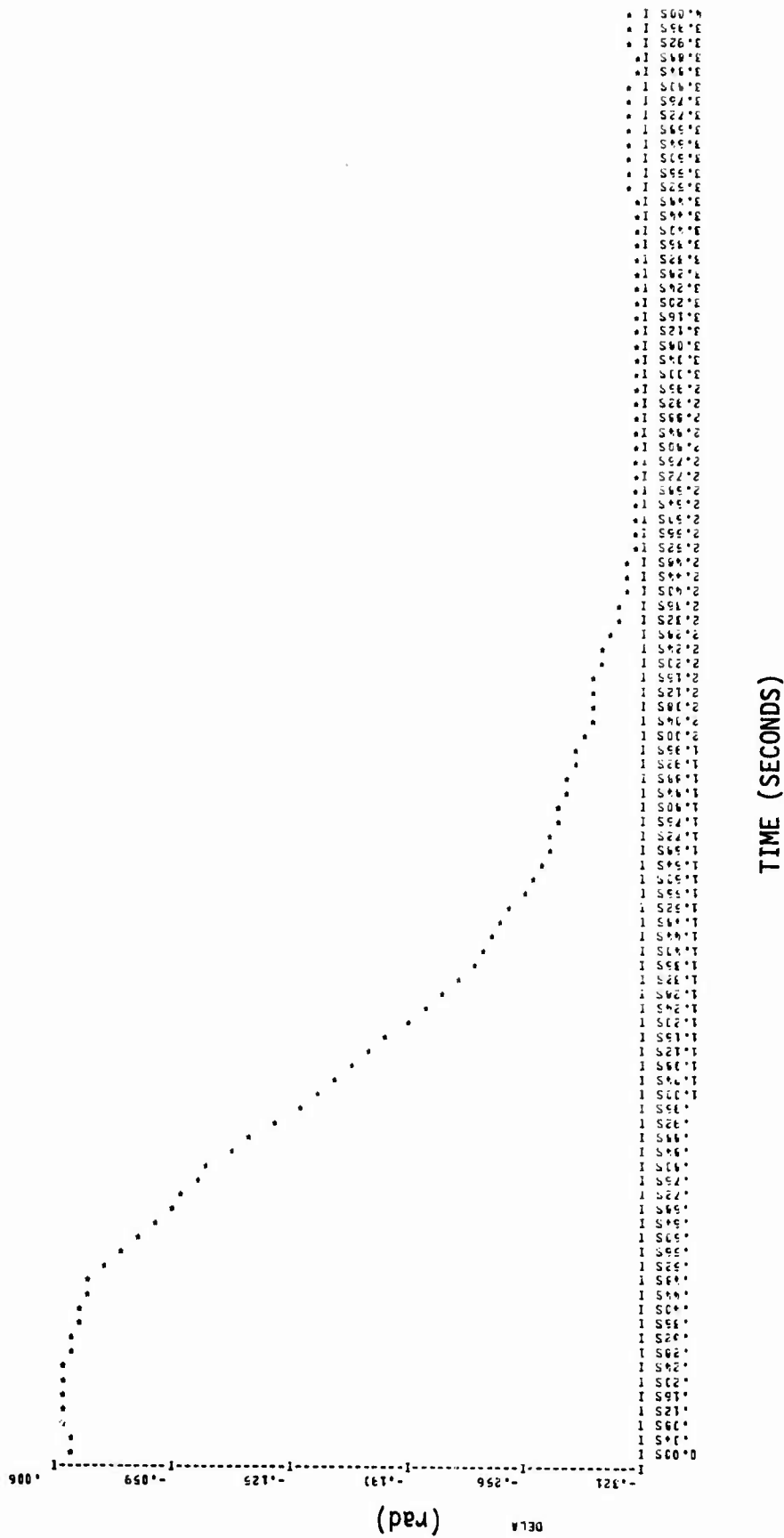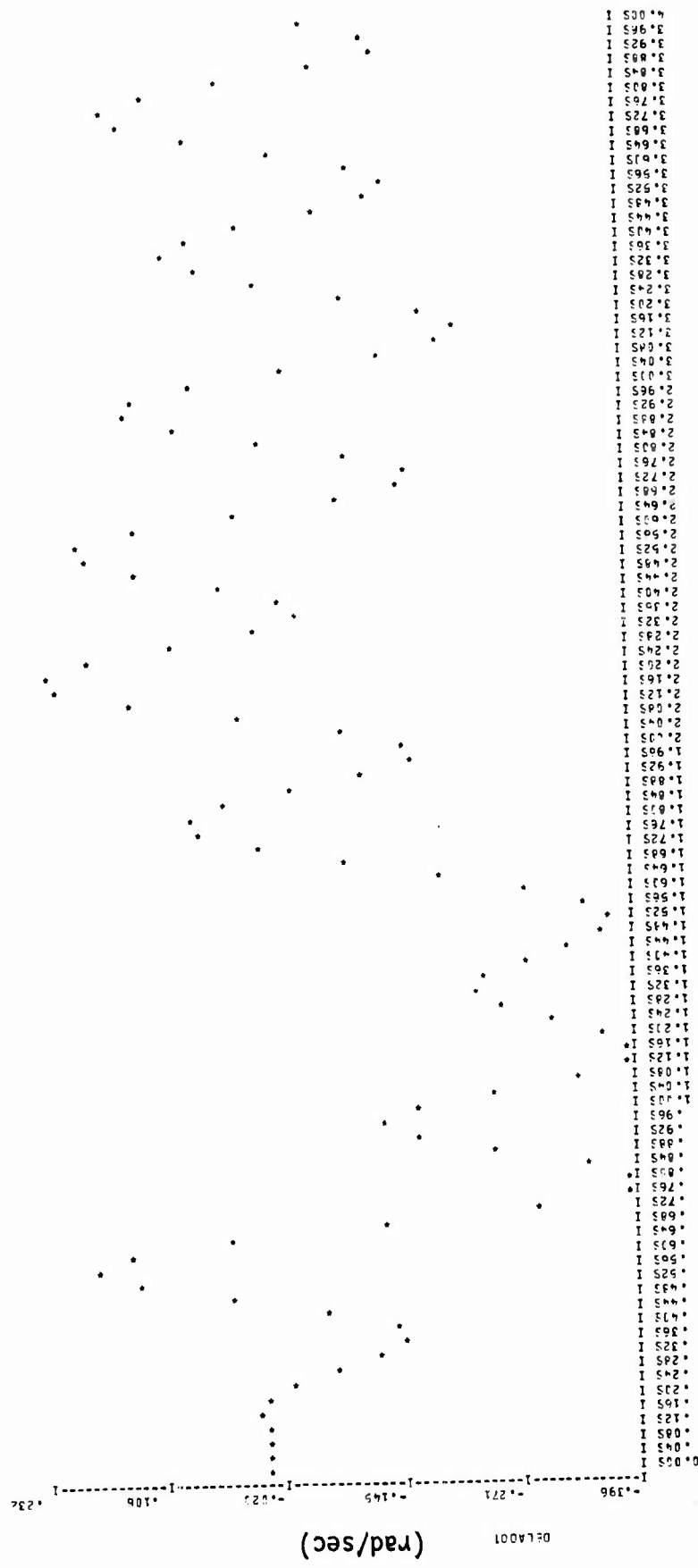Figure 142. Command Response Plot of ALDCS A/C with HG24RR Model (DELADOT)

260

TIME (SECONDS)

DELADOT (rad/sec)

Figure 143.   Command Response Plot of ALDCS A/C with F24RR Model (DELADOT)
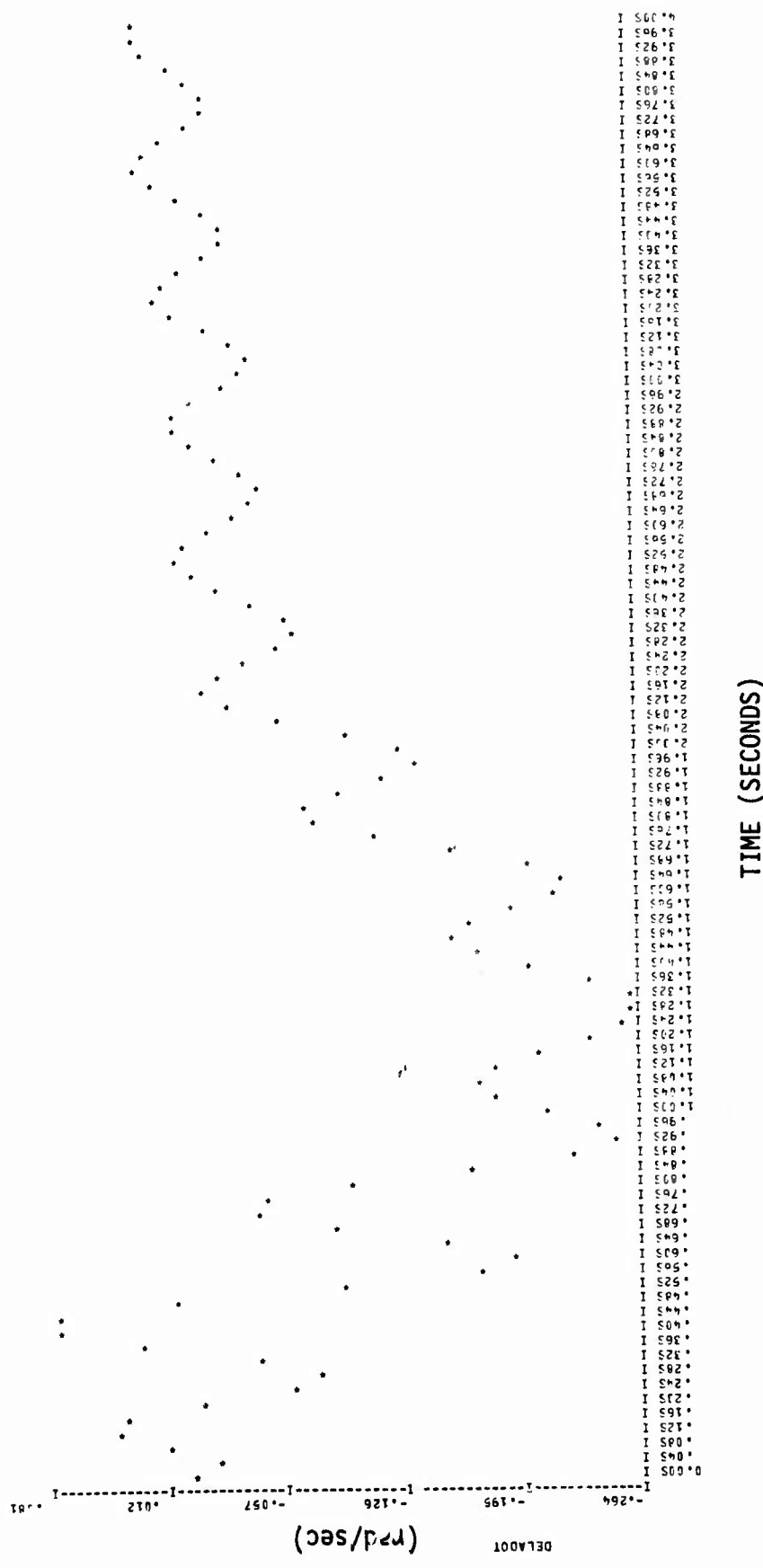
Figure 144.   Command Response Plot of ALDCS A/C with F24RT Model (DELADOT)

Figure 145. Command Response Plot of ALDCS A/C with F24TT Model (DELADOT)

TIME (SECONDS)

(rad/sec)

263

Figure 146. Command Response Plot of SAS A/C with HG24RR Model (ALPHA)

264

Figure 147. Command Response Plot of SAS A/C with F24RR Model (ALPHA)

265

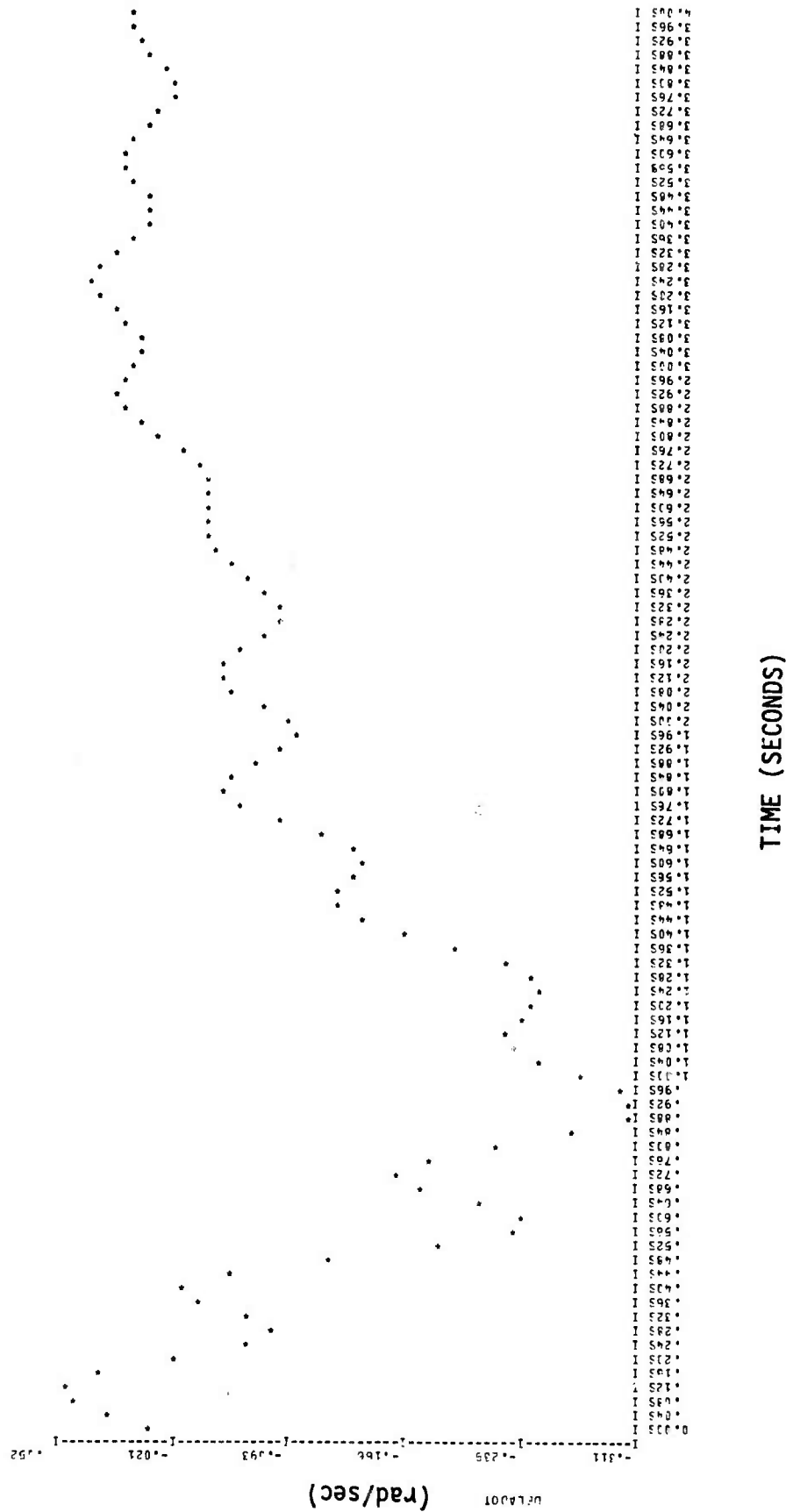Figure 148. Command Response Plot of ALDCS A/C with HG24RR Model (ALPHA)

TIME (SECONDS)

ALPHA (rad)

Figure 149. Command Response Plot of ALDCS A/C with F24RR Model (ALPHA)
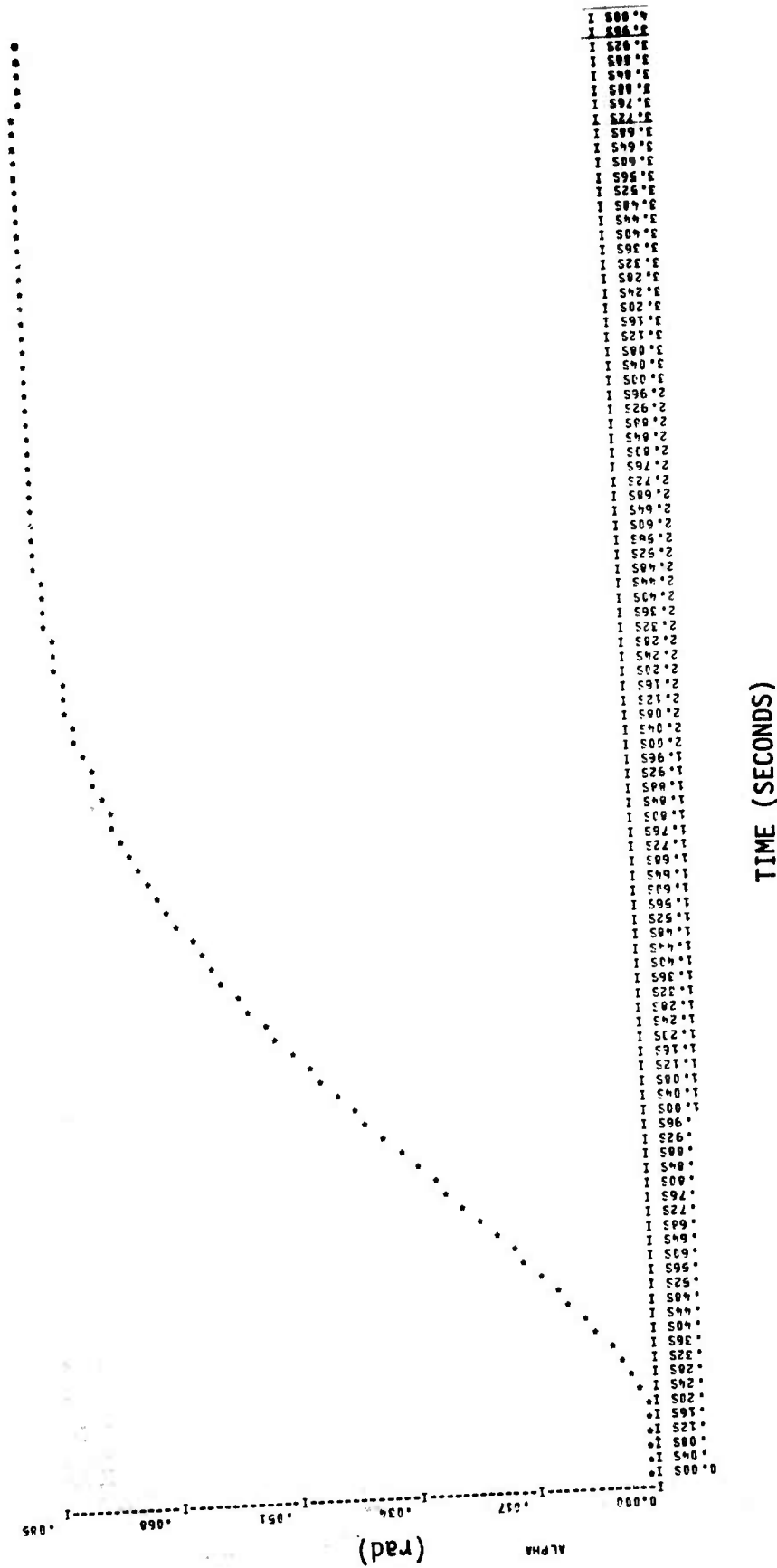
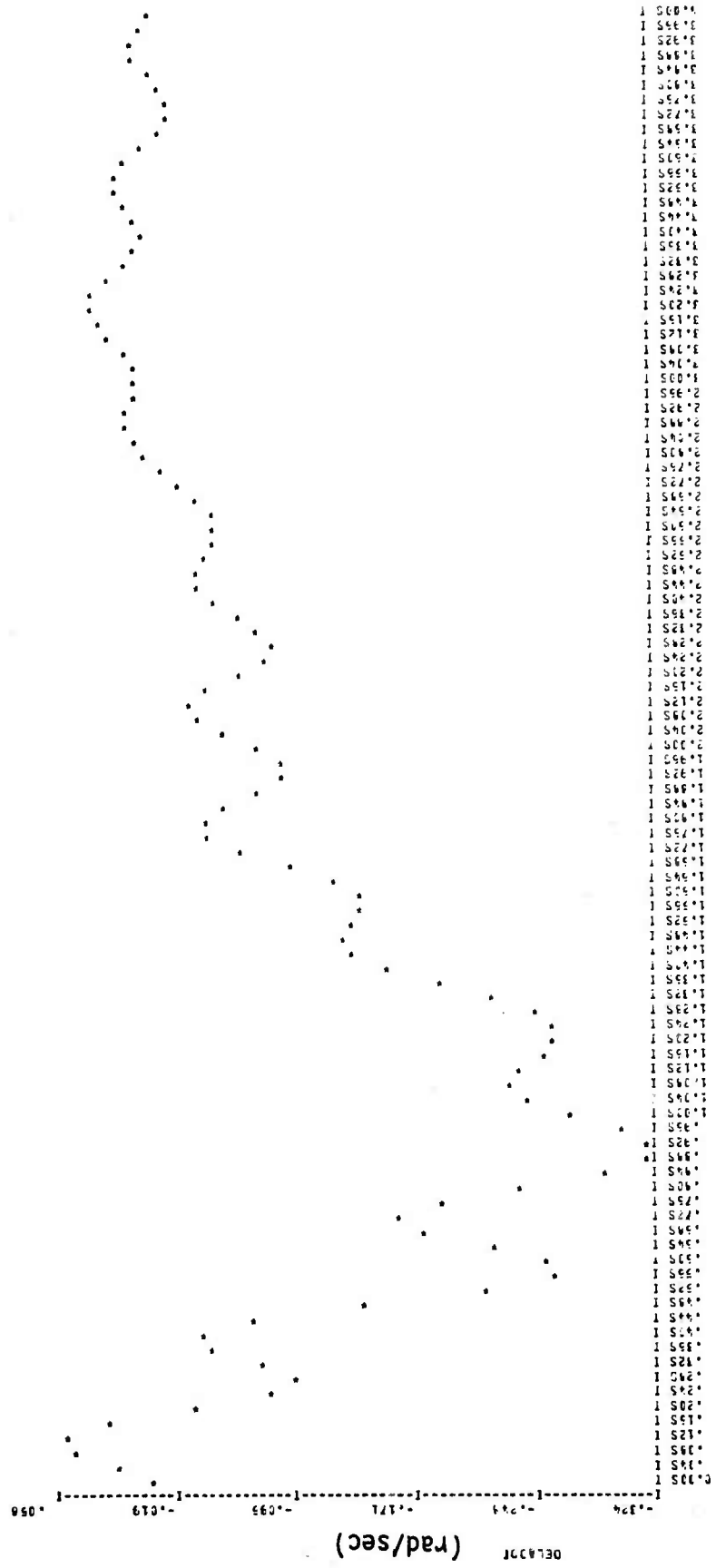Figure 150. Command Response Plot of ALDCS A/C with F24RT Model (Alpha)

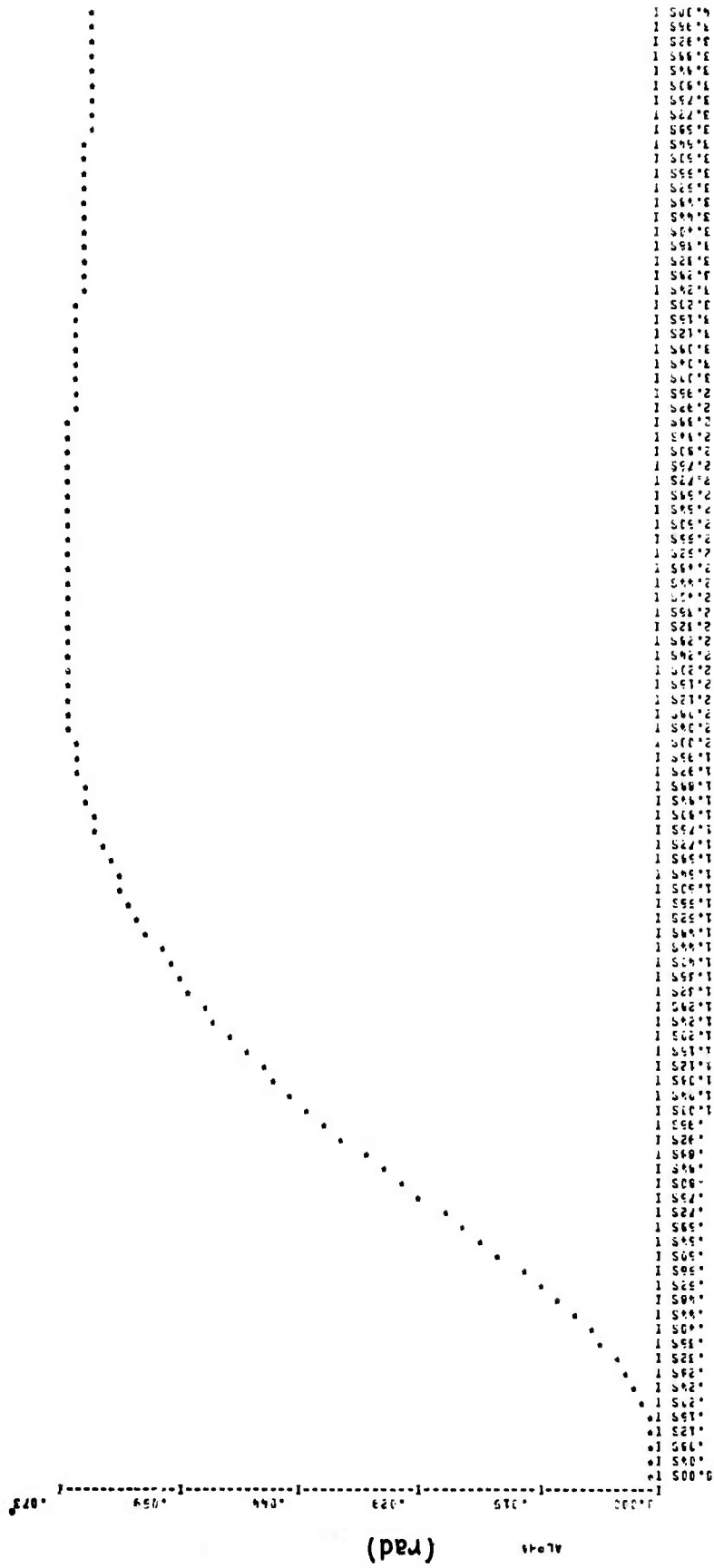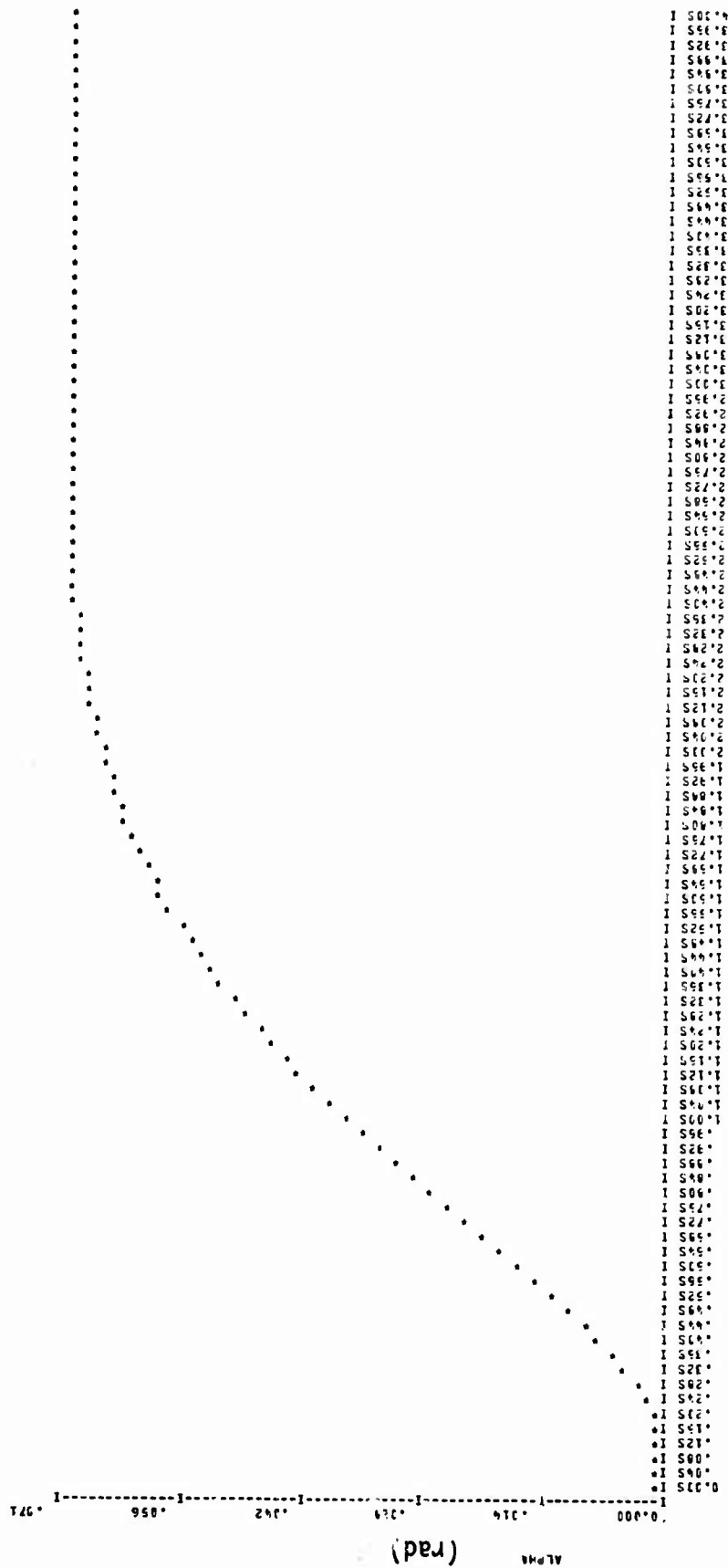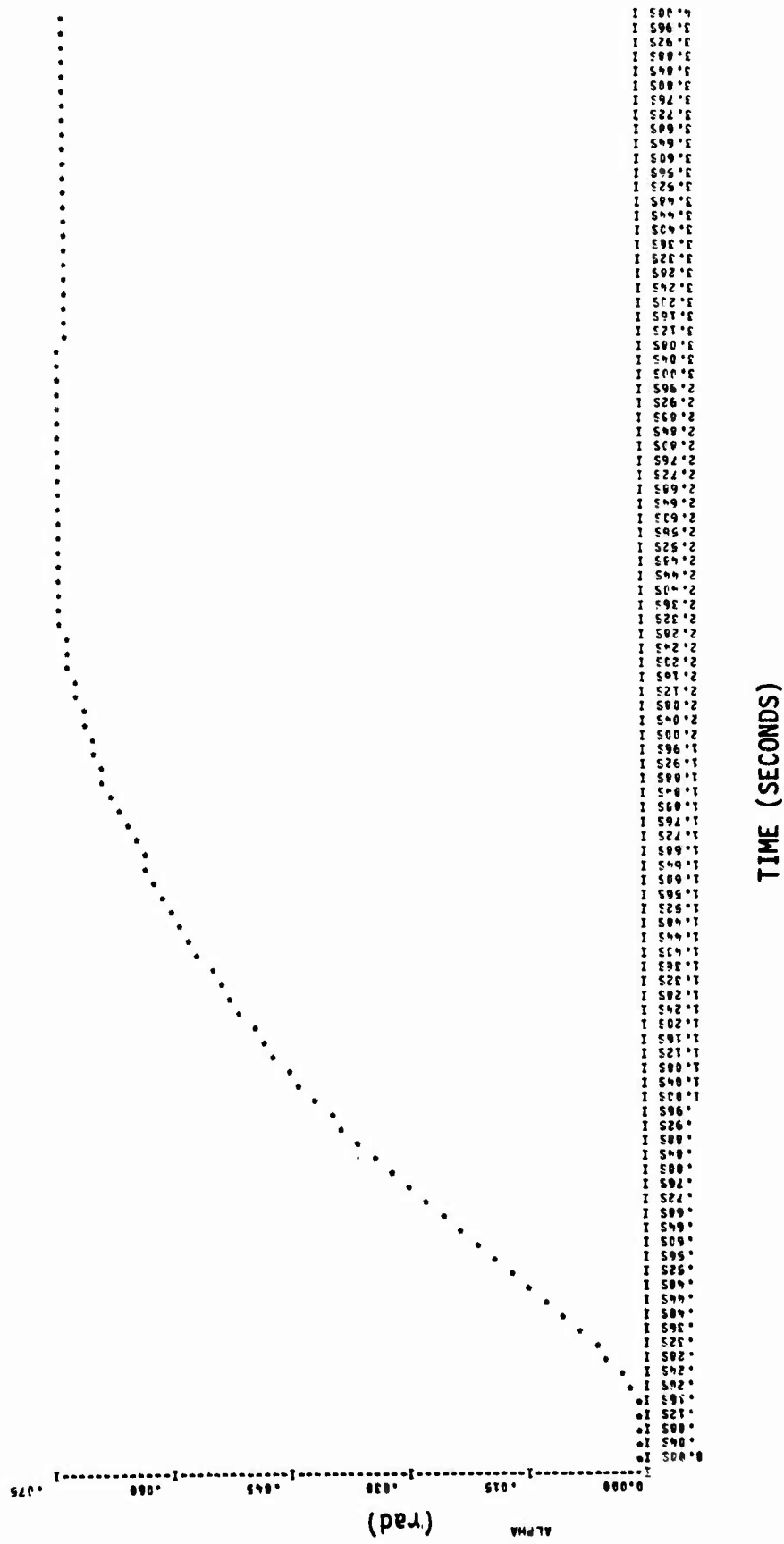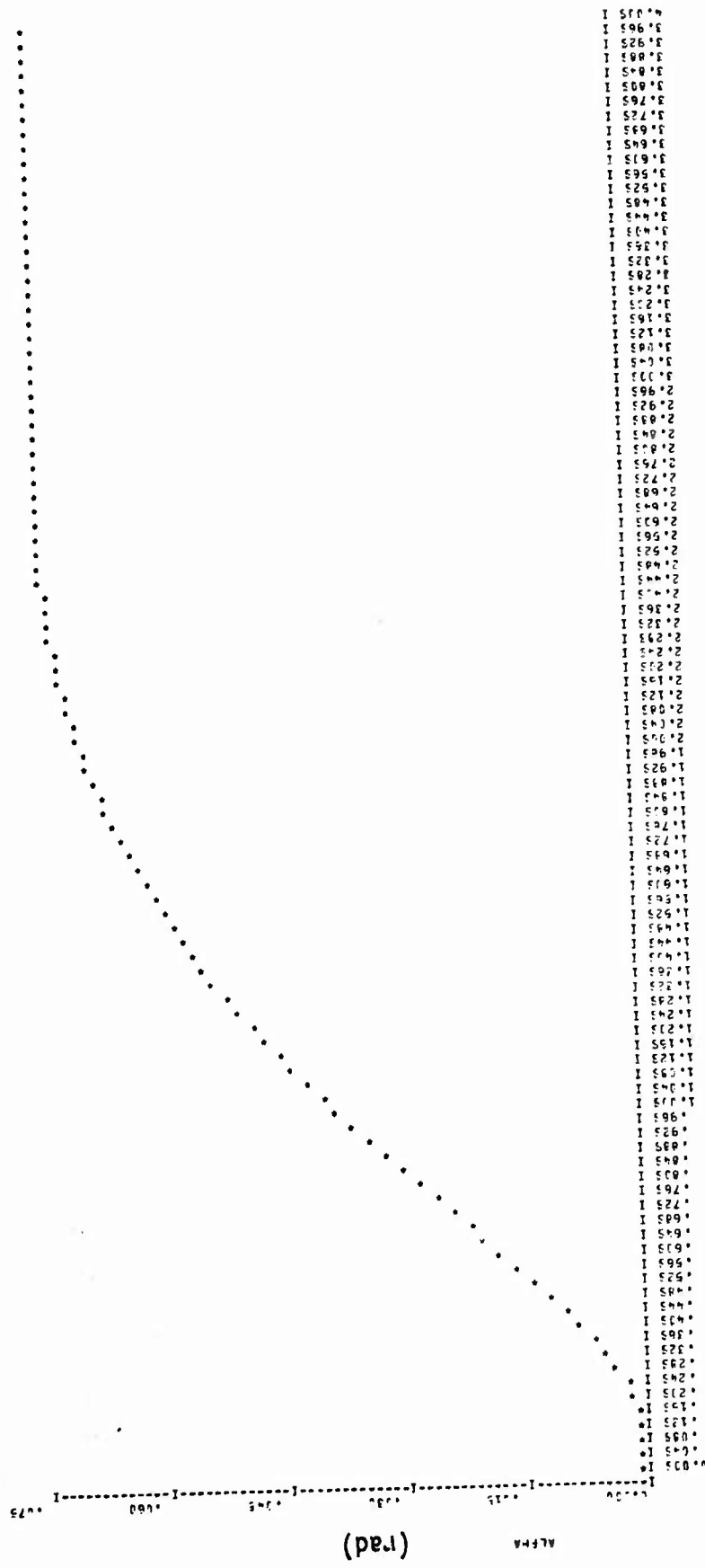TIME (SECONDS)

ALPHA (rad)

268

TIME (SECONDS)

ALPHA (rad)
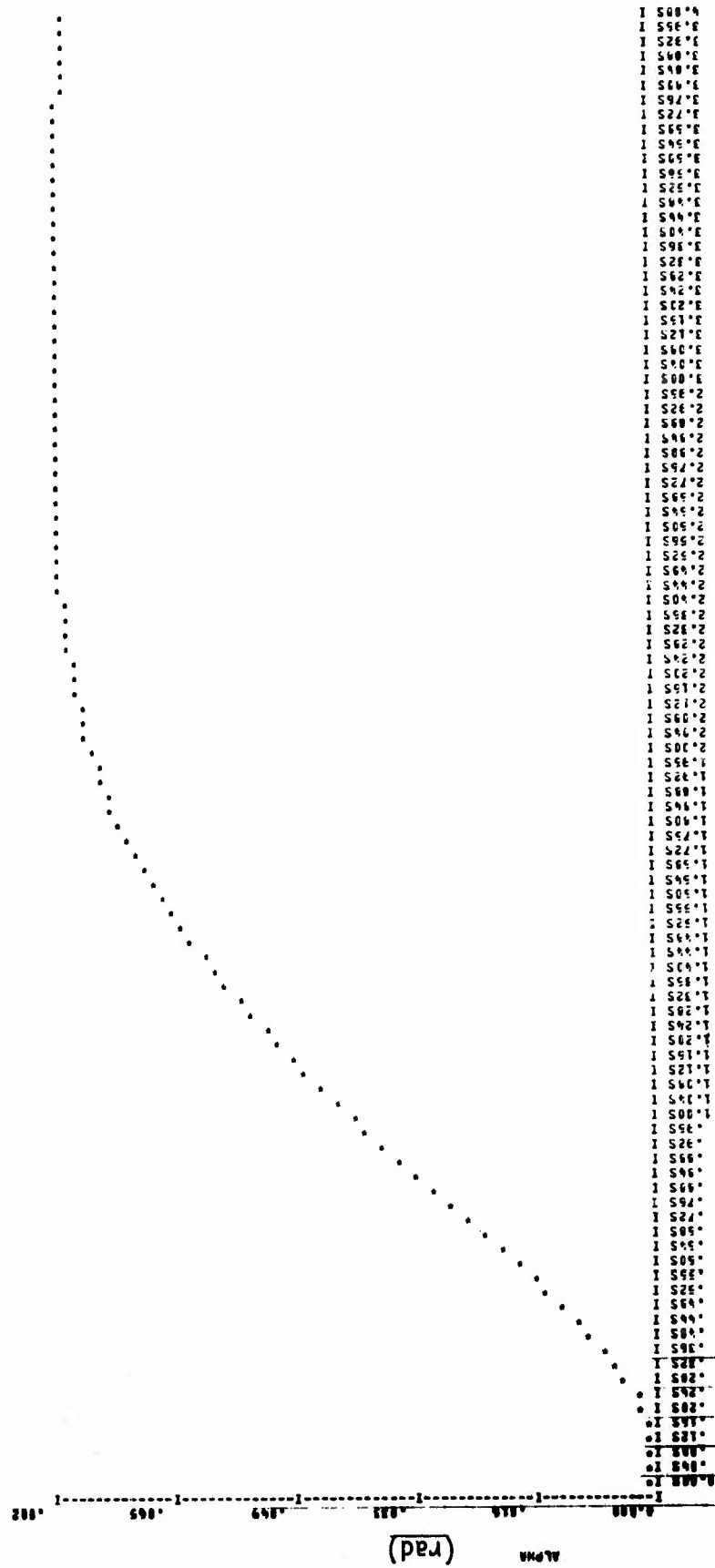
Figure 151. Command Response Plot of ALDCS A/C with F_ T Model (Alpha)

SECTION VII

CONCLUSIONS AND RECOMMENDATIONS

The objectives of this study were threefold: 1) develop an interface program between FLEXSTAB/LSA and Air Force-owned optimal control programs (DIAK and FFOC), 2) demonstrate the interface by using C-5A model and Active Lift Distribution Control System Design Procedure, and 3) conduct a brief study on model reduction procedures for design. The major emphasis has been on the interface software development.

These objectives were primarily met. The algorithms used in the interface and the results of demonstration example are documented in this report. The developed programs are listed in AFFDL-TR-75-146, Volume II. Users information for the programs is given in AFFDL-TR-75-146 Volume III.

In the following, the results and recommendations for future studies pertaining to the work in the area of analysis and synthesis and software developments are presented.

SIGNIFICANT RESULTS

- The work reported here established the total software system approach to Active Control Technology (ACT) and Control Configured Vehicles Design (CCV) problems.

270

- The chief benefit of the program was to provide integrated software for rapid development of vehicle model and control laws for ACT and CCV studies.

- The results of demonstration example with C-5A ALDCS show that FLEXSTAB program system generates valid models for preliminary control system synthesis.

- The results also show that the residualization procedure is better than truncation procedure when higher order models are reduced to low order models for design.

RECOMMENDATIONS FOR FUTURE ANALYTICAL WORK

- Development of efficient model reduction procedures is needed for feedback design of high order models representing unsteady aerodynamics and bending modes.

- Development of design procedures using residualized Riccati equations via singular perturbation and boundary layer techniques is needed to reduce design cost for high order systems.

- Development of efficient solution procedure is needed for constrained-optimal control problems to enforce conventional design criteria into optimal active control synthesis techniques.

RECOMMENDATIONS FOR FUTURE SOFTWARE DEVELOPMENT WORK

- Development of geometry definition interface module is needed

271

to generate vehicle configuration/performance sensitivities for Control Configured Vehicles design.

● Automatic weight selection and response selection modules should be developed to speed up the quadratic design process.

● Algorithms developed for the Constrained-Optimal Control problem should be implemented.

● Existing optimal control routines should be revised for higher computational efficiency.

● Optimal multirate digital control analysis and design capabilities should be added using the Air Force-owned programs.

CONCLUSIONS

A large-scale software system for automatic modeling and optimal design of active control systems was developed in this study. The software system was used to design controller for the C-5A vehicle with Active Lift Distribution Control System design procedure. Automatic dimensioning and user oriented statement features considerably improved the interface data mechanics for optimal design.

REFERENCES

1. A. J. VanDierendonck and G. L. Hartmann, "Quadratic Methodology," Volume II - Documentation for Computer Program, Honeywell Report No. F0161-FR, October 1973.

2. G. R. Hank et al., "A Method for Predicting the Stability Character-istics of Control Configured Vehicles," Volume II - FLEXSTAB 2.01.00 User's Manual, AFFDL-TR-74-91, November 1974.

3. A. F. Konar and J. K. Mahesh, "Computer Programs for Active Control Technology," Volume II, KONPACT Program Listings, AFFDL-TR-75-146 Vol. I, June 1976.

4. R. B. Beale, M. F. Barrett, and C. R. Stone, "Control Design for the C-5A Active Lift Distribution Control System," Honeywell Report No. RF-09523C, Volumes I and II, April 1974.

5. R. Schwanz, C. Stockdale, "Effect of Structural Idealization on the Aeroelastic Stability and Control Parameters of the C-5A Aircraft," AFFDL-TM-75-122-FGC, December 1975.

6. C. Stockdale and G. Grimes, "A Formulation of Dynamic Load Equations using the Level 2 FLEXSTAB Data Base for Control Configured Vehicles Design," AFFDL-TM-75-120, February 1976.

7. Phillips, A. C., Rosen, R. W., "A Note on Dynamic Data Storage in Fortran IV," Computer Journal, Vol. 18, No. 4, November 1975.

8. M. F. Barrett and R. C. McLane, "Design Procedure and Results for ALDCS," MR 12223, S&RC Honeywell, Minneapolis, September 1973.

9. E. N. Tinoco and J. E. Mercer, "FLEXSTAB, A Summary of the Functions and Capabilities of the NASA Flexible Airplane Analysis Computer System," NASA CR-2564, December 1975.

REFERENCES (Continued)

10. R. D. Miller et al., "Feasibility of Implementing Unsteady Aero-dynamics into the FLEXSTAB Computer Program System," NASA CR 132530, October 1974.

11. A. J. VanDierendonck et al., "Application of Practical Optimal Control Theory to the C-5A Load Improvement Control Systems (LICS)," AFFDL-TR-73-122, October 1973.

12. A. F. Konar, "Development of Weapon Delivery Models and Analysis Programs," AFFDL-TR-71-123, Volume I, April 1972.

13. G. L. Hartmann et al., "F-8C Digital CCV Flight Control Laws," NASA CR 2629, February 1976.

14. M. S. Borow et al., "Navy Digital Flight Control System Development," Honeywell Document No. 21857-FR, GAP, Minneapolis, December 1972.

15. C. R. Abrams, "A Performance Index for Response Evaluation of Highly Augmented Military Aircraft," NADC-AM-7103, Naval Air Development Center, Warminster, Pa., 12 October 1971.

16. "Military Specification - Flying Qualities of Piloted Airplanes," MIL-F-8785B (ASG), 7 August 1969.

17. "Military Specification - Control and Stabilization Systems: Automatic, Piloted Aircraft, General Specification For," MIL-C-18244A (WEP), 1 December 1962.

18. L. Edinger and T. Lahn, "C-5A Data Base for Load Alleviation and Mode Stabilization Program," Report 20564-DB1, Honeywell Inc., Government and Aeronautical Products Division, Minneapolis, Minn., 1 April 1968.

REFERENCES (Continued)

19. "Aircraft Load Alleviation and Mode Stabilization (LAMS): C-5A System Analysis and Synthesis," Technical Report AFFDL-TR-68-162, Wright-Patterson Air Force Base, Ohio, November 1969.

20. C. R. Stone, M. D. Ward, C. A. Harvey, M. E. Ebsen, E. E. McBride, and W. W. Hollenbeck, "Studies on the Compatibility of Relaxed Static Stability and Maneuver Load Control to C-5A-Type Aircraft," Volume I, Technical Report AFFDL-TR-72-38, Wright-Patterson Air Force Base, Ohio, June 1972.

21. Edinger, Schenk, and Curtis, "Study of Load Alleviation and Mode Suppression (LAMS) on the YF-12A Airplane," NASA CR-2158 , June 1972.

22. "Electronic Load Improvement Control System (LICS) Cost and Effectiveness Study for the C-5A, A Report to the C-5A Independent Structural Review Team," 13 September 1972.

23. G. Stein, A. H. Henke, "A Design Procedure and Handling-Qualities Criteria for Lateral-Directional Flight Control Systems," AFFDL-TR-70-152, May 1971.

24. A. J. VanDierendonck, "Design Method for Fully Augmented Systems for Variable Flight Conditions," AFFDL-TR-71-152, January 1972.

25. A. J. VanDierendonck, "Quadrater Methodology: A Short Course on the Application of Quadratic Optimal Control Theory to the Design of Practical Flight Control Systems (or any other similarly Modeled System)," prepared for AFFDL under contract No. F33615-72-C-2008.

26. C. R. Stone, M. D. Ward, C. A. Harvey, M. E. Ebsen, E. E. McBride, and W. W. Hollenbeck, "Studies in the Compatibility of Relaxed Static Stability and Maneuver Load Control to C-5A Type Aircraft," AFFDL-TR-72-38, Volume II, June 1972.

REFERENCES (Continued)

27. C. R. Stone, "From LICS to ALDCS with F.C. 37 of the C-5A," Honeywell Research Memo, MR 12184, 25 June 1973.

28. C. R. Stone, "LICS to ALDCS Revised," Honeywell Research Memo, MR 12195, 10 July 1973.

29. C. R. Stone, "Modeling of Flexible C-5A's for ALDCS," Honeywell Customer Engineering Letter to Lockheed Georgia Company, C.E.L. No. ALDCS-2, 27 July 1973.

30. J. G. Truxal, "Automatic Feedback Control System Synthesis," McGraw-Hill Book Co. Inc., New York 1955.

31. A. F. Konar and J. K. Mahesh, "Digital Control Systems for Tactical Fighters," AFFDL-TR-73-119, Volume I, June 1974.

32. Petar V. Kototovic and Ricard A. Yackel, "Singular Perturbation of Linear Regulators: Basic Theorems," IEEE Trans. Auto. Ctrl., Volume AC-17, No. 1, February 1972, pp. 29-37.

33. Richard A. Yackel and Petar V. Kokotovic, "A Boundary Layer Method for the Matrix Riccati Equation," IEEE Trans. Auto. Ctrl., Volume AC-18, No. 1, February 1973, pp. 17-24.

34. Y. Shamask, "Stable Reduced-Order Models Using Pade-Type Approximations," IEEE Trans. Auto Ctrl., October 1974, pp. 615-616.

35. Y. Shamask, "Linear System Reduction Using Pade Approximation to Allow Retention of Dominant Modes," Int. J. Ctrl., Volume 21, No. 2, 1975, pp. 257-272.

36. Y. Shamask, "Model Reduction Using the Routh Stability Criterion and the Pade Approximation Technique," Int. J. Ctrl., Vol. 21, No. 3, 1975, pp. 475-484.

REFERENCES (Continued)

37. M. Lal and R. Mitra, "A Comparison of Transfer Function Simplification Methods," IEEE Trans. Auto. Ctrl., October 1974, pp. 617-618.

38. Maurice F. Hutton and Bernard Friedland, "Routh Approximations for Reducing Order of Linear, Time-Invariant Systems" IEEE Trans. Auto. Ctrl., Vol. AC-20, No. 3, June 1975, pp. 329-337.

39. E. E. Yore and Y. Takahashi, "Identification of Dynamic Systems by Digital Computer Modeling in State Space," Journal of Basic Engineering, June 1967, pp. 295-299.

40. T. C. Hsia, "On the Simplification of Linear Systems," IEEE Trans. Auto Ctrl. June 1972, pp. 372-374.

41. R. B. Beale and N. E. Miller, "Turbine Engine Control Synthesis, Volume III: Experimental Engine Identification and Modeling," Aero Propulsion Lab Technical Report AFAPL-TR-75-14, March 1975.

42. R. Genesio and R. Pome, "Identification of Reduced Models from Noisy Data," Int. J. Ctrol, Volume 21, No. 2, 1975, pp. 203-211.

43. T. Subba Rao, "An Innovation Approach to the Reduction of the Dimensions in a Multivariable Stochastic System," Int. J. Ctrl., Volume 21, No. 4., 1975, pp. 673-680.

44. Lewis Meier and David G. Luenberger, "Approximation of Linear Constant Systems," IEEE Trans. Auto. Ctrl., October 1967, pp. 585-588.

45. C. T. Leondes and John F. Yocum, "Optimal Observers for Continuous Time Linear Stochastic Systems," Automatica, Volume II, 1975, pp. 61-73.

REFERENCES (Concluded)

46. Robert G. Schwendler and Richard H. MacNeal, "Optimum Structural Representation in Aeroelastic Analyses," Flight Dynamics Laboratory Report ASD-TR-61-680, March 1962.

47. Mihajlo D. Mesarovic, Theory of Hierarchal Multilevel Systems, Academic Press, 1970.

48. Krzysztof Cichocki, "Multilevel Control Systems," University of Minnesota, May 1975 (primarily a translation of Reference 49).

49. W. Findersen, "Multilevel Control Systems," (in Polish), PWN, Warzawa, 1974.

50. "A Method for Predicting the Stability Characteristics of Control Configured Vehicles," Volume I - FLEXSTAB 2.01.00 Theoretical Description, Boeing Commercial Airplane Company, AFFDL-TR-74-91, November 1974.

51. A. F. Konar and J. K. Mahesh, "Computer Programs for Active Control Technology, "Volume III, User's Manual, AFFDL-TR-75-146, Vol. III, June 1976.

52. "New Short Period Handling Quality for Fighter Aircraft," Boeing Document D6-17841 T/N, October 1965.

53. Kisslinger, R. L., and Wendl, M., "Survivable Flight Control System Interim Report No. 1, Studies Analysis and Approach," AFFDL-TR-71-20 Supplement 1, May 1971.

54. Dornfeld, G., Fraser, R., "Review of AFFDL Program, AFLOADS," The Boeing Commercial Airplane Company, Contract F33615-75-C-3132 Management Review Report, August 1976.